UNIVERSIDADE FEDERAL DE SANTA CATARINA
CENTRO TECNOLÓGICO
PROGRAMA DE PÓS-GRADUAÇÃO EM ENGENHARIA QUÍMICA

Julia Lemos de Oliveira

COENCAPSULATION OF DOXORUBICIN AND INDOCYANINE GREEN IN FUNCTIONALIZED POLYGLOBALIDE NANOPARTICLES

Florianópolis
2023

Julia Lemos de Oliveira

COENCAPSULATION OF DOXORUBICIN AND INDOCYANINE GREEN IN FUNCTIONALIZED POLYGLOBALIDE NANOPARTICLES

Dissertação submetida ao Programa de Pós-Graduação da Universidade Federal de Santa Catarina como requisito parcial para a obtenção do título de Mestra em Engenharia Química.
Orientadora: Prof.a Ana Paula Serafini Immich Boemo, Dr.a
Coorientadora: Prof.a Claudia Sayer, Dr.a
Coorientadora: Tamara Agner, Dr.a

Florianópolis
2023

Ficha de identificação da obra elaborada pelo autor,
através do Programa de Geração Automática da Biblioteca Universitária da UFSC.

de Oliveira, Julia Lemos
Coencapsulation of Doxorubicin and Indocyanine Green in Functionalized Polyglobalide Nanoparticles / Julia Lemos de Oliveira ; orientadora, Ana Paula Serafini Immich Boemo, coorientador, Claudia Sayer, coorientador, Tamara Agner, 2023.
166 p.

2. Nanopartículas de Poliéster (PGl). 3. Coencapsulação de Fotossensibilizador e Quimioterápico. 4. Fototerapia para Câncer. 5. Funcionalização com BSA. I. Boemo, Ana Paula Serafini Immich . II. Sayer, Claudia . III. Agner, Tamara IV. Universidade Federal de Santa Catarina. Programa de Pós Graduação em Engenharia Química. V. Título.

Julia Lemos de Oliveira

Coencapsulation of Doxorubicin and Indocyanine Green in Functionalized Polyglobalide Nanoparticles

O presente trabalho em nível de Mestrado foi avaliado e aprovado, em 15 de setembro de 2023 pela banca examinadora composta pelos seguintes membros:

Prof.a Ana Paula Serafini Immich Boemo, Dr.a
Universidade Federal de Santa Catarina

Prof.a Patrícia Bulegon Brondani, Dr.a
Universidade Federal de Santa Catarina, Blumenau

Camila Guindani, Dr.a
Universidade Federal do Rio de Janeiro

Certificamos que esta é a versão original e final do trabalho de conclusão que foi julgado adequado para obtenção do título de Mestre em Engenharia Química pelo Programa de Pós-Graduação da Universidade Federal de Santa Catarina.

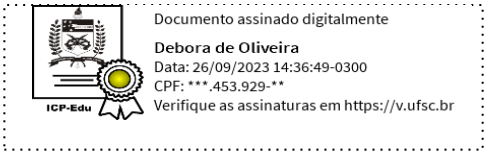

Coordenação do Programa de Pós-Graduação

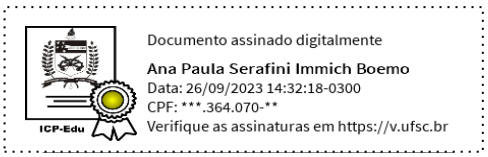

Prof.a Ana Paula Serafini Immich Boemo, Dr.a
Orientadora

Florianopólis, 2023

ACKNOWLEDGMENTS

À Deus e ao Mestre pela força, coragem e presença constante em minha vida para superar os desafios ao longo do desenvolvimento desse mestrado, com fé, alegria e certeza da vitória.

Aos meus pais, Josiano Alves de Lemos e Terezinha Maria de Oliveira Neri Lemos, e minha irmã, Laura Lemos de Oliveira Neri, por sempre acreditarem e investirem, me incentivando a dedicar aos estudos e por muitas vezes, abdicarem da presença física para que eu possa perseverar nos meus sonhos e apoiarem a seguir em frente quando o caminho se mostrou árduo. Essa vitória de certeza, é nossa!

Ao meu namorado, Daniel Queiroz, pela presença constante e apoio inabalável, que foram uma fonte de força e inspiração ao longo dessa jornada. Nos momentos de desafios, esteve ao meu lado, incentivando-me a superar obstáculos e acreditar em mim mesma. Suas palavras de ânimo, compreensão e paciência foram luzes que me guiaram nos momentos de incerteza. Isso demonstra que o nosso amor, independente da distância, é um sentimento genuíno que vale a pena a ser vivido. Essa dissertação é reflexo do nosso trabalho em equipe e mais uma celebração dos nossos esforços em união.

À minha orientadora, Ana Paula, por aceitar a transferência de orientação com presteza e contribuição ao longo deste período. Sua condução e orientações moldaram a qualidade da minha pesquisa e me ajudaram a crescer como estudante e pesquisador. Este é um marco significativo na minha jornada acadêmica, e seu papel como minha orientadora é parte integrante do meu crescimento e aprendizado.

À minha coorientadora, Claudia Sayer, cuja orientação, insights e encorajamento foram fundamentais para moldar este trabalho. Sua dedicação em partilhar conhecimento experiência e paciência ao guiar-me por desafios complexos foram inestimáveis para o desenvolvimento desse trabalho. Espero que possamos continuar trabalhando juntas em projetos futuros.

À minha coorientadora, Tamara, por ter me dado a mão, ensinado, auxiliado e por fazer esse trabalho se concretizar. Um exemplo de profissional, amiga e orientadora, o conhecimento e esperteza que me proporcionou, levarei em minha memória. Digo com certeza, que sem ela teria sido uma missão ainda mais árdua o desenvolvimento deste trabalho. Um pilar que me manteve motivada para perseverar mesmo nos dias desafiadores.

À colaboradora do estudo, Karina Cesca, pelo desenvolvimento de análises importantes para o trabalho, bem como pela orientação no laboratório de Cultura de Células. Sua contribuição e experiência foram fundamentais para o progresso do nosso estudo.

Ao Programa de Pós-Graduação em Engenharia Química – PósEnQ pela oportunidade concedida e por proporcionar um ambiente acadêmico e recursos que foram essenciais para a realização deste trabalho.

Ao Laboratório de Controle e Polimerização – LCP, Laboratórios de Simulação Numérica de Sistemas Químicos e de Transferência de Massa – LabSin-LabMassa e o Laboratório de Engenharia Biológica – LiEB, pela estrutura concedida e pelo ambiente que se tornou minha casa nesse período.

Aos técnicos da Central de Análise de Engenharia Química da UFSC, Fernanda e Leandro, e à Central de Análises do Departamento de Química da UFSC, ao Laboratório Interdisciplinar para o Desenvolvimento de Nanoestruturas – LINDEN e o Laboratório de Tecnologias Integradas (Intelab) da UFSC, por todo suporte, parceria e orientação prestados ao longo desse trabalho.

Aos amigos de trabalho, Tamara, Amanda, Marcelo, Isabela, Gabriel, Vanessa, Renato, Rosana, Luiz Paulo, Claudia, Danyelle, Karina, Maikon, Thuany, Thaíris, Camila, Thayli, Ricardo, Clara, Heloisa, Beatriz pela parceria, auxílio e amizade. Nos momentos de tensão, vocês foram fontes de alívio e descontração. Nas vitórias, vocês celebraram comigo, tornando cada conquista mais especial. Cada palavra de incentivo e cada momento compartilhado construíram uma rede de apoio que me sustentou.

Aos amigos que fazem parte da minha vida, tanto aqueles que me acompanham desde minha cidade natal quanto aqueles que conheci ao longo deste percurso enriquecedor, alegrando, me ajudando a chegar até aqui e contribuindo para a minha formação pessoal. Saber que eles estavam torcendo por mim, a cada passo do caminho, trouxe uma sensação de conforto e motivação. O apoio emocional e constante presença tornaram essa jornada mais significativa e memorável. Esta jornada não seria a mesma sem a contribuição única de cada um de vocês.

É com profunda gratidão que expresso meus sinceros agradecimentos neste momento significativo da minha jornada acadêmica. A conclusão desta dissertação de Mestrado marca o culminar de anos de dedicação, esforço e aprendizado, e não teria sido possível sem o apoio e contribuição dessas pessoas especiais.

"Science is much more than a body of knowledge. It's a way of thinking. It is not only compatible with Spirituality; she is a deep source of Spirituality. And somewhere, something amazing is waiting to be known."

Carl Sagan

RESUMO

A fototerapia tem despertado grande interesse na comunidade científica devido à sua baixa invasividade, toxicidade, efeitos adsorvidos reduzidos e falta de resistência a drogas no tratamento do câncer. Terapias como a Fotodinâmica e Fototérmica compreendem a administração de um fotossensibilizador (FS) que ao absorver luz no comprimento de onda específico, produz uma resposta citotóxica ao tecido tumoral, seja por liberação de espécies reativas citotóxicas de oxigênio ou liberação de calor. Apesar de ser uma técnica pouco invasiva, ainda existem limitações clínicas na aplicação devido ao baixo acúmulo do fotossensibilizador (FS) no tecido tumoral e ao seu curto tempo de circulação sanguínea, seja pela sua desativação por biomoléculas ou pela sua baixa solubilidade no meio. Essas limitações podem ser superadas com a encapsulação do fotossensibilizador, melhorando sua estabilidade e controlando sua fotoatividade. Este trabalho tem como objetivo encapsular o agente fotossensibilizador Verde de Indocianina (ICG) e o Quimioterápico Cloridrato de Doxorubicina (DOX) em nanopartículas (NPs) de Poli(Globalide) (PGl). O PGl foi sintetizado via Polimerização Enzimática de Abertura de anel a 65ºC usando Novozym 435, Candida antarctica B lipase imobilizada (Cal-B), como biocatalisador. Nanopartículas coencapsulando ICG e a DOX foram preparadas pela técnica de Dupla Emulsão por Evaporação do Solvente e foram analisadas quanto ao tamanho hidrodinâmico de partícula e índice de polidispersão (PDI) por Dispersão Dinâmica de Luz (DLS). O PGl e as NPs foram caracterizados quanto a sua estrutura química, propriedades térmicas e peso molecular. A eficiência de encapsulação (EE%), do ICG e DOX, foi determinada por Espectroscopia Ultravioleta-visível e Fluorescência, respectivamente. Diferentes formulações e condições experimentais foram avaliadas, sendo que nas condições otimizadas, NPs com menos de 300 nm e PDI < 0,2 foram obtidas. As imagens de TEM revelaram o formato esférico das nanopartículas e corroboraram com os tamanhos submicrométricos determinados por DLS. As EE% do ICG em PGL NPs, para as 4 formulações (em triplicata) foram maiores que 83.2 ± 0.4 % e de 59.5 ± 2.2 % para a DOX. Assim, a técnica de dupla emulsão provou ser uma estratégia eficiente para encapsular ICG e DOX, de maneira isolada (ICG) ou duplamente carregada em NPs de PGl. Corroborando com a literatura, houve um aumento na taxa de EE% do ICG quando adicionado à DOX na formulação de NPs, com aumento de cerca de 8,5%. Além disso, as nanopartículas foram funcionalizadas com Albumina Sérica Bovina (BSA) por adsorção e quantificadas pelo Método de Lowry, com adsorção de > 58%, resultando em um bom recobrimento da superfície. Durante 6 meses foi conduzido um estudo de 6 meses e as NPs demonstraram estabilidade, mantendo seu tamanho hidrodinâmico e pH. Foram investigados os perfis de liberação do ICG e DOX nas formulações F2 (5 mg de ICG) e F4 (5 mg de ICG e 1,25 mg de DOX) em diferentes valores de pH (5.5 e 7.4), simulando ambientes biológicos relevantes. Foi observado que a presença de DOX acelerou a liberação de ICG em pH fisiológico e ácido, com o ICG liberando mais rápido em pH fisiológico, enquanto a DOX demonstrou um aumento na liberação em pH 5.5. Para o estudo de citotoxicidade em células de fibroblastos L929, concentrações de NPs abaixo de 168,7 ng mL^{-1} (NPs sem funcionalização de BSA) não foram citotóxicas após 24 horas de incubação, com viabilidade celular acima de 70%. Nos testes em células de linhagem tumoral SKMEL-28, utilizando um laser de 808 nm, o tempo de irradiação foi um fator determinante na terapia fotodinâmica/fototérmica, irradiação em 10 minutos produziu os melhores resultados, com atividade metabólica entre 70% e 80%.

Palavras chaves: Carreadores de Nanopartículas de Poliéster; Dupla Emulsão, Coencapsulação de Fármacos Hidrofílicos; Fototerapia combinada em linhagem tumoral.

RESUMO EXPANDIDO

INTRODUÇÃO

O câncer é uma doença complexa e que demanda uma grande atenção por parte da comunidade científica. Atualmente, diversas abordagens são utilizadas para combater essa afecção, como a quimioterapia, radioterapia e imunoterapia. Apesar dos avanços significativos nesse campo, os tratamentos convencionais frequentemente apresentam efeitos adversos tóxicos, pois além de matar as células cancerígenas, matam as células saudáveis circundantes, dessa forma, podem ser debilitantes para os pacientes e prejudicar sua qualidade de vida. Uma solução emergente para mitigar os efeitos adversos indesejados é o uso de tratamentos não convencionais, como a fototerapia, a fotodinâmica e a fototérmica. Essas terapias envolvem a aplicação de luz para ativar substâncias fotossensibilizadoras específicas, induzindo a morte seletiva de células tumorais. Essa abordagem pode ser uma alternativa promissora aos tratamentos tradicionais, reduzindo a toxicidade geral no organismo do paciente. Uma das tendências atuais no campo da terapia fototérmica e fotodinâmica é o uso de Nanopartículas Poliméricas para encapsular fármacos fotossensibilizadores e quimioterápicos, como o Verde de Indocianina (ICG) e o Cloridrato de Doxorrubicina (DOX). Essas nanopartículas podem aprimorar o efeito terapêutico combinado, aumentando a eficiência da terapia fototérmica e fornecendo uma liberação controlada e direcionada dos agentes terapêuticos. A funcionalização das nanopartículas com a Albumina Sérica Bovina (BSA) visa melhorar ainda mais essa estratégia terapêutica, pois o BSA é uma proteína que apresenta alta afinidade por receptores expressos nas células cancerígenas, o que permite o transporte e maior acumulação das nanopartículas nas regiões tumorais, aumentando a seletividade e eficácia do tratamento. Além disso, o desenvolvimento de polímeros biocompatíveis e biodegradáveis que servirão de carreadores para esses fármacos, que apresentam propriedades de interesse para essas aplicações biomédicas, por exemplo, vem sendo estudado extensivamente nas últimas décadas. Nesse contexto, poliésteres emergem como uma classe de polímeros promissora como alternativas para materiais tradicionais devido a características como biocompatibilidade, biorresorbabilidade e biodegradabilidade. Adicionalmente, a possibilidade desses materiais serem obtidos por meio da polimerização por abertura de anel enzimática apresenta diversas vantagens em relação a catalisadores convencionais como condições de reação mais brandas e menor geração de resíduos tóxicos. Entre os poliésteres recentemente estudados, o Poli(Globalide) (PGl) apresenta um grande potencial de aplicações devido à presença da insaturação em sua unidade de repetição. Assim, o presente trabalho relata a síntese de PGl por polimerização enzimática por abertura de anel. O polímero obtido foi usado na preparação de nanopartículas pelo método de Dupla Emulsão com a evaporação de solvente e na encapsulação de ICG e DOX. Adicionalmente, as nanopartículas obtidas foram funcionalizadas com BSA. Por fim, as NPs foram aplicadas para ensaios de fototerapia combinada na linhagem celular de melanoma cutâneo (SKMEL-28).

OBJETIVOS

Objetivo Geral

Este trabalho teve como objetivo geral preparar e avaliar a utilização de Nanopartículas do Poliéster insaturado Poli(globalide) como potenciais nanocarreadores

do fotossensibilizador Verde de Indocianina (ICG) e o medicamento quimioterápico Cloridrato de Doxorrubicina (DOX), seguido de funcionalização com Albumina de Soro Bovino (BSA) para aplicação combinada em terapia fotodinâmica e fototérmica em linhagens celulares de melanoma cutâneo (SKMEL-28).

Objetivos específicos

a) Sintetizar Poli(globalide) via reação de polimerização enzimática por abertura de anel (e-ROP) utilizando a lipase imobilizada Novozym 435 e determinar sua estrutura química, peso molecular e dispersividade (*Đ*).

b) Avaliar o efeito da formulação e das condições operacionais nas características das Nanopartículas do poliéster Poli(Globalide).

c) Preparar PGl NPs através da técnica de Dupla Emulsão com evaporação do solvente e caracterizar as suas propriedades térmicas, estabilidade, tamanho hidrodinâmico, distribuição de tamanho, potencial Zeta, presença de grupos funcionais e morfologia.

d) Realizar testes de encapsulação, em diferentes formulações, com os fármacos ICG e DOX, preparados pela técnica de dupla emulsão com evaporação de solvente e caracterizar seu tamanho e morfologia, estabilidade, propriedades térmicas e eficiência de encapsulação.

e) Realizar ensaios de liberação in vitro de ICG e DOX sob condições controladas, em pH 5.5 e 7.4.

f) Funcionalizar as nanopartículas com BSA pelo método de adsorção e quantificar a incorporação superficial pelo Método de Lowry.

g)Realizar ensaios celulares como citotoxicidade (MTS) e aplicação fototerápica sinérgica de exposição da nanopartículas a laser infravermelho de 808 nm, com avaliação do efeito na apoptose das células tumorais de melanoma cutâneo (SKMEL-28).

METODOLOGIA

A síntese do polímero foi realizada pelo método de polimerização enzimática por abertura de anel de globalide (Gl). O polímero foi caracterizado em termos de peso molecular e estrutura química através das técnicas convencionais de cromatografia de permeação em gel (GPC) e espectroscopias por ressonância magnética nuclear (RMN) e de infra-vermelho por transformada de Fourier (FT-IR), respectivamente. Propriedades térmicas como entalpia e temperatura de fusão do polímero foram determinadas através de calorimetria diferencial de varredura (DSC). Visando a nanoencapsulação de ICG e DOX, nanopartículas (NPs) brancas de PGl foram produzidas pelo método de dupla emulsificação-evaporação de solvente e, em seguida, NPs carregadas de fármaco foram produzidas pelo mesmo método. As NPs foram então caracterizadas em relação a propriedades como tamanho hidrodinâmico, distribuição de tamanho de partícula e potencial zeta utilizando as técnicas de espalhamento dinâmico de luz (DLS) e a morfologia por meio de microscopia eletrônica de transmissão (TEM). As propriedades térmicas das NPs também foram verificadas por DSC e os grupos funcionais foram confirmados por (FT-IR). Além disso, as nanopartículas foram funcionalizadas com BSA pelo método de adsorção e quantificadas pelo método de Lowry. Por fim, a eficiência de encapsulação foi determinada pela quantificação por espectrofotometria de luz ultravioleta e visível (UV-Vis) e fluorescência, e ensaios de liberação em condições controladas análogas ao meio fisiológico e o microambiente mais ácido das células tumorais (pH=7,4 e 5,5, respectivamente, a 37 ºC) foram conduzidos. Após isso, foi

conduzido ensaios celulares como citotoxicidade (MTS) e aplicação fototerápica sinérgica, com exposição da nanopartículas a laser infravermelho de 808 nm, com avaliação do efeito na apoptose das células tumorais de melanoma cutâneo (SKMEL-28).

RESULTADOS E DISCUSSÃO

Para a síntese das nanopartículas, diferentes parâmetros nas formulações e condições experimentais (tempo e amplitude da etapa de emulsificação, aplicação de banho de gelo) foram avaliadas, dentre as melhores condições avaliadas as NPs produzidas apresentaram menos de 300 nm, PDI < 0,2 (distribuição estreita de tamanho), corroborados pela técnica de microscopia de eletrônica de transmissão, com tamanho submicrométrico e formato esférico. Durante esse processo, observou-se que ao aumentar o tempo de exposição ao ultrassom, o tamanho hidrodinâmico das partículas e o PDI diminuíram gradativamente. O tempo de sonicação na primeira etapa da emulsão dupla não teve impacto significativo no tamanho das partículas, enquanto, durante a segunda emulsão, o maior tempo de sonicação levou a tamanhos de partículas menores. Os resultados sugeriram que com quantidades decrescentes de PGl, o PDI da emulsão também diminuiu, indicando que a viscosidade da emulsão é crucial na homogeneidade da distribuição de tamanho resultante. Após estabelecer as condições de síntese das NPs branco foram estudadas 5 formulações, variando a concentração de ICG e mantendo ou não a presença da DOX. A Eficiência de Encapsulação (EE) foi determinada por análise espectroscopia ultravioleta-visível e fluorescência, do ICG e DOX, respectivamente, não encapsulado no sobrenadanre. As eficiências de encapsulação do ICG em PGL NPs, para as 4 formulações (em triplicata) foram maiores que 83.2 ± 0.4 e de 59.5 ± 2.2 %% para a DOX. Corroborando com a literatura, houve um aumento na taxa de eficiência de encapsulação do ICG quando adicionado ao DOX na formulação de nanopartículas, demonstrando um aumento de cerca de 8,5%. Além disso, as nanopartículas foram funcionalizadas com BSA pela técnica de adsorção. Dentre todas as formulações avaliadas, a maior quantidade de BSA que permaneceu adsorvida na superfície (NPs ICG 5mg + DOX + BSA) foi de 222,34 ± 33,36 μg de BSA por mL de emulsão. Isso significa que a quantidade de BSA por área de nanopartícula é de 6,44 ± 1,20 moléculas de $BSA.nm^{-2}$, o que representa cerca de $1,44x10^{6}$ ± $3,95\ x10^{5}$ moléculas de BSA por nanopartícula. Durante 6 meses foi conduzido um estudo de 6 meses e as NPs demonstraram estabilidade, mantendo seu tamanho hidrodinâmico e pH. Neste estudo, foi investigado os perfis de liberação ICG e DOX nas formulações F2 (5 mg de ICG) e F4 (5 mg de ICG e 1,25 mg de DOX) em diferentes valores de pH (5.5 e 7.4), simulando ambientes biológicos relevantes. Comparando os dois pH, foi perceptível que a presença da DOX na formulação F4 acelerou a liberação de ICG em pH fisiológico e pH ácido, além disso o ICG mostrou uma liberação mais rápida em pH 7.4 quando comparada ao pH 5.5, enquanto a DOX demonstrou um aumento na liberação em pH 5.5 (meio ácido), corroborando com a literatura. Após isso, foi realizado um estudo de citotoxicidade em células de fibroblastos L929, onde ao realizar diluições sequenciais, os resultados da atividade metabólica revelam que concentrações de nanopartículas a partir de 168,7 ng mL^{-1} (para nanopartículas sem funcionalização de BSA) são consideradas não citotóxicas após um período de incubação de 24 horas, a viabilidade celular permaneceu acima de 70%. Para os testes na células de linhagem tumorais em SKMEL-28, foi utilizando um laser 808nm e concluiu-se que o tempo de irradiação desempenhou um papel importante na terapia fotodinâmica/fototérmica. Quando foi aumentado o tempo de irradiação para

10 minutos, foi obtido um bom resultado dentre os outros, com atividade metabólica entre 70% e 80%. Dentre os experimentos não foi perceptível um aumento na temperatura.

CONSIDERAÇÕES FINAIS

Assim, a técnica de dupla emulsão provou ser uma estratégia eficiente para encapsular ICG e DOX, de forma isolada ou conjuntamente carregadas em nanopartículas de PGl. Além disso a funcionalização com BSA mostrou bons resultadosde recobrimento da superfície. Este estudo investigou a liberação de ICG e DOX em diferentes pHs e sua influência na terapia fotodinâmica/fototérmica. A DOX acelerou a liberação de ICG em pHs ácido e fisiológico, e liberou mais rápido em pH ácido, enquanto o ICG liberou mais rapidamente em pH 7.4. Testes de citotoxicidade mostraram que concentrações acima de 168,7 ng mL^{-1} não foram prejudiciais para células L929, e um tempo de irradiação de 10 minutos com laser de 808 nm teve os melhores resultados nas células SKMEL-28. Este estudo enfatiza a importância de ajustar vários parâmetros experimentais e destaca o potencial das nanopartículas na fototerapia.

Palavras-chave: Carreadores de Nanopartículas de Poliéster; Dupla Emulsão, Coencapsulação de Fármacos Hidrofílicos; Fototerapia combinada em linhagem tumoral.

ABSTRACT

Phototherapy has aroused great interest in the scientific community due to its low invasiveness, toxicity, reduced adsorbed effects and lack of drug resistance in the treatment of cancer. Therapies such as Photodynamic and Photothermal involve the administration of a photosensitizer (PS) that, when absorbing light at a specific wavelength, produces a cytotoxic response to the tumor tissue, either by releasing cytotoxic reactive oxygen species or releasing heat. Despite being a non-invasive technique, there are still clinical limitations in its application due to the low accumulation of the photosensitizer (FS) in the tumor tissue and its short blood circulation time, either due to its deactivation by biomolecules or its low solubility in the environment. These limitations can be overcome by encapsulating the photosensitizer, improving its stability and controlling its photoactivity. This work aims to encapsulate the photosensitizing agent Indocyanine Green (ICG) and the chemotherapy drug Doxorubicin Hydrochloride (DOX) in Poly(Globalide) (PGl) nanoparticles (NPs). PGl was synthesized via Ring Opening Enzymatic Polymerization at 65ºC using Novozym 435, immobilized Candida antarctica B lipase (Cal-B), as biocatalyst. Nanoparticles coencapsulating ICG and DOX were prepared by the Double Emulsion by Solvent Evaporation technique and were analyzed for hydrodynamic particle size and polydispersity index (PDI) by Dynamic Light Scattering (DLS). PGl and NPs were characterized regarding their chemical structure, thermal properties and molecular weight. The encapsulation efficiency (EE%) of ICG and DOX was determined by Ultraviolet-visible Spectroscopy and Fluorescence, respectively. Different formulations and experimental conditions were evaluated, and under optimized conditions, NPs with less than 300 nm and PDI < 0.2 were obtained. The TEM images revealed the spherical shape of the nanoparticles and corroborated the submicrometer sizes determined by DLS. The EE% of ICG in PGL NPs, for the 4 formulations (in triplicate) were greater than 83.2 ± 0.4% and 59.5 ± 2.2% for DOX. Thus, the double emulsion technique proved to be an efficient strategy to encapsulate ICG and DOX, singly (ICG) or doubly loaded in PGl NPs. Corroborating the literature, there was an increase in the EE% rate of ICG when added to DOX in the formulation of NPs, with an increase of approximately 8.5%. Furthermore, the nanoparticles were functionalized with Bovine Serum Albumin (BSA) by adsorption and quantified by the Lowry Method, with adsorption of > 58%, resulting in good surface coverage. A 6-month study was conducted and the NPs demonstrated stability, maintaining their hydrodynamic size and pH. The release profiles of ICG and DOX were investigated in formulations F2 (5 mg of ICG) and F4 (5 mg of ICG and 1.25 mg of DOX) at different pH values (5.5 and 7.4), simulating relevant biological environments. It was observed that the presence of DOX accelerated the release of ICG at physiological and acidic pH, with ICG releasing faster at physiological pH, while DOX demonstrated an increase in release at pH 5.5. For the cytotoxicity study on L929 fibroblast cells, concentrations of NPs below 168.7 ng mL-1 (NPs without BSA functionalization) were not cytotoxic after 24 hours of incubation, with cell viability above 70%. In tests on cells of the SKMEL-28 tumor lineage, using an 808 nm laser, the irradiation time was a determining factor in photodynamic/photothermal therapy, irradiation in 10 minutes produced the best results, with metabolic activity between 70% and 80% .

Keywords: Polyester Nanoparticle Carriers; Double Emulsion, Co-encapsulation of Hydrophilic Drugs; Combined phototherapy in tumor lineage.

LIST OF FIGURES

Figure 1. Search for the terms "nanoparticles", "phototherapy", "photothermal", "in vitro" and "polymers". a) Quantitative overview of publications relating polymeric nanoparticles to phototherapy per year, between 2013 and 2023; b) Overview of the subject areas of publications relating polymeric nanoparticles to phototherapy; c) Overview of types of publications relating polymeric nanoparticles to phototherapy... 34
Figure 2. Thematic map (VosViewer) with the most frequent keywords of publications relating polymeric nanoparticles to phototherapy between 2013 and 2023. 35
Figure 3 - Schematic representation of how photodynamic and photothermal therapies works. Phototherapy is used to induce apoptosis in cancer cells by employing light, heat, and radiation. Photosensitizers such as nanoparticles enhance the killing effect by targeting signaling pathways and the immune system. 36
Figure 4 - Thermal damage is caused by heat released during vibrational relaxation of the excited PTT agent, whereas chemical damage is caused by reactive oxygen species (ROS) generated through energy and/or electron transfer from the PDT agent after intersystem crossing of the excited singlet state to a longer-lived triplet state. 38
Figure 5 - Mechanism of contact of the nanomaterial with the synergistic action of PTT (effect of increasing the temperature of the microenvironment) and PDT (effect of releasing reactive oxygen species) 39
Figure 6: Nanostructured Delivery Systems used in the development of nanomedicines to treat cancer by PDT and PTT (nanosphere, nanocapsule, solid lipid nanoparticle, polymer micelle, dendrimer, liposome, gold nanoparticle, and nanoemulsion). 43
Figure 7 - Evolution of essential characteristics for the generation of biomaterials used at the time. 45
Figure 8 - Photothermal mechanism of action with the irradiation of a NIR laser on polymeric nanoparticles causing phototoxicity in cancer cells. 50
Figure 9 - Mechanism of action of the polymeric particle, with the application of the synergistic effect of the combined therapy of PTT and PDT (through the two-photon laser). 51

Figure 10 - Schematic representation of the PLA nanoparticle in the application of combined PDT and PTT therapy with NIR laser in cancer cells..... 53
Figure 11 - Scheme of techniques used for the preparation of polymeric nanoparticles. FSC: Supercritical Fluid; R C/V: Radical Controlled/Alive. 54
Figure 12 - Percentage of times each method was used. 57
Figure 13 – Diagram showing the delivery of specifically active and targeted PS drugs to tumors via receptor-mediated targeting. 60
Figure 14 – Schematic illustration of Ce6-loaded HANPs for combined fluorescent imaging and targeted photodynamic therapy..... 61
Figure 15 - Delivery Mechanism of Nanoparticle-mediated to Cancer Cells and their stimuli-responsive characteristics. 63
Figure 16 - ICG Chemical structure 71
Figure 17 - Structural formula of Doxorubicin hydrochloride. 73
Figure 18 - Schematic representation of globalide e-ROP. 80
Figure 19 – Preparation of PGl nanoparticles. 84
Figure 20 - Preparation of the first W_1/O emulsion of double emulsion technique using an ultrasound device. 85
Figure 21 - Preparation of the second emulsion ($W_1/O/W_2$) of double emulsion technique using an ultrasound device. 86
Figure 22 - Physicochemical and Morphological Characterization through Nanoparticles in Dispersion..... 88
Figure 23 - Physicochemical and Morphological characterization through Lyophilized Nanoparticles 89
Figure 24 – Scheme of sample preparation for quantification of ICG and DOX by the indirect method. 90
Figure 25 – Experimental procedure of ICG and DOX release study. 93
Figure 26 – Activities developed in in vitro studies. 94
Figure 27 - ^{1}H NMR spectrum of PGl and the respective peak attributions to its chemical structure 97
Figure 28 – FTIR spectrum of PGl 98
Figure 29 – Normalized molecular weight distributions GPC of different synthesized samples of PGl. 99

Figure 30 – TG/DTG curve for a PGl sample, carried out at 10 °C min^{-1} under nitrogen atmosphere. 100
Figure 31 - Thermal properties determined by DSC analysis for PGl sample. 101
Figure 32 - Evaluation of the effect of the sonication time of the 2nd emulsion during the preparation of blank PGl NPs. 106
Figure 33 - Hydrodynamic Size Distribution by Intensity of blank PGl NPs 108
Figure 34 – TEM analysis of Formulation F0 (blank NPs). 110
Figure 35 – DSC thermograms of NPs: (A) NPs ICG 1.25mg (F1), (B) NPs ICG 5 mg (F2), (C) NPs ICG 1.25 mg + DOX (F3), and (D) NPs ICG 5 mg + DOX (F4)..... 110
Figure 36 – (A) PGL, ICG, NPS ICG 1.25 mg (F1) and NPS ICG 5 mg (F2) spectra; (B) PGL, ICG, DOX, NPS ICG 1.25 mg + DOX(F3) and NPS ICG 5 mg + DOX (F4) spectra. 111
Figure 37 - Representation of the nanoparticle developed in this study, with the PGl shell, encapsulating ICG and DOX (F3 and F4) and functionalized with BSA. 115
Figure 38 - Hydrodynamic particle size and dispersity during 6 months of storage of blank PGl NPs 117
Figure 39 - Evaluation of the stability of the colloidal PGl dispersion 117
Figure 40 – ICG and DOX release at pH 5.5 and 7.4 A) F2 com 5mg de ICG, B) F4 com 5mg de ICG e 1,25mg de DOX (estudo do ICG) ; C) F4 com 5mg de ICG e 1,25mg de DOX (study of DOX). 118
Figure 41– Cytotoxicity assay in the 10 formulations F0 (Blank NPs), F1 (ICG 1.25mg), F2 (ICG 5mg), F3 (ICG 1.25mg + 1.25mg DOX), F4 (ICG 5mg + 1.25mg DOX), without or with addition of - BSA (Bovine Serum Albumin). 121
Figure 42 – Metabolic activity of SK-MEL-28 cells after 24 hours of laser phototherapy under different conditions in the presence of drug: C – Control cells, without nanoparticles; FO – Cells with white nanoparticles (No Drug); F2 – Cells with NPs 5mg of ICG; F4 – cells with NPs with 5mg of ICG + 1.25mg of DOX..... 123
Figure 43 – Metabolic activity of SK-MEL-28 cells after 48h of laser phototherapy under different conditions in the presence of drug: C – control cells, without nanoparticle; FO – cells with white nanoparticles (without drug); F2 – cells with NPs 5mg of ICG; F4 – cells with NPs with 5mg of ICG + 1.25mg of DOX..... 124
Figure 44 – Metabolic activity of SK-MEL-28 cells after 24h of laser phototherapy under different conditions in the presence of drug: C – Control cells, without Nanoparticles; FO

– Cells with Blank Nanoparticles (without drug); F2 – Cells with NPs 5mg of ICG; F4 – cells with NPs with 5mg of ICG + 1.25mg of DOX 125

LIST OF TABLES

Table 1 - Synthetic and natural polymers, their main source and properties, which have been applied in Phototherapy. 48
Table 2 - Advantages and limitations of main techniques used for drug encapsulation. 54
Table 3 - Studies that have been encapsulating ICG in polymeric nanoparticles by Double Emulsion with Solvent Evaporation 72
Table 4 – Formulations and experimental conditions evaluated for the preparation of the PGl NPs by the double emulsion solvent evaporation approach. 82
Table 5 - Formulations of PGl NPs 87
Table 6 - Molecular weight averages of synthesized polymers. 98
Table 7 – Formulations and experimental conditions evaluated for the preparation of the PGl NPs by the double emulsion solvent evaporation approach and their respective hydrodynamic size and PDI results. 103
Table 8 - Hydrodynamic particle size and polydispersity indices of the five formulations. 108
Table 9 - Encapsulation Efficiency (EE%) of ICG and DOX 113
Table 10 - Amount of BSA adsorbed to PGl NPs obtained by performing the Lowry protein. 115
Table 11 – Cumulative Release (%) of ICG over 7 days (168h) at pH 5.5 and pH 7.4 119
Table 12 - Cumulative Release (%) of DOX in the period of 8h, 24h and 48h at pH 5.5 and pH 7.4 119

LIST OF SCHEMES

Scheme 1 - Flowchart of the developed steps in this work 78

LIST OF ABBREVIATIONS AND SYMBOLS

^{1}H-NMR - Proton Nuclear Magnetic Resonance

$^{1}O_2$ - Singlet Oxygen

A - Unit of enzymatic activity (U g^{-1})

BSA - Bovine Serum Albumin

$CDCl_3$ - Deuterated Chloroform

Đ – Molecular weight Dispersity

DCM - Dichloromethane

DCM - Dichloromethane

DLS - Dynamic Light Scattering

DMSO - Dimethyl sulfoxide

DOX - Doxorubicin hydrochloride

Dp - Particle diameter (nm)

DSC - Differential Scanning Calorimetry

DSC - Differential Scanning Calorimetry

EDTA - Ethylenediaminetetraacetic Acid

G - Centrifugal Force

DMEM - Dulbecco's Modified Eagle's medium

EE - Encapsulation Efficiency (%)

e-ROP - Enzymatic ring-opening polymerization

F0 – Blank Nanoparticles

F1 - ICG 1.25mg

F2 - ICG 5mg

F3 - ICG 1.25mg + 1.25mg DOX

F4 - ICG 5mg + 1.25mg DOX

FDA - Food and Drug Administration

FPS - Fetal Bovine Serum

FT-IR - Fourier Transform Infrared

Gl – Globalide

GPC - Gel Permeation Chromatography

GPC - Gel Permeation Chromatography

HLB – Hydrophile/lipophile Balance

ICG – Indocyanine Green

LED - Light-Emiting Diode

Min - Minute

mL - Milliliter

M_n - Number Average Molecular Weight (g mol^{-1})

Mol% - Mol percentage

MTS – Metabolic Activity

M_w - Weight Average Molecular Weight (g mol^{-1})

Ng/mL – Nanograms per milliliter

NIR - Near Infrared

Nm – Nanometer

NMR - Nuclear Magnetic Resonance

NPs – Nanoparticles

NZ 435 - Novozym 435

O/W - Oil-in-water

OH – Hydroxyl

PBS - Phosphate buffered saline

PDI – Particle size polidispersion index

PDT - Photodynamic Therapy

PGl - Poly(globalide)

PS – Photosensitizer

PTT - Photothermal Therapy

PVA - Poly(Vinyl alcohol)

ROP - Ring-opening polymerization

ROS - Reactive Oxygen Species

SEM - Scanning Electron Microscopy

SKMEL-28 – Cutaneous melanoma cell line

T - Temperature (° C)

TEM - Transmission Electron Microscopy

TGA – Thermogravimetric analysis

THF - Tetrahydrofuran

T_m - Melting temperature (°C)

SUMMARY

1.CHAPTER 1 – INTRODUCTION……24
1.1 OBJECTIVES....26
1.1.1 GENERAL OBJECTIVE....26
1.1.2 SPECIFIC OBJECTIVES....26
2. CHAPTER 2 - LITERATURE REVIEW....32
2.1 INTRODUCTION....32
2.2 SCIENTOMETRICS ANALYSIS....33
2.3 PHOTOTHERAPY MEDIATED BY NANOMATERIALS....35
2.3.1. COMBINATION OF PHOTODYNAMIC THERAPY (PDT) WITH PHOTOTHERMAL THERAPY (PTT)....37
2.3.2 CHOICE OF LIGHT SOURCE....39
2.3.2.1 LASER LIGHT SOURCES....40
2.3.2.2 NON-LASER LIGHT SOURCES....41
2.4 POLYMERIC NANOPARTICLES IN PTT AND PDT....42
2.4.1 POLYMERIC NANOPARTICLES IN PDT/PTT: EVOLUTION OF PHOTOSENSITIZERS....44
2.4.2 POLYMERIC NANOPARTICULES IN PDT/PTT: POLYMER MATRICES……......47
2.4.3 POLYMERIC NANOPARTICLES IN PDT/PTT: ENCAPSULATION TECHNIQUES OF PHOTOSENSITIZERS....53
2.4.4. POLYMERIC NANOPARTICLES IN PDT/PTT: FUNCTIONALIZATION AND STIMULI-RESPONSIVE CHARACTERISTICS....53
2.4.4.1 FUNCTIONALIZED NANOPARTICLES....53
2.4.4.2 STIMULLI- RESPONSIVE CHARACTERISTICS....62
2.5 STATE OF ART APPLIED TO THE THESIS THEME…….…….65
2.5.1 BIODEGRADABLE POLYMERS: ALIPHATIC POLYESTERS……..….66
2.5.2 POLYMERS FROM MACROLACTONES…….….67
2.5.3 DOUBLE EMULSION WITH SOLVENT EVAPORATION METHOD……69
2.5.4 INDOCIANIN GREEN AND DOXORUBICIN DRUGS……..…70
2.5.5.SURFACE FUNCTIONALIZATION WITH BSA……...74

3. CHAPTER 03: ENCAPSULATION OF PHOTOSENSITIZER AND CHEMOTHERAPY AGENT IN POLY(GLOBALIDE) NANOPARTICLES FUNCTIONALIZED WITH BSA 76
3.1 INTRODUCTION **76**
3.2 MATERIAL AND METHODS **78**
3.2.1 MATERIALS 79
3.2.2 METHODS 79
3.2.2.1 SYNTHESIS OF POLYGLOBALIDE 79
3.2.2.2. CHARACTERIZATION OF THE POLYMER……80
3.3 PREPARATION OF POLYMERIC NANOPARTICLES 81
3.3.1 REFERENCE FORMULATION……81
3.3.2 PREPARATION OF BLANK NPS, ICG@NPS AND ICG~DOX@NPS BY THE DOUBLE EMULSION METHOD……84
3.3.3PHYSICAL-CHEMICAL AND MORPHOLOGICAL CHARACTERIZATION OF BLANK NANOPARTICLES AND ENCAPSULATING ICG OR ICG + DOX……87
3.4 DRUG ENCAPSULATION EFFICIENCY 90
3.5 FUNCTIONALIZATION OF PGL NPS, ICG@PGL NPS, AND ICG-DOX@PGL NPS WITH BOVINE SERUM ALBUMIN (BSA)……91
3.6 COLLOIDAL STABILITY OF NPS 92
3.7 DRUG RELEASE 92
3.8 IN VITRO STUDIES 93
3.8.1 METHODS: IN VITRO STUDIES 93
3.8.1.1 IN VITRO CYTOTOXICITY ASSAY 94
3.8.1.1.1 SAMPLE PREPARATION……94
3.8.1.1.2 CELL PREPARARION……..94
3.8.1.2. MTS ASSAY (METABOLIC ACTIVITY)……95
3.8.1.3 PHOTODYNAMIC AND PHOTOTHERMAL ACTIVITY ON MELANOMA CELLS: PHOTOXICITY STUDIES……...95
3.8.1.3.1 STATISTICAL ANALYSIS……..95
4. RESULTS AND DISCUSSION 96
4.1 SYNTHESIS OF POLY(GLOBALIDE) 96
4.1.1 CHARACTERIZATION OF THE POLYMER 97

4.2 PREPARATION OF POLYMERIC NANOPARTICLES 101
4.2.1REFERENCE FORMULATION……...……..…….101
4.2.2 PREPARATION OF BLANK NPS, ICG@NPS AND ICG~DOX@NPS BY THE DOUBLE EMULSION METHOD……107
4.2.2.1PHYSICAL-CHEMICAL AND MORPHOLOGICAL CHARACTERIZATION OF BLANK NANOPARTICLES AND ENCAPSULATING ICG OR ICG + DOX……..……107
4.3 DRUG ENCAPSULATION EFFICIENCY.....112
4.4 FUNCTIONALIZATION OF PGL NPS, ICG@PGL NPS, AND ICG-DOX@PGL NPS WITH BOVINE SERUM ALBUMIN (BSA) 114
4.5 COLLOIDAL STABILITY OF NPS 116
4.6 DRUG RELEASE 118
4.7 IN VITRO STUDIES 120
4.7.1 IN VITRO CYTOTOXICITY ASSAY.....120
4.7.1.1.MTS ASSAY (METABOLIC ACTIVITY)……..……...…120
4.7.2 PHOTODYNAMIC AND PHOTOTHERMAL ACTIVITY ON MELANOMA CELLS: PHOTOXICITY STUDIES…….……...122
5. CONCLUSIONS……...……...…127
6. REFERENCES…….……129

1. CHAPTER 1 – INTRODUCTION

Currently, conventional procedures for the treatment of cancer consist of surgery, radiotherapy, chemotherapy, hormone therapy, and immunotherapy (BOONMAN *et al.*, 2022). Although in recent years some of these traditional techniques employed have undergone substantial development, allowing an increase in the life span of cancer patients, patients treated with chemotherapy and radiotherapy may have serious adverse effects such as alopecia (hair loss), gastrointestinal disorders (nausea, vomiting, and diarrhea) and adynamia (physical prostration), making the treatment very painful for patients. In addition, surgical procedures for tumor removal can result in mutilation and severe physiological changes, such as damage to the aerodigestive tract and the excretory system and damage to psychological conditions (VARDY *et al.*, 2022).

Therefore, it is necessary to search for new therapeutic modalities capable of promoting a better treatment for this disease, with high efficiency and low toxicity. In this sense, phototherapy has aroused great interest in the scientific community due to its low invasiveness, insignificant toxicity, reduced adverse effects, and absence of drug resistance (AMARAL *et al.*, 2022). Currently, Photodynamic Therapy (PDT) and Photothermal Therapy (PTT) are techniques widely studied in the treatment of cancer, since they are local, minimally invasive therapies that do not require surgery, leaving the patient less debilitated and giving him a better ability to recover from illness (PINTO; POCARD, 2018).

Despite the continuous development of photodynamic therapy for the treatment of cancer, the advance of this therapy in clinical applications is still held back by the low accumulation of the photosensitizer (PS) in the tumor tissue and by its short blood circulation time, either due to its deactivation by biomolecules or due to its low solubility in the medium (CORREIA *et al.*, 2021).

The encapsulation of photosensitizers (PS) in nanostructured particles appears as an efficient tool to overcome the limitations associated with these therapeutic agents. These nanostructures can decrease the time required for PS to accumulate in the tumor, increase their power to accumulate in strategic locations within cancer cells, such as mitochondria and lysosomes (SARBADHIKARY *et al.*, 2021), and present greater penetration and retention in the tumor tissue, taking advantage of the irregular vasculature and the larger pores present in this type of tissue, compared to normal tissues (NAKAMURA *et al.*, 2016). In addition to improving tumor targeting, nanoparticles (NPs) enhance the therapeutic efficiency of PS by

protecting them from deactivation, preventing aggregation, and allowing control of their phototoxic activity (HUANG *et al.*, 2012). This protection provided by the NPs is extremely important to ensure that the PS maintain their therapeutic capacity until they reach the desired target, that is, the tumor cells, avoiding losses along the way (BERTRAND *et al.*, 2014).

The utilization of Indocyanine Green (ICG) and Doxorubicin (DOX) in photothermal and photodynamic therapy holds significant potential for advancing cancer treatment (CHEN *et al.*, 2021; HUNG *et al.*, 2016; LONG *et al.*, 2020; MANCHANDA *et al.*, 2010; SHEN *et al.*, 2019). ICG is a photosensitizer widely used in photodynamic and photothermal therapy, which, when activated by light of a specific wavelength (808 nm), generates reactive oxygen species capable of inducing the selective death of tumor cells (CHEN *et al.*, 2013). Doxorubicin, on the other hand, is a potent chemotherapeutic with the ability to insert itself into the DNA of cancer cells, inhibiting its replication and promoting cell apoptosis (KCIUK *et al.*, 2023). When encapsulated in polymeric nanoparticles, these therapeutic agents have a series of benefits that allow a controlled and targeted release of drugs, increasing their effectiveness and reducing toxicity to surrounding healthy tissues (PATRA *et al.*, 2018; XIAO *et al.*, 2022). The functionalization of the nanoparticle with Bovine Serum Albumin (BSA) is a promising approach to further improve this therapeutic strategy (MUNDEKKAD; CHO, 2022) since BSA is a protein that has a high affinity for receptors expressed in cancer cells, which allows a greater accumulation of nanoparticles in tumor regions, increasing the selectivity and effectiveness of the treatment (KARIMI *et al.*, 2016a).

These polymeric nanoparticles containing the therapeutic agents are then able to induce apoptosis in tumor cells more efficiently and specifically (MUNDEKKAD; CHO, 2022). This represents a significant advance in the search for more effective and less toxic cancer treatments. The search for innovative therapeutic approaches that can improve clinical outcomes and patient's quality of life is a priority for the scientific community. In this context, the immediatism and aim of this study is to prepare poly(globalide) nanoparticles (PGl NPs), encapsulating ICG and DOX followed by functionalization of the surface with BSA, for combined phototherapeutic application. This approach aims to combine the benefits of photothermal and photodynamic therapy with the effectiveness of drugs. By achieving this goal, this work can contribute to the evolution of cancer treatments and benefit scientific research on the subject.

This topic of polymeric nanoparticles encapsulating drugs for phototherapeutic application has been growing mainly in the last 5 years, with the publication of articles in

different fields in the area. Within this search, we can consider that until now, PGl has already been studied as a polymeric matrix of Nanoparticles and that it has already been synthesized by Enzymatic Ring Opening Polymerization (E-rop), including by work from the group itself. Furthermore, the coencapsulation of ICG and DOX has already been applied in polymeric nanoparticles and has shown good results including combined phototherapy, which has demonstrated greater efficacy and reduced side effects and toxicity. The novelty of the study is because PGl has not yet been applied in the co-encapsulation of medicines such as ICG and DOX, nor by double emulsion or any other method. It has potential biomedical applications, but has not yet been applied to phototherapy. Furthermore, PGl NPs have not yet been functionalized with BSA by adsorption, although it is a protein widely studied in the literature.

1.1 OBJECTIVES

1.1.1 GENERAL OBJECTIVE

To Prepare polyester (poly(globalide)) nanoparticles and encapsulate the drugs Indocyanine Green (ICG) and Doxorubicin hydrochloride (DOX), followed by functionalization with Bovine Serum Albumin (BSA) for combined application in photodynamic and photothermal therapy in cutaneous melanoma cell lines.

1.1.2 SPECIFIC OBJECTIVES

a)To obtain Poly(globalide) via enzymatic ring opening polymerization (eROP) mechanism with immobilized lipase Novozym 435 and determine its chemical structure, molecular weight (Mn), and dispersity (Đ).

b)To evaluate the effect of formulation and operating conditions on the characteristics of Poly(Globalide) polyester nanoparticles.

c)To synthesize PGl NPs by double emulsion-solvent evaporation technique and to characterize their thermal properties, stability, particle hydrodynamic size distributions, zeta potential, presence of functional groups, and morphology.

d)To perform encapsulation tests in different formulations with the drugs ICG and DOX, by the double emulsion technique with solvent evaporation and characterize their size and morphology, stability, thermal properties, and encapsulation efficiency.

e) Carry out in vitro release assays of ICG and DOX under controlled conditions.

f) To functionalize nanoparticles with BSA by adsorption method and quantify the conjugation.

g) Carry out cellular assays such as cytotoxicity, MTS and synergistic phototherapeutic application, with exposure of nanoparticles to an infrared laser of 808 nm, followed by evaluation of the effect on apoptosis of tumor cells (SKMEL-28).

CONCEPTUAL DIAGRAM

"COENCAPSULATION OF DOXORUBICIN AND INDOCYANINE GREEN IN FUNCTIONALIZED POLYGLOBALIDE NANOPARTICLES"

What?
Enzymatic polymerization of globalide (Gl) followed by preparation of nanoparticles encapsulating ICG and DOX by double emulsion with solvent evaporation, after functionalization with BSA by adsorption for application in combined phototherapy.

Why?	
I.	PDT and PTT are local, minimally invasive therapies that do not require surgery, leaving the patient less debilitated and giving him a better ability to recover from the disease.
II.	The synergistic or combined effect of the therapies enhances the effectiveness of the treatment and reduces the cost and time of the treatment because both require only one light source, so the photosensitizer and the photothermal agent are in a single nanostructure.
III.	Biocompatible and bioresorbable polyesters present interesting properties as alternative materials for biomedical applications.
IV.	The double emulsion by solvent evaporation is a simple method of producing nanoparticles and encapsulating a wide range of hydrophilic compounds.
V.	The coencapsulation of indocyanine green (ICG) and doxorubicin hydrochloride in polyester nanoparticles aims to take advantage of both compounds synergistically, improving their therapeutic efficacy and decreasing the adverse effects associated with the use of high dosages, as it allows the use of smaller doses of each therapeutic agent. In addition to having photothermal capacity as well as the ability to generate singlet oxygen.
VI.	Bovine serum albumin (BSA) has been used for interaction studies, as it has already been extensively characterized and has a role in transporting and extending the shelf life of the photosensitizer, for its ability to protect from degradation and stabilize these nanoparticles containing them.

State of the art	
I.	Enzymatic ring-opening polymerization (e-ROP) has been utilized to synthesize polyesters using various monomers, including globalide (Gl), with favorable outcomes.
II.	There are a few investigations that studied PGl as a polymer matrix for nanoparticles.
III.	The encapsulation of ICG and DOX has already been widely studied in polymeric nanoparticles and its application in phototherapy, even this double encapsulation has already obtained favorable results.
IV.	BSA is a widely studied protein commonly used as a model protein due to its well-characterized properties. It serves as a useful tool to investigate protein-nanoparticle interactions, stability, and drug delivery applications.
V.	Combined phototherapy has shown good results in the literature, with increased efficacy and reduced adverse effects and toxicity.
VI.	PGl has not yet been applied in the encapsulation of ICG and DOX drugs, nor by double emulsion or any other method. Furthermore, even though it has potential biomedical applications, it has not yet been applied to phototherapy.

Hypotheses	
I.	PGl nanoparticles obtained by double emulsion sizes less than 300 nm, narrow size distributions below 0.2, spherical in shape, as well as have thermal, functional, and morphological properties for biomedical applications.
II.	ICG and DOX can be efficiently encapsulated in PGl nanoparticles.
III.	ICG and DOX have a pH-sensitive and controlled release
IV.	BSA achieves good adsorption on the surface of PGl nanoparticles by the adsorption method.
V.	Exposure of cutaneous melanoma cell lineage to PGL nanoparticles, in combination with ICG and/or DOX, induces cellular apoptosis, thereby potentially facilitating phototherapeutic applications.

Which steps?	
I.	Synthesis of PGl via e-ROP.
II.	Characterization of PGl. Nanoparticles preparation followed by ICG and DOX encapsulation by double emulsion-solvent evaporation technique and characterization.
III.	Release study in vitro of ICG and DOX.
IV.	Functionalization of NPs with BSA by adsorption and quantification by the Lowry method.
V.	Cytotoxicity and metabolic activity assay
VI.	808 nm laser application of phototherapy in cutaneous melanoma cell lines (SKMEL-28) with controlled irradiation time.

Results	
I.	To obtain stable and narrow-size distributed PGl NPs.
II.	To achieve high drug loading in ICG and DOX encapsulation with the obtained polymers.
III.	To comprehend the effect of ICG and DOX release behavior from PGl NPs.
IV.	To obtain high incorporation of BSA on the surface of PGl nanoparticles by the adsorption method.
V.	The 808 nm laser used for photodynamic and photothermal therapy is viable and efficient.
VI.	Achieve that photothermal and photodynamic treatment with 808 nm laser exposure causes tumor cell death.

GRAPHICAL ABSTRACT

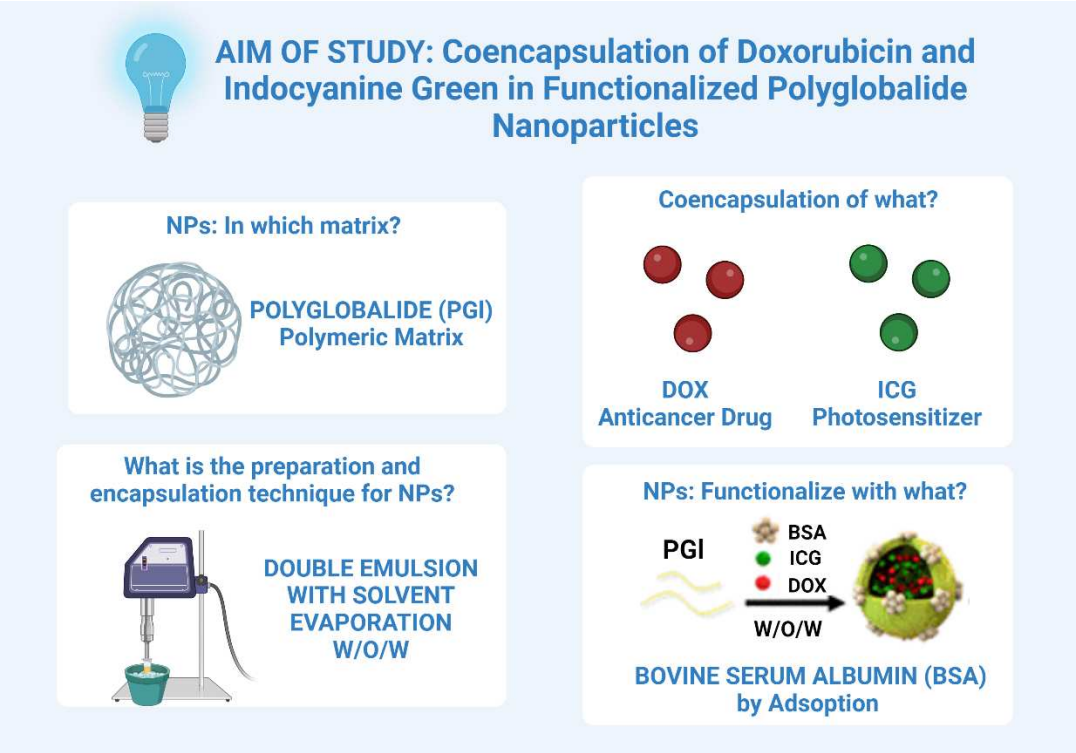

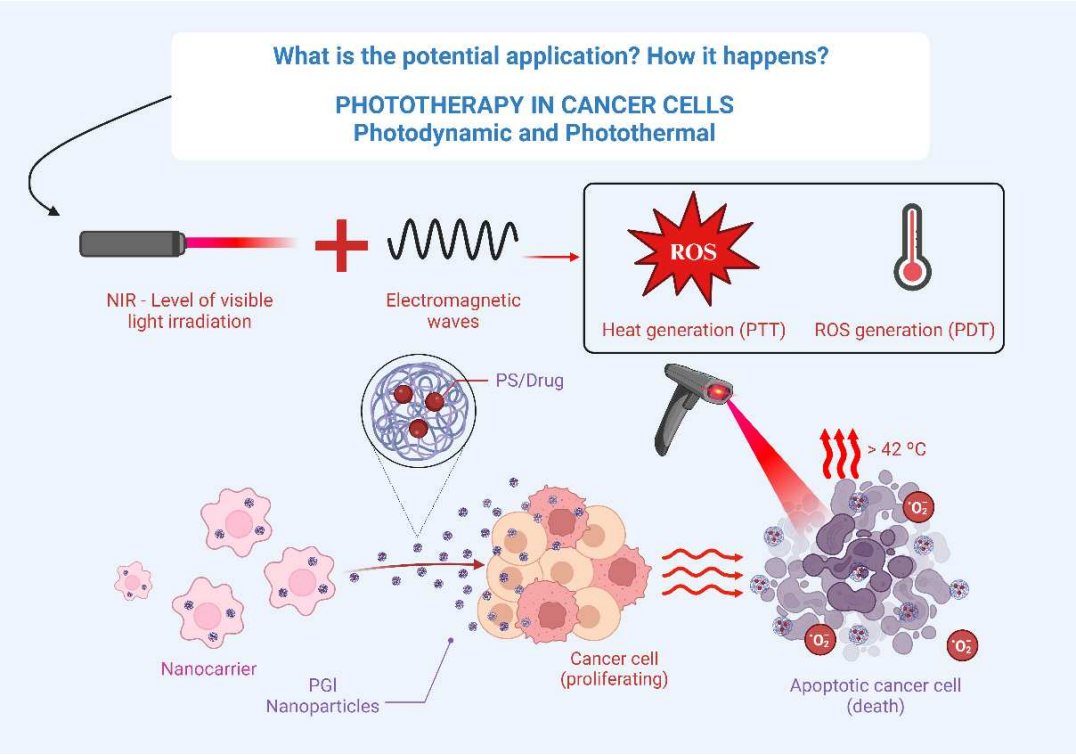

CHAPTER 2 - LITERATURE REVIEW

2.1 INTRODUCTION

Cancer is the main public health problem in the world and is already among the four main causes of premature death (before the age of 70) in most countries. The incidence and mortality from cancer have been increasing worldwide, partly due to aging, population growth, as well as changes in the distribution and prevalence of risk factors, especially those associated with socioeconomic development (MINISTÉRIO DA SAÚDE INSTITUTO NACIONAL DE CÂNCER, 2023).

About one million new cases of invasive cancer are diagnosed annually, excluding superficial skin cancers. According to the National Cancer Institute, Brazil registered 625,000 new cases of cancer each year in the 2020/2022 period (MINISTÉRIO DA SAÚDE INSTITUTO NACIONAL DE CÂNCER, 2023). According to the Real Instituto de Oncologia, in 2021, the number of Brazilians with various types of cancer reached 522,212 cases, of these, 260,000 lost their lives.

In Brazil, as in many other parts of the world, some procedures have been adopted with relative success in the fight against cancer. Currently, conventional procedures for the treatment of cancer consist of surgery, radiotherapy, chemotherapy, hormone therapy, and immunotherapy (BOONMAN *et al.*, 2022). Although in recent years some of these traditional techniques employed have undergone substantial development, allowing an increase in the life span of cancer patients, patients treated with chemotherapy and radiotherapy may have serious adverse effects such as alopecia (hair loss), gastrointestinal disorders (nausea vomiting, and diarrhea) and adynamia (physical prostration), making the treatment very painful (VARDY *et al.*, 2022). In addition, surgical procedures for tumor removal can result in mutilation and severe physiological changes, such as damage to the aerodigestive tract and the excretory system.

Therefore, it is necessary to search for new therapeutic modalities capable of promoting a better treatment with high efficiency and low toxicity. In this sense, phototherapy has aroused great interest in the scientific community due to its low invasiveness, insignificant toxicity, reduced adverse effects, and absence of drug resistance (AMARAL *et al.*, 2022).

Photodynamic Therapy (PDT) and Photothermal Therapy (PTT) are the most used and studied phototherapy modalities in the treatment of cancer, since they are local, minimally invasive therapies that do not require surgery, leaving the patient less debilitated and give the

same better ability to recover from the disease (PINTO; POCARD, 2018), thus becoming promising due to its specificity and cytotoxic potential (AMARAL *et al.*, 2022).

However, for high phototherapeutic efficiency, there is a need for excellent photosensitizing agents. Despite the continuous development of photodynamic therapy for the treatment of cancer, the progress of this therapy in clinical applications is still held back by the low accumulation of the photosensitizer (PS) in the tumor tissue or by its short blood circulation time, either by its deactivation by biomolecules or by its low solubility in the medium (CORREIA *et al.*, 2021).

To overcome these limitations, the encapsulation of photosensitizers has emerged as a useful tool, since in addition to reducing the time that PS takes to accumulate in the tumor, it also increases the accumulation in strategic points of the cancer cell, they also present greater penetration and retention in the tumor tissue, since this tissue has irregular vasculature and larger pores than the pores of normal tissues (SARBADHIKARY *et al.*, 2021).

Nanoscale drug delivery systems have shown their excellence in diagnosis, drug delivery, and therapy, specifically in cancer treatment, mainly in contrast to conventional drug delivery approaches, nanostructures have shown great potential in increasing the bioavailability of the drugs, prolonged circulation time, controlled drug release, and tumor targeting (YE *et al.*, 2019). In addition to these primary functions, new materials and emerging technologies may offer additional functions to nanocarriers for cancer diagnosis and treatment (TANG *et al.*, 2017).

Thus, the importance of polymeric nanoparticles applied as controlled drug delivery systems becomes clear, which has been corroborated by scientific publications in the area. These polymeric nanoparticles offer an attractive structure for the controlled delivery of photosensitizers and will be new biodegradable nanoplatforms that can be used without showing cross-resistance with other cancer treatments and therefore can be a component of combination treatments (BEGINES *et al.*, 2020).

1.1 SCIENTOMETRICS ANALYSIS

This literature review used a systematic methodology. First, the articles were selected from Scopus (Elsevier's abstracts and citations database), with the support of the bibliometric mapping software (VOSviewer) (VAN ECK; WALTMAN, 2014).

The search for the terms "nanoparticles", "phototherapy", "photothermal", "*in vitro*" and "polymers" in the period from 2013 to 2023 resulted in 282 documents. Publications were

classified into articles and reviews, as shown in Figure 1. Publications about phototherapy in medicine have been published since 1900, however, in the last 5 years, there has been a greater interest in evaluating polymeric nanoparticles applied to phototherapy, which have been successfully used in several tumor types.

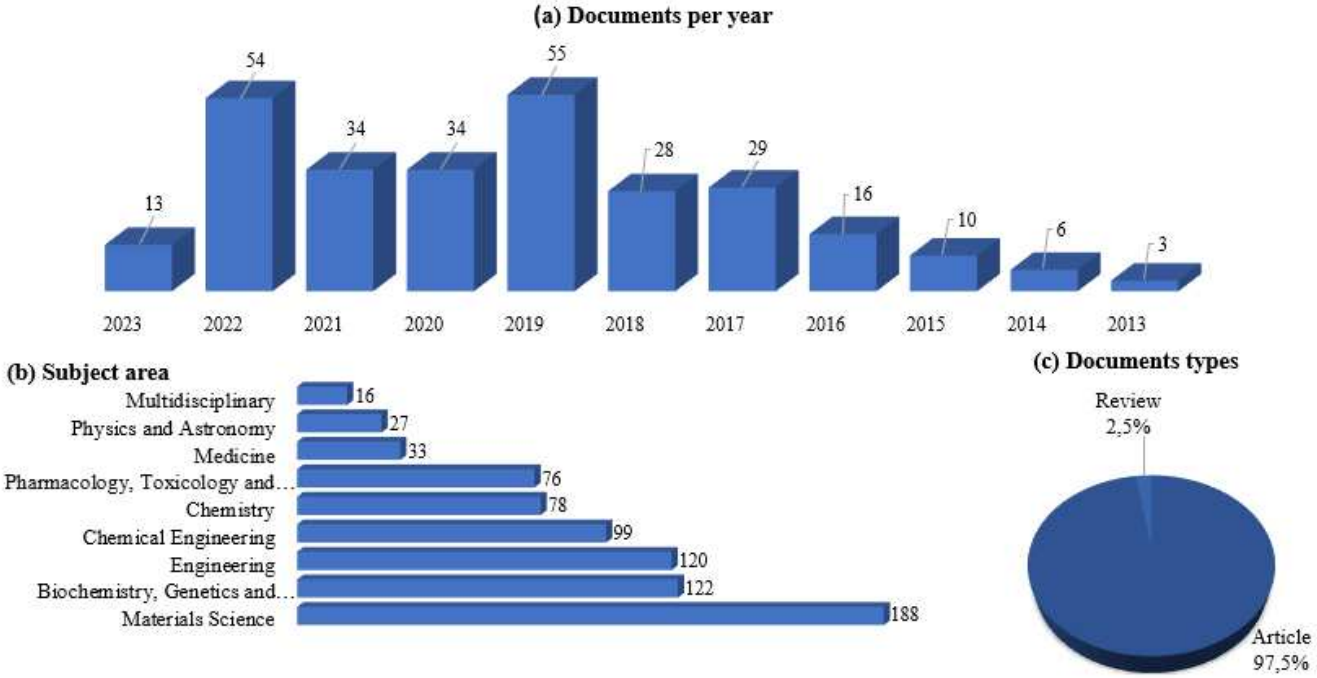

Figure 1. Search for the terms "nanoparticles", "phototherapy", "photothermal", "in vitro" and "polymers". a) Quantitative overview of publications relating polymeric nanoparticles to phototherapy per year, between 2013 and 2023; b) Overview of the subject areas of publications relating polymeric nanoparticles to phototherapy; c) Overview of types of publications relating polymeric nanoparticles to phototherapy.

Out of the documents found, more than 70% are concentrated in the broad field of engineering, including materials science, biochemistry, and chemical engineering. The other 30% of publications are concentrated on topics in the health area, such as medicine, genetics, molecular biology, pharmacology, toxicology, immunology, and microbiology.

The thematic map, Figure 2, shows the most frequent keywords cited by the authors, and theranostic nanomedicine, chemistry, cell death, synthesis, phototherapy, and polymer stand out as the most cited.

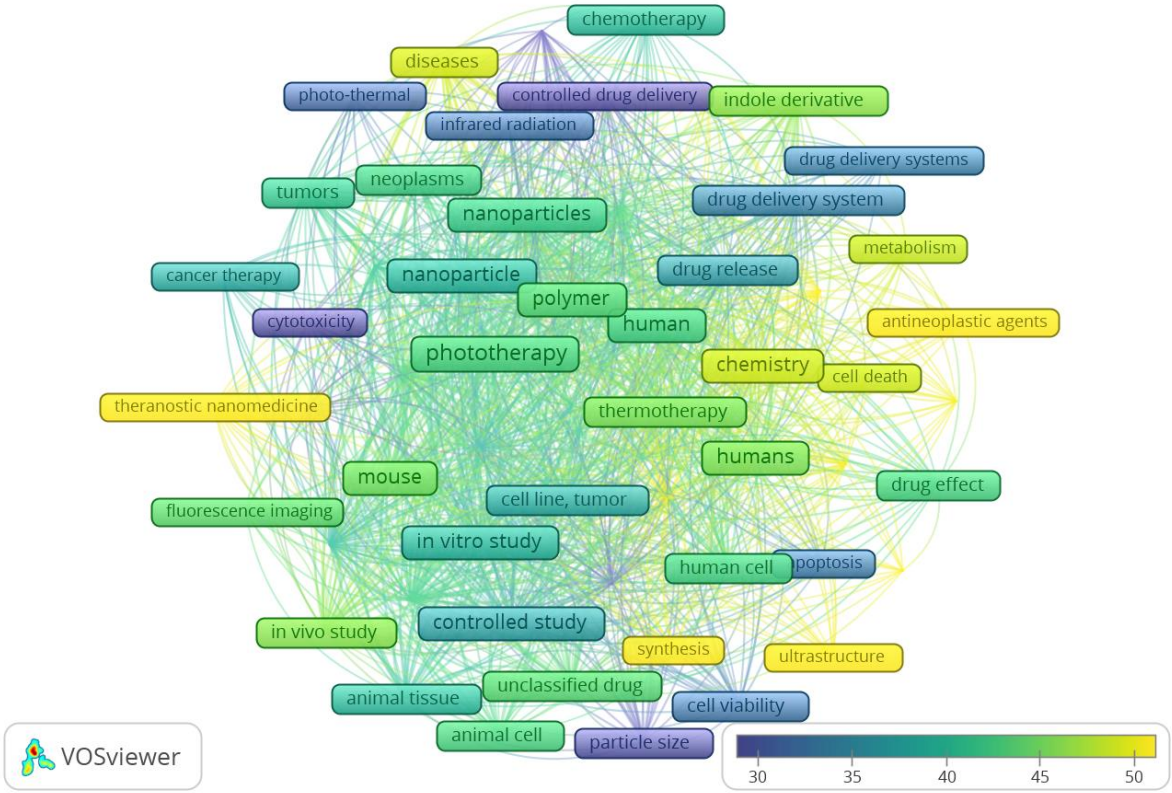

Figure 2. Thematic map (VosViewer) with the most frequent keywords of publications relating polymeric nanoparticles to phototherapy between 2013 and 2023.

To improve the comparison between the studies was specifically evaluated the encapsulation applying polymeric nanoparticles for phototherapy.

1.2 PHOTOTHERAPY MEDIATED BY NANOMATERIALS

Nanomaterials have revolutionized the field of biomedical applications, including phototherapy (MUNDEKKAD; CHO, 2022). Phototherapy is a non-invasive treatment option for cancer and other diseases that utilizes light-absorbing agents to generate cytotoxic effects (SHANG *et al.*, 2021). Nanomaterials have unique properties that make them ideal candidates for phototherapy applications (PIVETTA *et al.*, 2021).

One of the most promising applications of nanomaterials for phototherapy is photothermal therapy (PTT). PTT utilizes nanoparticles that absorb light and convert it into heat, which leads to the thermal ablation of cancer cells (Figure 3). The mechanism of PTT is

based on the photothermal effect, which is the ability of certain materials to absorb light and convert it into heat (CHEN *et al.*, 2022). Nanoparticles such as gold nanorods, carbon nanotubes, and graphene oxide have been extensively studied for PTT applications (due to their strong absorption in the near-infrared (NIR) region, which can penetrate deep into tissues without damaging healthy tissue (BAO *et al.*, 2016; HAN; CHOI, 2021).

Another approach to phototherapy is photodynamic therapy (PDT), which utilizes photosensitizers that generate reactive oxygen species (ROS) upon light activation (LIN *et al.*, 2021). ROS can damage cancer cells by inducing apoptosis or necrosis (ZHOU *et al.*, 2016) (Figure 3). Despite the growing popularity of PDT in the treatment of various types of cancer, such as cutaneous carcinoma, oropharyngeal cancer, and esophageal cancer, this treatment still has some shortcomings related to the low tissue penetration of the laser and the toxic effect of photosensitizers (PATEL; PRABHU, 2022).

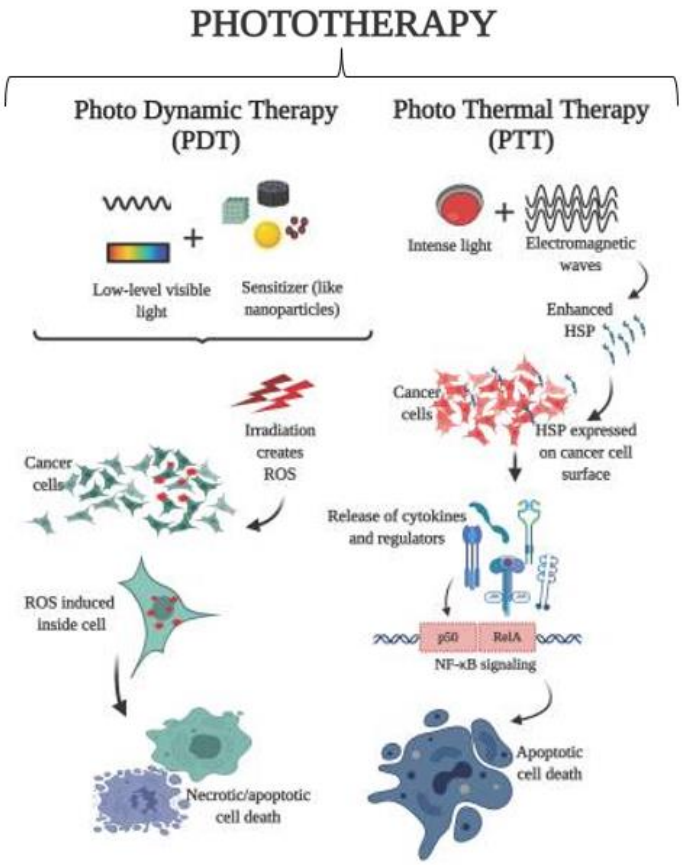

Figure 3 - Schematic representation of how photodynamic and photothermal therapies works. Phototherapy is used to induce apoptosis in cancer cells by employing light, heat, and radiation. Photosensitizers such as nanoparticles enhance the killing effect by targeting signaling pathways and the immune system. Source: (MUNDEKKAD; CHO, 2022)

Nanoparticles have been used to enhance the efficacy of PDT by improving the delivery and retention of photosensitizers in tumor tissues (CHEN *et al.*, 2022; KRUGER; ABRAHAMSE, 2018; LEE *et al.*, 2022; ZHAO *et al.*, 2021). For example, nanoparticles such as liposomes, silica nanoparticles, and polymer nanoparticles have been used to encapsulate photosensitizers and improve their targeting and retention in tumors (LEE *et al.*, 2022).

Nanoparticles have also been used as imaging agents in phototherapy applications. Imaging is an important component of phototherapy as it enables real-time monitoring of the treatment response (CHITGUPI *et al.*, 2017; LI *et al.*, 2023).. Nanoparticles such as quantum dots, gold nanoparticles, and up-conversion nanoparticles have been used as imaging agents due to their unique optical properties, such as fluorescence and luminescence (GERELKHUU *et al.*, 2022; LI *et al.*, 2020; LIANG *et al.*, 2020; RYVOLOVA *et al.*, 2012).

Despite the promising potential of nanomaterials for phototherapy applications, there are still challenges that need to be addressed. One of the major challenges is the potential toxicity of nanomaterials since nanoparticles can accumulate in organs and tissues, leading to cytotoxic effects. Therefore, optimizing the size, shape, and surface chemistry of nanoparticles is important to minimize toxicity and improve their biocompatibility (YUSUF *et al.*, 2023).

In conclusion, nanomaterials have shown great potential in the field of phototherapy for biomedical applications. The unique properties of nanoparticles, such as their strong light absorption, targeting ability, and imaging capabilities, make them ideal candidates for phototherapy applications. However, the challenges associated with toxicity and biocompatibility need to be addressed through further research and development. Nonetheless, the potential of nanomaterials for phototherapy applications continues to drive innovation in the field of biomedical research.

2.3.1. COMBINATION OF PHOTODYNAMIC THERAPY (PDT) WITH PHOTOTHERMAL THERAPY (PTT)

The combination of PTT and PDT can work synergistically to overcome the limitations of each method and improve treatment efficacy. The development of unique photosensitive agents capable of inducing PDT and PTT is therefore extremely advantageous and highly desired (BILICI *et al.*, 2021), explicit in Figure 4.

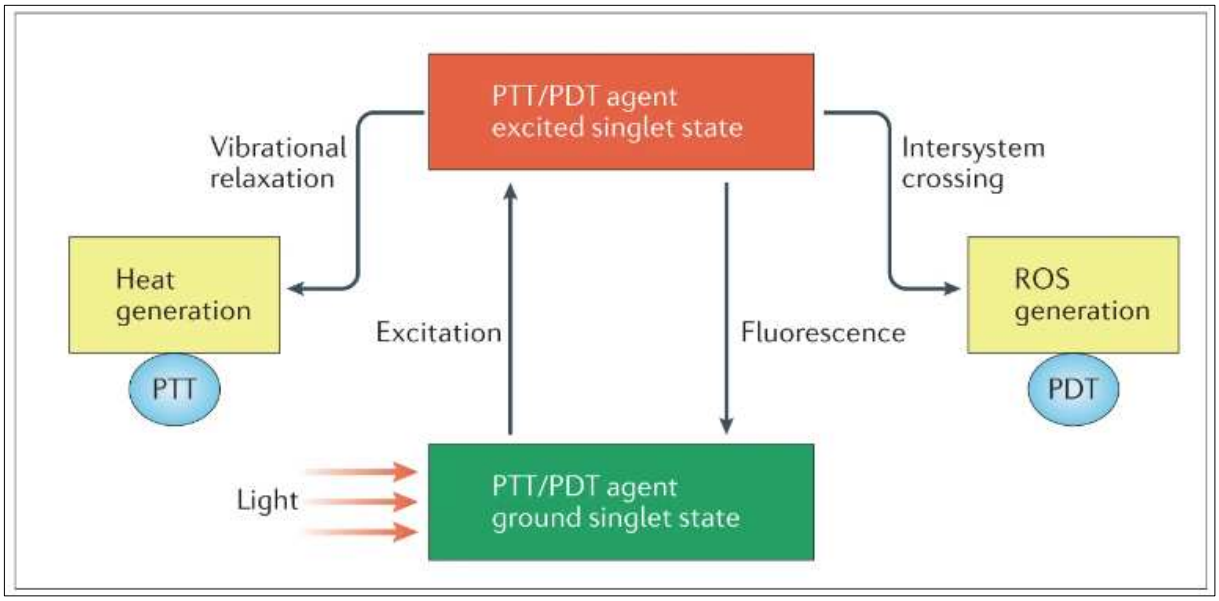

Figure 4 - Thermal damage is caused by heat released during vibrational relaxation of the excited PTT agent, whereas chemical damage is caused by reactive oxygen species (ROS) generated through energy and/or electron transfer from the PDT agent after intersystem crossing of the excited singlet state to a longer-lived triplet state. Source: Author (2023)

Generation of phototoxicity by irradiating photosensitive agents with no dark toxicity provides a long-desired locality in cancer treatment with an additional turn-on mechanism, dramatically reducing off-site toxicity. No cumulative toxicity, lack of resistance to multiple applications of phototherapies, and indications of reversal of multidrug resistance and influence on the metastatic tumor (GUO *et al.*, 2017; WEI *et al.*, 2019) accelerated the research efforts on phototherapy of cancer (DOS SANTOS *et al.*, 2019; JUNG *et al.*, 2018; LI *et al.*, 2016). PTT and PDT differ in the type of phototoxicity they generate. PTT is based on local temperature increase (HU *et al.*, 2018; JUNG *et al.*, 2018; LV *et al.*, 2020), and PDT is triggered by the formation of reactive oxygen species, especially singlet oxygen ($^1O^2$) (LI *et al.*, 2017, 2018) by irradiation of a photosensitizer (PS) at a molecule-specific wavelength, explicit in Figure 5.

A successful PS must meet the following requirements: 1) low toxicity in the dark; 2) strong absorbance at the excitation wavelength; 3) high quantum yield of $^1O^2$ for PDT and high thermal photoconversion efficiency for PTT; 4) tumor targeting ability to induce strong and selective phototoxicity to tumors (HU *et al.*, 2018; JAQUE *et al.*, 2014; LAN *et al.*, 2019). Furthermore, absorbance at long wavelengths and phototoxicity generated at low power

densities for safety and depth of penetration are also critical in the clinical translation of these approaches (HU *et al.*, 2022).

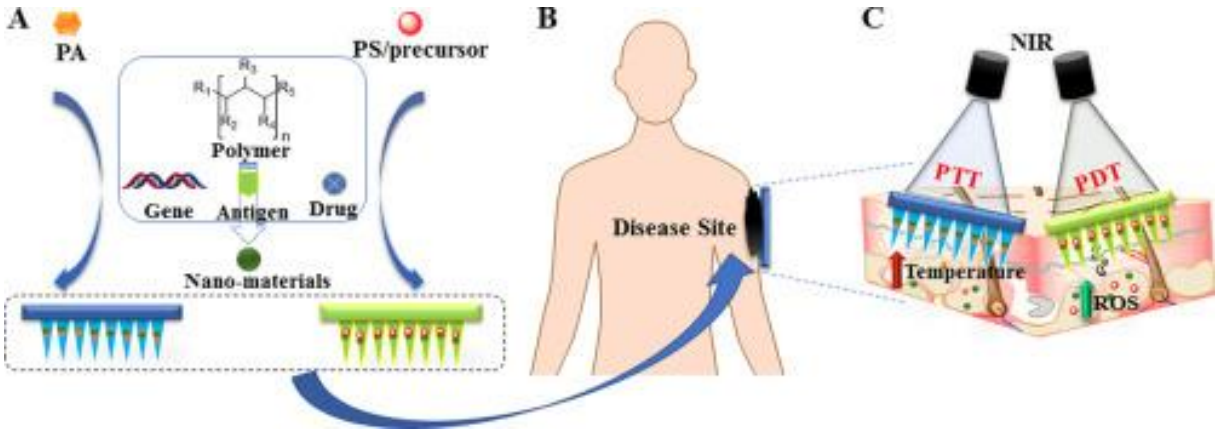

Figure 5 - Mechanism of contact of the nanomaterial with the synergistic action of PTT (effect of increasing the temperature of the microenvironment) and PDT (effect of releasing reactive oxygen species). Source: Author, 2023

This synergistic effect strategy has already been showing good results, but like any therapeutic method, PDT and PTT have limitations that need to be overcome for broader use and better therapeutic results (BHARATHIRAJA *et al.*, 2018; BILICI *et al.*, 2019; WANG, S. *et al.*, 2019; XIA *et al.*, 2019). In practice, if this can be achieved with a single PS, clinical translation would be relatively easy.

2.3.2.1 CHOICE OF LIGHT SOURCE

Just as important as in light-triggered drug release and photothermal therapy (FU *et al.*, 2015; LI *et al.*, 2015), the choice of light sources has an important role in PDT/PTT. Also, the correct light dose, sufficient photosensitizer concentration, and oxygen are needed within the tumor tissue (HUANG *et al.*, 2010). Since the parameters must be closely regulated, the light source must be del homogeneously delivered to the affected area ensure the treatment benefits reach the tissue.

Most PSs used for PDT/PTT have maximum absorption in the visible region (400 - 700 nm). To date, four types of laser light sources (argon-pumped lasers, metal-vapor-pumped lasers (Au- or Cu-vapor lasers), solid-state lasers (Nd:YAG lasers, Ho:YAG lasers, KTP:YAG/dye lasers), and diode lasers) and non-laser light sources (lamp light, light-emitting

diodes (LEDs)) have been tested in PDT/PTT (CALLAGHAN; SENGE, 2018; CHEN *et al.*, 2015; CLEMENT *et al.*, 2018; HSU *et al.*, 2018; LARUE *et al.*, 2018; REN *et al.*, 2018; TOGSVERD-BO *et al.*, 2013; TURAN *et al.*, 2016; WANG, R. *et al.*, 2018; WIEGELL *et al.*, 2008, 2012). Some of them have been used clinically, such as a red light argon dye laser, Nd:YAG laser, a red light (635 nm) LED lamp, a 570 - 670 nm wavelength red light lamp, green light (520 nm), 420-nm blue light-emitting diode, daylight (ETCHEVERRY *et al.*, 2016; JEON *et al.*, 2015; LERCHE *et al.*, 2016; MUNCK *et al.*, 2016).

2.3.2.1.1 LASER LIGHT SOURCES

The use of a multi-laser system is common when treating different diseases with PDT/PTT. The mono-chromaticity of lasers allows for irradiation with a precise wavelength at which a photosensitizer reaches its maximum absorption capabilities. These factors provide what is necessary to drive light to the targeted area of the body via optic fibers (CALIN *et al.*, 2011; CHEN *et al.*, 2022). The main types of laser light sources: are argon-pumped, solid-state and diode lasers.

The argon/dye laser is currently the primary light source for PDT employed in a medical setting. The high-powered argon/dye laser system can deliver light of continuous wave (CW) with a power of 1 to 7 W at a wavelength of 630 nm. However, argon/dye lasers have a “large frame” are often immobile and, need to be mounted to a structure, such as an optical bench (ETCHEVERRY *et al.*, 2016). For use in PDT procedures, the unit should be less cumbersome and require little optical adjustment to maintain sufficient power. In a study by Li and his group (2022), upon 808 nm laser irradiation, GOx@PCoS exhibit photothermal and photodynamic effects with a high photothermal conversion efficiency (45.06%) and generation capacity of the toxic superoxide anion (O_2^-) for photothermal therapy (PTT) and photodynamic therapy (PDT). The synergetic antitumor effects can be realized by GSH depletion, starvation, and combined PTT, and PDT with enhanced efficacy (LI *et al.*, 2022). Another study with the same 808 nm laser at extraordinarily low output power promptly demonstrated local hyperthermia. This allowed for a remarkable contrast in local temperature and drug release between the “silent” state (before phototriggering) and the “activated” state (after phototriggering). This NIR light-activated local hyperthermia and drug delivery provided the basis for the combination of chemotherapy and photothermal therapy (PTT) in antitumor treatment and exhibited excellent therapeutic efficacy (LI *et al.*, 2022).

Solid-state lasers take advantage of solid-state gain media. These lasers utilize arc or flash lamps as optical pumps (JEON *et al.*, 2015), such as Nd:YAG lasers, Ho:YAG lasers, and KTP:YAG/dye lasers. These all have applications in PDT/PTT, much like argon and metal vapor lasers. Among the advances in newly developed laser processes is the use of biocompatible silica optical-fiber delivery systems; this has driven development in treatment procedures. The Ho:YAG laser is a multipurpose laser used in urology, this is due to the laser's ability to penetrate multiple soft- and hard tissues. This system provides advantages in PDT/PTT including low cost, durability, portability, tenability, and ease of use (SONG, R. *et al.*, 2018). Khulugurov et al. demonstrated the possibility of the treatment of animals with malignant neoplasms using 608 nm solid-state laser radiation by means of photodynamic therapy (PDT) (KHULUGUROV *et al.*, [*s. d.*]).

Diode lasers are based on semiconductors. There is a lot of potential for incorporating these lasers into clinical use because they are portable and easy to use. They are considered ideal for endoscopic PDT and are generally coupled with optical fibers (YANG *et al.*, 2019). However, these systems are under development to adapt the laser for use with multiple wavelengths (TEYMOURI *et al.*, 2016). An advantage of using a system of lasers as a way of delivering light for PDT/PTT is the easy incorporation of the same light into fiber optics, allowing for the activation of photons to happen directly at the target site. Shirazian et al. investigated the effects of diode lasers on cancer cell proliferation and invasion. According to the results of this study, laser irradiation at 0 and 24 h resulted in a significant inhibitory effect on cell proliferation, especially at 660 nm/80 mW and 810 nm/200 mW (SHIRAZIAN *et al.*, 2021).

2.3.2.1.2 NON-LASER LIGHT SOURCES

Photonics technology is constantly under development. New light sources are being designed and improved for use with PDT/PTT on a large scale soon. Lamp light sources are being explored as an alternative to laser lights with highly successful results; these novel light sources include the use of halogen, xenon, and metal-halide lamps (TAWFIK *et al.*, 2018). When comparing lamps to lasers, the lamps provide a wider spectral output. They are advantageous in that they are portable, easy to use, can cover a large area, and can be used cooperatively with cross-section light guides (KIM; DARAFSHEH, 2020).

The use of LED in PDT has already been elucidated (WEIJER *et al.*, 2015). LED light sources can emit high-energy light at a specific wavelength, nd have customizable shapes and

configurations. LED provides diverse treatment options, allowing customization for PDT that can treat brain tumors and fit into balloon catheters intraoperatively, while also being useful for treating minimally invasive procedures such as the implantation of a flexible LED catheter into a tumor percutaneously (YANG *et al.*, 2019). Comparing a 660 nm LED desk lamp to the LD670–05 diode and the metal-halide lamps, it was evaluated at the LED desk lamp was not only more potent but required half as much irradiation time to produce the same effects (TAKAHASHI *et al.*, 2014). LEDs have advantages over other PDT/PTT light sources, such as low cost and low hazard (TURAN *et al.*, 2016), also they are compact, lightweight, and require low amounts of energy when producing desired wavelengths. According to Etcheverry et al. LED lights can be produced at different wavelengths such as 630, 670, and 690 nm, useful for PDT methods requiring flat surface illumination (ETCHEVERRY *et al.*, 2016).

2.4 POLYMERIC NANOPARTICLES IN PTT AND PDT

Several studies (BAHMANI *et al.*, 2014; GÜNEY AKKURT; GÜLSOY, 2022; HU *et al.*, 2022; HUNG *et al.*, 2016; LIU, B. *et al.*, 2021a; LIU, J. *et al.*, 2021; MA *et al.*, 2012; MANCHANDA *et al.*, 2010; PATEL *et al.*, 2012; SAXENA *et al.*, 2004b; SHEN *et al.*, 2019; TING *et al.*, 2021; WATANABE *et al.*, 2017; YAO *et al.*, 2021; ZHAO *et al.*, 2014) have reported that the use of nanoparticles in the encapsulation of photosensitizers makes these agents very selective for the diseased tissue and also reduces the time that PS takes to accumulate in the tumor, and present a greater penetration and retention in the tumor tissue since this tissue has irregular vasculature and larger pores than the pores of normal tissues (SONGCA, 2023). In addition, nanoparticles increase the PS accumulation power in strategic points of the cancer cell, such as, for example, in mitochondria and lysosomes (LIU *et al.*, 2020); thus, resulting in better patient compliance, minimal toxicity, and reduced dosage (KRISHNAN; MITRAGOTRI, 2020).

NPs increase the therapeutic efficiency of PS by protecting them from deactivation, preventing aggregation, and allowing control of their photoactivity (TADA; BAPTISTA, 2015). Recently, nanoparticle carriers have gained more attraction due to their potential application in targeted action, food technologies, and cosmetics. The main characteristics of nanoparticles are shown in Figure 6.

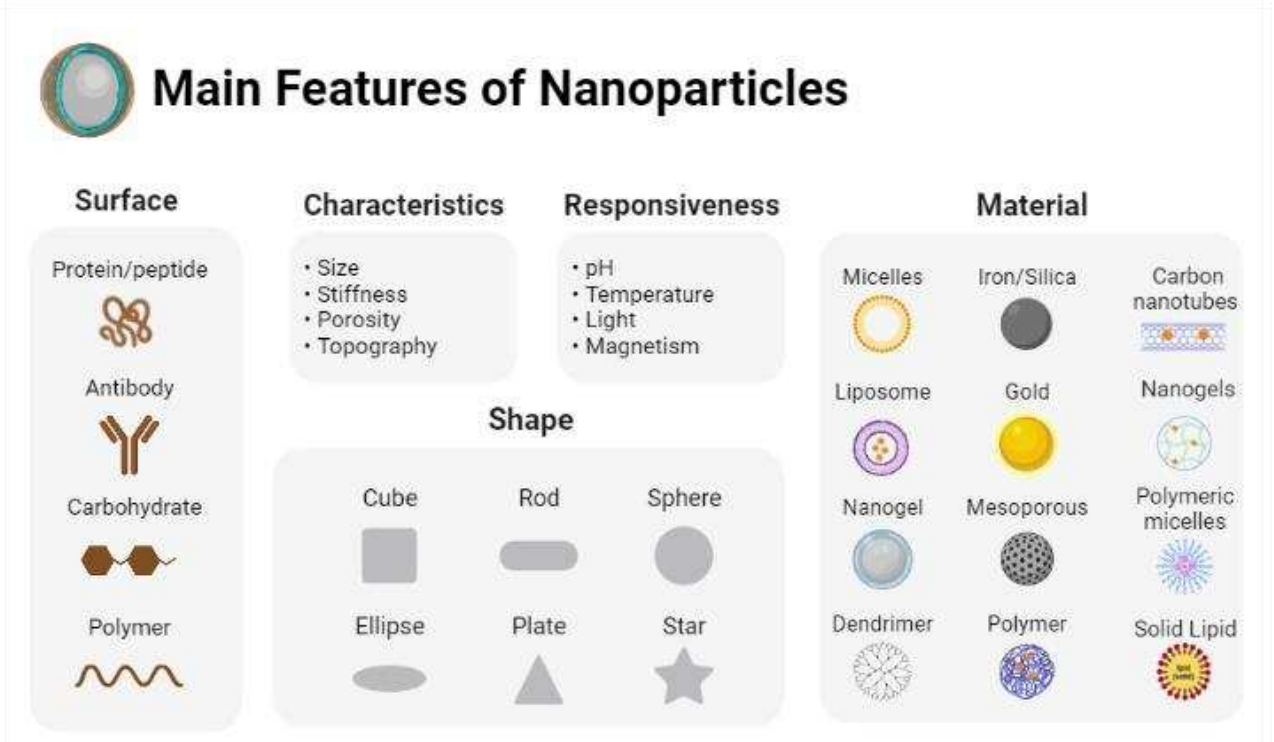

Figure 6: Nanostructured Delivery Systems used in the development of nanomedicines to treat cancer by PDT and PTT (nanosphere, nanocapsule, solid lipid nanoparticle, polymer micelle, dendrimer, liposome, gold nanoparticle, and nanoemulsion). Source: Author, 2023.

The main types of nanosystems used for PDT and PTT are liposomes, dendrimers, polymeric nanoparticles, lipid nanoparticles, metallic nanoparticles, and carbon nanotubes (XU *et al.*, 2023). However, polymeric nanoparticles are often used as they can enhance the solubility of drugs as well as provide the drug's stability and sustained release (GANGOPADHYAY *et al.*, 2015). For example, polymeric nanoparticles were used to encapsulate the photosensitizer zinc phthalocyanine, and as a result, the phototoxicity showed a 500 times increase compared to the free drug in a lung cancer cell line (MEHRABAN *et al.*, 2019). In addition, its main raw material is easy to obtain, the production processes are relatively simple, it is possible to use biocompatible and biodegradable matrices and there is a wide variety of polymers. The latter have very diversified physicochemical characteristics, allowing the formation of systems with different degradation rates and release control in the organism (SONG, L. *et al.*, 2018).

2.4.1 POLYMERIC NANOPARTICLES IN PDT/PTT: EVOLUTION OF PHOTOSENSITIZERS

Therefore, despite the continuous development of photodynamic and photothermal therapy for the treatment of cancer, the advance of these therapies in clinical applications is still held back by the low accumulation of the photosensitizer (PS) in the tumor tissue and by its short blood circulation time, either by its deactivation by biomolecules or by its low solubility in the medium (PINTO; POCARD, 2018).

PSs are chromophore-containing compounds, which are either natural or synthetic in chemical composition (DEBELE *et al.*, 2015). PSs can absorb light at a particular wavelength and generate cytotoxic ROS, which in turn allows PDT/PTT treatments to induce chemical or physical damage in target cancer tissues (HU, 2014). However, within PDT/PTT PS drugs need to have a high molar absorption coefficient within the PDT therapeutic red region of the visible light spectrum (650 – 780 nm), as ensure minimal patient photosensitivity before PS excitation, as well as to avoid light absorption by other endogenous human body pigments (CALIXTO *et al.*, 2016; CHEN *et al.*, 2016). However, these particular wavelength parameters also ensure maximum light absorption for PS excitation and ROS generation, as well as optimal tissue penetration at targeted tumor sites, to warrant effective PDT/PTT cancer treatments (DEBELE *et al.*, 2015; MOKWENA *et al.*, 2018).

Commonly, PSs are classified into three groups according to their functional capabilities namely, first, second and third generation (MOKWENA *et al.*, 2018), explicit in Figure 7.

The second-generation PSs are single compounds synthesized, derived from porphyrin, bacteriochlorophyll, phthalocyanine, chlorin, benzoporphyrin, curcumin, methylene blue derivatives, etc. Compared with the first-generation PSs, the second-generation PSs have a longer absorption spectrum (visible-near-infrared region), higher $^1O_2$ yields, and better tumor targeting. Third-generation PS consists of second-generation PSs which have bound to passive targeting nanoparticles (NPs) or active targeting agents (aptamers, peptides, antibodies, amino acids, polypeptides, or by encapsulation into highly biocompatible nanocarriers to improve the ability of PS improve accumulation of PSs at the targeted tumor sites ((BASKARAN *et al.*, 2018) and so tend to report enhanced uptake and the best PDT/PTT treatment outcomes in cancer patients (DEBELE *et al.*, 2015; MOKWENA *et al.*, 2018).

Lastly, research is beginning to focus on the development of fourth-generation PS (Figure

7), a second-generation PS encapsulated in a NP delivery system—making it a third-generation PS, with a co-encapsulated small-molecular inhibitor capable of blocking tumor survival pathways post PDT treatment to improve its overall efficacy in clinical settings and so halt possible tumor reoccurrence (KATAOKA *et al.*, 2017; WEIJER *et al.*, 2015).

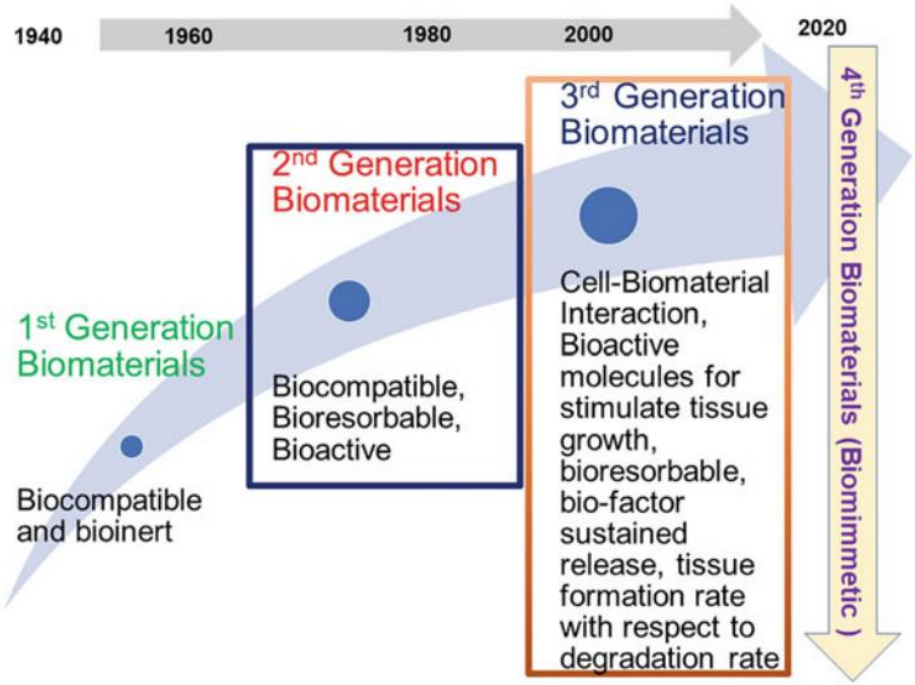

Figure 7 - Evolution of essential characteristics for the generation of biomaterials used at the time. Source: Author, 2023

Many other photoactive dyes, small synthetic organic compounds, have been found to have photodynamic/phototermal properties in either antimicrobial applications or anti-cancer applications. Common dyes that have been investigated for PDT/PTT include phenothiazinium salts (methylene blue and toluidine blue), rose Bengal, squaraines, boron-dipyrromethene, phenalenones, and indocyanine green (WATANABE *et al.*, 2017).

Indocyanine green (ICG), an FDA-approved medical contrast agent for intravenous administration, has received considerable attention as a phototherapeutic agent given its photothermal effect and cytotoxic ROS generation upon NIR laser irradiation also exhibit combined PTT-PDT effects (DENG *et al.*, 2015; NOMURA *et al.*, 2020). In particular, ICG has been used as an effective NIR-absorbing PTT/PDT agent with excellent light-to-heat conversion efficiency for cancer treatment (SHIRATA *et al.*, 2017). ICG, whose absorption

peak is around 800 nm, was evaluated as a suitable dye for PDT in melanoma cells in vitro (WATANABE *et al.*, 2017). Barth and colleagues successfully targeted ICG-loaded nanoparticles for PDT to leukemia *in vivo* beyond the solid tumors (BARTH *et al.*, 2011). These nanoparticles enable deep light tissue penetration which improves PDT efficacy. CD117-ICG-loaded calcium phosphosilicate nanoparticles were able to specifically target leukemia stem cells and improve survival by 29% in leukemic mice (BARTH *et al.*, 2011).

In 2011, a pilot clinical study showed the feasibility of ICG for the treatment of metastatic breast cancer. A total of 10 patients with advanced-stage metastatic breast cancer received laser immunotherapy consisting of the local injection of ICG and glycated chitosan, followed by 805-nm laser irradiation at a power density of 1 W/cm^2. NIR laser-based immunotherapy achieved an objective response rate of 62.5% and a clinical benefit response rate of 75%. There were no significant adverse events after treatment, aside from limited local thermal injury (LI *et al.*, 2011).

A combination of indocyanine green (ICG), polydopamine (PDA), and tirapazamine (TPZ) have shown remarkable antitumor efficacy against subcutaneous U87MG tumors and orthopedic B16F10 tumors combining PDT and PTT. In the study by Huang et al., (HUANG *et al.*, 2019) PDA was used as a photothermal conversion agent along with ICG, a widely used photosensitizer. Both PDA and ICG have absorption maxima in the NIR range. Tirapazamine is a hypoxia-activated chemotherapeutic drug that damages DNA when the photosensitizer consumes oxygen to produce ROS. CaCO3/TPGS hybrid was used as a carrier to prepare ICG-PDA-TPZ NPs (HUANG *et al.*, 2019). PDA is also used in the mesoporous form to serve as a nanocarrier along with showing its PTT effects. Hence, it is easy to achieve synergistic effects by loading the photosensitizer or chemotherapeutic agents onto mesoporous PDA (MPDA) (WU *et al.*, 2022)

A combination of different therapies for different drug treatment of cancer increases therapeutic efficacy and helps to overcome the limitations of single therapy. Chemotherapy is a front-line strategy for treating cancer using chemical drugs. Doxorubicin (DOX) is a widely used chemotherapeutic that hinders DNA replication by inhibiting topoisomerase (HAK, et al., 2021). This co-delivery of two different drugs requires a nanoscale drug delivery system. The covalent conjugation of the photosensitizer and the chemotherapy drug is another strategy for the co-delivery of both drugs (HAK *et al.*, 2021).

Studies developed by Luo et al. focused on the development of polymeric nanoparticles with co-encapsulation of Doxorubicin and a photosensitizer. To avoid the known toxicity of

Doxorubicin, the strategy used was to link DOX to the polymer, a link that can be cleaved by ROS, and thereby the activation of the nanoparticle is ROS-dependent. They encapsulated the catalase enzyme to act on the intracellular H_2O_2 to produce more O_2 and functionalized particles with a peptide IF7 to target the tumor. This versatile and complex system (IF7-ROSPCNP) was shown to be an effective nanoparticle with accurate tumor targeting, that was able to inhibit tumor growth and prolong survival time when submitted to laser irradiation. Mice treated with ROSPCNP and IF7-ROSPCNP, but not irradiated, were also submitted to histopathological studies, which showed that other tissues were no different from the control group, which suggests that the nanoparticles were safe (LUO *et al.*, 2019).

Deng and collaborators developed systems with tetrakis(4-carboxyphenyl) porphyrin as a photosensitizer, where the drug Doxorubicin was encapsulated forming π-π interactions with polymeric nanoparticles (PNP) to enhance the drug loading. These researchers obtained high drug loading (17.9%) and encapsulation efficiency (89.3%) associated with π-π interactions, as proven by the fluorescence method. Furthermore, in vivo studies showed that the PNPs developed were able to inhibit the growth of breast tumor in Balb/c mice when exposed to laser irradiation. The studies discussed in this topic were a few examples among many reports of photodynamic/photothermal therapies exploiting PNPs in several types of cancer, such as cervical adenocarcinoma, glioblastoma, highly aggressive breast cancer, and hepatocellular carcinoma, showing the versatility of combining PNPs and PDT/PTT for cancer treatment (DENG *et al.*, 2015; GANGOPADHYAY *et al.*, 2015; JAMALI *et al.*, 2018; WANG, Q. *et al.*, 2019).

2.4.2 POLYMERIC NANOPARTICULES IN PDT/PTT: POLYMER MATRICES

The choice of polymers for the development of polymeric nanoparticles for application in dynamic and photothermal phototherapy is a fundamental process to guarantee the efficacy and safety of these therapeutic systems. These polymers play a crucial role in encapsulating and transporting these photosensitizing agents and/or photothermal agents, which are responsible for generating therapeutic effects when activated by light (LEE; KOPELMAN, 2011).

Several criteria must be considered when selecting suitable polymers for these applications. One of the key factors is biocompatibility, as polymers must be safe for use in living organisms and not have adverse reactions. The potential toxicity of polymers and their degradation products is a critical aspect to be evaluated (BARANWAL *et al.*, 2022).

Another important aspect is the ability of the polymer to encapsulate and protect the therapeutic agent during administration, preventing its premature release and ensuring its stability. The selective permeability of the polymeric matrix is essential to control the release of the therapeutic agent in the target area, as well as its therapeutic efficacy (LIECHTY *et al.*, 2010).

In addition, the choice of polymer should also consider its physicochemical properties, such as solubility, stability under different conditions, ease of processing, loading and unloading capacity with the therapeutic agent. The structure of the chemical can influence its degradation, biodistribution, and interaction with the biological environment (LIU *et al.*, 2009).

Different types of polymers have been explored for this purpose (Table 1), including synthetic and natural polymers. Synthetic polymers, such as poly(lactide-co-glycolide) (PLGA), polyethylene glycol (PEG), Poly(vinyl alcohol) (PVA), and Polymethylmethacrylate (PMMA), are widely used due to their versatile properties and modulation capacity (REDDY *et al.*, 2021).

Natural compounds, such as chitosan, alginate, collagen, and gelatin, have also been investigated due to their biocompatible, biodegradable, and hidden properties with the biological environment. These natural polymers may provide a more sustainable and less toxic approach to polymer nanoparticle development (REDDY *et al.*, 2021).

Table 1 - Synthetic and natural polymers, their main source and properties, which have been applied in Phototherapy.

Materials	**Main sources**	**Properties**	**References**
Poly(lactic acid) (PLA)	Acid lactic	Biocompatibility, biodegradability	(WANG, J. *et al.*, 2018; WATANABE *et al.*, 2017)
Poly(glycolic acid) (PGA)	Acid glycolic	Biocompatibility, hydrophobicity, biodegradability	(DURO-CASTANO *et al.*, 2021)
Poly(ethylene glycol)-poly(L-lactic acid) (PLGA)	Acid lactic and acid glycolic	Biodegradable, biocompatible, FDA-approved, tunable release rate, high drug-loading capacity	(ANSARINIK *et al.*, 2022), (GERMANOVA *et al.*, 2022)

Poly(vinyl alcohol) (PVA)	Vinyl acetate	Biocompatibility, biodegradability	(JIN, 2022)
Polymethyl methacrylate (PMMA)	Methyl methacrylate	Biocompatibility, high mechanical properties, chemical stability, bioinert	(FEUSER *et al.*, 2016; SMITH *et al.*, 2022)
Poly ε-caprolactone (PCL)	ε-caprolactone	Biodegradable, biocompatible, tunable release rate, high drug-loading capacity, low toxicity	(MOAZZAMI GOUDARZI *et al.*, 2022)
Polyethylene glycol (PEG)	Ethylene oxide	Biodegradable, biocompatible, high drug-loading capacity, versatile chemistry, low toxicity	(LIU *et al.*, 2018; VIVEK *et al.*, 2018; ZHAO *et al.*, 2014)
Poly(thioether-ester)	α,ω-diene diester	Biodegradability, biocompatibility, and antioxidant activity	(FREIRE *et al.*, 2022)
Collagen	Cartilage, tendons, and marrow from animal bones	Biocompatibility and ability to interact with cells and the extracellular matrix	(WANG *et al.*, 2021; ZHU *et al.*, 2023; ZIAUDDIN *et al.*, 2022)
Gelatin	Bovine or porcine collagen	Biocompatibility and ability to interact with cells and the extracellular matrix	(LIU, B. *et al.*, 2021b)
Chitosan	Exoskeleton of crustaceans	Biodegradable, biocompatible, mucoadhesive, versatile chemistry, low toxicity, immunomodulatory, stimuli-responsive	(AHMADY *et al.*, 2022; MATICA *et al.*, 2019)
Alginate	Brown algae	Biocompatibility and biodegradability	(ABDELBASSET *et al.*, 2022; BALDE *et al.*, 2022; CHANG *et al.*, 2020; LIU *et al.*, 2022; QIAN *et al.*, 2022;

			SPOIALĂ *et al.*, 2022; STAGNOLI *et al.*, 2023)
Cellulose	Plants	Porosity, hydrophilicity, swelling behavior in aqueous media, large surface area, ability to chemically modify the surface as well as sensitivity to pH and temperature	(CHANDRA *et al.*, 2022; LAKHANI *et al.*, 2018)

Polymers such as poly(lactic-co-glycolic acid)/PLGA and poly(ethylene glycol)/PEG are FDA-approved polymers that have shown promising results in treating cancer. Marasini and Aryal. synthesized a core–shell biocompatible nanocarrier envelope made up of a phospholipid conjugated with PEG as a shell, while PLGA was used as a core to encapsulate IR-820 dye. The IR-820-loaded nanoparticles were prepared by nanoprecipitation and characterized for their physicochemical properties and photothermal efficiency (MARASINI; ARYAL, 2022) (Figure 8).

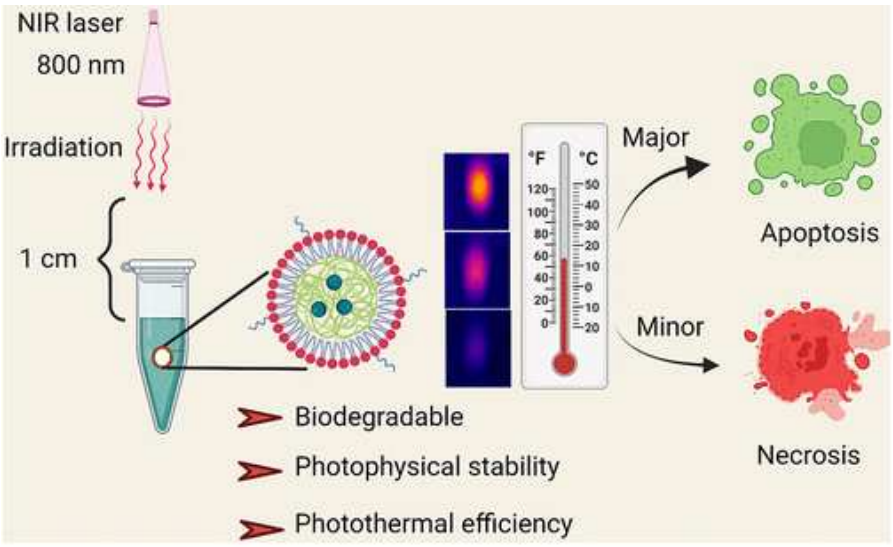

Figure 8 - Photothermal mechanism of action with the irradiation of a NIR laser on polymeric nanoparticles causing phototoxicity in cancer cells. Source: (MARASINI; ARYAL, 2022).

The IR-820-loaded nanocarrier showed excellent biocompatibility in the dark, whereas remarkable phototoxicity was observed with breast cancer cells (MCF-7) upon NIR laser excitation. Therefore, the IR-820-loaded phospholipid mimicking biodegradable lipid-polymer

composite nanoparticles could have great potential for cancer theranostics (MARASINI; ARYAL, 2022).

In another study which also used an NIR laser a sophisticated photosensitive polymeric material (An-NP) that allows sustained $^1O_2$ generation and sufficient oxygen supply during the entire phototherapy was engineered by alternatively applying PDT and photothermal therapy (PTT) controlled by two NIR laser beams (YANG *et al.*, 2019). In addition to a photosensitizer that generates $^1O_2$, An-NP consists of two other key components: a molecularly designed anthracene derivative capable of trapping/releasing $^1O_2$ with superior reversibility and a dye J-aggregate with superb photothermal performance. Thus, in 655 nm laser-triggered PDT process, An-NP generates abundant $^1O_2$ with extra $^1O_2$ being trapped; while in the subsequent 785 nm laser-driven PTT process, the converted undergoes thermolysis to liberate the captured $^1O_2$ and regenerates An-NP. The intratumoral oxygen level can be replenished during the PTT cycle for the next round of PDT to generate $^1O_2$. The working principle and phototherapy efficacy were preliminarily demonstrated in living cells and tumor-bearing mice, respectively (YANG *et al.*, 2021).

Another alternative, only now using two-photon activated, was the research by the group of Wang et al. (Figure 9), where a type of polymeric nanoparticles loading indocyanine green and Pt(II)-porphyrins (ICG-Pt-NPs) was constructed to achieve a synergistic effect of combined photothermal photodynamic therapy. The nanoparticle core comprises the photosensitizer Pt(II)-porphyrins (PtTFPP), and organic semiconducting polymer (PFO) that acts as a two-photon antenna (WANG *et al.*, 2017).

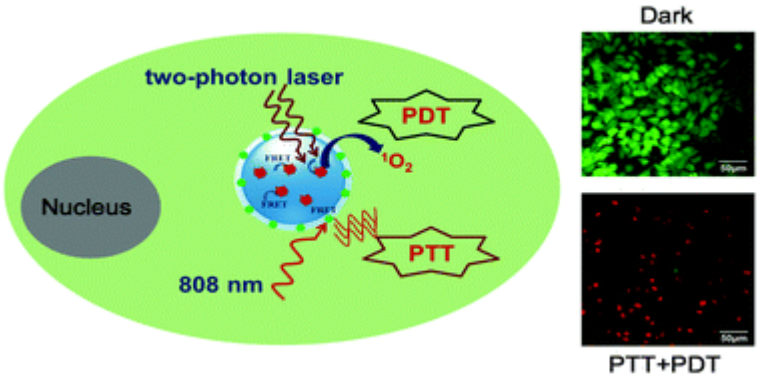

Figure 9 - Mechanism of action of the polymeric particle, with the application of the synergistic effect of the combined therapy of PTT and PDT (through the two-photon laser). Source: (WANG *et al.*, 2017).

Negative ICG molecules, a NIR-absorbing photothermal dye, can be loaded into the positively charged poly-L-lysine (PLL) shell of the polymeric nanoparticles *via* electrostatic interaction. In these carefully designed ICG-PtTFPP integrated nanoparticles, PtTFPP absorbs the photonic energy transferred by the PFO polymer under two-photon laser excitation at 740 nm to induce photodynamic cancer cell death, while ICG offers nanoparticles a strong photothermal performance under 808 nm laser irradiation. Compared with photodynamic therapy or photothermal therapy alone, the combined therapy had a significantly synergistic effect and improved the therapeutic efficacy with near-infrared irradiation (WANG *et al.*, 2017).

Palao-Suay and his group also developed a study applying the combined therapy of PDT and PTT, the aim of the work was the generation of a multifunctional nanopolymeric system that incorporates IR-780 dye, a near-infrared (NIR) imaging probe that exhibits photothermal and photodynamic properties; and a derivate of α-tocopheryl succinate (α-TOS), a mitochondria-targeted anticancer compound. IR-780 was conjugated to the hydrophilic segment of copolymer PEG-b-polyMTOS, based on poly(ethylene glycol) (PEG) and a methacrylic derivative of α-tocopheryl succinate (MTOS), to generate IR-NP, self-assembled nanoparticles (NPs) in aqueous media which exhibit a hydrophilic shell and a hydrophobic core (PALAO-SUAY *et al.*, 2017). They developed nanotheranostic particles showed distinct fluorescence and photothermal behavior after excitation by a laser light emitting at 808 nm. Treatment of MDA-MB-453 cells with IR-NP or IR-NP-eIR resulted in an efficient internalization of the IR-780 dye, while subsequent NIR-laser irradiation led to a severe decrease in cell viability. Photocytoxicity conducted by IR-NP, which could not be attributed to the generation of lethal hyperthermia, responded to an increase in the levels of intracellular reactive oxygen species (ROS). Therefore, the fluorescence imaging and inducible phototoxicity capabilities of NPs derived from IR-780-PEG-b-polyMTOS copolymer confer high value to these nanotheranostics tools in clinical cancer research (PALAO-SUAY *et al.*, 2017).

Poly(lactic acid) (PLA), which is biodegradable and possesses an ultrasound signaling capability, was used as a polymeric nanoparticle in Peban's et al., study (Figure 10). IR-775, a hydrophobic photosensitizer, was used in combination with polyphenols (p)-rich ethyl acetate extract from Terminalia chebula to treat cancer. IR-775 dye and polyphenols were encapsulated in a poly(lactic acid) polymeric nanosystem (PpIR NPs) to increase the cell bioavailability (PEBAM *et al.*, 2022).

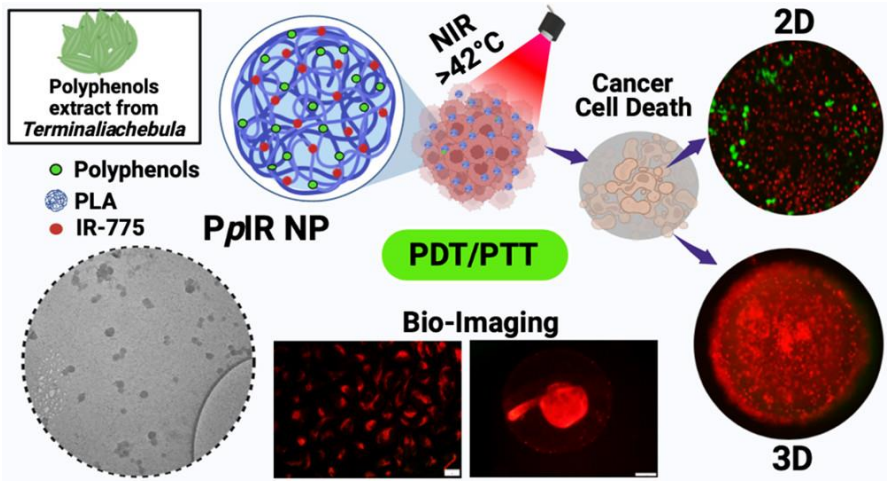

Figure 10 - Schematic representation of the PLA nanoparticle in the application of combined PDT and PTT therapy with NIR laser in cancer cells. Source: (PEBAM *et al.*, 2022).

The nanosystem showed enhanced cellular uptake in a lung cancer cell line (A549). Cell cytotoxicity results indicate that PpIR NPs showed more than 82.46 ± 3% cell death upon NIR light treatment compared to the control groups. Both PDT and PTT generate reactive oxygen species (ROS) and cause hyperthermia, thereby enhancing cancer cell death. Qualitative and quantitative analyzes have depicted that PpIR NPs with NIR light irradiation have decreased protein expression of HSP70 and PARP, and increased γ-H2AX, which collectively lead to cell death. After NIR light irradiation, the relative gene expression patterns of HSP70 and CDK2Na were also downregulated. Further, PpIR NPs uptake has been studied in 3D cells and in ovo bioimaging in zebrafish models. In conclusion, the PpIR NPs show good cancer cell cytotoxicity and present a potential nanosystem for bioimaging (PEBAM *et al.*, 2022).

2.4.3. POLYMERIC NANOPARTICLES IN PDT/PTT: ENCAPSULATION TECHNIQUES OF PHOTOSENSITIZERS

The method of preparation mainly depends on the nature of the drug (hydrophilic or hydrophobic) to be encapsulated (ALI *et al.*, 2014). In drug delivery systems, colloidal carriers like nanoparticles are becoming more important due to their smaller size, which allows them to permeate through biological membranes (RIZVI; SALEH, 2018). Depending on the type of drug to be loaded in the polymeric NPs and their requirements for a particular administration route, different methods can be used to produce the particles (JAWAHAR; MEYYANATHAN,

2012). In general, two main strategies are employed (Figure 11, Table 2), namely, the dispersion of preformed polymers or the polymerization of monomers (AMGOTH *et al.*, 2020).

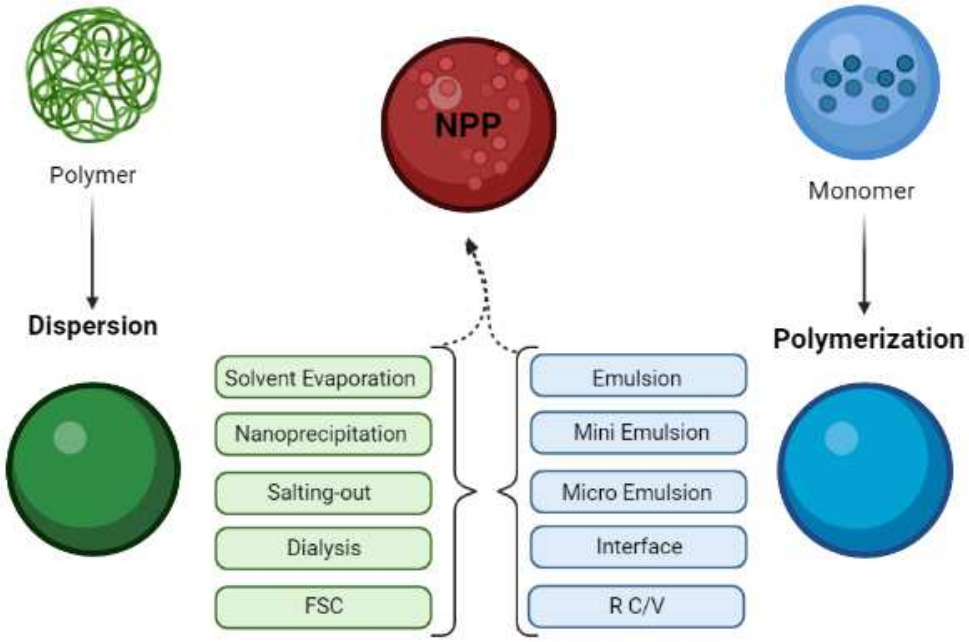

Figure 11 - Scheme of techniques used for the preparation of polymeric nanoparticles. FSC: Supercritical Fluid; R C/V: Radical Controlled/Alive adapted from (RAO; GECKELER, 2011).

Table 2 - Advantages and limitations of main techniques used for drug encapsulation.

Encapsulation Technique	Advantages	Disadvantages	Examples
Single emulsion solvent evaporation	1. Provides high retention of lipophilic actives. 2. Particle size is adjustable by changing homogenization speed, amount of stabilizer, and viscosity of organic and aqueous phases.	1. Trapping of hydrophilic drugs is bad. 2. Difficult to scale up. 3. Usually requires high-shear devices.	(DOS SANTOS *et al.*, 2019; FREIRE *et al.*, 2023; G. NAVA-ARZALUZ *et al.*, 2012; MANCHANDA *et al.*, 2010)
Double emulsion solvent evaporation	1. Provides an encapsulation advantage for both hydrophilic and hydrophobic actives. 2. Structured nanoparticles.	1. Large, non-uniform (polydisperse) particles. 2. Two-step process. 3. Leakage of the hydrophilic active into	(LIU *et al.*, 2018; PARK *et al.*, 2017; PATEL *et al.*, 2012)

Encapsulation Technique	Advantages	Disadvantages	Examples
		the external aqueous phase. 4. Difficult to scale up. 5. Usually requires high-shear devices.	
Emulsion diffusion method	1. Allows the incorporation of thermosensitive drugs. 2. Reduces average particle size and narrow size distribution. 3. Good batch-batch reproducibility. 4. Greater entrapment of lipophilic drugs. 5. Use of non-toxic solvents. 6. Easy to scale up.	1. Possible residues of organic solvents in the final formulation. 2. Poor encapsulation of hydrophilic drugs. 4. Requires more time for stirring the emulsion. 5. Requires a greater volume of water for the formation of nanoparticles. 6. Solvent must be partially soluble in water.	(ANVARI *et al.*, 2013; BAHMANI *et al.*, 2014; MA *et al.*, 2012)
Emulsion polymerization	1. It's fast and scalable. 2. Organic solvent-free method. 3. Does not require high-shear devices. 4. Particle concentration and solids content may be very high.	1. Complexity of particle nucleation rendering encapsulation less straightforward 2. May use toxic organic monomers. 3. Difficulty removing residual monomers, initiators, and surfactants from the final product.	(GHARIEH *et al.*, 2019; LOVELL; SCHORK, 2020)
Miniemulsion polymerization	1. It's fast. 2. Organic solvent-free method. 3. Particle concentration and solids content may be very high. 4. Particle concentration and solids content may be very high.	1. Requires high-shear devices. 2. May use toxic organic monomers. 3. Difficulty removing residual monomers, initiators, and surfactants from the final product.	(BERNARDY *et al.*, 2010; FEUSER *et al.*, 2016; FRIZZO *et al.*, 2019; GHARIEH *et al.*, 2019)
Microemulsion Technique	1. Reduces mean particle size and narrow size distribution.	1. High concentration of surfactants and co-surfactants.	(DENG *et al.*, 2003; SALABAT;

Encapsulation Technique	Advantages	Disadvantages	Examples
	2. Organic solvent-free method. 3. No power consumption process. 4. Easy to scale up. 5. Particle concentration may be very high.		MIRHOSEINI, 2022)
Nanoprecipitation	1. Simple and fast. 2. Uses non-highly toxic solvents. 3. High batch-batch reproducibility. 4. Does not require high-shear devices. 5. Monodisperse particles.	1. Mainly limited to hydrophobic active encapsulation. 2. The size of nanoparticles mainly depends on the polymer concentration. 3. The solvent must be soluble in water.	(HUNG *et al.*, 2016; ZHAO *et al.*, 2014)
Salting out	1. Does not require high shear stress. 2. Applicable to heat-sensitive medicine. 3. High loading efficiency for lipophilic drugs. 4. Easy to scale up. 5. High reproducibility.	1. Extensive nanoparticle washing step. 2. Exclusively applicable for lipophilic drugs.	(WANG *et al.*, 2016)

When encapsulating hydrophobic compounds, two of the most used techniques are the emulsification-solvent evaporation technique and the nanoprecipitation technique (HAQUE *et al.*, 2018; HERNÁNDEZ-GIOTTONINI *et al.*, 2020; PAGEL *et al.*, 2014). The emulsification technique occurs in two stages and is based on a mixture of a volatile non-water miscible solvent and an aqueous solution, which are emulsified by the application of high shear force. Then the volatile solvent is evaporated, forming in the process the PNP. This method is advantageous because it is non-toxic and produces very small particles. Nevertheless, a disadvantage of the technique is the high energy used in the process, which could affect the stability of certain drugs (MASOOD, 2016; YANG *et al.*, 2015).

The solvent evaporation method is an example of a two-step procedure where an emulsion is created, homogenized, or sonicated, and then an evaporation step is required to remove the organic solvent in which the polymer was dissolved. On the other hand, nanoprecipitation is a one-step procedure where the polymer and drug are dissolved in a solvent miscible in water and

dripped in an aqueous solution containing a stabilizer. In both methods, organic solvents are employed, and although toxic solvents such as chloroform are no longer used, ether and acetone are currently used for the preparation of nanoparticles. In these cases, evaporation and purification methods are required to remove solvent residues from the dispersion (AMOABEDINY *et al.*, 2018; CRUCHO; BARROS, 2017; MACHADO *et al.*, 2019).

Biodegradable polymers such as poly(lactide-co-glycolide) (PLGA) have been popularly employed as matrix materials for PS encapsulation (LEE; KOPELMAN, 2011). PLGA was utilized to achieve topical photodynamic therapy using ALA prodrugs (SHI *et al.*, 2013). ALA was efficiently encapsulated in PLGA nanoparticles by the double emulsion solvent evaporation method, resulting in ca. 66% encapsulation efficiency. ALA-loaded amorphous PLGA nanoparticles were effectively internalized by squamous cell carcinoma cells and mediated photocytotoxicity, which was more efficient than free ALA of the same concentration.

Analyzing the articles used in this bibliographic review, it is observed that the most used method of obtaining is nanoprecipitation (36 %) (Figure 12). This may occur due to the characteristics of the procedure already mentioned above, such as simplicity, speed, low cost, and ease of reproduction (SALATIN *et al.*, 2017).

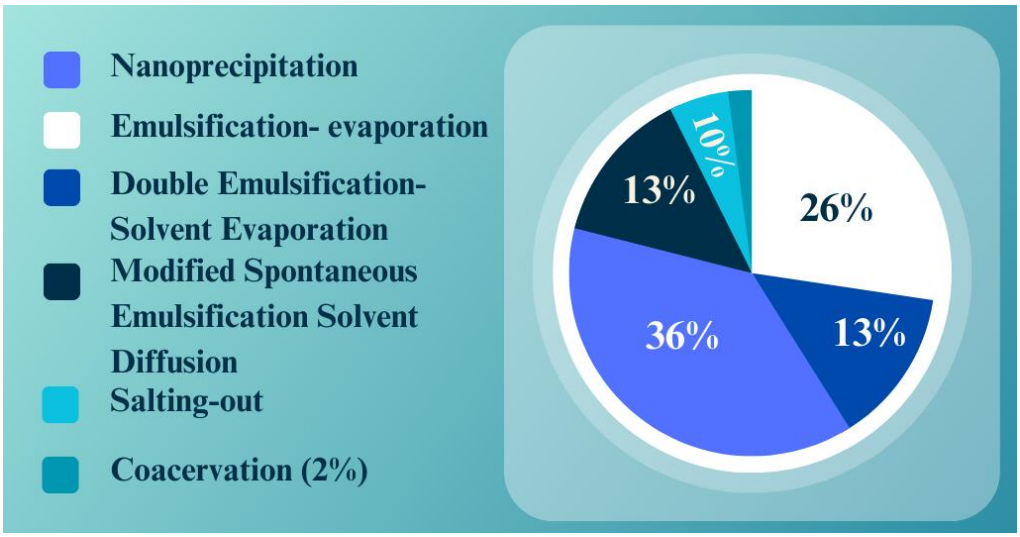

Figure 12 - Percentage of times each method was used.

Solvent emulsification-evaporation is also a widely used method, ranking second with 26% of publications. Because it requires high energy for homogenization, the transposition to large-scale production becomes a limitation of this procedure. As for nanoprecipitation, theoretically, it could be more easily adapted (HERNÁNDEZ-GIOTTONINI *et al.*, 2020).

Coacervation was the least used method for obtaining nanoparticles. Among the publications raised, its application was restricted to the use of polymers of natural origin that have an electric charge and, therefore, naturally favor the formation of nanoparticles by these methods.

2.4.4 POLYMERIC NANOPARTICLES IN PDT/PTT: FUNCTIONALIZATION AND STIMULI-RESPONSIVE CHARACTERISTICS

Recently, stimuli-responsive nanoparticles have also been proposed as a promising active targeting strategy for tumor treatment (DE *et al.*, 2022; RAVI KIRAN *et al.*, 2021; SHARIFI *et al.*, 2021; ZHANG, S. *et al.*, 2022; ZHOU *et al.*, 2019, 2016). Specifically, an acidic environment, high levels of reactive oxygen species (ROS) and glutathione (GSH), and overexpression of specific enzymes in the tumor microenvironment (TME) can contribute to the development of stimuli-responsive nanoparticles for targeted drug delivery, as these nanoparticles maintain their stealth features in the normal physiological environment but upon homing to targeted sites or the local microenvironment are responsive and release encapsulated agents (DE *et al.*, 2022; RAVI KIRAN *et al.*, 2021; ZHANG, J. *et al.*, 2022; ZHOU *et al.*, 2019). Moreover, functionalized nanoparticles can also be activated by external stimuli including magnetic fields, light, and ultrasound, to realize efficient tumor accumulation and controlled drug release in a temporal and spatial-specific fashion (ZHAO *et al.*, 2017). It should be noted that these stimuli-responsive nanoparticles also overcome many of the disadvantages of conventional nanoagents by site-specific tumor targeting and controlled drug release, such as providing improved therapeutic agent delivery, overcoming the off-target adverse effects, and enhancing the therapeutic benefits.

2.4.4.1 FUNCTIONALIZED NANOPARTICLES

Most NP PSs need to be prepared and functionalized according to the TME that they are targeting for a successful biophysiological interaction to occur, as to ensure effective PS drug uptake and retention for active indirect PS drug targeting (ASHFAQ *et al.*, 2017; MASTER *et al.*, 2013).

Tumor cell/tissue-specificity of PS drug delivery can be significantly increased via the surface modification of NP PSs to bind with targeting surface receptor moieties for active direct PS drug targeting (HONG *et al.*, 2016; OLIVO *et al.*, 2010). The surface functionalization of

PS nanodrug carrying systems with targeting receptor moieties which are overexpressed in tumor sites only, allows nanocarriers to precisely recognize targeted tumors and so allow for active absorption and uptake of PS drugs in these specific cancer cells only (Figure 13) (DEBELE *et al.*, 2015; HONG *et al.*, 2016). This particular type of drug targeting system is known as the "magic bullet" or "smart drug delivery systems" in PDT/PTT cancer therapy (HONG *et al.*, 2016; KYDD *et al.*, 2017). PDT/PTT active cancer nanodrug therapy targeting implies the use of externally conjugated target moieties to a NP PS drug delivery system in order to enhance PS uptake and concentration in specific tumor cells (KYDD *et al.*, 2017).

Biomolecules or surface molecules for active tumor targeting include antibodies, aptamers, peptides, or small molecules that recognize tumor cell-specific or tumor associated antigens in the TME (Figure 13) (BARAKAT *et al.*, 2011). Researches have shown that this approach improves and concentrates PS drug localization and active uptake in specific tumor cells only, while reducing the undesirable adverse effects of PS drugs to surrounding healthy tissues and unwanted phototoxicity (CALIXTO *et al.*, 2016; EDIRIWICKREMA; SALTZMAN, 2015). Thus, for targeted and effective PDT, functionalized NPs are often used in research to efficiently incorporate and deliver hydrophobic PS drugs into only specific target tissues/cells, whereby via light activation they only produce ROS in tumorous tissues, destroying only cancer cells and leaving healthy tissues unharmed (CALIXTO *et al.*, 2016), Figure 13.

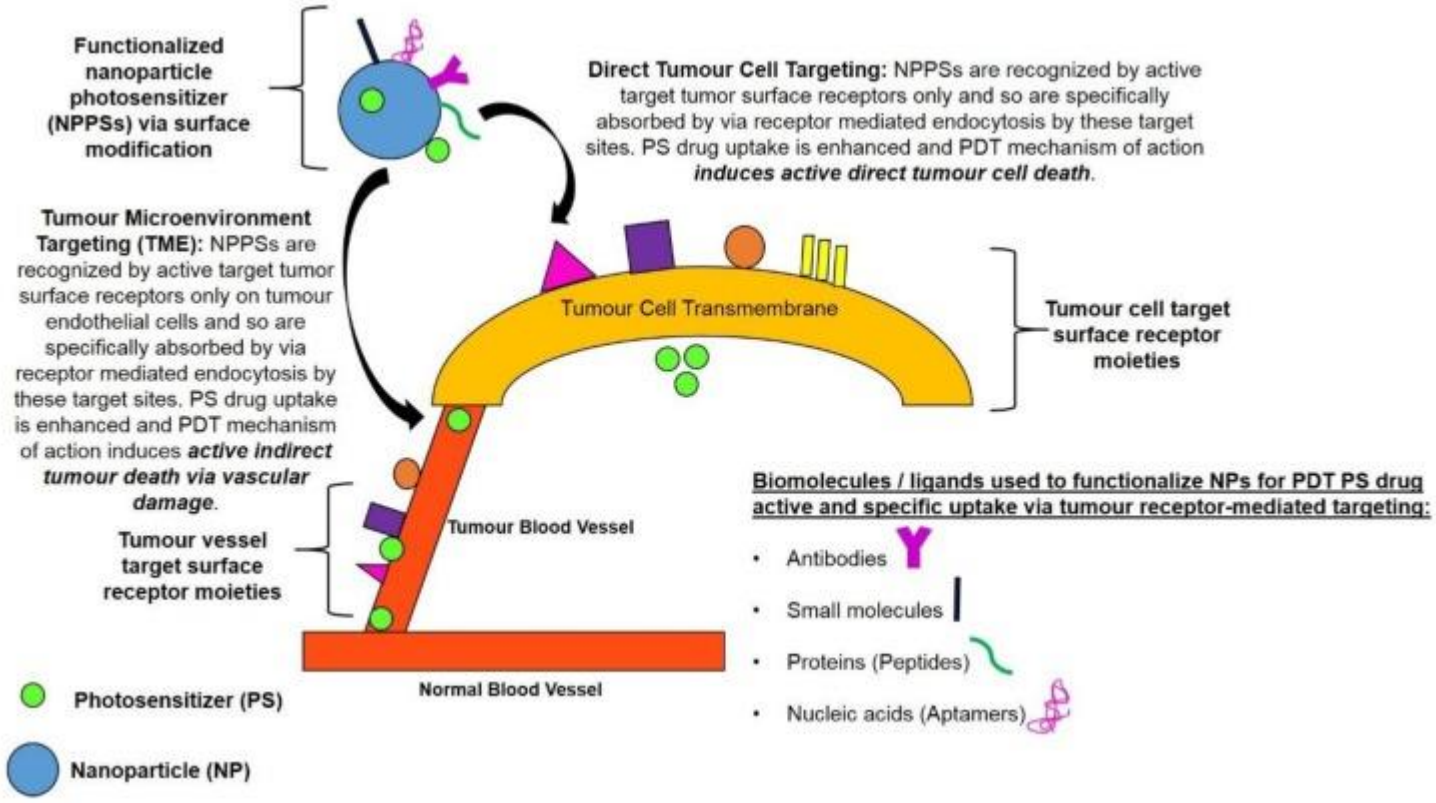

Figure 13 – Diagram showing the delivery of specifically active and targeted PS drugs to tumors via receptor-mediated targeting.

Several recent studies have shown that the application of molecules such as folic acid (EBRAHIMNEJAD *et al.*, 2022), biotin (LI *et al.*, 2017), hyaluronic acid (SODAGAR TALEGHANI *et al.*, 2019), and macromolecules like monoclonal antibodies (IANNAZZO *et al.*, 2017) that have specific receptors on the surface of cancer cells as active targeting can target cancer cells. These ligands bind to specific receptors on the surfaces of the target cells, so they can effectively increase the concentration of phototherapeutics in the tumor area, enhance cellular uptake of drug-loaded nanocarriers, greatly reduce the adverse effects of the drug and thereby improve therapeutic efficacy (SHIRAZIAN *et al.*, 2021).

Transferrin receptors, for example, are overexpressed in breast cancer. Regarding this, Jadia et al. (JADIA *et al.*, 2018) functionalized prepared nanoparticles containing the drug benzoporphyrin monoacid with a peptide (hTf) that can bind to transferrin receptor. As expected, functionalized nanoparticles exhibited specificity to the cell line (triple-negative breast cancer) and enhanced the phototoxicity compared to non-functionalized nanoparticles.

Hyaluronic acid (or hyaluronan) (HA) is a polysaccharide that is found within extracellular body fluids and is responsible for cellular growth, differentiation, and migration

in normal body cells (GAO *et al.*, 2017). However, HA is often found to be elevated in various types of tumor cancer cells and so gives them the ability to invade and metastasize in other tissues. Recently, researchers have started to investigate HA as a targeting moiety for NP PS enhanced drug delivery in PDT, since it can specifically bind to various cancer cells that over-express glycoprotein CD44 which is a HA tumor receptor (ABRAHAMSE *et al.*, 2017; GAO *et al.*, 2017; KYDD *et al.*, 2017; YANG; GAO, 2017).

Kesharwani et al. (KESHARWANI *et al.*, 2022) used a similar strategy to target nanoparticles to CD44 expressing cancer cells. HA nanoparticles modified with acrolac acid were seen to be internalized by squamous carcinoma cells in vitro which was attributed to overexpression of CD44 on the surface. In vivo, based on fluorescence originating from the tumor, HA nanoparticles concentrated in the region of the tumor indicating high tumor specificity for CD44 expressing tumors. Unmodified HANPs were not as effective and were cleared out in an hour thus proving HA modification to be a necessary step to provide longer half-life and effective targeting abilities (KESHARWANI *et al.*, 2022)

Effective tumor-targeting PDT using Ce6-loaded hyaluronic acid (HA) nanoparticles (Ce6-HANPs) was also investigated as described in (Figure 14) (YOON *et al.*, 2012). Ce6-HANPs showed stable structural integrity in aqueous conditions and rapid cellular uptake into cancer cells. Moreover, rapid biodegradation of Ce6-HANPs by hyaluronidases abundant in cytosol of cancer cells was observed implying efficient intracellular release of Ce6 at the tumor tissues.

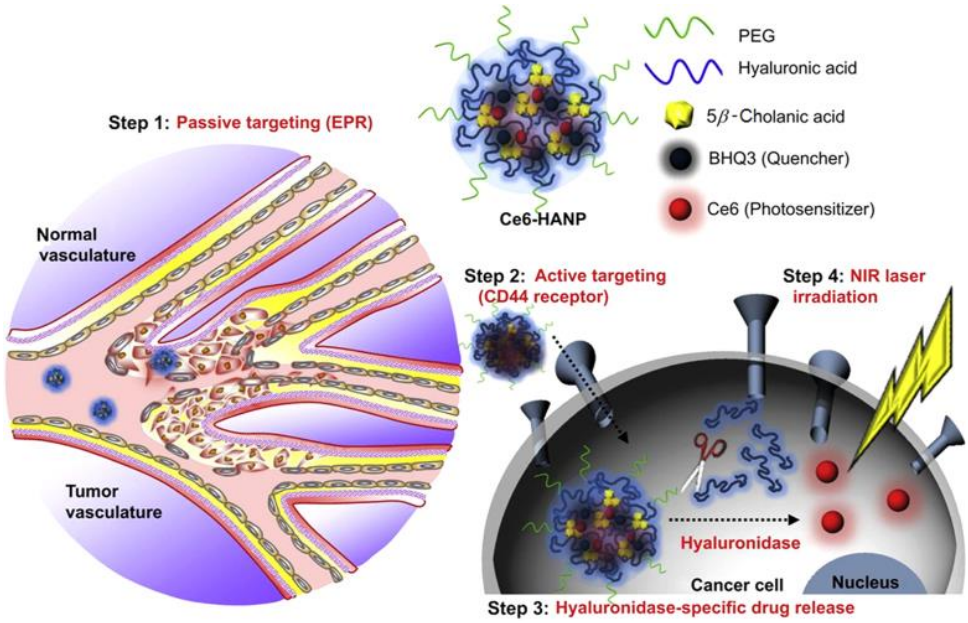

Figure 14 – Schematic illustration of Ce6-loaded HANPs for combined fluorescent imaging and targeted photodynamic therapy. Source: (YOON *et al.*, 2012)

Intravenously injected Ce6-HANPs into tumor-bearing mice efficiently targeted the tumor tissue *via* the enhanced permeability and retention (EPR) effect – the property characterized by an increased accumulation of macromolecules, such as liposomes, drugs, and NPs in tumors versus in normal tissues – and readily entered tumor cells through HA receptor–mediated endocytosis. It was observed that Ce6 released from the HANPs could generate singlet oxygen inside tumor cells under 671 nm light irradiation for PDT, simultaneously generating fluorescence for *in vivo* imaging (YOON *et al.*, 2012).

A protein that is also used in studies is Bovine Serum Albumin (BSA). BSA is a protein that has a high affinity for receptors expressed in cancer cells, which allows a greater accumulation of nanoparticles in tumor regions, increasing the selectivity and effectiveness of the treatment (KARIMI *et al.*, 2016a). In a study by Guindani et al., (2019) the surface of poly(globalide-co-ε-caprolactone) (PGlCL) nanoparticles containing double bonds in the main polymer chain is covalently functionalized with bovine serum albumin (BSA) by thiol-ene chemistry, producing conjugates which are resistant to dissociation. The successful formation of the covalent conjugates was confirmed and the presence of a protein layer surrounding the NPs can be observed. After conjugation with BSA, NPs present reduced cell uptake by HeLa and macrophage RAW264.7 cells, in comparison to uncoated NP. These results demonstrate that it is possible to produce stable conjugates by covalently binding BSA to PGlCL NP through thiol-ene reaction (GUINDANI *et al.*, 2019).

With the same protein, in another study by Guindani et al., (2019) the conjugation of BSA, poly(methyl methacrylate) (PMMA) NPs were conjugated by a non-covalent method, was also evaluated. The successful conjugation of BSA to PMMA NPs was confirmed by a set of different techniques, such as dynamic light scattering, zeta potential, transmission electron microscopy, Lowry protein quantification assay and flow cytommacroetry. Cell uptake assays showed that the conjugation of BSA on PMMA NPs increased cellular uptake by HeLa cells in comparison to uncoated PMMA NPs, which is an important feature for successful drug delivery applications. These results were important evidence that it is possible to control the interaction of nanocarriers with cells, by designing a pre-formed protein corona through simple non-covalent conjugation (GUINDANI *et al.*, 2019).

2.4.4.2 STIMULLI- RESPONSIVE CHARACTERISTICS

In addition, nanoparticles have potential for further engineering and can be successfully used to exploit the cancer microenvironment to design stimulus-responsive drug delivery systems, including responsive to pH, light, redox, temperature, ultrasound, enzymes, magnetic field, and multi-responsive systems for selective delivery of drugs and genes to prevent the emergence of multidrug-resistant cancers (KESHARWANI *et al.*, 2019), as can be summarized in the following Figure 15.

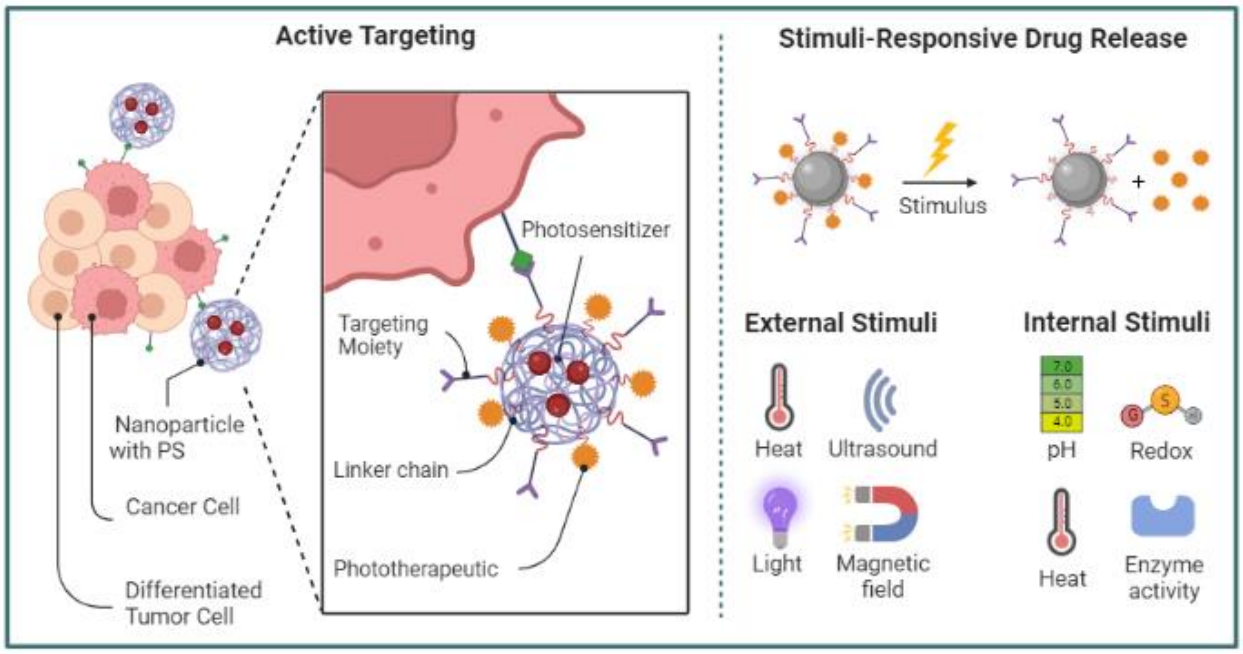

Figure 15 - Delivery Mechanism of Nanoparticle-mediated to Cancer Cells and their stimuli-responsive characteristics.

Stimuli-responsive nanoparticles are designed to respond to specific triggers or stimuli in their surrounding environment (CHANG *et al.*, 2021). These nanoparticles possess unique properties that allow them to undergo changes in structure, behavior, or release profile in response to external or internal cues. This characteristic enables precise control over drug delivery, release, and therapeutic activity, making stimuli-sensitive nanoparticles highly attractive for various biomedical applications (CHANG *et al.*, 2021).

There are several types of stimuli that can be utilized to trigger the response of nanoparticles, including pH, temperature, light, enzymes, and magnetic fields. Each stimulus has its advantages and can be tailored to the specific requirements of the application. Here, we discuss some of the commonly used stimuli and their applications in stimuli-sensitive nanoparticles (MI, 2020).

pH-Responsive Systems: pH-responsive systems are widely used to achieve triggered drug release within the acidic tumor microenvironment. Polymeric nanoparticles can be designed using pH-sensitive polymers. These changes facilitate the release of encapsulated photosensitizers or therapeutic agents, improving treatment efficacy (KARIMI *et al.*, 2016b). A pH-sensitive nanoparticles of polycaprolactone (PCL) co-delivers Fe-TPP and DOX. PCL was modified with histidine, which coordinates with PEGylated Fe-TPP via metal-coordinated interaction. This interaction leads to the formation of supramolecular assemblies, on which DOX can be loaded. In the acidic intracellular microenvironment, this metal-coordinated interaction is reduced, which releases the drug and photosensitizer subsequently. The *in vitro* teston HeLa and MCF-7 cells show enhanced killing effects (HAK *et al.*, 2021). Another study that evaluated pH responsiveness was Wang et al., they developed an intelligent polymer drug vehicle (Mal-PAH-PEG-DMMA/ poly (ethylene imine (PEI)) – poly(ε-caprolactone (PCL)) block polymers, MPPD/PEI-PCL) based on pH-responsive to deliver docetaxel (DTX) and photosensitizer (IR825) for photothermal combination therapy (MPPD@IR825/DTX NPs). MPPD@IR825/DTX NPs could undergo charge conversion in a slightly acidic microenvironment (pH 6.8), resulting in strong electrostatic repulsion to withdraw the shell of the polymer nanoparticles (MPPD), enhanced cellular uptake, and increased drug release. MPPD@IR825/DTX NPs presented nanometric sizes, monodisperse size distribution, and stability, triggered DTX release in response to acidic environment and NIR stimulation, at the same time providing excellent photothermal conversion efficiency. In vitro and in vivo experiments confirmed that charge-reversal polymeric nanoparticles improved antitumor efficiency in 4T1 tumor cell modal than non-charge-reversal polymeric nanoparticles. Furthermore, in comparison with photothermal therapy in a single treatment mode, photothermal combination therapy of MPPD@IR825/DTX NPs with laser irradiation showed highly efficient tumor ablation. In addition, the polymeric nanoparticles exhibited good biocompatibility and safety (WANG *et al.*, 2022).

Light-Responsive Systems: Light-responsive systems offer precise spatiotemporal control over drug release or localized photothermal therapy. Polymeric nanoparticles can be functionalized with photoactive moieties or plasmonic nanoparticles that absorb specific wavelengths of light. Upon light irradiation, these nanoparticles generate heat or undergo photothermal conversion, resulting in triggered drug release or localized hyperthermia, respectively (SCHOPPA *et al.*, 2021). Such systems allow for targeted therapy and minimize damage to healthy tissues. Shoppas et al. (2021) developed a redox and photo dual-responsive,

folate receptor-targeted nanourchin carriers for chemo, photodynamic, and photothermal therapy prepared by the amalgamation of an outer layer of polyethylene glycol (PEG)-S-S-methotrexate (MTX) and an inner core of indocyanine green (ICG)-loaded bismuth sulfide (Bi_2S_3). MTX introduces the carrier to folate receptors resulting in the internalization of nanoparticles into cancer cells, specifically and increasingly. In the reducing environment inside cancer cells, MTX was cleaved, resulting in a burst release that effectively inhibited tumor growth. Simultaneously, the fusion of Bi_2S_3 and ICG in the inner core absorbed energy from a near-infrared radiation (NIR) laser to generate heat and reactive oxygen species, which further ablated the tumors and synergistically enhanced the anticancer activity of MTX. These results indicate the successful preparation of combined nanourchins (Nus) showing GSH-induced and laser-responsive release of MTX and ICG, accompanied by hyperthermia via Bi_2S_3 and ICG. Effective in vitro cellular internalization, cellular cytotoxicity, and pro-apoptotic behavior of the nanoparticles were achieved through a targeting, redox, and NIR-responsive combination strategy. In vivo biodistribution and photothermal imaging also revealed tumor-selective and -retentive, as well as thermally responsive attributes. Ultimately, this in vivo antitumor study shows an effective tumor ablation by these nanourchins without affecting the vital organs. Their findings indicate that using these targeted redox- and laser-responsive combination therapeutic carriers can be a promising strategy in folate receptor-expressing tumors (SCHOPPA *et al.*, 2021)**.**

Temperature-Responsive Systems: Temperature-responsive systems use the temperature difference between the tumor and normal tissues to trigger drug release (ABUWATFA *et al.*, 2022). Thermosensitive polymers, such as poly(N-isopropylacrylamide) (PNIPAAm) (XU *et al.*, 2020), undergo reversible sol-gel phase transitions in response to temperature changes. Below the lower critical solution temperature (LCST), the polymer is hydrated and swells, while above the LCST, it collapses and forms a gel-like structure, leading to drug release (XU *et al.*, 2020). This approach provides precise control over drug release in response to local temperature changes.

In summary, stimuli-responsive systems for polymeric nanoparticles in phototherapy applications offer controlled drug release, spatiotemporal selectivity, and targeted therapy. pH-responsive, light-responsive, temperature-responsive systems provide strategies to improve the performance of polymeric nanoparticles in phototherapy.

2.5 STATE OF ART APPLIED TO THE THESIS THEME

The encapsulation of photosensitizers in polymeric nanoparticles has shown to be a promising strategy to improve the efficacy and safety of phototherapy in the treatment of several diseases, especially in the field of oncology (XIA *et al.*, 2021).

Polymeric nanoparticles are systems that allow the incorporation of photosensitizers into their interior. These photosensitizers are substances capable of generating reactive oxygen species when activated by light of a specific wavelength, resulting in the induction of selective RIZI death of tumor cells. Encapsulating these agents in nanoparticles protects them from early degradation, ensuring they remain intact and active until they reach their desired target, reducing toxicity to surrounding healthy cells (YOUSEFI RIZI *et al.*, 2022).

Proper selection of polymeric materials used in nanoparticles is essential to ensure the biocompatibility, stability, and targeting of particles to tumor tissues. In addition, it is possible to functionalize the surface of nanoparticles with specific molecules that increase selectivity for cancer cells, further improving therapeutic targeting. Polymeric nanoparticles also allow precise control of the release of photosensitizers and respond to internal and external stimuli in the tumor microenvironment, enabling a more effective and personalized therapy, as it extends the time of exposure and deactivation of nanoparticles in the body (MITCHELL *et al.*, 2021).

2.5.1 BIODEGRADABLE POLYMERS: ALIPHATIC POLYESTERS

Recently, the field of polymer science has made great strides in transforming the use of biodegradable polymers as an environmentally friendly alternative to conventional plastics. These changes have led to the widespread use of these materials in important biomedical fields (MCBRIDE; GILLIES, 2013). Biodegradable polymers are characterized by chemical and physical degradation under certain conditions, leading to complete degradation (ABHILASH; THOMAS, 2017). In addition, these polymers must remain biologically inert and must not produce harmful substances during degradation.

Biodegradable polymers encompass a range of polymer structures that undergo hydrolytic or enzymatic cleavage, ultimately breaking down into soluble byproducts (ATANASE *et al.*, 2022; TIAN *et al.*, 2012; TSCHAN *et al.*, 2012). These polymers can be derived from natural sources such as polysaccharides, proteins, and bacterial polyesters, or they can be synthetically produced, including polyamides, polyureas, polyurethanes, polyesters, polyethers, polyanhydrides, and polypeptides. The degradation characteristics of these polymers, along

with their physical properties, are influenced by various factors, such as the chemical composition of the polymer backbone, molecular weight, dispersity, and crystallinity (TSCHAN *et al.*, 2012).

Aliphatic polyesters have emerged as highly appealing biodegradable polymers for biomedical applications due to their ease of synthesis, tunable properties, and excellent biocompatibility (POLLONI *et al.*, 2020; TIAN *et al.*, 2012). These characteristics position them as sustainable alternatives comparable to conventional materials like polyethylene (PE) (GONÇALVES *et al.*, 2017; KOBAYASHI, 2010; WILSON *et al.*, 2019). Among the commonly used synthetic polyesters in biomedicine are poly(lactic acid), poly(glycolic acid), poly(lactic-co-glycolic acid), and poly(ε-caprolactone) (PCL) (ATANASE *et al.*, 2022; URBÁNEK *et al.*, 2019).

2.5.2 POLYMERS FROM MACROLACTONES

Aliphatic polyesters were initially developed by the condensation polymerization of hydroxyl acids or diacids and diols (FLORY, 1946; WILSON *et al.*, 2019). Condensation polymerization, on the other hand, has certain limitations, including the necessity for extensive monomer purification, precise stoichiometry, and high reaction temperatures that might result in unwanted side reactions (WILSON *et al.*, 2019). To produce aliphatic polyesters, three different polymerization processes may be used: (1) ring-opening polymerization (ROP) of cyclic ketene acetals, (2) stepgrowth polymerization of lactones, and (3) ROP of lactones. When compared to ROP of lactones, the first two processes have disadvantages, such as limited selectivity and rather large molecular weight distributions (LECOMTE; JÉRÔME, 2011). As a result, several instances of either live or controlled polymerization applying this process and various types of catalysts and initiators have been described, allowing the production of high molecular weight aliphatic polyesters with low molecular weight dispersity.

Considering that macrolactones (composed of 12 or more carbon atoms) have minimal ring tension, the entropic gain that comes from ring opening is the fundamental driving aspect behind the ROP. This allows for less impeded chain rotation, resulting in a minor enthalpic benefit (WILSON *et al.*, 2019). Slower kinetics are seen when organometallic catalysts are employed to polymerize macrolactones, and polymers with low molecular weight are frequently generated (DUDA *et al.*, 2002). Thus, in such cases, enzymatic ring-opening polymerization is a better alternative.

Macrolactones are frequently employed in the pharmaceutical and chemical industries to enhance the scent or fragrance of various products. Macrolactones containing 14 – 16 carbons are particularly notable for their musk-like odor and are often found in natural sources such as plants and animal hormones (CHIARADIA, 2019). Furthermore, macrocyclic polyesters have been extensively studied for their potential use in synthesizing biodegradable polymers (POLLONI *et al.*, 2017).

The application of enzymes as biological catalysts in ring-opening polymerization reactions (e-ROP) is an excellent demonstration of how the polymerization process may be enhanced by producing cleaner, which is required by modern biomedical applications (CHIARADIA *et al.*, 2018). Enzymatic polymer synthesis reactions have high chemoselectivity, regioselectivity, mild reaction conditions regarding temperature, pressure, and pH, and low energy consumption (KOBAYASHI, 2010; SULMAN *et al.*, 2019).

Furthermore, these polymerizations proceed in mild reaction conditions without the use of toxic substances, which contributes to sustainable production techniques and easy catalyst recyclability (POLLONI *et al.*, 2018).

Novozym 435 (NZ435), an immobilized lipase B from Candida Antarctica, is one of the most widely utilized lipases in enzymatic polymerization for the synthesis of polyesters including macrolactones (POLLONI *et al.*, 2017; VAN DER MEULEN *et al.*, 2008, 2011; ZHANG *et al.*, 2014). There is a wide range of publications on its activity and catalyst efficiency available in the literature, and the use of these biological catalysts has attracted interest in the biomedical area, for example, as an option to decrease toxicity concerns (GUINDANI *et al.*, 2017). NZ435 also demonstrates thermosetting immobilization and considerable activity in a wide range of organic solvents (ZHANG *et al.*, 2014).

Aliphatic polyesters are highly versatile and exhibit excellent mechanical properties, hydrolyzability, and biocompatibility, making them top contenders in the biomedical and pharmaceutical industries. They can be used as resorbable implant materials as well as components of controlled drug delivery systems and other medical applications (ALBERTSSON; VARMA, 2003). Over the last decade, researchers have extensively investigated the potential of using polyesters made from macrolactones as biodegradable carriers for biomedical applications (MANAVITEHRANI *et al.*, 2016). Despite their inherent potential, the homopolymers of macrolactones are generally poorly biodegradable/bioresorbable due to their semi-crystalline structure and high hydrophobicity (VAN DER MEULEN *et al.*, 2011).

Among the most recently investigated macrolactones, Globalide has aroused interest due to its potential biomedical application. It is an unsaturated, biocompatible and non-toxic macrolactone, widely used in the perfumery industry, which has 15 carbon atoms and a double bond in position 12 or 13 (VAN DER MEULEN *et al.*, 2008). As a result of its nature, globalide is easily polymerizable by e-ROP, and it has been investigated for its modification/functionalization potential (presence of double bonds in the main polymer chain), adaptability, and biomedical material synthesis applications (CHIARADIA *et al.*, 2019; DE OLIVEIRA *et al.*, 2017; GUINDANI *et al.*, 2019; POLLONI *et al.*, 2020; VAN DER MEULEN *et al.*, 2008).

2.5.3 DOUBLE EMULSION WITH SOLVENT EVAPORATION METHOD

Emulsions are compositions of two or more liquids that do not dissolve in each other, with one or more liquids dispersed through another. Water-in-oil (W/O), oil-in-water (O/W), oil-in-water-in-oil (O/W/O), and water-in-oil-in-water (W/O/W) emulsions are often used in pharmaceutical applications (JENJOB *et al.*, 2019). Colloidal dispersions include emulsions, miniemulsions (or nanoemulsions), and microemulsions, in which one component (the dispersed phase) is dispersed in another substance (the continuous phase). They differ in the size of the dispersed phase droplets and the methods employed for producing them, though (JAISWAL *et al.*, 2015).

The selection of a specific technique for an efficient drug encapsulation is generally determined by the hydrophilicity or hydrophobicity of the drug molecules (JELVEHGARI; MONTAZAM, 2012). The double emulsion technique is an appropriate method often used for the encapsulation of hydrophilic molecules, in which first, the aqueous phase is dispersed in an immiscible polymer-containing organic solvent to form a primary emulsion (W_1/O), followed by homogenization of the primary emulsion into the external aqueous phase (W_2) containing emulsifier to obtain the double emulsion using high shear homogenizer. Subsequently, evaporation of the organic solvent from the emulsion (IQBAL *et al.*, 2015b; PALAMOOR; JABLONSKI, 2014).

The double emulsion process is very versatile and can be used to manufacture various types of polymeric particles, including nanoparticles with hollow structures (IQBAL *et al.*, 2015b). The emulsion droplets can be used as templates for further processing to form core-shell nanostructures by emulsifying the dispersed phase containing the polymer into the outer

aqueous phase and then removing the organic solvent by evaporation or diffusion, leaving the polymeric dispersion (JELVEHGARI; MONTAZAM, 2012).

Double emulsion is a two-step emulsification process that usually requires two surfactants, a low HLB one, designed to stabilize the first emulsion (W1/O), and another of high HLB for the second emulsion (O/W2) (BECKER PERES *et al.*, 2016). Stabilizers make it possible to maintain the physicochemical state of dispersion of two or more immiscible phases and prevent the separation of phases, thus making the emulsion system more stable. The commonly used stabilizers in the double emulsion process include PVA, Tween 80, and Span 80. However, polyvinyl alcohol (PVA) is one of the most frequently used stabilizers in the double emulsion process for the encapsulation of different active moieties (LIU *et al.*, 2005; RIZKALLA *et al.*, 2006). It is a well-known hydrophilic, biocompatible polymer and possesses good mechanical strength, low fouling potential, and lasting temperature stability and pH stability. These properties of PVA make it a suitable candidate to be used in the encapsulation of various pharmaceuticals and biopharmaceuticals (XIA; XIAO, 2012).

Ultrasonic emulsification is an efficient method to obtain a finely dispersed emulsion; typical results are comparable to the best high-pressure homogenizers (AGNER *et al.*, 2017; TAHA *et al.*, 2020). The advantages of ultrasound include lower energy consumption, production of a more homogeneous emulsion, with a smaller droplet size, and a more stable emulsion compared to mechanical homogenization using less surfactant (TAHA *et al.*, 2020). Several parameters affect the ultrasonic emulsification process, including hydrostatic pressure, continuous phase viscosity, oil/water ratio, surfactant concentration, ultrasonic horn position at the oil-water interface, ultrasonic power, and tip exposure time (AWAD *et al.*, 2012; MENDOZA-MUÑOZ *et al.*, 2016).

2.5.4 INDOCIANIN GREEN AND DOXORUBICIN DRUGS

Indocyanine green (ICG) is a non-toxic anionic indotricarbocyanine derivative with a molecular weight of 774.96 g composed of two totally lipophilic polycyclic structures (bezoindotricarbocyanine), linked by a carbon chain (DESMETTRE *et al.*, 2000). Its chemical structure is shown in Figure 16.

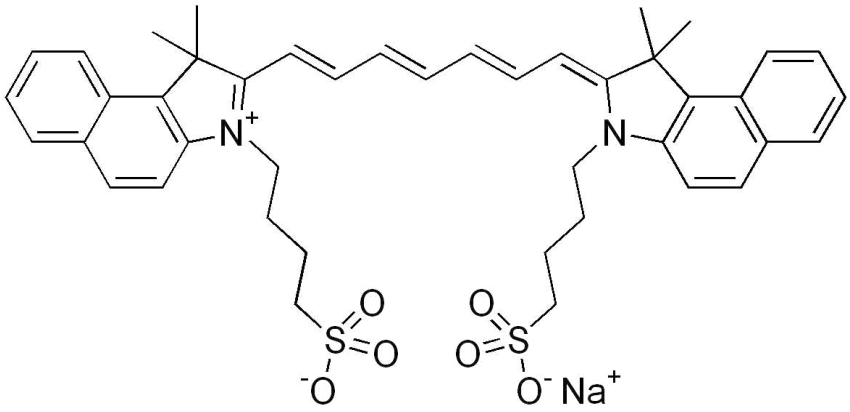

Figure 16 - ICG Chemical structure

Due to the negative charge of sulfonic groups, ICG presents amphiphilic character, which means that it has a hydrophilic part (affinity for water) and a hydrophobic part (affinity for non-polar substances), with a propensity to self-aggregate at low micromolar concentrations in water, and its logP has been measured to be 1.81 ± 0.06 when the aqueous phase is phosphate buffer (100 mM, pH 7.4) (GAMAGE; SMITH, 2022)- the LogP (octanol-water partition coefficient) is a measure of the hydrophobicity or lipophilicity of a molecule, which is related to its affinity for organic or aqueous systems. Molecules with higher LogP values tend to be more lipophilic and less soluble in water. This solubility in water provides a good characteristic for the application of ICG as a photosensitive drug, as it allows relative stability of the drug when in aqueous solution and can be administered rather quickly intravenously (COSTA *et al.*, 2001). Another important feature is that ICG is a relatively large molecule, and can bind to plasma proteins such as albumins, globulins, and mainly to lipoproteins, allowing to improve the penetration of pigments in the ocular regions, in hemorrhages and fluids, exhibiting selective retention in the abnormal neovessels of the choroid and around them, not interacting with the epithelial spaces (MORDON *et al.*, 1998).

ICG is a widely investigated contrast agent and is approved by U.S. Food and Drug Administration (FDA) for diagnostic imaging in humans (KIM *et al.*, 2010; SAXENA *et al.*, 2004b). Being a fluorescence dye, when being irradiated, ICG strongly absorbs light at 780 nm and emits light at 820 nm (ALTINOĞLU *et al.*, 2008; ZHENG *et al.*, 2011). This absorption region allows the light beam to adequately penetrate the tissues without interference from blood constituents, ensuring greater drug activation capacity. ICG has shown excellent thermal properties. When irradiated by light, ICG absorbs light and converts it into heat, which can be used for photothermal treatments (ZHENG *et al.*, 2011). Hence, photodynamic therapy using ICG serves as a promising method for the destruction of tumors (KIM; DARAFSHEH, 2020;

TANG; MCGORON, 2009; ZHENG *et al.*, 2011). However, ICG is prone to aqueous instability and photo-bleaching, has a low quantum yield, and is not target specific, all of which limit its applicability for prolonged target specific applications (SAXENA *et al.*, 2004b; XU *et al.*, 2009).

In recent years, biodegradable-biocompatible, FDA-approved PLGA carriers are one of the most common particulate systems employed to enhance ICG for quantitative imaging and therapeutic applications (GOMES *et al.*, 2006; SAXENA *et al.*, 2004b; XU *et al.*, 2009). PLGA nanoparticles are associated with enhanced permeation and retention (EPR) effect that allows passive targeting from the bloodstream into the tumor site. In addition, targeting ligands can be conjugated to PLGA nanoparticles to make them cancer specific (GOMES *et al.*, 2006; SAXENA *et al.*, 2004b; XU *et al.*, 2009). ICG encapsulation protects ICG from aggregation and protein interaction, thereby stabilizing its optical characteristics. It not only preserves the aqueous, thermal, and photo-stability of ICG but also increases the circulation half-life to ∼14 min, which is three to seven times more than that of free ICG (SAXENA *et al.*, 2004a).

ICG can be used for destroying superficial tumors by photodynamic (PDT) and photothermal (PTT) therapy. Studies with ICG showed its in vitro absorption by cancer cells and efficient photodynamic/photothermal effect (ABELS *et al.*, 2000; FICKWEILER *et al.*, 1997).

Table 3 - Studies that have been encapsulating ICG in polymeric nanoparticles by Double Emulsion with Solvent Evaporation

Polymer	Photosentisizer	Reference
PLGA	Indocyanine Green and PIN	(PATEL *et al.*, 2012)
PLGA	Indocyanine Green	(WANG, S. *et al.*, 2019)
PLGA	Indocyanine Green	(SHI et al., 2013)
PLGA-PEG-PCL	Indocyanine Green and Arginine	(SUN *et al.*, 2021)
PLGA	Indocyanine Green and Doxorubicin	(SHEN *et al.*, 2019)
PLGA- PEG	Indocyanine Green and Paclitaxel	(LIU et al., 2018)

In addition, the use of different encapsulation methods allows obtaining particles with specific characteristics, such as size, morphology, controlled release, and stability, expanding

the application possibilities of these nanostructured systems in several areas of materials science and medicine.

Doxorubicin (also known as adriamycin) and Doxorubicin hydrochloride are two forms of the same active substance, used in different formulations for drug delivery. The main difference between them is the salt form and water solubility. Doxorubicin in its pure form is relatively insoluble in water, hydrophobic, which makes intravenous administration difficult. The addition of the hydrochloride increases the solubility, making it suitable for medical use, allowing it to be administered intravenously more easily. Both forms have the same base molecule, with similar functional groups (MOHAN; RAPOPORT, 2010).

Thus, Doxorubicin hydrochloride (DOX) (Figure 17), used in this study, is a hydrophilic drug used in a wide variety of clinical applications, one of the most effective antitumor drugs for solid tumors including breast, ovarian, lung, and prostatic cancers (MOHAMMADI ABANDANSARI *et al.*, 2018; PRADOS *et al.*, 2015; WAKHARDE AA, 2018). Doxorubicin alone or in combination with other photossensitizer is a common first-line therapy for numerous cancers including breast, ovarian, bladder, and lung (PRADOS *et al.*, 2012).

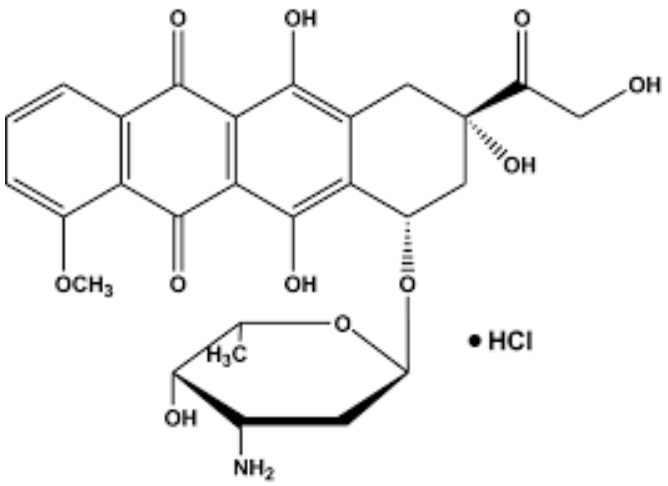

Figure 17 - Structural formula of Doxorubicin hydrochloride.

Although the mechanism of action for DOX is still being studied, proposed mechanisms include intercalation into DNA disrupting gene expression, generation of reactive oxygen species, and inhibition of topoisomerase II, a gyrase important for DNA synthesis and replication (CHATTERJEE *et al.*, 2010).

Doxorubicin, from the anthracycline family that is widely used in breast cancer chemotherapy (GUDKOV *et al.*, 1993; HENDERSON; CANELLOS, 1980), inhibits

topoisomerase II (topo II), a key enzyme in DNA replication (YU *et al.*, 2007). Doxorubicin acts by intercalating into DNA, thereby inhibiting macromolecular biosynthesis (WANG *et al.*, 2010). However, one of the inherent problems of DOX-based chemotherapy is that this anticancer agent does not specifically target breast cancer cells but affects healthy tissue as well, thus causing toxicity and adverse effects that limit the maximum tolerable dose of the drug (WU *et al.*, 2011). DOX is known to be cardiotoxic and its use can lead to the development of cardiomyopathy, which sometimes does not respond to common medications and can progress to biventricular failure and even death (WU *et al.*, 2011). To avoid these complications, new forms of drugs with optimized pharmacokinetics and pharmacodynamics that specifically target the tumor are under development. In this respect nanoparticles, are currently being investigated as possible candidates (WANG *et al.*, 2010).

Diverse types of nanoparticle drug carriers have been developed and tested for systemic delivery and release of DOX at the tumor site. Chitosan is a linear biodegradable polysaccharide in which NPs have been formulated to deliver chemotherapy (KAMRA VERMA *et al.*, 2018; MITRA *et al.*, 2001) and nucleic acids (MANSOURI *et al.*, 2006). In an early study, the group of Maitra incorporated a dextran-DOX conjugate into chitosan nanoparticles (MANSOURI *et al.*, 2006). They compared conventional “free” DOX, the dextran conjugate alone, and the chitosan-dextran conjugate NP groups for reducing tumor size (subcutaneously implanted J774A.1 macrophage tumor) and prolonging survival in Balb/c mice. Treatment was initiated when the tumor size was about 200 mm^3 and 4 weekly intravenous dosages were administered. The NP group (16 mg/kg/dose) was the most effective with about a 50% regression in tumor size at day 90 compared to a maximum size at day 45. Moreover, the group treated with the nanoparticle had prolonged survival with 50% of the mice alive at day 90. In contrast, all mice in the free DOX group died by day 60, and only 25 % of mice in the dextran-conjugate group survived by day 90 (MITRA *et al.*, 2001) Similarly, a recent study found that DOX-loaded chitosan NP markedly inhibited tumor growth and prolonged survival of mice compared to free Dox (KAMRA VERMA *et al.*, 2018). Notably, in both studies, there was little to no evidence of toxicity observed in mice that received the DOX-loaded chitosan NPs. Loading of doxorubicin in nanoparticles increases its bioavailability and anti-tumor activity, DNA affinity and reduces its severe adverse effects (GOMARI *et al.*, 2019; MIRZAEI-KALAR *et al.*, 2020; SINGH *et al.*, 2019).

2.5.5. SURFACE FUNCTIONALIZATION WITH BOVINE SERUM ALBUMIN

BSA can act as a stabilizing agent for nanoparticles, preventing their aggregation and maintaining their colloidal stability. This is particularly crucial in applications where nanoparticles need to be dispersed in solution for an extended period (ZUO *et al.*, 2015). By conjugating BSA on the surface of nanoparticles, it can enhance their biocompatibility and reduce potential adverse effects when interacting with biological environments, such as cells, tissues, or organisms, and provides a platform for attaching specific ligands or antibodies (SPADA *et al.*, 2021). When nanoparticles are introduced into biological fluids, proteins present in the surrounding environment can adsorb onto their surface, forming a protein corona. The composition and characteristics of the protein corona can influence the biological interactions and behavior of nanoparticles (CORBO *et al.*, 2016).

Overall, conjugating BSA on the surface of nanoparticles through adsorption offers benefits such as stability, biocompatibility, modulation of the protein corona, targeting capabilities, and ease of functionalization. These factors contribute to improved performance and functionality of nanoparticles in various biomedical applications (SPADA *et al.*, 2021).

In this way, the coencapsulation of doxorubicin and indocyanine green in functionalized polyglobalide nanoparticles presents an innovative concept. Although multiple investigations have deepened the capabilities of PGl polymer for biomedical applications, our approach takes a pioneering stance by starting with the enzymatic polymerization by ring opening of PGl in solution, already pre-established in the literature, later advancing to the preparation of PGl nanoparticles and the encapsulation of ICG and DOX drugs. Moving forward, the research revolves around surface functionalization of these nanoparticles via BSA adsorption, all with the overall goal of implementing a combined phototherapy strategy within a cutaneous melanoma cell line.

CHAPTER 03: ENCAPSULATION OF PHOTOSENSITIZER AND CHEMOTHERAPY AGENT IN POLY(GLOBALIDE) NANOPARTICLES FUNCTIONALIZED WITH BSA

3.1 INTRODUCTION

Future challenges in the field of polymer development are dependent on the discovery of new synthetic materials and methods that can enhance the features of polymers, customize their properties, lower costs, reduce their environmental impact, and lessen their toxicity (ATANASE *et al.*, 2022). For prospective applications in the biomedical industry, characteristics like biodegradability, bioresorbability, and biocompatibility are particularly appealing (GUINDANI *et al.*, 2017). Among the category of biodegradable polymers, aliphatic polyesters represent a broadly used class of materials, particularly in biomedical applications (SEYEDNEJAD *et al.*, 2011). According to Kobayashi (2010), Polloni et al. (2017a), and Wilson et al. (2019), long-chain aliphatic polyesters have properties such as high hydrophobicity and semicrystalline structure, as well as hydrolysis-based degradation, biocompatibility, and bioresorbability (KOBAYASHI, 2010; POLLONI *et al.*, 2017; WILSON *et al.*, 2019).

As a result, they are appealing alternatives for traditional polymers utilized in various applications. The ring-opening polymerization (ROP) of lactones is a typical process for producing several types of aliphatic polyesters in bulk or solution, with numerous potential purposes such as biomedical applications, food packaging, textiles and apparel, agriculture, adhesives and coatings, drug delivery, and environmental remediation. Numerous initiators and catalysts for the lactone polymerization process have been described in the literature (ALBERTSSON; VARMA, 2003; LECOMTE; JÉRÔME, 2011). Enzymes have been studied as a greener alternative to typical chemical catalysts in polymerization reactions. Specificity, high efficiency, reusability, low toxicity, and the necessity of mild reaction conditions are all benefits of enzymatic ring-opening polymerization (e-ROP) over chemical catalysis (CHIARADIA *et al.*, 2018; POLLONI *et al.*, 2017). One alternative of a reactant that could be used in combination with biocatalysis is globalide (Gl), a macrolactone composed of two isomers with 15 carbons containing a double bond in positions 11 or 12 (VAN DER MEULEN *et al.*, 2008). The resulting polymer, polyester poly(globalide) (PGl) was already synthesized by enzymatic route in several studies (CHIARADIA, 2019; DE OLIVEIRA *et al.*, 2017; GUINDANI *et al.*, 2019; VAN DER MEULEN *et al.*, 2008).

Regarding biomedical applications, polymeric nanoparticles have emerged as a highly promising approach for phototherapy due to their unique properties, which include high stability, biocompatibility, and the ability to encapsulate and transport photosensitizing agents (MISHRA *et al.*, 2019; TANG *et al.*, 2016). Incorporating drugs into nanoformulated systems, for example, can increase their quicker start of therapeutic effects, as well as controlled and targeted release at the specified place. This technique seeks to improve therapeutic efficacy while minimizing total treatment toxicity, hence increasing selectivity in attacking cancer cells (JOSEPH *et al.*, 2022; ROCHA *et al.*, 2014). ICG, a photosensitizer, and DOX, an effective chemotherapeutic, are widely used in photodynamic and photothermal therapy, in which they generate reactive oxygen species and cause an increase in temperature in the tumor microenvironment, increase specificity and selectiveness in tumor cells, and result in their apoptosis when activated by light of a specific length (WU *et al.*, 2022).

Combining photothermal and photodynamic therapy with chemotherapeutic action has a synergistic therapeutic effect, enhancing treatment against cancer cells at multiple stages of the cell cycle. Thus, encapsulating ICG and DOX in polymeric nanoparticles has multiple advantages, including the preservation of therapeutic compounds from early degradation, enhanced therapeutic efficiency, and reduced undesired adverse effects (KONG; CHEN, 2022). Polymeric nanoparticles can be functionalized, for example, with Bovine Serum Albumin, to increase their selectivity towards tumor cells, allowing for the selective accumulation of drugs in cancerous tissue (MUNDEKKAD; CHO, 2022). Among so many advantages, BSA is a protein that is naturally present in the blood and is highly biocompatible, which means it is easily absorbed by the human body and has a low potential for generating immunological or inflammatory reactions, in addition to the capacity to bind to expressed receptors in tumor cells and in the endothelial cells of the blood arteries that supply the cancers (KARIMI *et al.*, 2016b).

This work aims to present an innovative concept hitherto unexplored in the literature. Numerous studies have explored the potential of the PGl polymer for biomedical applications, so our approach starts with the synthesis of PGl using enzymatic ring-opening polymerization in solution and subsequently, we prepare PGl nanoparticles and encapsulate the ICG and DOX drugs. The next step involves the surface functionalization of these nanoparticles through BSA adsorption, with the final proposal of applying combined phototherapy in a cutaneous melanoma cell line.

3.2 MATERIAL AND METHODS

This section presents the methodology used. Scheme 1 shows a flowchart of the developed steps.

Scheme 1 - Flowchart of the developed steps in this work

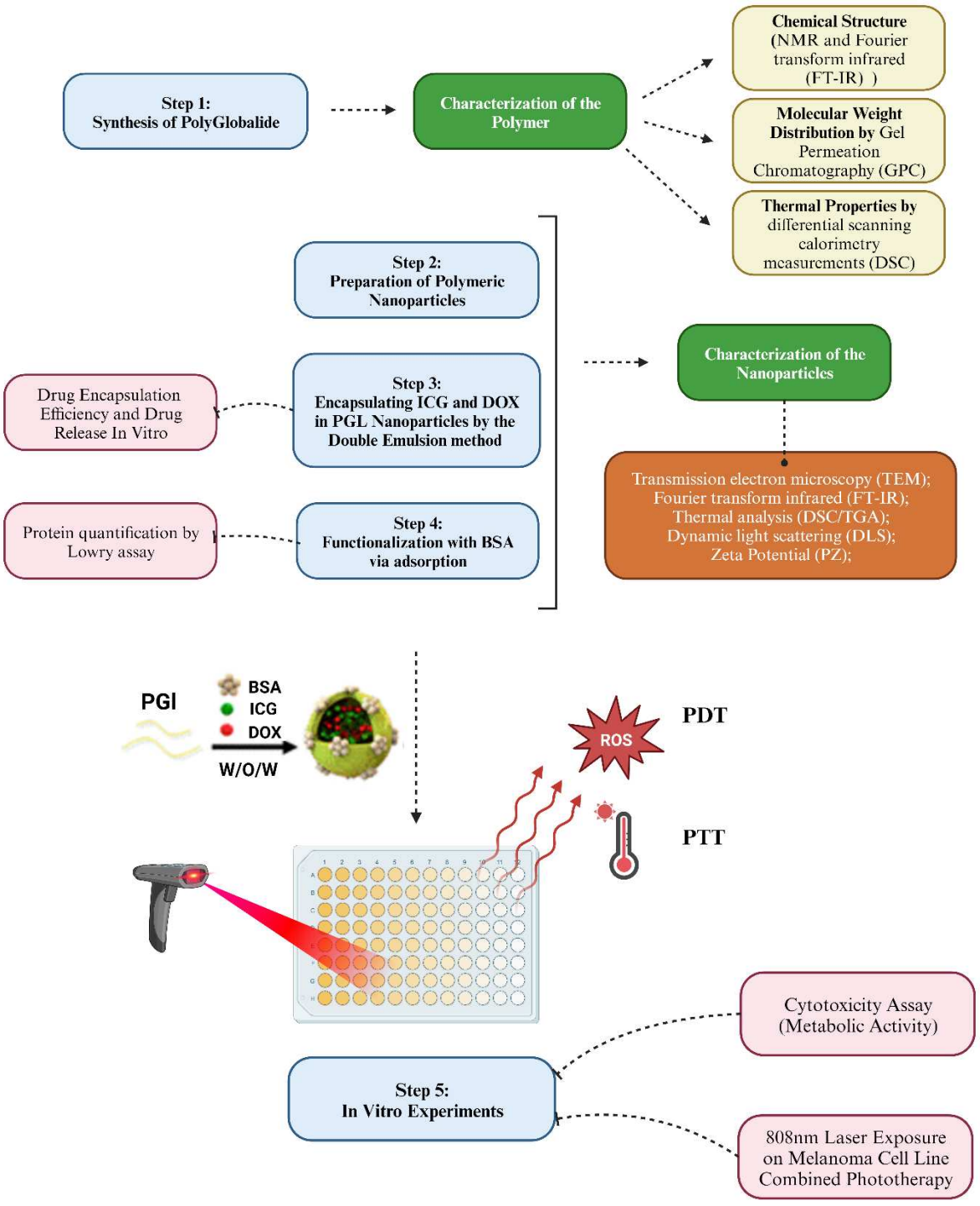

3.2.1 MATERIALS

The monomer globalide (90 % purity) was purchased from Symrise Aromas e Fragâncias LTDA (Brazil). Novozym 435 (commercial lipase B from *Candida antarctica* immobilized) was kindly donated by Novozymes S/A (Brazil). Chloroform (99.8%, Panreac), toluene (99.8%, Sigma-Aldrich), and Doxorubicin Hydrochloride (DOX, Eurofarma) were used as received. Dichloromethane (99.8 %, DCM) and ethanol (99.8 %, EtOH) were purchased from Synth (Brazil). Methanol (99.5 %, MetOH) and tetrahydrofuran (99,9 %, THF) were purchased from Neon Química (Brazil) and used as received. Indocyanine Green (ICG, 90 %, Toronto Research Chemicals) and Poly(vinyl alcohol) (PVA, 87-90%, 30-70 kDa, Sigma-Aldrich; 88%, 78.000Da, Polyscience). Murine cell line of fibroblasts (L929, Thermo Scientific, Brazil), Immortalized human SK-MEL-28 melanoma, PBS, for in vitro cell culture were cultivated in a culture medium containing sodium carbonate (Sigma Aldrich), penicillin-streptomycin (pens/strep), Dulbecco's Modified Eagle's medium (DMEM), fetal bovine serum (FBS). TrypLE Express Enzyme, phosphate buffered saline (PBS), CellTiter 96® Aquous One Solution (MTS [3-(4,5-dimethylthiazol-2-yl)-5-(3-carboxymethoxyphenyl)-2-(4-sulfophenyl)-2H-tetrazolium]) (Promega Biotecnologia do Brasil, Brazil), glutaraldehyde and formaldehyde were also used in several assays.

3.2.2 METHODS

3.2.2.1 SYNTHESIS OF POLYGLOBALIDE

Polyglobalide (PGl) was synthesized via enzymatic ring opening polymerization (e-ROP), as previously reported by works of the group that involved globalide homo-and copolymerization and other similar polyesters (CHIARADIA, 2019; GUINDANI *et al.*, 2017; POLLONI *et al.*, 2018), in a sealed glass vial at 65 ºC. Both globalide and the enzymes were dried under vacuum at 70 °C and 60 °C for 24 h, respectively, and stored in a desiccator over silica and 4 Å molecular sieves. After this, the enzyme (Novozym-435), monomer (Globalide), and toluene (solvent, when used) were weighed on a precision scale balance (Shimadzu ATX224, Philippines with 0.0001 g accuracy) in the reaction vial.

For the polymerization, the toluene solution of monomer (containing 66,6wt.% of globalide, 2:1 monomer (Gl) to solvent (toluene) ratio) was mixed with the enzyme. The

concentration of enzyme was 5 wt.% concerning the e-ROP monomer. The reaction vial was placed in a sand bath under magnetic stirring at 65 °C. After the reaction, 30 mL of dichloromethane was added to the final mixture, to deactivate and filter the enzyme. This is the amount required for the solution to separate the enzyme from the polymeric solution. Thereafter, the polymer was precipitated in cold methanol and dried for 24 h at 60 °C to remove residual solvent. Reaction yield was determined gravimetrically (mass of final polymer in relation to the mass of monomer used in the reactions). Figure 18 shows a schematic representation of globalide e-ROP, with the terminal groups, H and OH, since water is the initiator of the reaction.

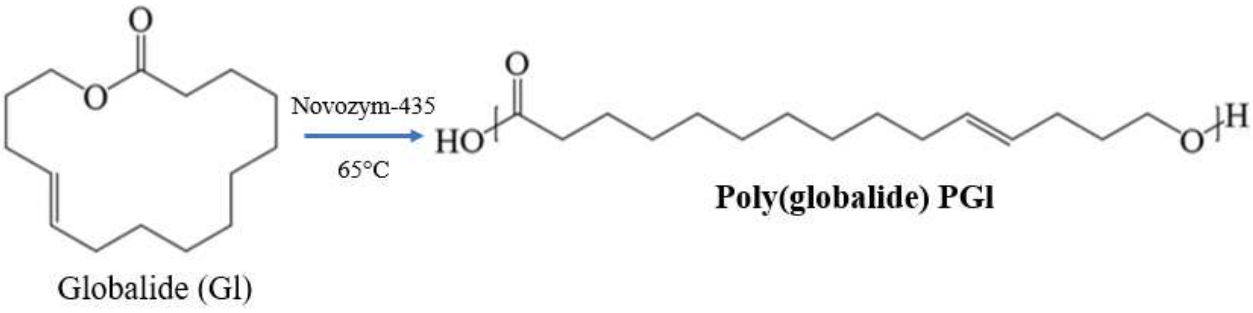

Figure 18 - Schematic representation of globalide e-ROP.

3.2.2.2. CHARACTERIZATION OF THE POLYMER

Chemical Structure: The chemical composition of PGl was determined by 1H NMR spectroscopy using a Bruker AC-200F NMR, operating at 200 MHz. Chemical shifts are reported in ppm, relative to tetramethyl silane (TMS) 0.01 % (v/v) (δ=0.00). Sample of 20 mg was solubilized in 0.5 mL of CDCl3 (δ=7.26 for 1H NMR). Fourier transform infrared (FT-IR/ATR) spectroscopy was performed to identify the chemical structure characteristics of PGl. The analysis was performed by Attenuated Total Reflectance (ATR) on KBr pellet Cary 600 model (Model: Agilent Technologies CARY 600) spectrometer with ZnSe window Transmission infrared spectra were recorded in a wavenumber range of 650-4000 cm1.

Chemical shifts were reported in parts per million (ppm) using tetramethylsilane (TMS,0.01% v/v) (δ = 0.00) as internal standard. The dried polymer was solubilized in CDCl3 (δ = 7.27 for 1H NMR).

1H-NMR (200 MHz, CDCl3): δ (ppm) = 5.55 – 5.30 (m, CH=CH), 4.16 – 4.04 (m, CH2O(C=O)), 3.66 (m, CH), 2.48 – 2.15 (m, CH2(C=O)O), 2.18 – 1.87, 1.81 – 1.5, 1.28 (m, CH2).

The tests were carried out at the Central de Análises Química do Departamento de Química at the Federal University of Santa Catarina (UFSC) in Florianópolis - SC.

Molecular Weight Distribution: Number average molecular weight (Mn), weight average molecular weight (Mw), and dispersity (*Đ*) were determined by Gel Permeation Chromatography (GPC) with high-performance liquid chromatography equipment (HPLC, model LC 20-A, Shimadzu) with a refraction index detector (RID-10A), one pLgel MiniMIX-C PL1510-1500 guard column (5 µm, 4.6 x 50 mm), and two pLgel MiniMIX-C PL1510-5500 main columns (5 µm, 4.6 x 250 mm (GPC804 and GPC807, Shimadzu). THF was used as an eluent with a volumetric flow rate of 1 mL·min^{-1} at 40 °C. Calibration was performed against styrene standards with molecular weights ranging from 580 to 3,000,000 g mol^{-1}. For the analysis, approximately 0.02 g of the PGl was dissolved overnight in 4 mL of THF and filtered through a nylon syringe filter, pore: 0.45 µm, before injection. The tests were carried out at the Laboratory of Control and Polymerization Processes (LCP) at the Federal University of Santa Catarina (UFSC) in Florianópolis - SC.

Thermal Properties: Thermal analyses of poly(globalide) were performed by differential scanning calorimetry measurements (DSC) and thermogravimetric analysis (TGA) on the STA 449 F3 Jupiter equipment, Netzsch, that allows the simultaneous measurement of TGA-DSC. The analysis was performed using approximately 10 mg of dry polymer, under an inert atmosphere (N_2, 60 mL min^{-1}), from 20 °C to 600 °C with a heating of 10 °C min^{-1}. Melting enthalpie and temperature were determined from the first heating cycle. The analysis did not remove the thermal history. The tests were carried out at the Laboratory of Control and Polymerization Processes (LCP) at the Federal University of Santa Catarina (UFSC) in Florianópolis - SC.

3.3 PREPARATION OF POLYMERIC NANOPARTICLES

3.3.1 REFERENCE FORMULATION

The construction of a reference emulsion for the preparation of nanoparticles addresses a variety of parameters and is a critical step in the process since it directly influences the final characteristics of the particles produced.

The method chosen for preparing the Polyglobalide Nanoparticles and drug encapsulation was Double Emulsion technique with solvent evaporation and it was adapted from IQBAL et al., (2015) (IQBAL *et al.*, 2015b).

For this study, different parameters were adjusted in the formulation of the emulsion for the preparation of PGl nanoparticles by the Double Emulsion technique (Table 4), including the mass of the internal aqueous phase, the mass ratio between the polymer and the organic solvent used to solubilize it, the mass molar, degree of hydrolysis, concentrations of the components in the external aqueous phase and the respective volume used. In addition, different experimental conditions, such as the time and amplitude of the sonication probe, as well as the application of an ice bath for temperature control, were also evaluated. All these variables have a direct influence on the results of the nanoparticles, such as hydrodynamic size and dispersity. Through the systematic study of the effect of these parameters, it is possible to establish a reference emulsion that will provide the solid basis for obtaining nanoparticles with the desired characteristics, guaranteeing a successful and efficient preparation.

Table 4 – Formulations and experimental conditions evaluated for the preparation of the PGl NPs by the double emulsion solvent evaporation approach.

Test formulations	**Parameters of the 1st Emulsion (W/O)**				**Parameters of the 2nd Emulsion (O/W)**		
	Internal Aqueous Phase W1 (g)	Organic Phase (O) (g)		Sonication time (min)*	Mw of PVA (0.5% Solution, kDa)	External Aqueous Phase W2 (g)	Son. time (min)*
	Mili-Q Water	Polymer (PGl)	Solvent (DCM)				
NPs PGl 01	0.35	0.7	10.50	5 [a]	N/A		
NPs PGl 02	0.35	0.7	10.50	5 [b]	78 [c]	112	8 [b]
NPs PGl 03	0.50	1.01	10.18	5 [b]	78 [c]	112	8 [b]
NPs PGl 04	0.93	1.86	9.33	5 [b]	78 [c]	112	8 [b]
NPs PGl 05	0.50	1.01	10.18	5 [b]	30-70 [d]	112	8 [b]
NPs PGl 06	0.50	1.01	10.18	5 [b]	30-70 [d]	112	10 [b]
NPs PGl 07	0.50	1.01	10.18	5 [b]	30-70 [d]	112	12 [b]
NPs PGl 08	0.50	1.01	10.18	5 [b]	30-70 [d]	112	14 [b]
NPs PGl 09	0.50	1.01	10.18	5 [b]	30-70 [d]	112	16 [b]

N/A: No result was obtained because the Solvent DCM evaporated during the sonication of the 1st emulsion.

* Amplitude of 70% of the sonication tip and pulse regime (10on 5 off) constant.

[a] No ice bath application.

[b] With ice bath application.

[c] PVA with a degree of hydrolysis of 88%.

[d] PVA with a degree of hydrolysis of 87-90%.

After this study of the parameters, in search of the reference formulation and evaluating the results obtained from hydrodynamic size and the polydispersion index (PDI), we established the reference formulation NPs PGl 09 (Table 4) for the preparation of nanoparticles by the Double Emulsion method.

3.3.2 PREPARATION OF BLANK NPS, ICG@NPS AND ICG~DOX@NPS BY THE DOUBLE EMULSION METHOD

After the definition of the reference emulsion, 5 formulations (Figure 19) were established, which will be discussed below along the methodology.

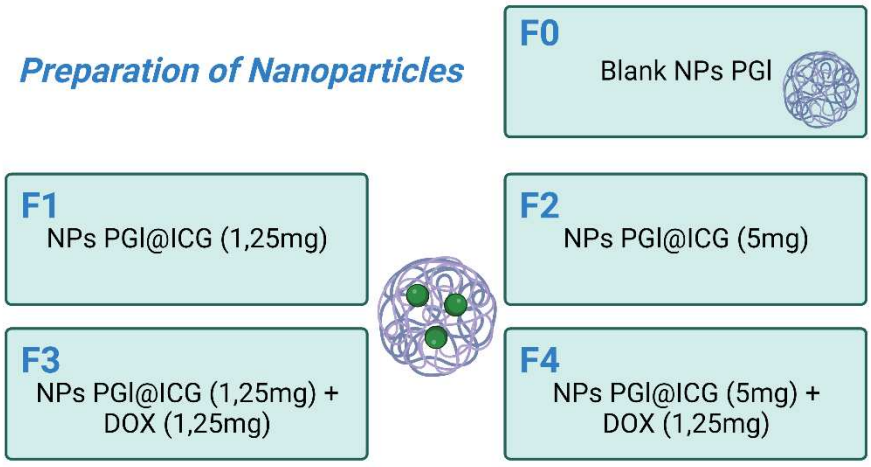

Figure 19 – Preparation of PGl nanoparticles.

For this, formulations were established by varying the amount of the ICG drug (0 mg, 1.25 mg, and 5.0 mg) and the mass of DOX remained constant (1.25 mg), as described in Figure 20 and Table 5. The first emulsion (water-in-oil) was prepared by adding 0.5 g of water or DOX solution or ICG and DOX solution, as summarized in Table 5, to the organic phase (1.01 g PGl

in 10.18 g of DCM) under magnetic stirring (300 rpm), followed by miniemulsification with a sonicator (Sonics, Vibra Cell) with a ½" tip at 70% amplitude for 5 min (10s on/ 5 off). The whole process was performed sheltered from light, due to the photosensitivity of the drug and the miniemulsification was in an ice bath, to minimize the evaporation of DCM.

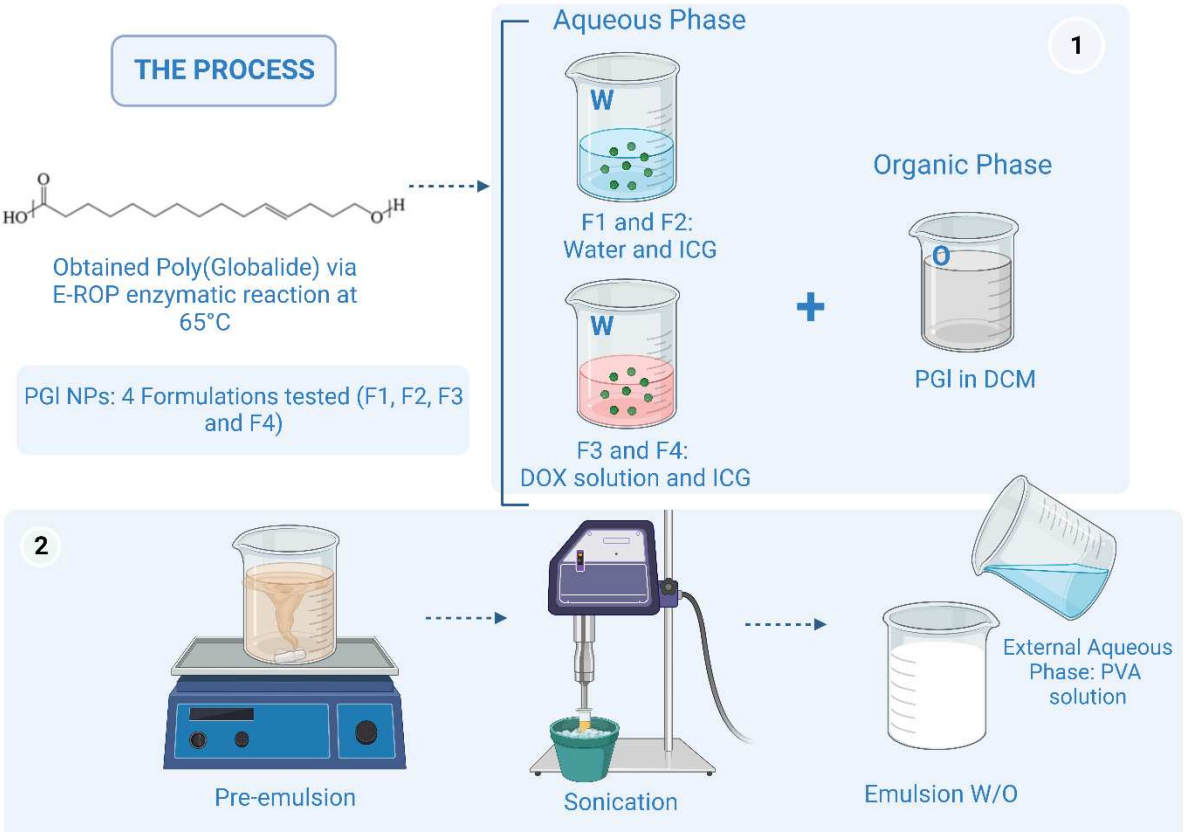

Figure 20 - Preparation of the first W_1/O emulsion of double emulsion technique using an ultrasound device.

So, this first emulsion (W_1/O) was then added to 112 g of PVA aqueous solution (0.5 wt%) and sonified to form the second emulsion ($W_1/O/W_2$) at 70% amplitude for 12 min (10s on/ 5 s off). This sonication time was established in preliminary sonication tests in which sonication time was from 8 min to 16 min. Then, the DCM was evaporated and the particle size and PDI were analyzed by Dynamic Light Scattering – DLS (Zetasizer Nano-S, Malvern Instruments).

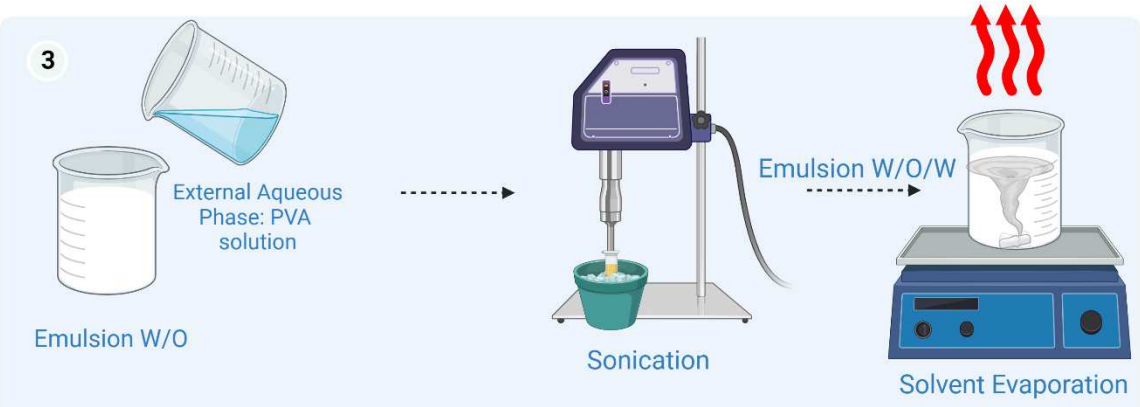

Now, the colloidal dispersion of solid polymeric nanoparticles, containing the encapsulated drug, was destined for three different steps (Figure 21) : 1) centrifugation for the determination of the encapsulation efficiency, 2) lyophilization for DSC/TGA and FTIR characterization and 3) kept as dispersion for DLS, TEM, Zeta Potential measurements.

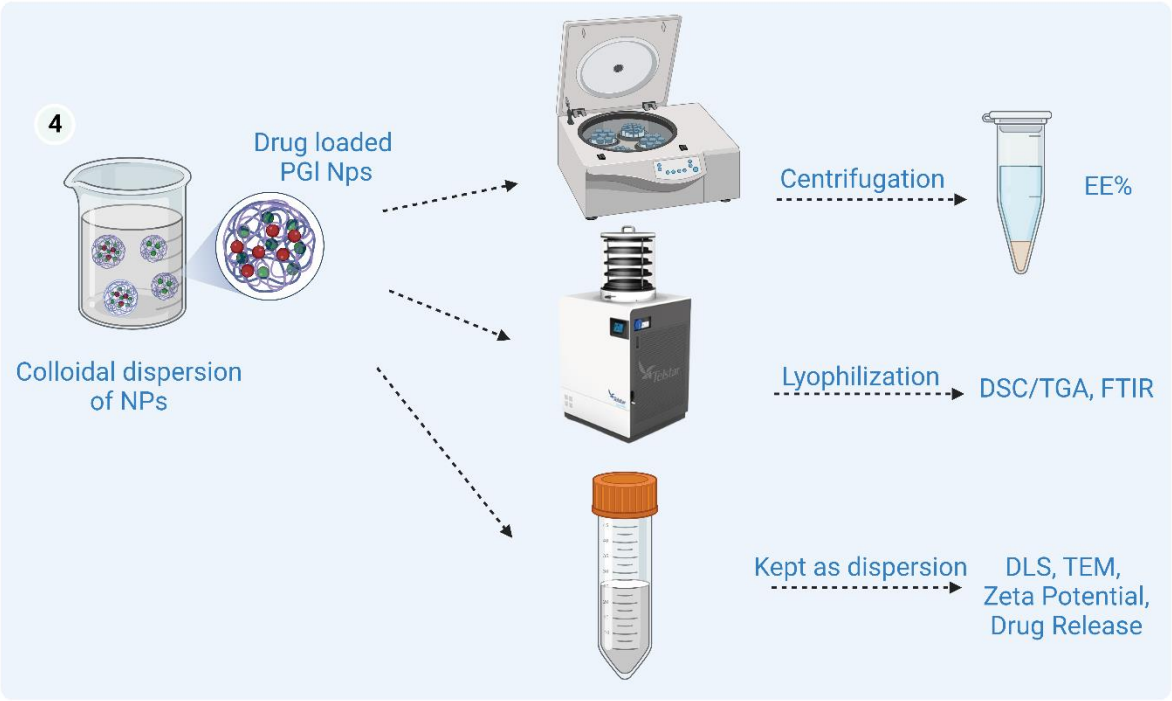

Figure 21 - Preparation of the second emulsion ($W_1/O/W_2$) of double emulsion technique using an ultrasound device.

For the preparation of blank particles without the drug, only a volume of Milli-Q water was added to the internal aqueous phase, following the protocol previously described.

Table 5 - Formulations of PGl NPs

		FO	F1	F2	F3	F4
Internal Aqueous Phase	**Water (Mili-Q) (g)**	0.5	0.5	0.5	0.5	0.5
	ICG (g)	-	0.00125	0.005	0.00125	0.005
	DOX (g)	-	-	-	0.00125	0.00125
Organic Phase	**PGl (g)**	1.01	1.01	1.01	1.01	1.01
	DCM (g)	10.18	10.18	10.18	10.18	10.18
External Aqueous Phase	**(0,5% PVA Solution) (g)**	112	112	112	112	112
	PVA (g)	0.56	0.56	0.56	0.56	0.56

3.3.3 PHYSICAL-CHEMICAL AND MORPHOLOGICAL CHARACTERIZATION OF BLANK NANOPARTICLES AND ENCAPSULATING ICG OR ICG + DOX

To carry out the analyses that will be mentioned below, it removed an aliquot of the nanoparticle dispersion (Figure 22).

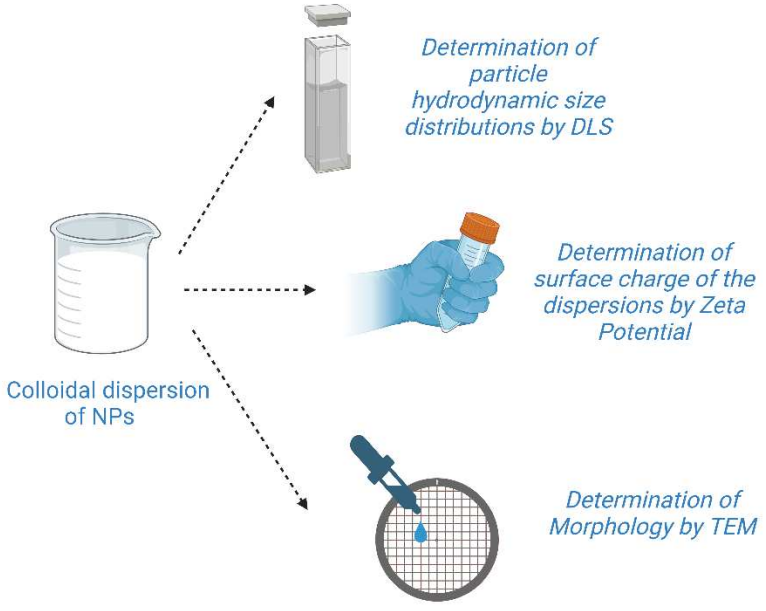

Figure 22 - Physicochemical and Morphological Characterization through Nanoparticles in Dispersion

Determination of particle hydrodynamic size distributions and Zeta Potential

Dynamic light scattering: The intensity average diameters of polymer particles (Dp) and the polydispersion index were determined at 25 °C by Dynamic Light Scattering (DLS) measurements, using the Zetasizer Nano S equipment (Malvern Instruments). The equipment performs non-invasive measurements by "backscatter optic" (NIBS), made at a detection angle of 173º, and the cuvette measurement position is automatically determined by the equipment software. The equipment performed an average of 12 determinations for each analysis. Latexes were diluted in ultrapure water obtained by the Milli Q® system and placed in glass cuvettes with an optical path of 1 cm. Given the dilution, the viscosity of the dispersing medium was that of water, and the diameters (nm) were the average of three runs. Each sample was diluted before each analysis. The tests were carried out at the Laboratory of Control and Polymerization Processes (LCP) at the Federal University of Santa Catarina (UFSC) in Florianópolis–- SC.

Zeta Potential: The surface charge of the dispersions was measured as zeta potential, determined by the electrophoretic mobility of the dispersed particles subjected to an electric field. Measurements were performed at different pH values (pH 2 ± 0.2, pH 3 ± 0.2, pH 5 ± 0.2, pH 7 ± 0.2, pH 9 ± 0.2, pH 11 ± 0, 2) in aqueous dispersant (10−3 M NaCl or HCl) at 25 ° C. The analyzes were carried out in the Zetasizer 3000HS equipment using an electrophoretic cell at the Interdisciplinary Laboratory for the Development of Nanostructures (LINDEN) of the Federal University of Santa Catarina (UFSC) in Florianópolis – SC.

Determination of Morphology

Transmission Electron Microscopy – TEM: The transmission electron microscopy technique was used to evaluate the morphology and size of the nanoparticles, as well as the presence of aggregates. The technique consists of an electron beam that is emitted towards a very small amount of sample. The transmitted electrons that interact with the sample form an image on a fluorescent screen and then it is passed on to a capture device via computer. The samples were dispersed in a beaker with distilled water and placed in the ultrasonic bath for 30 s. With the aid of a pipette, a drop of this solution was deposited on a 300# grid and then dried

for 24 h before performing the test. The equipment used is the JEOL brand, model JEM-2100 TEM 100 kV Transmission Electron Microscope (TEM), with magnifications of 10,000x, 20,000x and 50,000x. The tests were carried out at the Central Laboratory of Electron Microscopy (LCME) of the Federal University of Santa Catarina (UFSC) in Florianópolis–-SC.

For the analyzes performed below, it was necessary to freeze-dry the nanoparticles to remove water (Figure 23), stabilize the nanoparticles, and prepare the sample for spectroscopic analysis. This allows for obtaining more accurate and representative results of the properties and characteristics of nanoparticles.

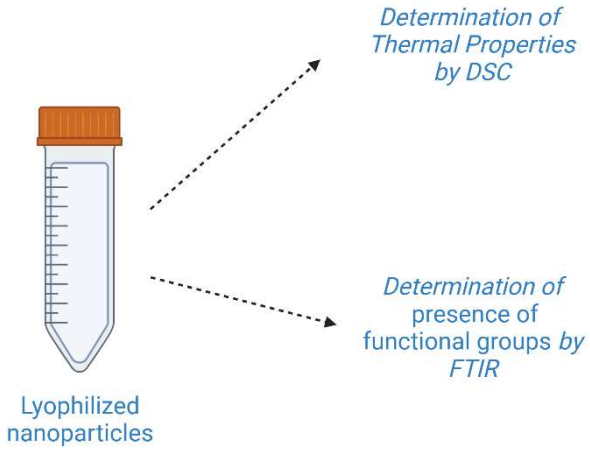

Figure 23 - Physicochemical and Morphological Characterization through Lyophilized Nanoparticles

Determination of Thermal Properties

Differential Exploratory Calorimetry –- DSC: For the evaluation of thermal properties, such as melting temperature (Tm), differential scanning calorimetry (DSC) techniques was used. Thermal analyzes of nanoparticles of Poly(globalide) were performed on the STA 449 F3 Jupiter equipment, Netzsch. The analyzis was performed using approximately 10 mg of dry polymer, under an inert atmosphere (N2, 60 mL min-1), from 20 °C to 600 °C with a heating of 10 °C min-1. Melting enthalpy and temperature were determined from the first heating cycle. The analysis did not remove the thermal history. The tests were carried out at the Laboratory

of Control and Polymerization Processes (LCP) at the Federal University of Santa Catarina (UFSC) in Florianópolis - SC.

Fourier Transform Infrared Spectroscopy – FTIR: The technique of Fourier transform infrared spectroscopy was used to evaluate the presence of functional groups. The samples were prepared in potassium bromide (KBr) pellets and the analyzes were performed at wavenumber intervals between 4000 cm^{-1} and 500 cm^{-1} by attenuated total reflectance (ATR) . The equipment used was an Agilent Technologies spectrophotometer, model Cary 600 Series FTIR Spectrometer. The tests were carried out at the Analysis Center of the Department of Chemical Engineering and Food Engineering at the Federal University of Santa Catarina (UFSC) in Florianópolis - SC.

3.4 DRUG ENCAPSULATION EFFICIENCY

Determination of drug encapsulation efficiency of ICG and DOX

The encapsulation efficiency refers to the amount of drug encapsulated in the PGl polymeric particles as compared to the total amount of drug added in the formulations. The determination of the encapsulation efficiency of ICG and DOX was carried out through the indirect method, shown in Figure 24. The process involves the separation of nanocarriers from the continuous aqueous phase (W_2) using ultrafiltration, followed by quantifying the amount of the substance that was not encapsulated and remained in the W_2. The dispersion was placed in ultrafiltration tubes (Amicon®, MWCO 100 KDa) with a membrane that generates pressure under centrifugal force and allows the material to filter, classifying it according to pore size. A centrifugal force of 12100 x g was used for 30 min for the ultrafiltration process.

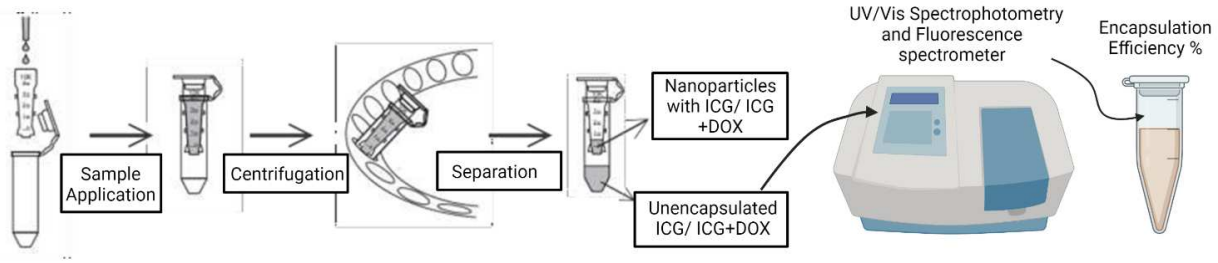

Figure 24 – Scheme of sample preparation for quantification of ICG and DOX by the indirect method.

The absorbance of ICG at 780 nm and the DOX fluorescence in the range (Excitation = 488 nm, Emission = 595nm) were determined, by a UV-Vis SpectraMax Spectrophotometer and a fluorescence spectrometer (SpectraMax® GEMINI EM Dual-Scanning Microplate Spectrofluorometer, Sunnyvale, California), respectively. An absence of overlap ensures the specificity of the fluorescence readings.

ICG and DOX calibration curves were prepared before measurements to verify the spectral characteristics, linearity range, and degree of overlap between the spectra of the drug. For ICG samples, aliquots of the supernatant were placed in 4.5 mL glass cuvettes, and for the DOX samples, the supernatants were then transferred to a black microplate of 96 wells, and measurements were carried out immediately after preparation.

The W_2 of blank nanoparticles (without drugs) was used as a blank for background correction. Spectral emission readings were recorded at 1 nm intervals up to 870 nm. All measurements and sample handling were performed in triplicate and under dimmed lighting conditions, and instrument operating conditions were held constant.

ICG and DOX concentrations were determined from the peak emission wavelength, subtracting that of the corresponding blank NPs, using the previously obtained calibration curves of ICG and DOX in water. The encapsulation efficiency of ICG and DOX in PGl nanoparticles were calculated in triplicate using the Equation 1:

Equation 1 – Quantification of encapsulation efficiency of ICG and DOX by the indirect method

$$EE(\%) = \frac{(Total\ mass\ of\ drug\ (ICG\ or\ DOX) - Mass\ of\ \ drug\ (ICG\ or\ DOX)\ in\ W_2)}{(Total\ mass\ of\ drug\ (ICG\ or\ DOX))}\ x100 \quad (\text{Eq. } 1)$$

3.5 FUNCTIONALIZATION OF PGL NPS, ICG@PGL NPS, AND ICG-DOX@PGL NPS WITH BOVINE SERUM ALBUMIN (BSA)

Non-Covalent Functionalization of Nanoparticles with Bovine Serum Albumin (BSA)

Following the methodology described by Guindani et al. (2020), for the functionalization of the PGl NPs, a BSA solution (3 mg mL ^{1}) was prepared in 0.1 M sodium phosphate buffer solution, pH 8.0 containing 1 mM EDTA. Then, an aliquot (1.15 mL) of BSA solution was added to 10 mL of polymeric dispersion, and incubated overnight at 4 °C. On most surfaces, the amount of albumin that occupies a monolayer is near 0.15 μg/cm^2 (MURA-GALELLI *et*

al., 1991; SOKOLOV *et al.*, 1998). The amount of BSA used was established as $5x10^{-6}$ mol of BSA per mL of emulsion, as this amount is theoretically sufficient to cover the surface of this these PGl NPs. After incubation, the dispersion containing BSA + conjugated PGl NPs was washed and centrifugated (Amicon filtration tubes MWCO: 100 kDa, 12100 x g, 10 min) three times to remove the weakly adsorbed BSA. The supernatant containing free BSA was removed, and the conjugates were redispersed in distilled water and stored in a refrigerator (4 °C) until the characterization was carried out.

Protein quantification by Lowry assay

The Lowry assay was performed to determine the amount of BSA conjugated to the nanoparticle surface. The BSA + PGl NPs conjugates were centrifuged (12100 x g for 30 min) and the supernatant containing free BSA was analyzed. Protein content in the supernatant was determined according to the method described by Lowry et al. using Folin's phenol reagent (phosphomolybdicphosphotungstic acid reagents) (LOWRY *et al.*, 1951). Bovine serum albumin (BSA) was used as a standard. Absorbance was measured at 700 nm on a SpectraMax spectrophotometer. A calibration curve of BSA was prepared before measurements to verify the spectral characteristics, linearity range, and degree of overlap between the spectra. In this assay, the amount of free BSA removed during the purification of the conjugates was determined by the analysis of the supernatant.

3.6 COLLOIDAL STABILITY OF NPS

Blank PGl dispersions were stored at 4 °C to determine their long-term stability. From its preparation, every 30 days, with a final deadline of 6 months, 1 mL of the sample was analyzed by DLS. Each measurement was performed in triplicate.

3.7 DRUG RELEASE

The *in vitro* drug release of drugs was adapted from Aghda et al., (2020) (HESHMATI AGHDA *et al.*, 2020) and studied for 20 days. Release studies were performed by placing 2 mL of the NPs latex (13.5 mg/mL) in a dialysis membrane that was immersed in 20 mL of PBS solution (pH 7.4 or 5.5) at 37 °C under continuous agitation in a shaker. These pH values were

chosen to simulate the biological environments in which drug delivery systems can be applied. pH 7.4 is close to the physiological pH of the human body, when in equilibrium, and pH 5.5 simulates the more acidic microenvironment of tumor cells. At predetermined time intervals (30 min, 1 h, 2 h, 4 h, 6 h, 8 h, 10 h, 12 h, 24 h, 36 h, 48 h, 60 h, 72 h, 96 h and so every 24 h up to 480 h) the concentration of DOX and ICG released in the dialysate (buffer solution containing the permeate) was determined by Fluorescence Spectrum (480 nm) and UV–Vis Absorption Spectroscopy (780 nm), respectively. The experiment and all measurements were done in duplicate. An individualized dialysis tube was prepared for each measurement. The experimental apparatus and procedure are presented in Figure 25.

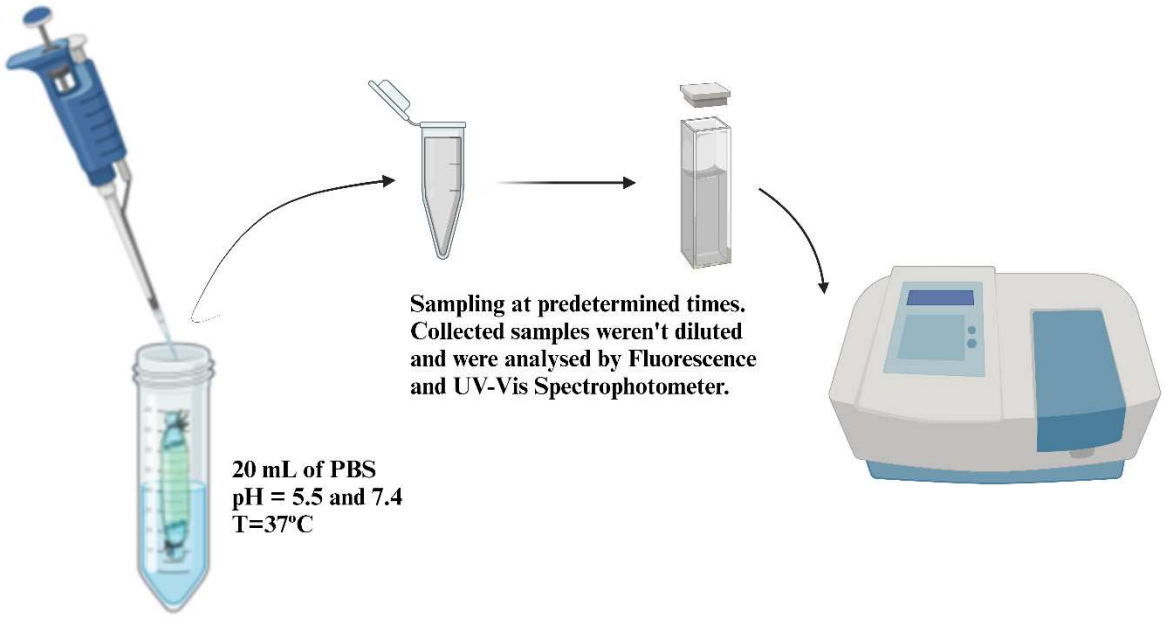

Figure 25 – Experimental procedure of ICG and DOX release study.

3.8 IN VITRO STUDIES

3.8.1 METHODS: IN VITRO STUDIES

The activities developed in the in vitro studies are described in Figure 26.

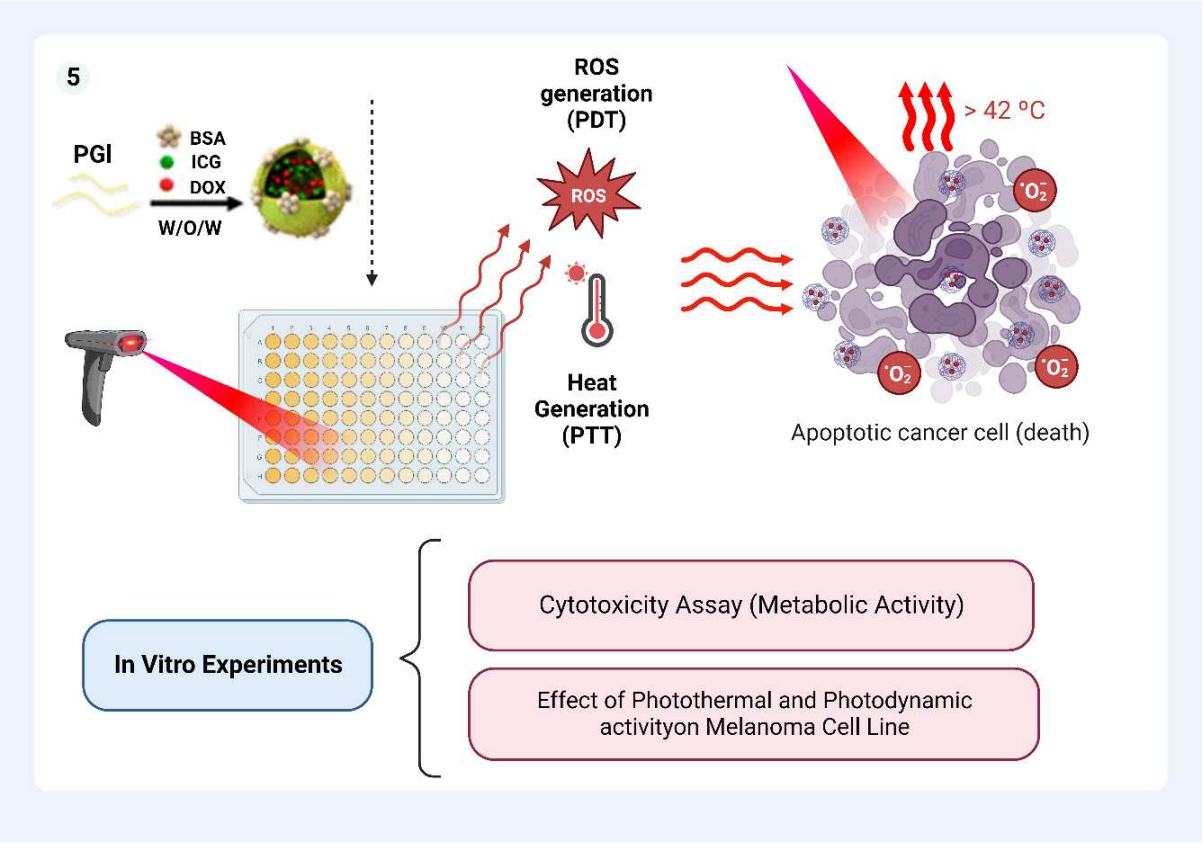

Figure 26 – Activities developed in in vitro studies.

3.8.1.1 IN VITRO CYTOTOXICITY ASSAY

3.8.1.1.1 SAMPLE PREPARATION

The samples were diluted in the medium at different concentrations quadruplicate (0.7 ng/mL to 675 ng/mL (without dilution)). For the direct contact assay, the different concentrations were plated directly on the cells.

3.8.1.1.2 CELL PREPARATION

Cell viability was evaluated with a murine cell line of fibroblasts - L929, seeded in 96-well cell culture plates. Cells were kept under a moist atmosphere at 37 °C with 5% CO2 and cultured in DMEM, supplemented with 10% FBS and 1% penicillin/streptomycin. The Cell culture medium was refreshed every 2 days until cells reached 85–90% confluence. The Cells were detached using Tryplex and placed in 96-well plates at a density of 1·104 cells/well. After

24 h, different concentrations were added to the cell wells and kept under a moist atmosphere at 37 °C with 5% CO2 for more 24 hours. Subsequently, the cells were washed twice in PBS and cell viability (MTS) was evaluated.

3.8.1.2 MTS ASSAY (METABOLIC ACTIVITY)

The cells were then incubated for 24, h at 37 °C, 5% CO2 and 90% humidity. The control wells containing culture medium only were also incubated. After the time, the cells were rinsed with PBS (PBS, Gibco® USA), and cell viability was measured with AQueous One solution proliferation assay (CellTiter 96, MTS, Promega). In each well, a mixture of 20 μL cell MTS reagent (Promega Corporation® USA) and 100 μL medium was added and cultured in an incubator (Ultrasafe HF 212UV, Brazil) at 37 °C for 24 h with 5% CO2. Afterward, the remaining medium was transferred into 96-well plates for optical density measurements at 490 nm wavelength. The analyses were performed on a spectrophotometer (Molecular Devices, Spectra Max Plus 348) with four parallel replicates for each sample. The culture medium was used as a control group and the results showed metabolic activity (MELGAR AGUILAR *et al.*, 2021).

3.8.1.3 PHOTODYNAMIC AND PHOTOTHERMAL ACTIVITY ON MELANOMA CELLS: PHOTOXICITY STUDIES

SKMEL-28 cells were seeded into 6-well plates at 2·105 cells/well in DMEM (2.0 mL) containing 10% FBS and 1% penicillin and incubated at 37 °C overnight under 5% CO2. The cancer cells were treated with C, NPs, F2 and F4 for 6 h. After washing with PBS twice, the cancer cells were harvested with Triplex and then treated with 808 nm laser for 2.5; 5; 7.5 and 10 min. The cancer cells were reseeded on 96-well plates at a concentration of 1·104 cells/well and incubated at 37 °C under 5% CO2 for 24 and 48 h. To determine the cell viability of cancer cells, MTS was used, followed by re-incubation at 37 °C for 2 h. The absorbance of each well at 490 nm was determined by the microplate reader. For control, the cancer cells were treated only with C, NPs, F2 and F4 for 6 h without further photo-irradiation.

3.8.1.3.1 STATISTICAL ANALYSIS

Metabolic activity of L929 cells was analyzed using OriginPro® (OriginLab Corporation, Northampton, Massachusetts, USA) expressed as the mean ± standard error from three independent assays and their triplicates. Statistical evaluation was performed using one way analysis of variance (ANOVA), followed by Tukey's test with $p < 0,05$ considered as statistically significant).

4. RESULTS AND DISCUSSION

4.1 SYNTHESIS OF POLY(GLOBALIDE)

The e-ROP yield averaged 74% (experiments conducted in triplicate). This result can be compared with other studies that synthesized PGl by the same methodology, the study by Chiaradia et al. for example, obtained a yield of 80 to 90% with the same reaction time and using 6% of the NZ435 enzyme in with respect to the monomer (POLLONI *et al.*, 2018). Another study carried out by Rowley et al. obtained a whitish crystalline polymer (PGl) with a yield of 69% in 4 hours of reaction (ROWLEY *et al.*, 2020).

Precise control of the amount of water in the e-ROP polymerization reaction using the NZ435 enzyme is essential to obtain a high polymerization yield and control over the molecular weight as water acts as initiator in these ROP. In addition, excess water can also lead to hydrolysis and degradation of the formed polymer. Loeker et al. (2004) conclude that the amount of water in the reaction medium has a direct influence on molecular weight.

The denaturing temperature of the NZ435 enzyme can vary depending on experimental conditions such as pH, and substrate concentration. Generally, however, the NZ435 enzyme, like many other enzymes, has a relatively high denaturing temperature due to its thermophilic origin. Although there are no specific data available for the denaturing temperature of NZ435, thermophilic enzymes in general can maintain their enzymatic activity over a wide temperature range, up to 80 °C. Poojari et al. (2013) reported that the NZ-435 shows high thermal stability up to 100 °C and maintains its catalytic activity when incubated in toluene at 80 °C for up to one month without denaturing. In this way, the drying temperature of 60 °C for NZ-435 and the reaction temperature (65º C) are within the recommended range.

The need for the enzyme to use a small amount of water to activate its active site makes this characteristic the main parameter that affects the e-ROP reaction. The amount of water is related to the maintenance of the active three-dimensional conformation, its integrity, the

polarity of the active site, flexibility, and stability of the protein regardless of whether it is in free form or covalently attached to a support (BELLTRAME, 2022). Thus, the presence of water functions as a nucleophile, when in the presence of other nucleophiles, it will result in the formation of chains with different terminal groups (HENDERSON *et al.*, 1996).

3.1.1 CHARACTERIZATION OF THE POLYMER

Chemical Structure: ^{1}H NMR spectroscopy is in good agreement with the literature as Figure 27 shows (ATES *et al.*, 2011; CHIARADIA, 2019; GUINDANI *et al.*, 2017; VAN DER MEULEN *et al.*, 2008)

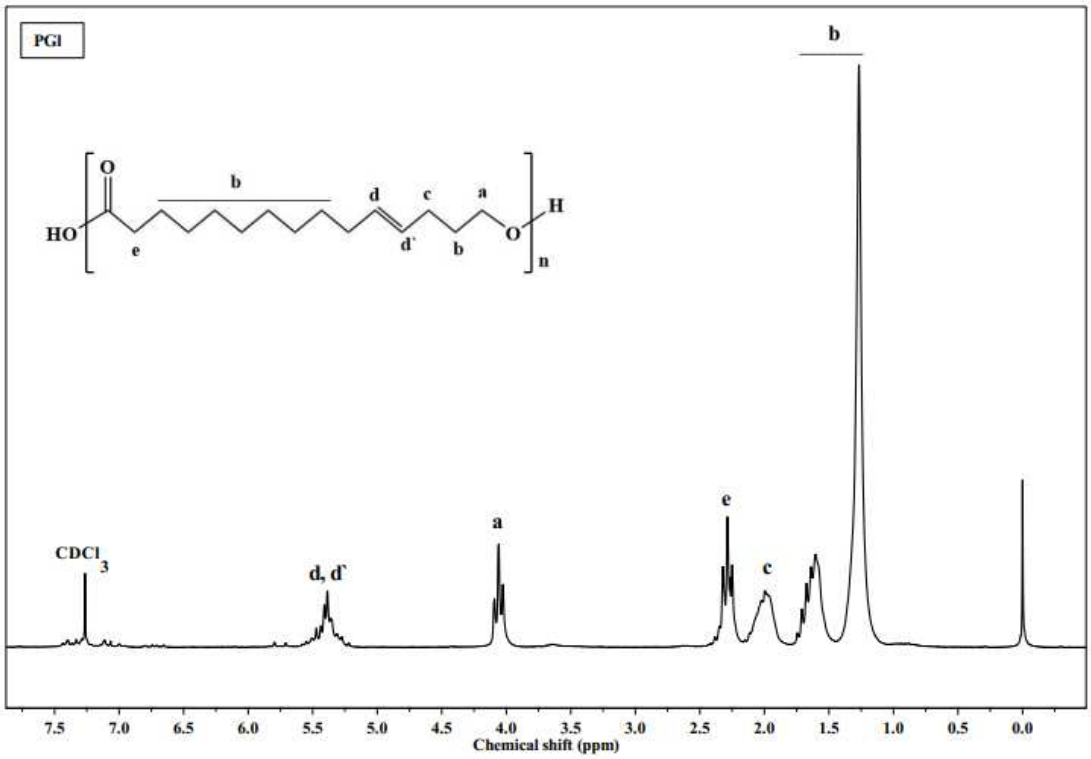

Figure 27 - ^{1}H NMR spectrum of PGl and the respective peak attributions to its chemical structure

Structural characterization of PGl was also performed by FT-IR spectroscopy. Figure 28 shows the FT-IR/ATR spectrum of the synthesized PGl. The characteristic bands of PGl are: 721 cm^{-1} (cis RCH = CHR); 970 cm^{-1} (trans RCH=CHR); 1177 cm^{-1} (COC); 2925, 2848 and 1463 cm^{-1} (C–H); and 1739 cm^{-1} (C=O) (SAVIN *et al.*, 2018).

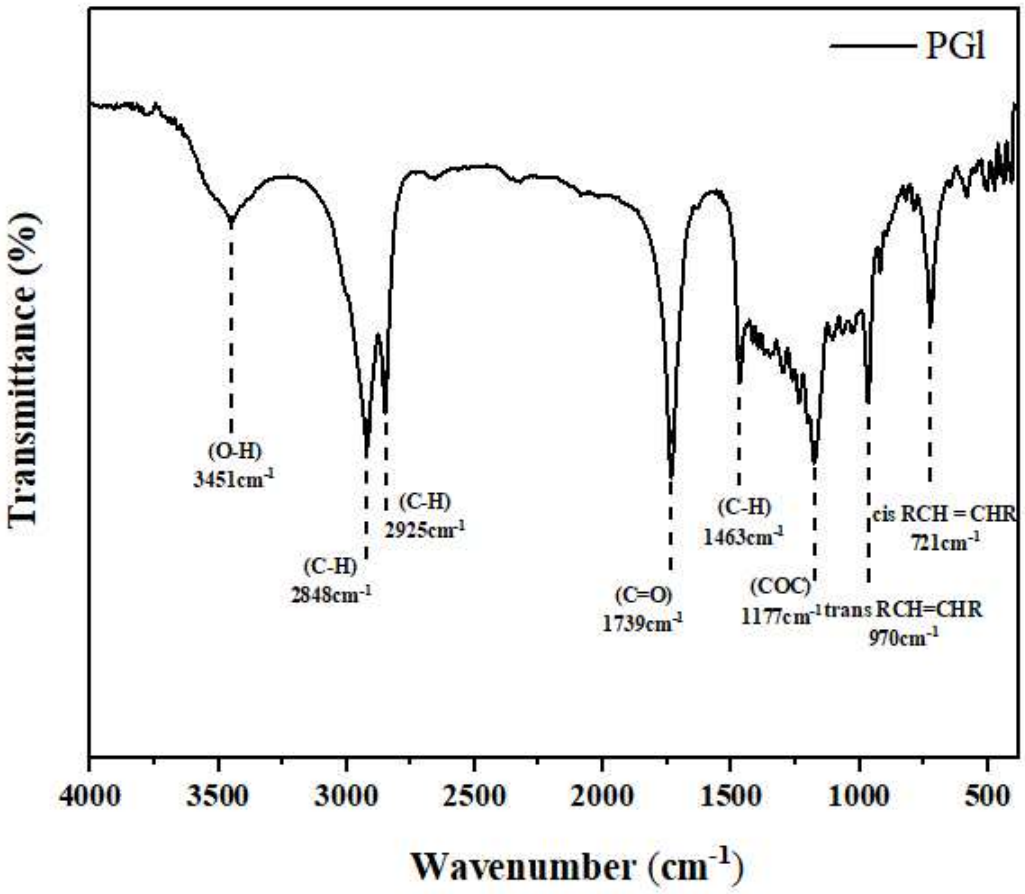

Figure 28 – FTIR spectrum of PGl

Molecular Weight Distribution: The molecular weight of the PGl (synthesized in triplicate) was determined using GPC. The average molecular weights in number (Mn) and weight (Mw) were 9584 ± 2007 g·mol^{-1} and 30000 ± 2255 g·mol^{-1}, respectively, resulting in an average dispersivity (*Đ*) of 3.22 ± 0.49. The molecular weight averages and dispersions of each reaction are shown in Table 6, and the molecular weight distributions are in Figure 29. The width of the distribution can be related to the growth mechanism of this e-ROP and the back biting reactions that lead to the formation of cyclic oligomers of low molar weight broadening the distribution.

Table 6 - Molecular weight averages of synthesized polymers.

Synthesized Polymers	M_n, g mol^{-1}	M_w, g mol^{-1}	*Đ* (-)
PGl_01	10133	30547	3.01
PGl_02	11723	32449	2.76
PGl_03	6898	27006	3.91

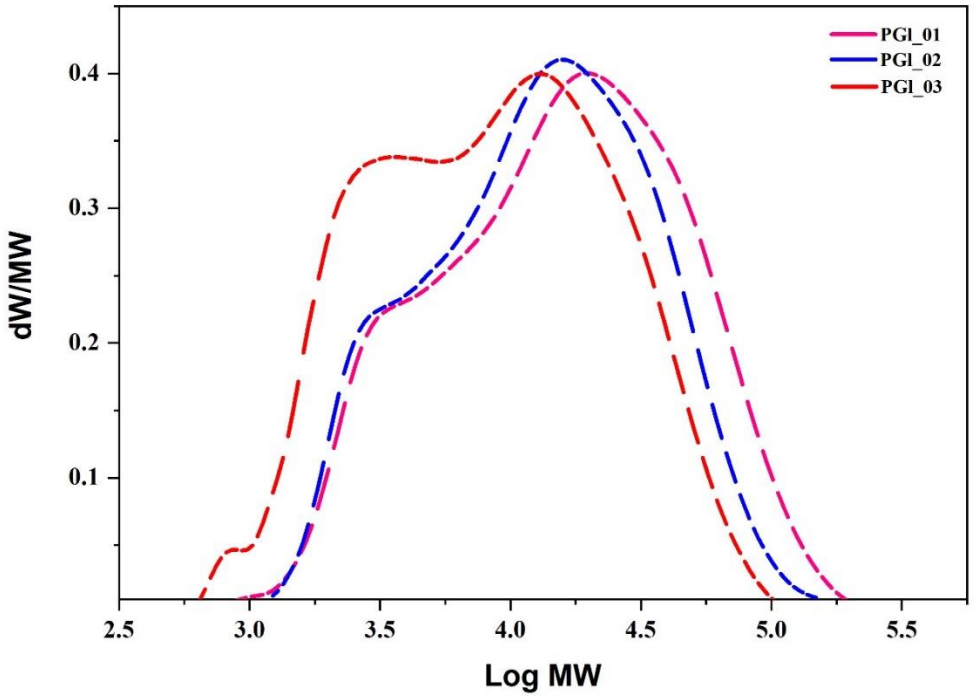

Figure 29 – Normalized molecular weight distributions GPC of different synthesized samples of PGl.

The variation in the results obtained can be explained by the arbitrary loss of oligomers during the purification step and also be due to the amount of water present in each system and external conditions, such as air humidity. The presence of water plays a crucial role in polymerization kinetics and molecular weight in ring-opening polymerization (e-ROP) systems, as it plays the role of initiator (nucleophile) (CHIARADIA *et al.*, 2018).

Some studies have already involved the synthesis of PGl using enzymes as catalysts in ROP reactions (ALBERTSSON *et al.*, 2009). The most used route to produce PGl is ring opening polymerization (ROP), as it is capable of synthesizing polymers with high molecular weight (CHIARADIA *et al.*, 2018; POLLONI *et al.*, 2018). Guindani et al. (2022) synthesized PGl with Mn around 8362 g mol^{-1} and 15222g mol^{-1}, and *Đ* with values between 1.66 and 3.67, using pressurized fluids.

In contrast to condensation polymerizations, e-ROP polymerization has the convenience of not generating output groups during the reaction (BELLTRAME, 2022; DOUKA *et al.*, 2018). This allows to obtain polyesters with a high degree of control about molecular weight and dispersion, under relatively moderate reaction conditions.

Thermal Properties: Thermogravimetric analysis (TGA) was performed in order to access the mass loss curve caused by thermal decomposition of PGl, Figure 30 shows the weight loss curve. The analyzed PGl sample presented 50% mass loss at 420 °C, and a mass loss of 88% at 470 °C. Similar results were previously reported by Ates et al., (2014) and Guindani (et al., 2022).

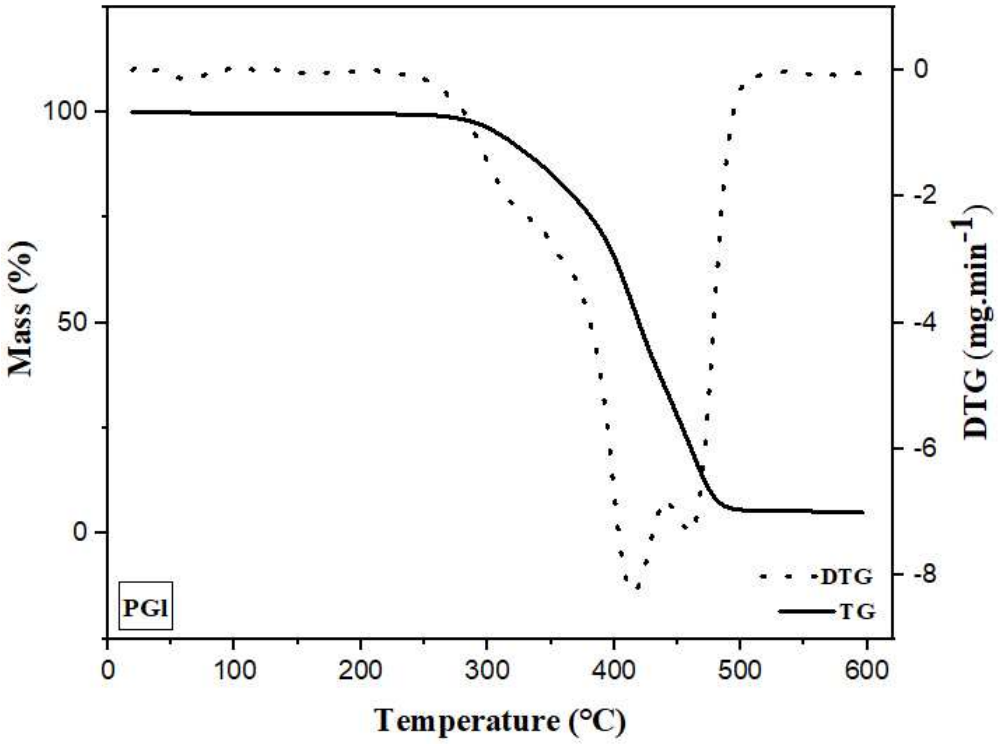

Figure 30 – TG/DTG curve for a PGl sample, carried out at 10 °C min^{-1} under nitrogen atmosphere.

With the derived thermogravimetric curve (DTG) it is possible to identify in how many stages the thermal decomposition occurs. The PGl thermogravimetric curve showed four thermal events. Event I, slow and discrete started at 43.8 °C and ended at a final temperature of 103.8 °C due to evaporation of the water still present in the sample. The second event, more pronounced, started at 285.0 °C and ended at 367.4 °C, with 35.71% of mass decomposition, soon followed by sequential events, event III, which was marked by an initial temperature of 386.4 °C and a final temperature of 436.6 °C, with 61.27 % mass decomposition, and event IV, starting at 444.1°C and ending at 466.3°C, with 85.96 % of mass decomposition, indicating that practically all residual mass degraded completely, being possible to identify that at 600 ºC only 4.94 % of mass remained during the thermodegradation process, indicates that the majority of the material has undergone decomposition by that point in the process.

Then, the thermal behavior of the obtained PGl samples was evaluated by means of DSC analysis, as shown in Figure 30.

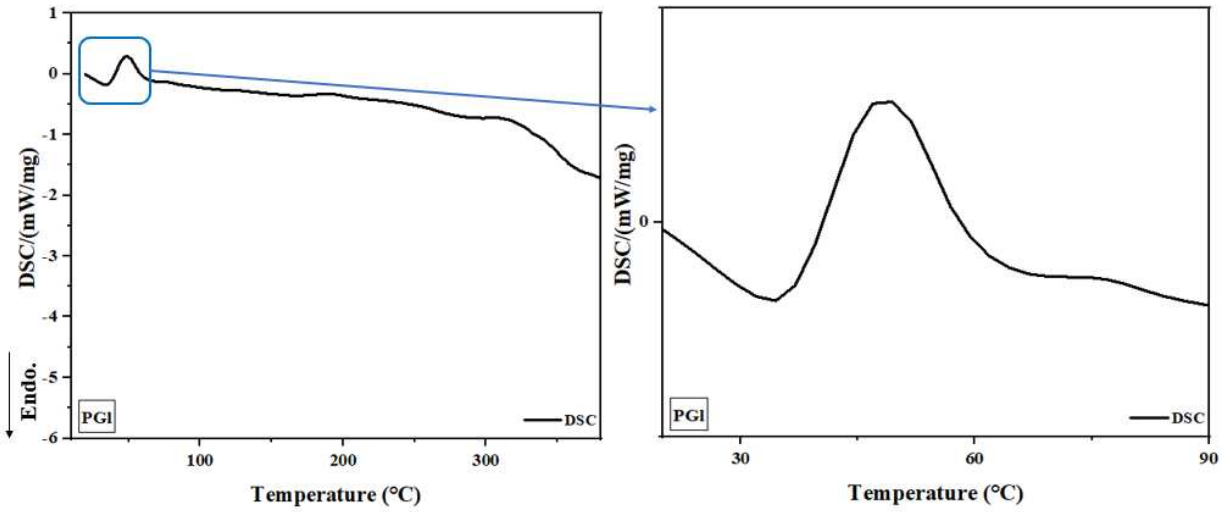

Figure 31 - Thermal properties determined by DSC analysis for PGl sample.

PGl has a semi-crystalline structure and, among other properties of interest, has a relatively low melting temperaI (T_m), as demonstrated by the analysis, around 49.4 ºC, corroborating with Chiaradia et al. (2018) and Guindani et al. (2017). In practice, this temperature corresponds to the maximum of the differential scanning calorimetry (DSC) curve in the melting of the polymeric material, representing an exothermic peak. This characteristic, together with the presence of a potentially biodegradable ester group and of a double bond in each repetitive unit of the polymer chain, makes PGl a very attractive polymer from an industrial point of view and for NPs coating applications.

4.2 PREPARATION OF POLYMERIC NANOPARTICLES

4.2.1 REFERENCE FORMULATION

Double $W_1/O/W_2$ emulsion involves the dispersion of an aqueous phase W_1 (containing the drugs) in an organic phase (O) consisting of a polymer and solvent, followed by a second dispersion of the organic phase in an external aqueous phase (W_2) containing a stabilizer. First the inner aqueous phase (W_1) and subsequently the organic phase (O) are broken into droplets by the application of external energy (by sonication). Several factors can influence the preparation and the final characteristics of nanoparticles, such as hydrodynamic size, PDI

(Polydispersity Index), and efficiency in encapsulating drugs. The selection of formulation components, including polymers, solvents, and surfactants, can lead to different interactions and colloidal stabilities, affecting the final particle size. The concentration of the components in the formulation is also crucial. Changes in concentrations can lead to changes in solubility, viscosity, and stability. Furthermore, process conditions, such as temperature, emulsification device and amount of energy provided also affect the homogeneity of the formed particles (AGNER *et al.*, 2017). However, excessive energy input can also lead to unwanted effects, such as overheating or damaging sensitive components.

The polymer amount may be an important factor influencing the particle's characteristics and encapsulation efficiency. In this work, three PGl masses were evaluated for the nanoparticle preparation (0.7 g; 1.01 g, and 1.86 g). Formulations and experimental conditions evaluated for the preparation of the PGl NPs by the double emulsion solvent evaporation approach are in Table 7.

Table 7 – Formulations and experimental conditions evaluated for the preparation of the PGl NPs by the double emulsion solvent evaporation approach and their respective hydrodynamic size and PDI results.

Test formulations	**Parameters of the 1st Emulsion (W/O)**				**Parameters of the 2nd Emulsion (O/W)**			**Dp (nm)**	**PDI**
	Internal Aqueous Phase W1 (g)	Organic Phase (O) (g)		Sonication time (min)*	Mw of PVA (0.5% Solution, kDa)	External Aqueous Phase W2 (g)	Son. time (min)*		
	Mili-Q Water	Polymer (PGl)	Solvent (DCM)						
NPs PGl 01	0.35	0.7	10.50	5 [a]		N/A		N/A	N/A
NPs PGl 02	0.35	0.7	10.50	5 [b]	78 [c]	112	8 [b]	406.2 ± 1.5	0.27 ± 0.053
NPs PGl 03	0.50	1.01	10.18	5 [b]	78 [c]	112	8 [b]	474.7 ± 1.3	0.34 ± 0.006
NPs PGl 04	0.93	1.86	9.33	5 [b]	78 [c]	112	8 [b]	527.9 ± 2.4	0.63 ± 0.094
NPs PGl 05	0.50	1.01	10.18	5 [b]	30-70 [d]	112	8 [b]	292.5 ± 1.0	0.19 ± 0.006
NPs PGl 06	0.50	1.01	10.18	5 [b]	30-70 [d]	112	10 [b]	274.8 ± 1.9	0.15 ± 0.009
NPs PGl 07	0.50	1.01	10.18	5 [b]	30-70 [d]	112	12 [b]	244.5 ± 1.4	0.13 ± 0.009
NPs PGl 08	0.50	1.01	10.18	5 [b]	30-70 [d]	112	14 [b]	243.6 ± 0.9	0.13 ± 0.006
NPs PGl 09	0.50	1.01	10.18	5 [b]	30-70 [d]	112	16 [b]	278.8 ± 0.8	0.18 ± 0.016

N/A: No result was obtained because the Solvent DCM evaporated during the sonication of the [1s]t emulsion.

* Amplitude of 70% of the sonication tip and pulse regime (10on 5 off) constant.

[a] No ice bath application.

[b] With ice bath application.

[c] PVA with a degree of hydrolysis of 88%.

[d] PVA with a degree of hydrolysis of 87-90%.

The results obtained (Table 7) indicate that at a small amount (0.7 g) of polymer small particles were obtained (406.2 ± 1.5 nm) but as the amount of polymer was increased 1.01 and 1.86g, the particle size increased to 474.7 ± 1.3 nm, and 527.9 ± 2.4 nm, respectively. Similar results were reported by Ibraheem et al., (2014). This is because an increase in the amount of polymer is associated with an increase in the viscosity of the organic phase, turning more difficult droplet deformation and breakage and, consequently, emulsification (IBRAHEEM *et al.*, 2014). This observation was further supported by Colmán et al., 2011, who affirmed that elevated quantities of pre-dissolved polymer augment the proportion of generated particles, signifying its promotion of the droplet nucleation mechanism. Nevertheless, the investigation also highlighted a threshold in incorporating pre-dissolved polymers, as exceedingly high viscosities of the organic phase result in inadequate dispersion of monomer droplets (COLMÁN *et al.*, 2011).

In this study, initially the polymer-solvent ratio 1:5 (NPs PGl 01 and NPs PGl 02) was evaluated, at this higher ratio, the viscosity was so high that the emulsification efficiency was reduced. In sequence, this ratio was decreased to 1:10 (NPs PGl 03) and 1:15 (NPs PGl 04). Attempting to balance between the amount of solvent and organic phase viscosity that still allows an efficient emulsification, the 1:10 polymer-solvent was chosen and used in the subsequent experiments PGl 05, 06, 07, 08, and 09.

The results suggested that with decreasing amounts of PGl, the PDI of the emulsion also decreased, indicating that the viscosity of the emulsion is crucial in the homogeneity of the resulting size distribution of the nanoparticles.

Polyvinyl alcohol (PVA) was used as stabilizer in the external aqueous phase W_2 to reduce the interfacial tension between the aqueous and organic phases, preventing the droplets from coalescing during the solvent evaporation process (LOVELL; SCHORK, 2020). The colloidal stabilization of the NPs is essential to ensure uniform and well-dispersed nanoparticles

(KYRYCHENKO *et al.*, 2017). The most used stabilizers in those articles working with the double-emulsion process include PVA, Tween 80, and Span 80. However, PVA stands out (DEVRIM GÖKBERK; ERDINÇ, 2023; EBRAHIMIAN *et al.*, 2017, 2022; IQBAL *et al.*, 2015b; ÖZDAL *et al.*, 2022). PVA is a well-known hydrophilic polymer that is biocompatible and has good mechanical strength, low fouling potential, and long-lasting temperature and pH stability (IBRAHEEM et al., 2014; NAZARI; ABDELRASOUL, 2022). These properties of PVA make it a suitable candidate for use in the encapsulation of various pharmaceuticals and biopharmaceuticals

Two different molecular weight PVA were used as stabilizers, one with molecular weight of 78 kDa and degree of hydrolysis of 88 % (PVA^c) and other with molecular weight of 30 – 70 kDa and 87 – 90 % (PVA^d) of degree of hydrolysis. The degree of hydrolysis refers to the proportion of acetate groups in the polymer that have been replaced by hydroxyl groups, resulting in a modification of the PVA structure. It was observed that the use of PVA^c resulted in nanoparticles with larger hydrodynamic size and a higher PDI (polydispersion index) compared to the use of PVA^d in the formulations.

Another important factor is the time of exposure to the ultrasound probe. The energy supply is very important because a too-short sonication provides insufficient energy to the system, while a long sonication, besides of increasing process time and energy consumption, can also lead to the breakdown of the double emulsion, which in turn will lead to a low trapping efficiency and difference in particle size. In this experiment (Figure 32), only the sonication time of the second emulsion was changed, as demonstrated in other studies of double emulsion with tip (BECKER PERES *et al.*, 2016; DEVRIM GÖKBERK; ERDINÇ, 2023; IBRAHEEM *et al.*, 2014; IQBAL *et al.*, 2015a) where the duration of sonication during the initial emulsion (W1/O) phase does not notably impact particle size. However, the subsequent sonication stage holds more sway over the ultimate average particle size than the initial step. Hence, optimizing particle size reduction is achieved most effectively by prolonging the sonication period during the second emulsification phase.

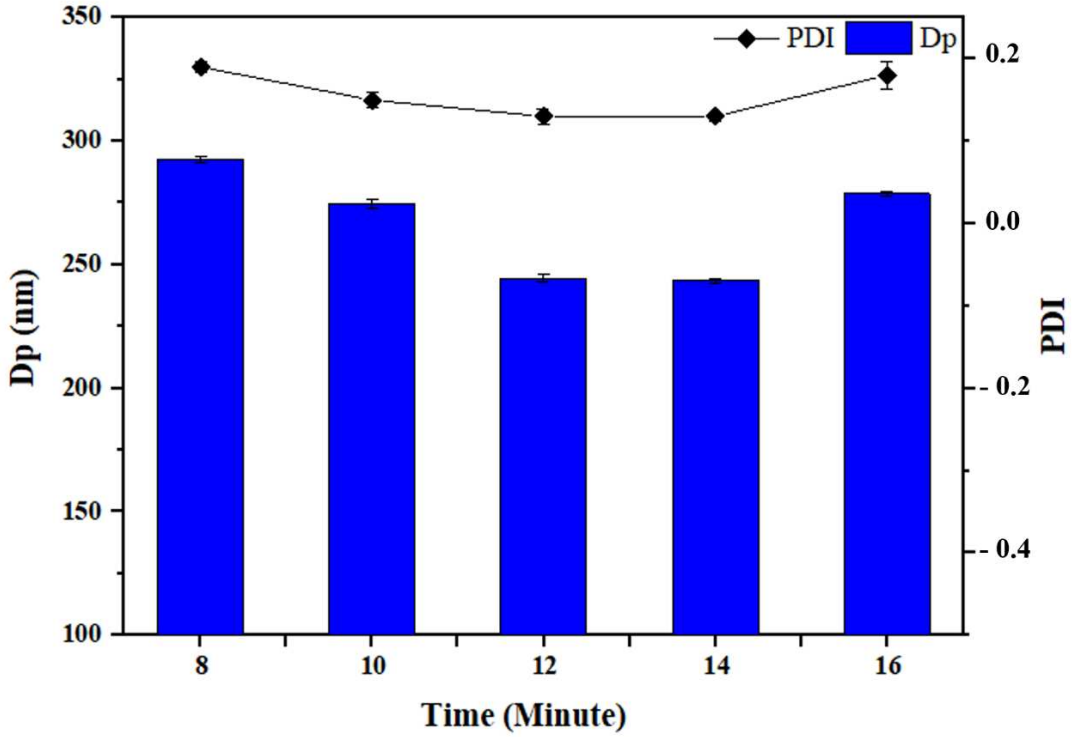

Figure 32 - Evaluation of the effect of the sonication time of the 2nd emulsion during the preparation of blank PGl NPs.

Five formulations were prepared with different sonication times of the second emulsion (8 min, 10 min, 12 min, 14 min and 16 min) and the particle sizes achieved were 292.5 ± 1.0 nm, 274.8 ± 1.9 nm, 244.5 ± 1.4 nm, 243.6 ± 0.9 nm and 278.8 ± 0.8 nm and their PDIs 0.19 ± 0.006; 0.15 ± 0.009; 0.13 ± 0.009; 0.13 ± 0.006 and 0.18 ± 0.016, respectively (Figure 32). It was verified that, with the increase of the ultrasound exposure time, the hydrodynamic size of the particles and PDI gradually decreased. This increase in energy with elongated exposure time to ultrasound causes more fragmentation of the droplets and, consequently, decreases the final size of the particles.

It is then possible to understand that an adequate sonication time is necessary to obtain small and monodisperse particles and to avoid the aggregation of the formed particles, however, this sonication time must not exceed a certain limit to the point of reducing the efficiency of the system, which was what happened in experiment NPs PGl 09, with an increase in the hydrodynamic size of the particles and their respective PDI.

4.2.2 PREPARATION OF ICG@NPS AND ICG~DOX@NPS BY THE DOUBLE EMULSION METHOD

The co-encapsulation of Indocyanine green (ICG) and Doxorubicin hydrochloride (DOX) in a polymeric nanoparticle aims to improve the therapeutic efficacy (CHEN, J. *et al.*, 2019; DANHIER *et al.*, 2010; HESHMATI AGHDA *et al.*, 2020; HUNG *et al.*, 2016; LONG *et al.*, 2020; MANCHANDA *et al.*, 2010; SHEN *et al.*, 2019; TANG *et al.*, 2010). Co-encapsulation can improve the biodistribution and pharmacokinetics of compounds and allow controlled release of encapsulated compounds at optimal levels, increasing blood circulation and preferential accumulation in the target tissue. This can result in a reduction in toxicities and unwanted adverse effects (CHEN, H.-H. *et al.*, 2019; FREIRE *et al.*, 2023; HESHMATI AGHDA *et al.*, 2020; HUNG *et al.*, 2016; LONG *et al.*, 2020)

4.2.2.1 PHYSICAL-CHEMICAL AND MORPHOLOGICAL CHARACTERIZATION OF BLANK NANOPARTICLES AND ENCAPSULATING ICG AND ICG + DOX

Hydrodynamic size distributions, morphology and zeta potential of nanoparticles.

Particle size influences release, biodistribution and absorption of nanoparticles (GAUMET *et al.*, 2008; ROUSSAKI *et al.*, 2014). The hydrodynamic intensity average particle size (D_p) and dispersity (PDI) of each PGl NPs sample were examined and are shown in Table 8. The presented values are the average of at least 3 independent measurements. As Table 8 shows, PGl NPs presented low PDI values, indicating the formation of a narrow size distribution (Figure 33). All the NPs were smaller than 300 nm, which means they can be good candidates for passive targeting based on the EPR effect (SUBHAN *et al.*, 2023) and phototherapy applications. Research suggests that suitable particle size generally depends on the target tissue; however, the upper size limits typically fall within the range of 20 – 400 nm (ROUSSAKI *et al.*, 2014).

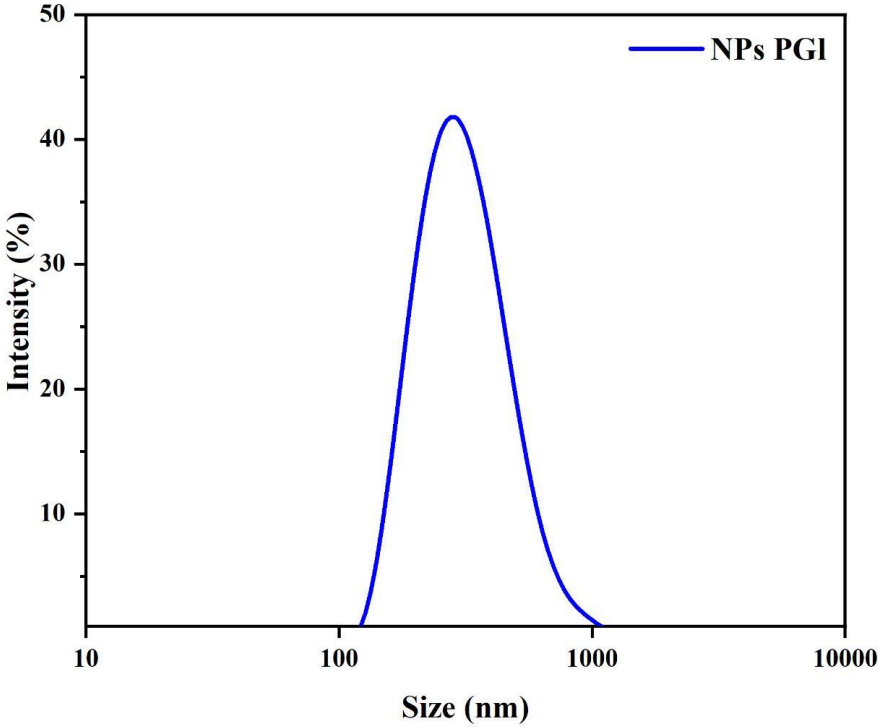

Figure 33 - Hydrodynamic Size Distribution by Intensity of blank PGl NPs (F0, Table 8)

The formulations that contain ICG in different concentrations (F1 and F2) and with the addition of DOX (F3 and F4) presented slightly bigger average sizes (Table 8).

Table 8 - Hydrodynamic particle size and polydispersity indices of the five formulations

PGl NPs	D_p (nm)	PDI (-)
F0 (Blank)	244.50 ± 1.40	0.13 ± 0.01
F1 (1.25mg of ICG)	252.87 ± 1.85	0.15 ± 0.03
F2 (5mg of ICG)	257.77 ± 1.70	0.14 ± 0.03
F3 (1.25mg of ICG + DOX)	261.80 ± 1.65	0.14 ± 0.03
F4 (5mg of ICG + DOX	265.17 ± 1.40	0.15 ± 0.02

This increase is often observed when the drugs are incorporated with certain efficiency inside the polymeric nanoparticle matrix, this can be explained by the fact that they occupy additional space within the polymeric matrix, the need for these drugs to be solubilized in the internal aqueous phase or also due to the interaction with the polymeric matrix through bonds or forces of attraction, all of which may lead to an increase in particle size (CHENTHAMARA

et al., 2019). It is important to emphasize that the increase in hydrodynamic size is not necessarily deleterious, as long as it is within an acceptable range for the desired application.

The size of nanoparticles directly influences their ability to transport and release encapsulated drugs, thus allowing their efficient penetration into target tissues, and cells directly affecting the effectiveness of the treatment. It also influences its biodistribution in the body, preventing rapid elimination by the immune system, allowing greater circulation in the blood, and increasing exposure to target tissues or organs (AFZAL *et al.*, 2022). In addition to being important for the colloidal stability of nanoparticles, a narrow size distribution and low PDI indicate that the particles are more uniform, reducing the likelihood of agglomeration or sedimentation. This is essential to maintain suspension homogeneity and ensure nanoparticle stability during storage and administration (MASARUDIN *et al.*, 2015).

In addition, inappropriate size and PDI can trigger unwanted immune responses or increase the toxicity of nanoparticles. Very large particles can be recognized as foreign bodies, activating the immune system. On the other hand, very small particles can accumulate in specific organs and cause dose-related toxicity (ZOLNIK *et al.*, 2010).

The zeta potential reflects the strength of the colloidal particles electrical barrier and is used as a parameter in evaluating the electrostatic stabilization of colloidal dispersions (IQBAL *et al.*, 2015a). To point out the effect of pH on the particles surface charge density, the zeta potential of PGl nanoparticles was determined as a function of pH, with a blank sample.

Between pH 3 and 12 the zeta potential of PGL nanoparticles oscillated between 2.0 mV and −2.0 mV, which could be considered near to zero. This result can be attributed to uncharged chemical nature of PGl and also to the screening effect of PVA. Normally, for charged particles, the use of non-charged stabilizer leads to the surface charge screening effect and shift in sleeping plan position far from particles surface, which induce decreases in the absolute value of the zeta potential (IQBAL et al., 2015a). Thus, PVA provides a steric stabilization to the nanoparticle dispersion. PVA provides colloidal stability over a wide range of temperature and ionic strength, whereas particles produced with ionic surfactants flocculate in moderate ionic strength solutions upon collapse of the hydrogel as the temperature is increased (LEE et al., 2010).

The TEM images, as shown in Figure 34, provided an insight into the morphology of the nanoparticles. These images revealed that the nanoparticles exhibited a spherical shape, confirming the submicron sizes previously determined through DLS analysis.

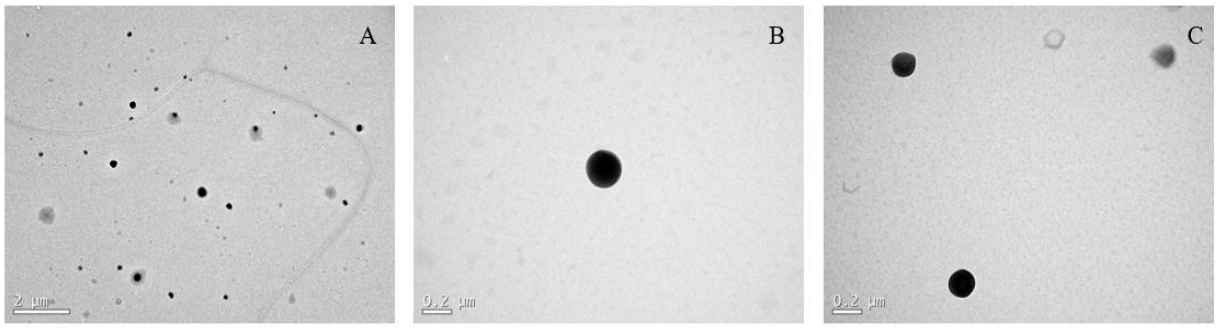

Figure 34 – TEM analysis of Formulation F0 (blank NPs).

Figure 37 shows the profile of the heating curves comparing the four formulations and highlights the incorporation and miscibility of ICG and DOX, comparing this figure with the DSC thermogram of PGl (shown in Figure 35), we can see that the Tm found was 50.75 ºC, 50.93 ºC, 51.22 ºC, 51.71 ºC, for formulations F1, F2, F3, F4, respectively.

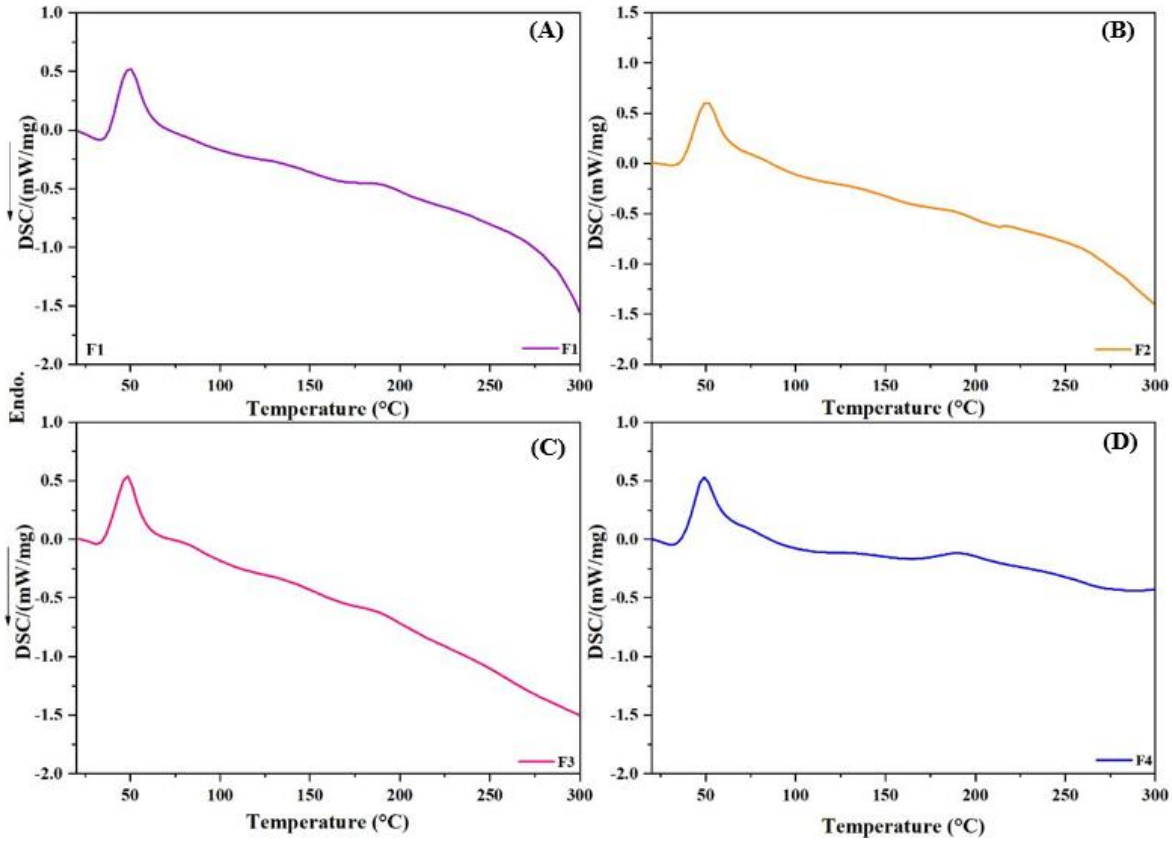

Figure 35 – DSC thermograms of NPs: (A) NPs ICG 1.25mg (F1), (B) NPs ICG 5 mg (F2), (C) NPs ICG 1.25 mg + DOX (F3), and (D) NPs ICG 5 mg + DOX (F4)

Fourier Transform Infrared Spectroscopy – FTIR: As shown in Figure 38, in the samples, F1, F2, F3, F4, all infrared spectra exhibited absorption bands at 3384 cm^{-1}, attributed to the elongation of –OH, which may indicate the presence of water. There are several hydroxyl groups (OH) in the structure of doxorubicin hydrochloride, which are attached to the aromatic rings and both ICG and DOX, because they are amphiphilic (with high solubility in water) and hydrophilic, have the ability to absorb water.

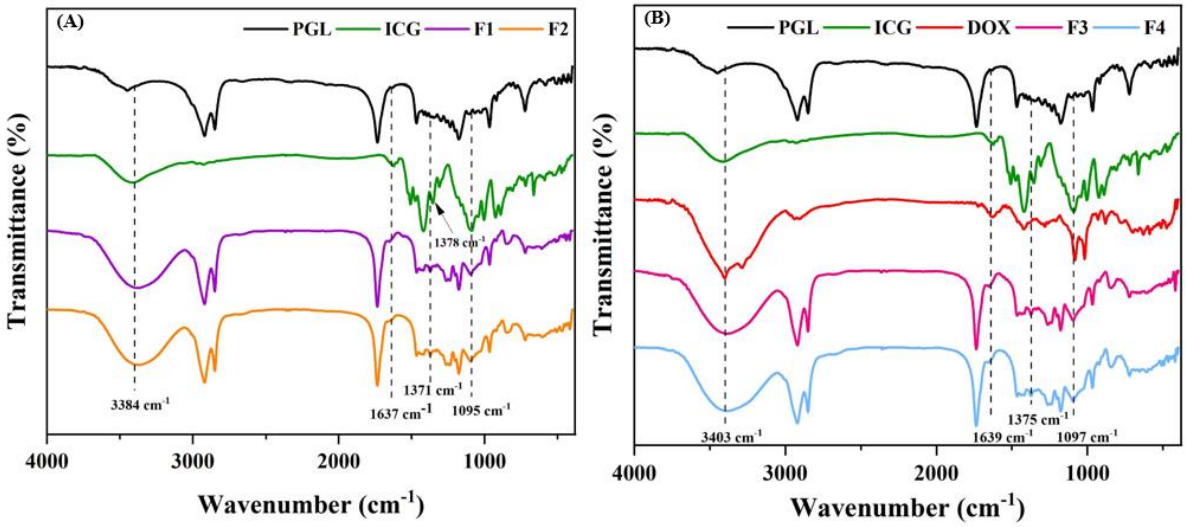

Figure 36 – (A) PGL, ICG, NPS ICG 1.25 mg (F1) and NPS ICG 5 mg (F2) spectra; (B) PGL, ICG, DOX, NPS ICG 1.25 mg + DOX(F3) and NPS ICG 5 mg + DOX (F4) spectra.

The results showed the absorption spectra of pure PGl and ICG (A), as well as the nanoparticles (NPs) prepared from these compounds. The shifts at 2927, 2852 are associated with the C–H stretching; 1736 cm^{-1} corresponds to the C=O stretching; 1468 cm^{-1} is associated with a bending vibration (ZHANG et al., 2021); 721 cm^{-1} reflects cis RCH = CHR; 965 cm^{-1} corresponds to trans RCH = CHR; 1174 cm^{-1} is associated with C-O-C bonds and 1093 cm^{-1} with a C–OC– vibration, characteristic bands of poly(globalide) nanoparticles (SAVIN *et al.*, 2018).

Additionally, a band was observed at 1641 cm^{-1} with low intensity in both F1 and F2. This band is attributed to the bending of the H–O–H bond, characteristic of ICG. The presence of this band indicates that some characteristics of ICG are present in the NPs but with shifts and lower intensity, due to the low ICG:PGl ratio. Another characteristic band of ICG observed in the NPs is at 1374 - 1358 cm^{-1}, representing the stretching vibrations of CO in carboxylic groups. The peak at 1095 cm^{-1}, attributed to ICG, was also present in both F1 and F2 (YU *et*

al., 2023). This observation reinforces the idea that both compounds are present in the NPs, leading to changes in the intensities of the absorption bands. The results suggest that the PGl nanoparticles encapsulated the ICG, as its spectroscopic characteristics differ from those of its pure forms.

Overlapping peaks in the Fourier Transform Infrared (FTIR) spectrum is a common challenge in the characterization of complex samples, in this case involving the encapsulation of compounds such as DOX. DOX is a drug with functional groups that may present infrared absorption bands similar to those of the polymer or other components present in the system, making it difficult to directly and isolate identify the bands corresponding to the encapsulated compound. The FTIR technique can be considered a complementary analysis to the quantitative determination of encapsulation efficiency by spectroscopy.

4.3 DRUG ENCAPSULATION EFFICIENCY

ICG and DOX Encapsulation Efficiencies

ICG is a promising therapeutic agent for several types of cancer. However, studies on the effects of polymeric nanoparticles incorporating only ICG in PDT and PTT are few, as most of the existing literature on these systems also includes a chemotherapeutic agent to achieve better suppression of cancer cells.

In this way, the development of nanocarriers that co-encapsulate ICG and DOX has become an efficient strategy to increase the stability of ICG (CHEN, J. et al., 2019; GÜNEY AKKURT; GÜLSOY, 2022; ZHENG et al., 2013), minimize the adverse effects of DOX (cardiotoxicity, myelosuppression, mucositis, and alopecia) (GÜNEY AKKURT; GÜLSOY, 2022) and increase the efficiency of encapsulation of ICG and its accumulation in the tumor through passive targeting (TANG *et al.*, 2010).

Here, we were able to co-encapsulate two therapeutic agents, ICG and DOX, in different concentrations, by Double Emulsion Method based on previous studies which also encapsulated ICG and DOX in polymeric particles (FERREIRA *et al.*, 2021; HESHMATI AGHDA *et al.*, 2020; HUNG *et al.*, 2016; MANCHANDA *et al.*, 2010; SHEN *et al.*, 2019), however, they were performed using different methods since and polymers there are no studies in the literature so far that describe the same approach used in this study. The drug encapsulation efficiency (EE) of the NPs is crucial for their clinical application. The encapsulation efficiencies, both of

ICG (in formulations F1, F2, F3, and F4) and DOX (F3 and F4), are shown in Table 9 and represent the average values of triplicate experiments of each formulation.

Table 9 - Encapsulation Efficiency (EE%) of ICG and DOX

	ICG (EE%)	**DOX (EE%)**
F1	83.2 ± 0.4 %	-
F2	91.7 ± 4.6 %	-
F3	90.3 ± 1.7 %	63.4 ± 1.7 %
F4	93.1 ± 5.0 %	59.5 ± 2.2 %

Comparing the results found in this study with those reported in the literature (nanoparticles that encapsulated only ICG), it can be observed that often the efficiencies were higher. For example, Kim et al., (2010) reported efficiency of ICG loading ranged from 39 – 78% depending on the concentration of ICG, while other studies reported 58.4% (WATANABE et al., 2017), 65.2 ± 1.1% (MA *et al.*, 2012), 74% (SAXENA *et al.*, 2004b), 74.5 ± 2.2% (SAXENA *et al.*, 2004b), and 89 ± 6.8% (RODRIGUEZ *et al.*, 2008).

Other studies in which ICG and DOX have been co-encapsulated within polymeric NPs have reported similar EE% for ICG, 92.1% and 96.8% (ZHANG *et al.*, 2018), 98% (WU *et al.*, 2020) and 98.4% (SHU *et al.*, 2018). In contrast, it was also possible to find articles that had lower efficiency values, such as 44.4 ± 1.6% (MANCHANDA *et al.*, 2010), 47.8% (ZHENG *et al.*, 2013), 45.2 ± 1.4% ICG (SRINIVASAN *et al.*, 2014). Thus, it is possible to conclude that ICG has been successfully encapsulated in these PGl nanoparticles by the double emulsion solvent evaporation technique.

Evaluating the efficiency values for Doxorubicin Hydrochloride, the values found in the literature for different types of NPs and using different encapsulation methods are between 40% and 96%, 43.8% (ZHENG et al., 2013), 70.3 ± 3.4% (SRINIVASAN et al., 2014), 71.6% (SHEN et al., 2019), 71.8%, (SHU et al., 2018), 74.3 ± 1.9% (MANCHANDA et al., 2010), 85% (WU et al., 2020) and 96.2% (ZHANG et al., 2018). In addition, it was also possible to corroborate with a study of Tewes et al., who prepared PLGA particles loaded with doxorubicin. The hydrodynamic size of DOX-loaded particles was found to be 316 nm and its encapsulation efficiency was 67 %. Thus, we can state that the efficiency is within the values found in the literature, however, comparing with some of these same works, the encapsulation efficiency rate was lower, which can be explained by the competition with other components

in the formulation, or adverse interaction during the nanoparticle formulation process (TEWES *et al.*, 2007).

As shown in Table 9, ICG efficiency slightly increased with increasing ICG concentration (from 2.5 mg/mL to 5.0 mg/mL). This can be explained by the fact that there is a greater amount of drug molecules available to interact with the polymer during the encapsulation process eventually leading to stronger non-covalent interactions between molecules, promoting greater retention of the drug in the polymeric matrix.

Corroborating to the literature, there was an increase in the ICG encapsulation efficiency rate when added to DOX in the formulation of nanoparticles, in F1, for example, it was 83.2 ± 0.4% and became 90.3 ± 1.7% in F3, demonstrating an increase of about 8.5%.

Previous research has shown that concentrations of 5 μM of ICG and 10 μM of DOX are effective in producing hyperthermia in combination with that singlet oxygen and chemotherapy (MANCHANDA et al., 2010), thus considering good results, together with the fact that the high efficiency of drug trapping and the small particle size are desirable characteristics for the process.

4.4. FUNCTIONALIZATION OF PGL NPS, ICG@PGL NPS, AND ICG-DOX@PGL NPS WITH BOVINE SERUM ALBUMIN (BSA)

Functionalization of Nanoparticles with Bovine Serum Albumin (BSA)

The functionalization of the surface of PGl nanoparticles with BSA can improve stability, biocompatibility, forming a protein corona and having specific targeting and interactions, in addition to improving drug delivery (SHANWAR et al., 2021). The adsorption of BSA can be influenced by pH, temperature, and ionic strength, which affect the surface charge of both the nanoparticles and the BSA protein (ACUÑA-NELSON *et al.*, 2020).

The representation of the nanoparticle developed in this study, with the PGl shell, encapsulating ICG and DOX (F3 and F4) and functionalized with BSA is shown in Figure 39.

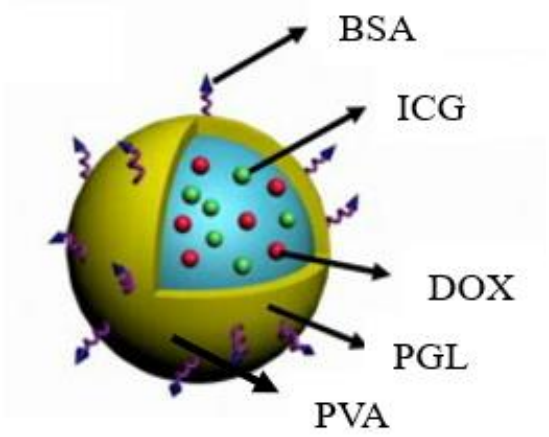

Figure 37 - Representation of the nanoparticle developed in this study, with the PGl shell, encapsulating ICG and DOX (F3 and F4) and functionalized with BSA.

Protein quantification by Lowry assay

PGl NPs were successfully prepared by double emulsion-solvent evaporation method. In sequence, NPs were functionalized with the model protein BSA, by the adsorption method. Particle size and dispersity (PDI) were determined by DLS measurements. For uncoated PGl NPs, the mean particle diameter was determined to be around 244.5 ± 1.4 nm, with a PDI value of 0.13 ± 0.009. After functionalization with BSA, the nanoparticles kept a uniform size distribution, but the mean particle diameter value increased from 244.5 ± 1.4 nm to 260.4 ± 1.23 nm. This slight increase in hydrodynamic size is probably associated with the development of a layer of BSA (bovine serum albumin) that surrounds the nanoparticles (NPs). This fact can be evidenced by the study by Guindani et al., (2020), who concluded that after conjugation with BSA in PMMA NPs, the conjugates maintained a uniform size distribution and the mean value of the particle diameter increased from 151 ± 1 nm to about 179 ± 2 nm (GUINDANI *et al.*, 2020). Simon et al. (2018) also reported a similar increase of approximately 15 nm in particle diameter when conjugating amino and carboxy functionalized polystyrene NPs with IgG-depleted plasma. This remarkable increase in mean particle diameter further indicates the effective conjugation of BSA on the surface of NPs (SIMON *et al.*, 2018).

The amount of BSA adsorbed to PGl NPs was obtained by performing the Lowry protein quantification assay, according to Table 10.

Table 10 - Amount of BSA adsorbed to PGl NPs obtained by performing the Lowry protein.

	Diameter part. (nm)	Adsorption Efficiency (%)	Mass of adsorbed BSA per mL emulsion (ug/mL)	BSA molecules per area (nm^2)	BSA molecules / NPs (x 10^{-6})
F1 + BSA	266.87 ± 13,07	58.95 ± 2,27 %	203.37 ± 7,84	5.59 ± 0,14	1.13 x 10^6 ± 1,34 x 10^5
F2 + BSA	271.77 ± 11,73	63.42 ± 5,97 %	218.99 ± 20,40	6.17 ± 0,81	1.30 x 10^6 ± 2,73 x 10^5
F3 + BSA	275.80 ± 9,08	63.76 ± 4,44 %	219.96 ± 15,32	6.29 ± 0.64	1.37 x 10^6 ± 2.23 x 10^5
F4 + BSA	279.17 ± 10,06	64.45 ± 7,89 %	222.34 ± 27,24	6.44 ± 0.98	1.44 x 10^6 ± 3.22 x 10^5

According to the results obtained by Lowry's assay, all formulations presented rather similar adsorption efficiencies around 62 ± 3 % and > 58%. The interaction between the protein and the surface of the nanoparticle governs the adsorption process. Electrostatic forces and group interactions are often involved. By adsorbing BSA onto the surface of nanoparticles, it provides an accessible platform for subsequent applications.

4.5. COLLOIDAL STABILITY OF NPS

The stability of nanoparticles is an essential aspect of their application in several areas, including nanomedicine. The stability of blank PGl NPs was evaluated over a period of six months, Figure 41, starting from the moment they were prepared, using the Dynamic Light Scattering (DLS) technique, Figure 40. Initially, the hydrodynamic size of the particles was 244.5 ± 1.4 nm with a PDI value of 0.13 ± 0.009. Even after 6 months, the nanoparticles maintained remarkable stability, with a hydrodynamic size of 264 ± 0.77 nm and PDI of 0.10 ± 0.02.

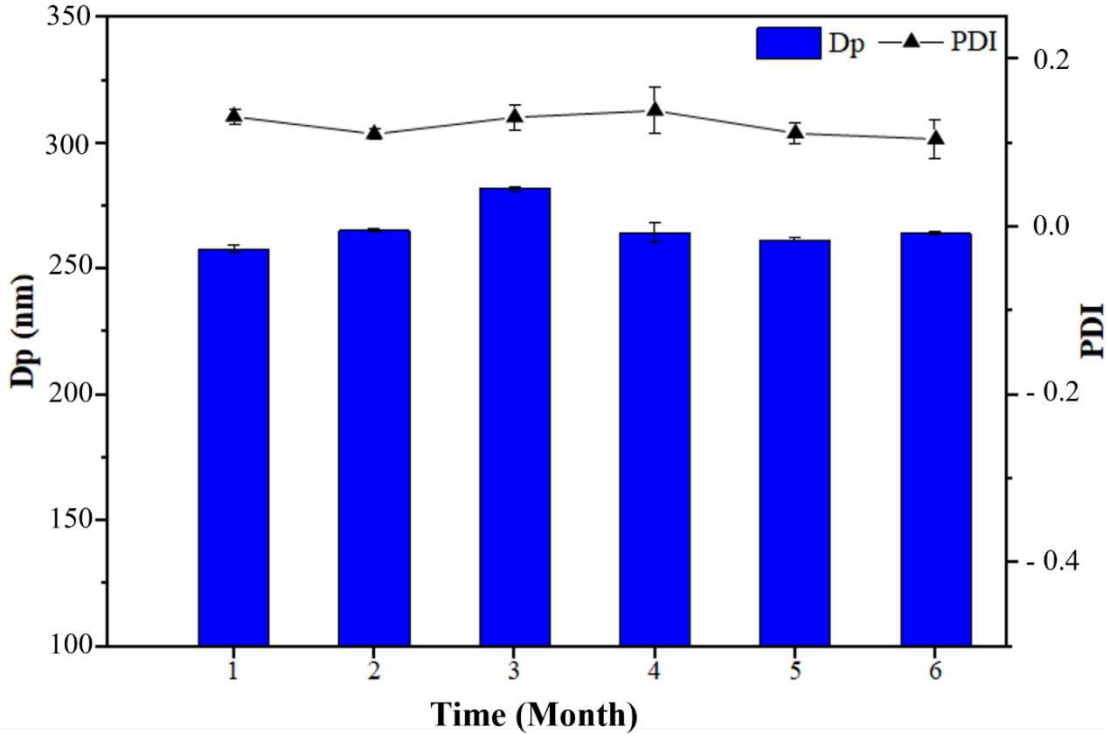

Figure 38 - Hydrodynamic particle size and dispersity during 6 months of storage of blank PGl NPs

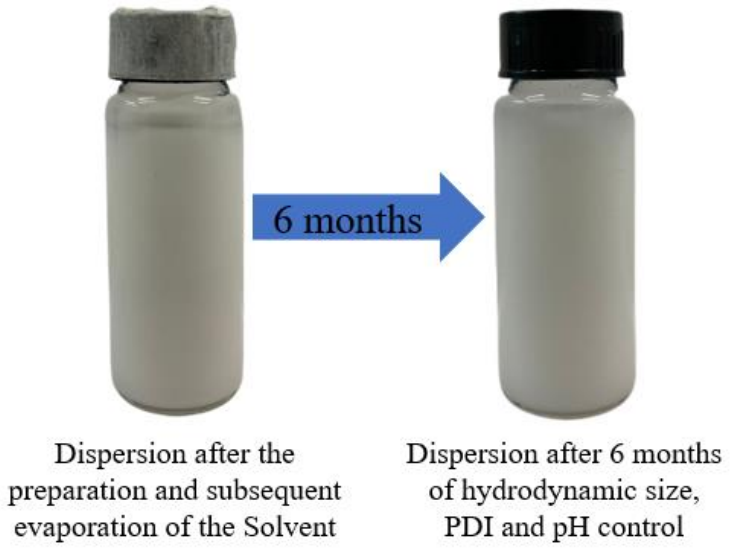

Figure 39 - Evaluation of the stability of the colloidal PGl dispersion

In addition, it is important to note that the pH of the system remained relatively constant 6.1 (right after preparation) and 6.9 after six months, which may have contributed to the preservation of the stability of the nanoparticles. These results are promising, suggesting that

nanoparticles remain with stability characteristics that make them potentially suitable for applications in therapeutic formulations that require stable particles in solution.

4.6 DRUG RELEASE

Figure 42 shows the results of the controlled release of nanoparticles containing ICG and DOX drugs.

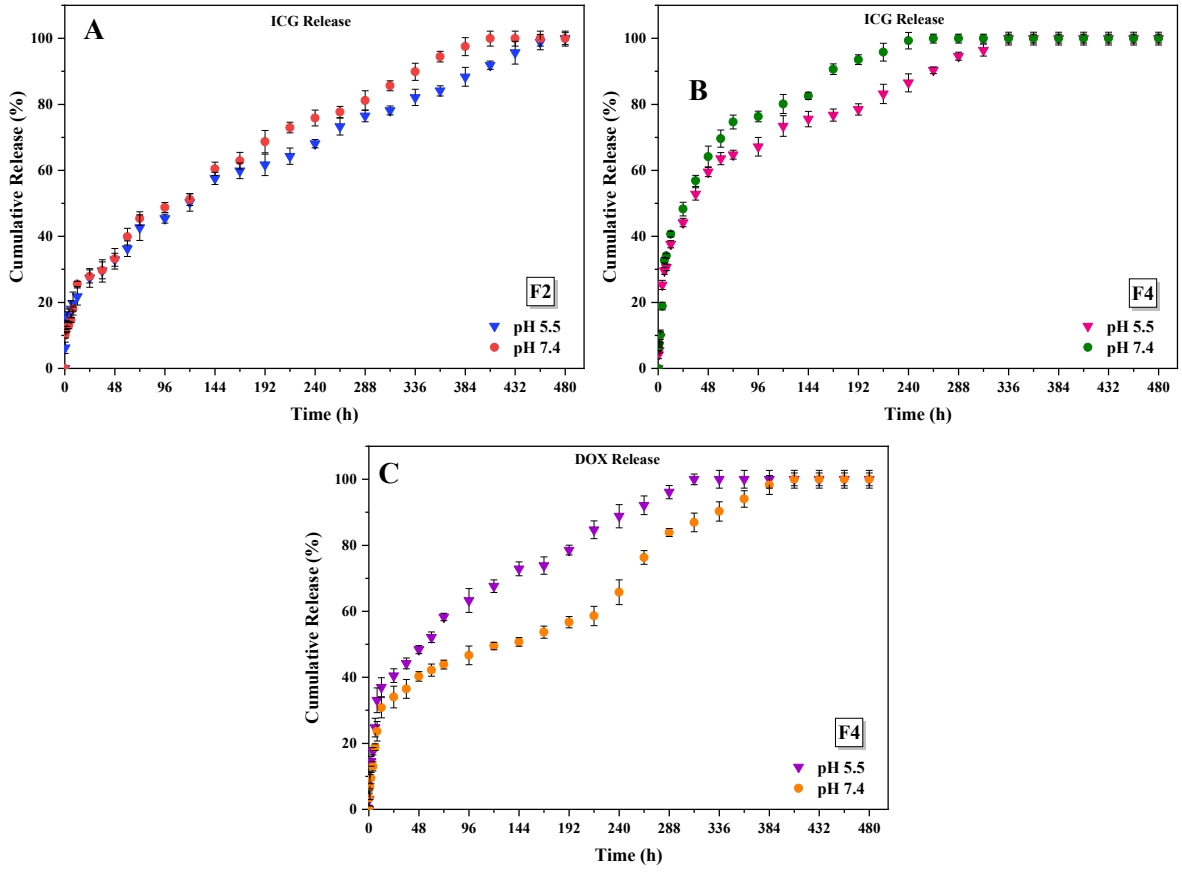

Figure 40 – ICG and DOX release at pH 5.5 and 7.4 A) F2 com 5mg de ICG, B) F4 com 5mg de ICG e 1,25mg de DOX (estudo do ICG) ; C) F4 com 5mg de ICG e 1,25mg de DOX (study of DOX).

In this study, we investigated the release of Indocyanine Green (ICG) and Doxorubicin (DOX) in formulations F2 (5 mg of ICG) and F4 (5 mg of ICG and 1.25 mg of DOX) at different pH values, simulating biological environments relevant.

At pH 5.5, both formulations exhibited moderate release of ICG, with F2 releasing approximately 27% after 24 h and 32% at 48 h and F4 releasing approximately 48% at 24 h and 59% at 48 h. The difference in release rate can be explained by the presence of DOX in the F4

formulation. DOX is a water-soluble drug that can cause a change in the structure of the polymeric matrix of nanoparticles, making it more permeable and, therefore, allowing a faster release of ICG. Furthermore, DOX is known to be a reducing agent, which can lead to polymer matrix degradation in acidic environments, such as pH 5.5 (WANG, S. *et al.*, 2019). This additional degradation may contribute to a faster release of ICG in the F4 formulation compared to the F2 that contains only ICG. This gradual release profile suggests that these formulations may be suitable for applications that require a more controlled release of ICG in acidic environments, such as tumor detection and treatment. The ability of nanoparticles to release drugs more quickly in acidic environments can be leveraged to target treatment to the tumor more effectively while minimizing exposure to healthy tissue.

Table 11 – Cumulative Release (%) of ICG over 7 days (168h) at pH 5.5 and pH 7.4

	F2	F4
pH 5.5	59%	76%
pH 7.4	62%	90%

Comparing F2 and F4, at different pH, it was noticeable that at pH 7.4 the formulations showed a faster ICG release compared to pH 5.5. Furthermore, it also suggests that the presence of DOX (at F4) may have influenced accelerating ICG release at physiological pH and acidic pH (SUN *et al.*, 2018).

Already evaluating the release of DOX, it was faster at pH 5.5 compared to pH 7.4, information corroborated by the studies by Zhao et al. (2017) , Zhang et al., (2018) and Hu et al., (2022), who concluded an increased release of DOX in an acid medium (HU *et al.*, 2022; ZHANG *et al.*, 2018; ZHAO *et al.*, 2017).

Table 12 - Cumulative Release (%) of DOX in the period of 8h, 24h and 48h at pH 5.5 and pH 7.4

	8 h	24 h	48 h
pH 5.5	33%	44%	48%
pH 7.4	23%	34%	40%

The kinetic profile of release at pH 7.4 may be similar to that previously reported by the group of Manchanda et al., (2009) and Srinivasan et al., (2014) (SRINIVASAN *et al.*, 2014)

which achieved a sustained release of DOX of 48 ± 2% in 48 hours. DOX release is also consistent with literature reports of DOX-loaded PLGA nanoparticles, where a biphasic drug release profile is displayed. The two drug release phases refer to an initial rapid release followed by a slow and sustained release of DOX (CHITTASUPHO *et al.*, 2009; TANG *et al.*, 2010; YANG *et al.*, 2007).

Furthermore, as can be seen in Figure 42, over 12 days (288 h), in F4, ICG release was faster than DOX release at pH 7.4, where ICG had 99% release while DOX presented 83%. This agrees with the results of Kalaria et al. (2009), who showed a slower release of DOX when compared to ICG in a certain period of days (KALARIA *et al.*, 2009).

The tests showed the controlled and gradual release profiles of the compounds of interest under different pH conditions. This result makes NPs versatile for diverse clinical applications, including tumor-targeted therapies. The pH response allows these formulations to adjust to the specific needs of the biological environment, ensuring accurate and effective drug delivery. The controlled, gradual release allows the drug concentration at the target site to be maintained within an effective therapeutic range for an extended period. In addition, it reduces drug concentration peaks in the body, minimizing unwanted adverse effects that may occur with the administration of high single doses.

4.7 IN VITRO STUDIES

4.7.1 IN VITRO CYTOTOXICITY ASSAY

4.7.1.1 MTS ASSAY (METABOLIC ACTIVITY)

MTS assay, Figure 41, was carried out to measure the cell viability and the metabolic activity of murine cell line of fibroblasts - L929, and then to determine the cytotoxicity of the nanoparticles with 11 different concentrations (0.7, 1.4, 2.6, 5.3, 10.5, 21.1, 42.2, 84.4,1 68.7, 337.5 and 675 ng/mL) at 24 h. The initial nanoparticles concentration employed in the assay, 675 ng mL^{-1}, resulted in a sample comprising 50% culture medium and 50% nanoparticles, signifying an excessive nanoparticle concentration. Consequently, nearly all samples exhibited cytotoxicity at this concentration. However, upon conducting sequential dilutions, the metabolic activity results reveal that concentrations of nanoparticles starting from 168.7 ng mL-1 (for nanoparticles without BSA functionalization) are deemed non-cytotoxic following a 24-

hour incubation period, (Figure 41), and cell viability remained above 70 %. This is important information, as it indicates that the nanoparticles did not cause significant damage to the cells and are safe to use in subsequent experiments.

Through the MTS, the concentration that was used for the phototherapy test was determined, and it was decided to use the first dilution (168.7 ng/mL ~ second dilution), which exhibited no signs of toxicity.

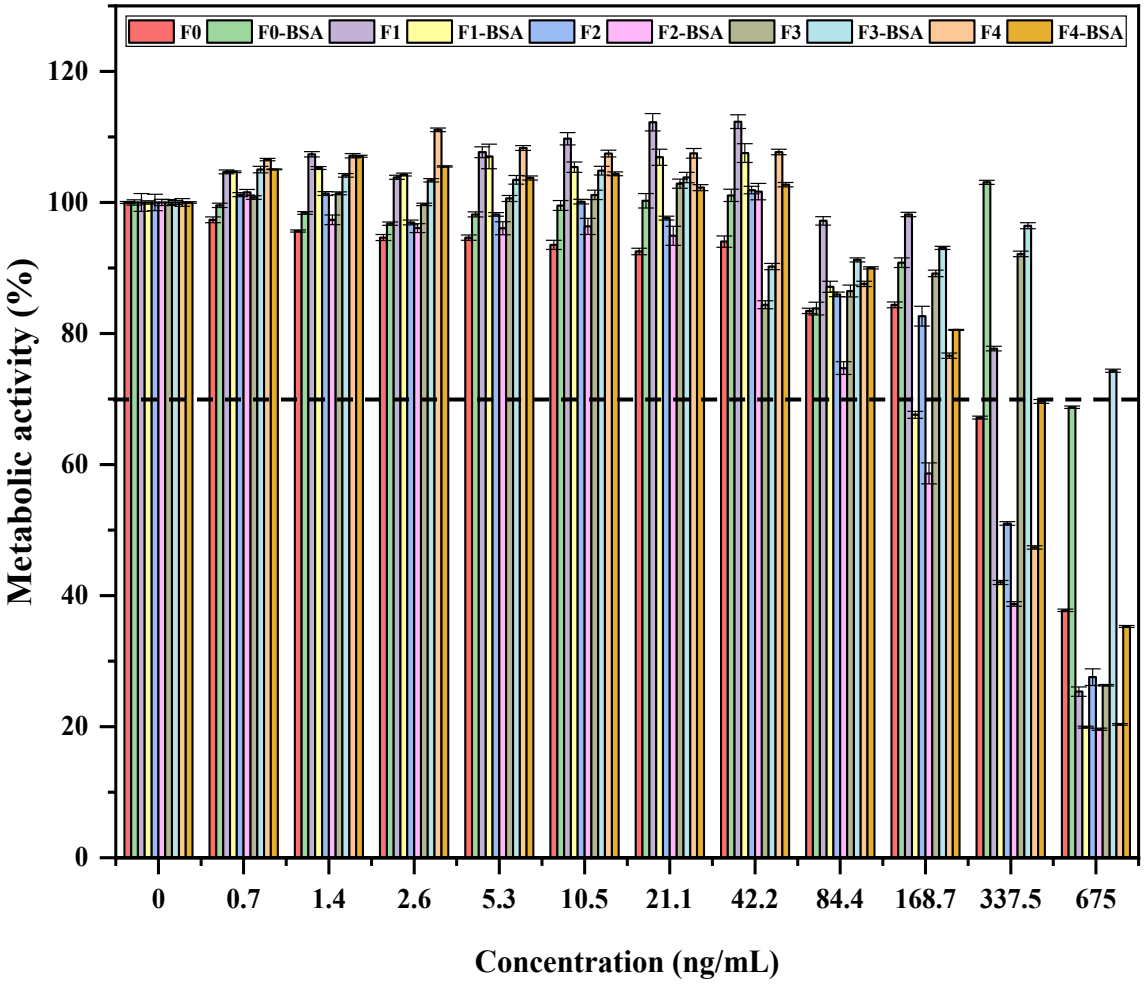

Figure 41– Cytotoxicity assay in the 10 formulations F0 (Blank NPs), F1 (ICG 1.25mg), F2 (ICG 5mg), F3 (ICG 1.25mg + 1.25mg DOX), F4 (ICG 5mg + 1.25mg DOX), without or with addition of -BSA (Bovine Serum Albumin).

By choosing a concentration that is not necessarily cytotoxic for the phototherapeutic assay, we guarantee that final result will be more accurate, because in themselves, the nanoparticles will not cause significant damage to the cells or tissues in question, thus allowing

a more correct assessment of the effects of the encapsulated drug with the application of phototherapy.

4.7.2. PHOTODYNAMIC AND PHOTOTHERMAL ACTIVITY ON MELANOMA CELLS: PHOTOXICITY STUDIES

The therapeutic potential of the developed nanoparticles was assessed by examining the metabolic activity of SKMEL-28 cells (melanoma) following their incubation with the nanoparticles and subsequent laser irradiation at 808 nm. The experimental procedure involved an initial 24-hour incubation period for cell adhesion and proliferation. Subsequently, the cells were exposed to non-toxic nanoparticle doses and incubated again to facilitate nanoparticle internalization. After 6 hours of internalization (CHEN, H.-H. *et al.*, 2019), the cells underwent a washing step to remove non-internalized material. Following this, a single laser irradiation (808 nm) was administered at varying exposure durations (2.5, 5, 7.5, and 10 minutes). Following irradiation, the cells were once again incubated, and metabolic activity was assessed at 24h and 48h post-irradiation using MTS assays.

The results of the phototherapy assay with SKMEL-28 cells in 24h are shown in Figure 42.

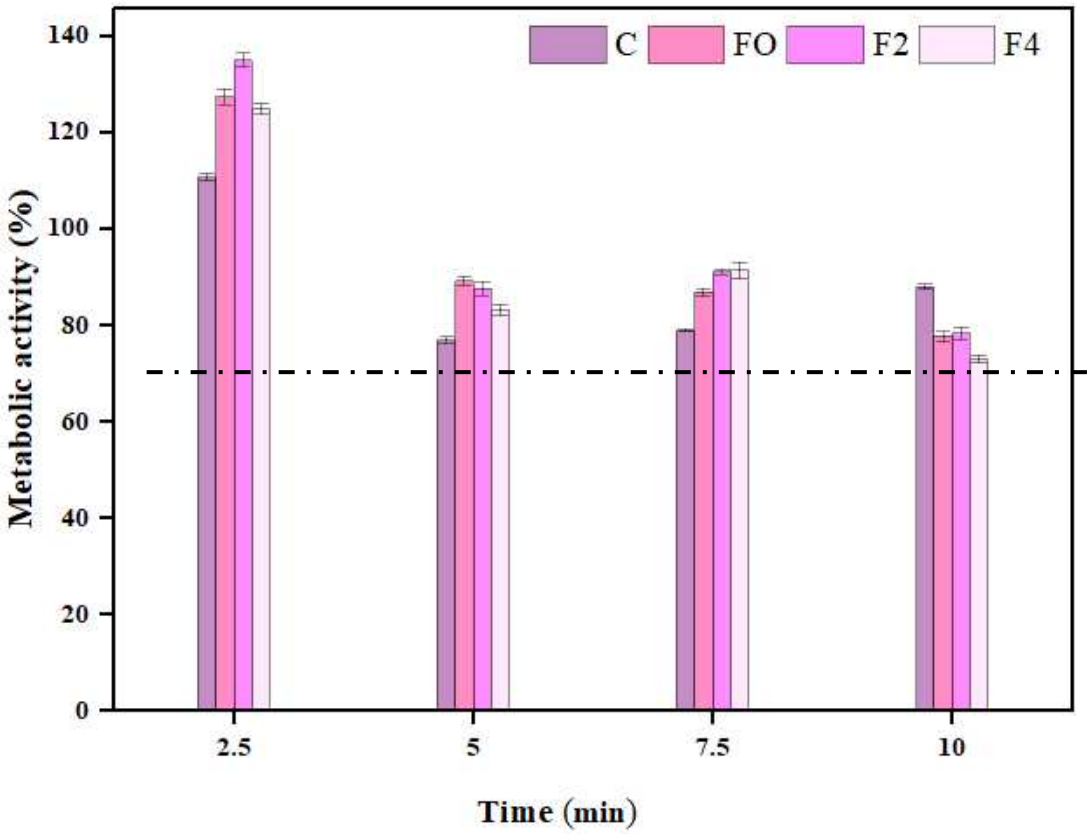

Figure 42 – Metabolic activity of SK-MEL-28 cells after 24 hours of laser phototherapy under different conditions in the presence of drug: C – Control cells, without nanoparticles; FO – Cells with white nanoparticles (No Drug); F2 – Cells with NPs 5mg of ICG; F4 – cells with NPs with 5mg of ICG + 1.25mg of DOX

The irradiation time with the 808nm laser played an important role in photodynamic/photothermal therapy. In this experiment, it was observed that a time of 2.5 minutes was insufficient to obtain positive results, that is, a decrease in metabolic activity. This could be because such a short time may not provide enough energy to effectively activate the nanoparticles or induce biological responses in cells.

When the irradiation time increased to 5 and 7.5 minutes, a decrease in metabolic activity was observed, which is an indication of the drug's cytotoxic activity during phototherapy. This may indicate that this time interval is necessary to allow the nanoparticles to absorb laser energy and release this energy effectively, so that drug activation occurs and triggers reactions that affect cells, such as the generation of reactive oxygen species. (ROS) that can damage target cells. Finally, when was increased the irradiation time to 10 minutes, was obtained the best results, with metabolic activity between 70% and 80%. This fact showed that a longer cumulative time of irradiation resulted in greater therapeutic efficacy, that is, cell death of the tumor lineage, information corroborated by Zheng et al., (2013) and Wu et al., (2020) (WU *et al.*, 2020; ZHENG *et al.*, 2013).

Following the assessment of metabolic activity conducted 24 hours post-irradiation, the cells were subsequently re-incubated and subjected to analysis 48 hours later. In this new assessment of metabolic activity, Figure 43 reveals that there were positive alterations in metabolic activities. Following the second incubation period post-irradiation, the cells underwent a recovery in their metabolic activity, leading to proliferation, as the capacity of cancer cells to multiply is their most prominent trait. This observation suggests the potential requirement for additional irradiation cycles to confirm the sustained phototherapeutic effect of the nanoparticles.

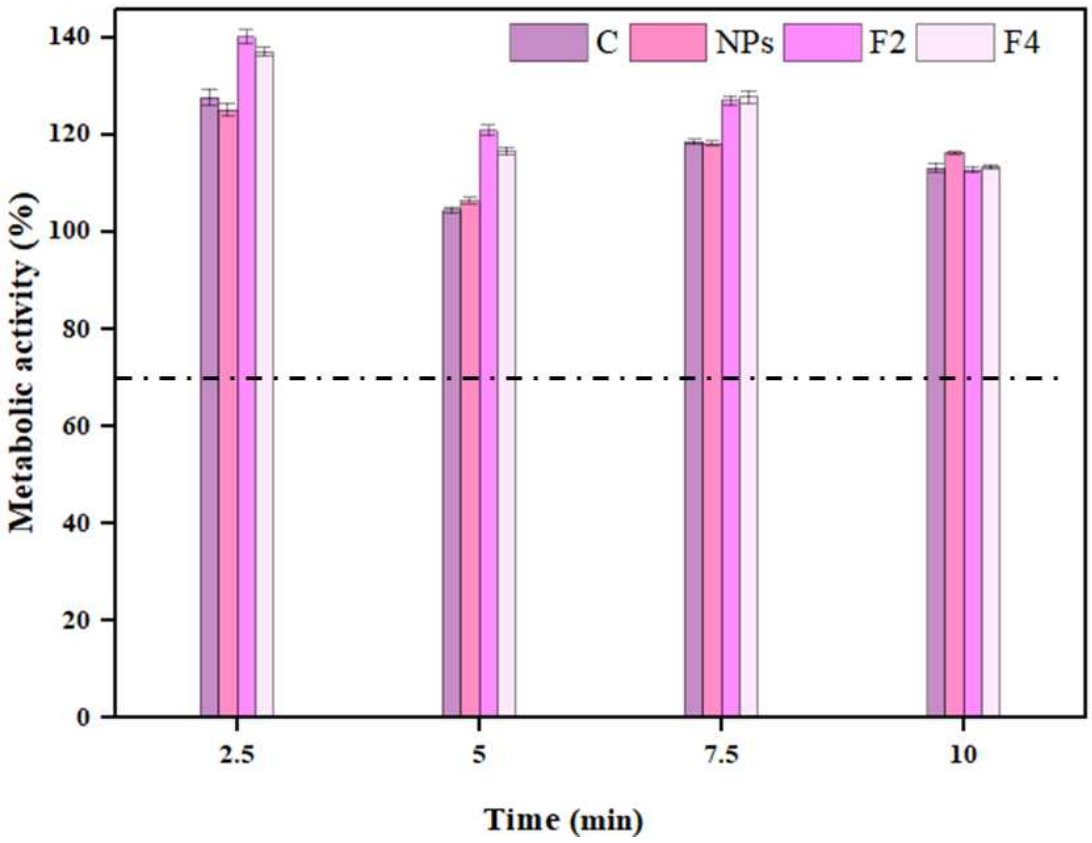

Figure 43 – Metabolic activity of SK-MEL-28 cells after 48h of laser phototherapy under different conditions in the presence of drug: C – control cells, without nanoparticle; FO – cells with white nanoparticles (without drug); F2 – cells with NPs 5mg of ICG; F4 – cells with NPs with 5mg of ICG + 1.25mg of DOX

The presented findings suggest a limited therapeutic efficacy of nanoparticles in addressing melanoma cancer cells. This outcome could be attributed to various factors, including the potential suboptimal methodology owing to time constraints during the research. Many of the conditions employed were based on parameters found in previously published studies, encompassing sample irradiation durations, internalization time of nanoparticles by cells (CHEN, H.-H. *et al.*, 2019; GÜNEY AKKURT; GÜLSOY, 2022; HESHMATI AGHDA *et al.*, 2020; ZENG *et al.*, 2021), other parameters were randomly chosen, such as the irradiation distances. Considering this crucial parameter, we replicated the experiment with varying irradiation distances between the laser lamp and the samples. The initial distance of 25 cm proved insufficient to induce temperature alterations in the medium. Consequently, a new experiment was conducted with a reduced distance of 15 cm between the lamp and the sample, as illustrated in Figure 44. Despite this adjusted distance still not causing significant

temperature changes in the medium, it does underscore the previously presented finding that 10-minute radiation exposures elicit a more pronounced cytotoxic effect on the examined cells, with metabolic activity below 70%. The F4 formulation was very close to the limit of metabolic activity (70%), based on other similar reports, the hypothesis that a slightly higher level of toxicity in the F4 within the 10 min period was raised, which may be due to the higher oxidative stress generated, which can induce cell apoptosis as the laser exposure time increases (PUJARI-PALMER *et al.*, 2016).

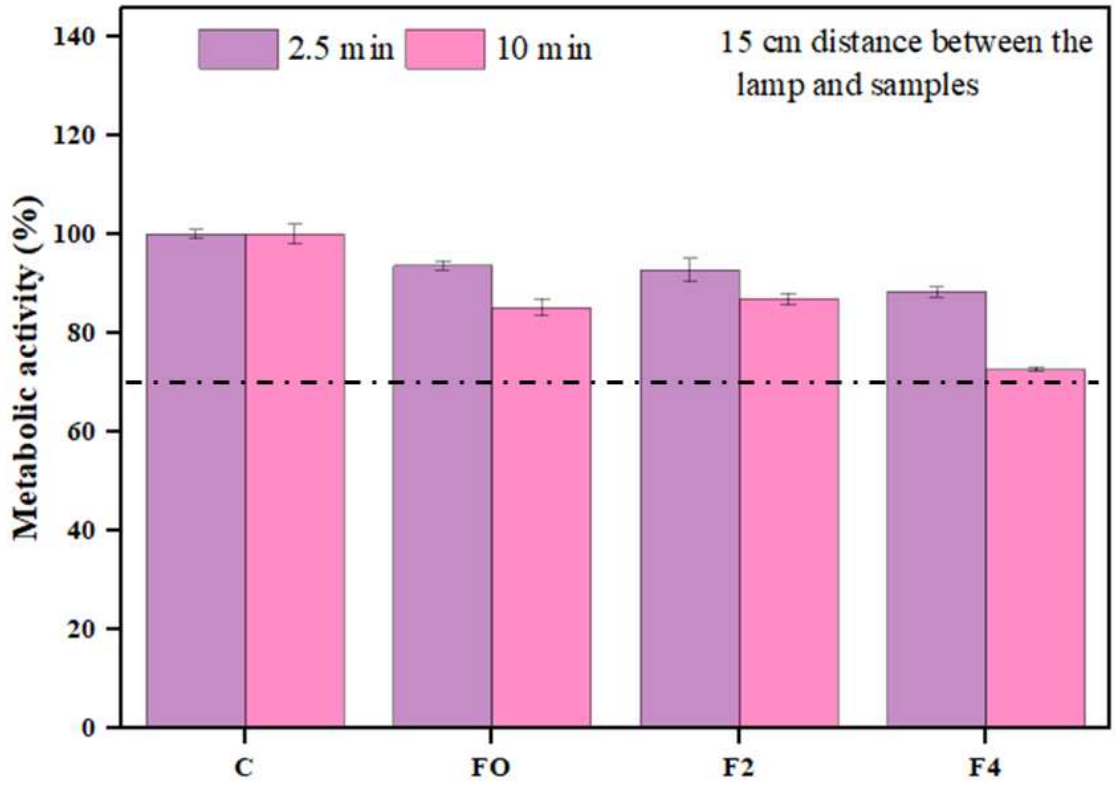

Figure 44 – Metabolic activity of SK-MEL-28 cells after 24h of laser phototherapy under different conditions in the presence of drug: C – Control cells, without Nanoparticles; FO – Cells with Blank Nanoparticles (without drug); F2 – Cells with NPs 5mg of ICG; F4 – cells with NPs with 5mg of ICG + 1.25mg of DOX with a distance of 15 cm between the samples and the lamp

The obtained results fell short of our expectations, and we can outline several potential explanations. Firstly, the encapsulation of drugs with PGl may have inadvertently shielded the drug, rendering its activity ineffective in the context of phototherapeutic treatment. Secondly, the drug encapsulation with PGl could have contributed to safeguarding the nanoparticles, reducing their accessibility for interaction with target cells during phototherapy. This

phenomenon may elucidate the absence of a pronounced cytotoxic effect, particularly when dealing with encapsulated drugs crucial for inducing cytotoxicity.

Furthermore, the irradiation distance may also not have been adequate, and could be further reduced with a longer exposure time to actually cause an increase in temperature. The 25 cm distance may have been inadequate to ensure effective exposure of the cells to the laser light, as reducing the distance to 15 cm may not have caused significant variations in the results, as it was still not close enough to focus the energy. the laser effectively into the cells.

As noted, an increase in laser exposure time from 2.5 minutes to 10 minutes resulted in increased metabolic activity between 70% and 80%. This suggests that a longer exposure time may be required to trigger the desired cytotoxic effect. However, it is important to ensure that this increase in exposure time does not cause thermal damage to the cells due to the increased temperature. The lack of considerable changes in metabolic activity after 24 hours and 48 hours may indicate that the cytotoxic or therapeutic effects of the nanoparticles are not long-lasting or that the cells were able to recover over time.

Another crucial parameter warranting more in-depth investigation is the duration of nanoparticle internalization by cells. In this study, a 6-hour internalization period was employed. Following this interval, the cells underwent a thorough washing process to eliminate non-internalized nanoparticles. This factor may have considerably influenced the therapeutic efficacy of the nanoparticles. Given that a comprehensive assessment of internalization kinetics was not conducted, it's possible that a more extended incubation period is required to facilitate efficient internalization, potentially leading to a more notable therapeutic impact.

Overall, the results indicate that it is important to consider a number of experimental factors, including exposure time, irradiation distance, and analysis time, when optimizing photodynamic/photothermal therapy with nanoparticles. It is possible that tweaking these variables or exploring different nanoparticle formulations could lead to more effective results in the future.

5 CONCLUSIONS

In this study, the successful synthesis of the Poly(globalide) was confirmed through characterization techniques, allowing the analysis of its chemical structure, molecular weight and thermal properties. For the preparation of nanoparticles, some formulations and process conditions were evaluated. Among them, the mass of the internal aqueous phase, the proportion of polymer and solvent in the organic phase, the degree of hydrolysis and molar mass of the components of the external aqueous phase, as well as the evaluation of the effect of process conditions, such as exposure time to the sonication tip and its respective amplitude, and the use or not of an ice bath. The investigation of these parameters was essential to reach an ideal formulation of Poly(globalide) Nanoparticles with hydrodynamic size in the desired range and controlled PDI, crucial factors to guarantee the homogeneity and stability of the nanomaterial.

The double emulsion technique proved to be highly effective in encapsulating Indocyanine Green and Doxorubicin Hydrochloride in Poly(globalide) Nanoparticles. These photosensitizers and chemotherapeutics can be loaded either individually or in combination, expanding their therapeutic potential. The technique allowed more precise control over the load of therapeutic agents, being especially suitable for hydrophilic compounds.

This study achieved hydrodynamic nanoparticle sizes of less than 300 nm, with a narrow size distribution < 0.2. TEM images revealed the spherical shape of the nanoparticles and corroborated the submicrometer sizes determined by DLS. Nanoparticles remained stable for a period of 6 months with evaluation of hydrodynamic size and pH. The ability to maintain the integrity of these nanostructured systems over time is crucial in practical applications, especially in the formulation of pharmaceutical and therapeutic products, where nanoparticles play an essential role in drug delivery.

Furthermore, encapsulation efficiencies reached values greater than 89 % for Indocyanine Green and >58 % for Doxorubicin Hydrochloride. This level of encapsulation is of great importance in applications such as nanomedicine and phototherapeutic therapies, where substance loading efficiency is crucial for successful treatments and diagnoses. Corroborating the literature, there was an increase in the encapsulation efficiency rate of ICG when added to DOX in the nanoparticle formulation, demonstrating an increase of about 8.5%.

In addition, the adsorption efficiency of Bovine Serum Albumin in all formulations exceeded approximately 58%, another relevant aspect, which may facilitate the circulation of

these systems in the body and increase their blood half-life, which is particularly advantageous for medical applications.

In this study, the ICG and DOX release profiles were investigated in formulations F2 (5 mg of ICG) and F4 (5 mg of ICG and 1.25 mg of DOX) at different pH values (5.5 and 7.4), simulating biological environments relevant. Comparing the two pH, it was noticeable that the presence of DOX in the F4 formulation accelerated the release of ICG at physiological pH and acidic pH, in addition, the ICG showed a faster release at pH 7.4 when compared to pH 5.5, while DOX showed an increase on release at pH 5.5 (acid medium). Thus, a pH-sensitive effect was observed on the release of compounds, an important characteristic for targeting therapies to specific sites in the body, such as tumors.

In the cytotoxicity assay, concentrations of nanoparticles from 168.7 ng mL-1 did not demonstrate cytotoxicity in L929 fibroblast cells after 24 hours of incubation, maintaining cell viability above 70%. In tests with SKMEL-28 tumor cells, the 808 nm laser irradiation time played a crucial role in photodynamic/photothermal therapy, with a time of 10 minutes producing the best results.

In summary, this trial highlighted the importance of considering a variety of experimental factors when optimizing photodynamic/photothermal therapy with nanoparticles, including exposure time, irradiation distance, and analysis time. Adjustments to these variables or exploration of different formulations may lead to even more effective results in the future.

Thus, this study represents a contribution to research on therapeutic nanosystems, with emphasis on photodynamic and photothermal therapy. The combination of therapies, the development of nanoparticles and the ability to control the release of therapeutic agents have the potential to revolutionize the way diseases are treated, offering hope for patients and opportunities for advances in science and human health.

6 REFERENCES

ABDELBASSET, W. K.; JASIM, S. A.; SHARMA, S. K.; MARGIANA, R.; BOKOV, D. O.; OBAID, M. A.; HUSSEIN, B. A.; LAFTA, H. A.; JASIM, S. F.; MUSTAFA, Y. F. **Alginate-Based Hydrogels and Tubes, as Biological Macromolecule-Based Platforms for Peripheral Nerve Tissue Engineering: A Review**. [*S. l.*]: Springer, 2022.

ABELS, C.; FICKWEILER, S.; WEIDERER, P.; BÄUMLER, W.; HOFSTÄDTER, F.; LANDTHALER, M.; SZEIMIES, R.-M. Indocyanine green (ICG) and laser irradiation induce photooxidation. **Archives of Dermatological Research**, [*s. l.*], v. 292, n. 8, p. 404–411, 2000.

ABHILASH, M.; THOMAS, D. Biopolymers for Biocomposites and Chemical Sensor Applications. *Em*: BIOPOLYMER COMPOSITES IN ELECTRONICS. [*S. l.*]: Elsevier, 2017. p. 405–435.

ABRAHAMSE, H.; KRUGER, C. A.; KADANYO, S.; MISHRA, A. Nanoparticles for Advanced Photodynamic Therapy of Cancer. **Photomedicine and Laser Surgery**, [*s. l.*], v. 35, n. 11, p. 581–588, 2017.

ABUWATFA, W. H.; AWAD, N. S.; PITT, W. G.; HUSSEINI, G. A. Thermosensitive Polymers and Thermo-Responsive Liposomal Drug Delivery Systems. **Polymers**, [*s. l.*], v. 14, n. 5, p. 925, 2022.

ACUÑA-NELSON, S.-M.; BASTÍAS-MONTES, J.-M.; CERDA-LEAL, F.-R.; PARRA-FLORES, J.-E.; AGUIRRE-GARCÍA, J.-S.; TOLEDO, P. G. Nanocoatings of Bovine Serum Albumin on Glass: Effects of pH and Temperature. **Journal of Nanomaterials**, [*s. l.*], v. 2020, p. 1–11, 2020.

AFZAL, O.; ALTAMIMI, A. S. A.; NADEEM, M. S.; ALZAREA, S. I.; ALMALKI, W. H.; TARIQ, A.; MUBEEN, B.; MURTAZA, B. N.; IFTIKHAR, S.; RIAZ, N.; KAZMI, I. Nanoparticles in Drug Delivery: From History to Therapeutic Applications. **Nanomaterials**, [*s. l.*], v. 12, n. 24, p. 4494, 2022.

AGNER, T.; ZIMMERMANN, A.; DI LUCCIO, M.; DE ARAÚJO, P. H. H.; SAYER, C. Monomer-in-water miniemulsions by membrane emulsification. **Chemical Engineering and Processing - Process Intensification**, [*s. l.*], v. 120, p. 251–257, 2017.

AHMADY, A. R.; RAZMJOOEE, K.; SABER-SAMANDARI, S.; TOGHRAIE, D. Fabrication of chitosan-gelatin films incorporated with thymol-loaded alginate microparticles for controlled drug delivery, antibacterial activity and wound healing: In-vitro and in-vivo

studies. **International Journal of Biological Macromolecules**, [*s. l.*], v. 223, p. 567–582, 2022. Disponível em: Acesso em: 23 abr. 2023.

ALBERTSSON, A.-C.; VARMA, I. K. Recent Developments in Ring Opening Polymerization of Lactones for Biomedical Applications. **Biomacromolecules**, [*s. l.*], v. 4, n. 6, p. 1466–1486, 2003.

ALBERTSSON, A.; VARMA, I. K.; SRIVASTAVA, R. K. Polyesters from Large Lactones. *Em*: HANDBOOK OF RING-OPENING POLYMERIZATION. [*S. l.*]: Wiley, 2009. p. 287–306.

ALI, T.; SHOAIB, M. H.; YOUSUF, R. I.; JABEEN, S.; MUHAMMAD, I. N.; TARIQ, A. Use of hydrophilic and hydrophobic polymers for the development of controlled release tizanidine matrix tablets. **Brazilian Journal of Pharmaceutical Sciences**, [*s. l.*], v. 50, n. 4, p. 799–818, 2014.

ALTINOĞLU, E. I.; RUSSIN, T. J.; KAISER, J. M.; BARTH, B. M.; EKLUND, P. C.; KESTER, M.; ADAIR, J. H. Near-Infrared Emitting Fluorophore-Doped Calcium Phosphate Nanoparticles for *In Vivo* Imaging of Human Breast Cancer. **ACS Nano**, [*s. l.*], v. 2, n. 10, p. 2075–2084, 2008.

AMARAL, S. I.; COSTA-ALMEIDA, R.; GONÇALVES, I. C.; MAGALHÃES, F. D.; PINTO, A. M. Carbon nanomaterials for phototherapy of cancer and microbial infections. **Carbon**, [*s. l.*], v. 190, p. 194–244, 2022.

AMGOTH, C.; PHAN, C.; BANAVOTH, M.; ROMPIVALASA, S.; TANG, G. Polymer Properties: Functionalization and Surface Modified Nanoparticles. *Em*: ROLE OF NOVEL DRUG DELIVERY VEHICLES IN NANOBIOMEDICINE. [*S. l.*]: IntechOpen, 2020.

AMOABEDINY, G.; HAGHIRALSADAT, F.; NADERINEZHAD, S.; HELDER, M. N.; AKHOUNDI KHARANAGHI, E.; MOHAMMADNEJAD AROUGH, J.; ZANDIEH-DOULABI, B. Overview of preparation methods of polymeric and lipid-based (niosome, solid lipid, liposome) nanoparticles: A comprehensive review. **International Journal of Polymeric Materials and Polymeric Biomaterials**, [*s. l.*], v. 67, n. 6, p. 383–400, 2018.

ANSARINIK, Z.; KIYANI, H.; YOOSEFIAN, M. Investigation of self-assembled poly(ethylene glycol)-poly(L-lactic acid) micelle as potential drug delivery system for poorly water soluble anticancer drug abemaciclib. **Journal of Molecular Liquids**, [*s. l.*], v. 365, p. 120192, 2022. Disponível em: Acesso em: 23 abr. 2023.

ANVARI; LYTLE; WALKER; GUPTA; VULLEV; ANVARI. Effects of nanoencapsulation and PEGylation on biodistribution of indocyanine green in healthy mice:

quantitative fluorescence imaging and analysis of organs. **International Journal of Nanomedicine**, [*s. l.*], p. 1609, 2013.

ASHFAQ, U. A.; RIAZ, M.; YASMEEN, E.; YOUSAF, M. Z. Recent Advances in Nanoparticle-Based Targeted Drug-Delivery Systems Against Cancer and Role of Tumor Microenvironment. **Critical Reviews in Therapeutic Drug Carrier Systems**, [*s. l.*], v. 34, n. 4, p. 317–353, 2017.

ATANASE, L. I.; SALHI, S.; CUCOVEICA, O.; PONJAVIC, M.; NIKODINOVIC-RUNIC, J.; DELAITE, C. Biodegradability Assessment of Polyester Copolymers Based on Poly(ethylene adipate) and Poly(ε-caprolactone). **Polymers**, [*s. l.*], v. 14, n. 18, p. 3736, 2022.

ATES, Z.; THORNTON, P. D.; HEISE, A. Side-chain functionalisation of unsaturated polyesters from ring-opening polymerisation of macrolactones by thiol–ene click chemistry. **Polym. Chem.**, [*s. l.*], v. 2, n. 2, p. 309–312, 2011.

AWAD, T. S.; MOHARRAM, H. A.; SHALTOUT, O. E.; ASKER, D.; YOUSSEF, M. M. Applications of ultrasound in analysis, processing and quality control of food: A review. **Food Research International**, [*s. l.*], v. 48, n. 2, p. 410–427, 2012.

BAHMANI, B.; GUERRERO, Y.; BACON, D.; KUNDRA, V.; VULLEV, V. I.; ANVARI, B. Functionalized polymeric nanoparticles loaded with indocyanine green as theranostic materials for targeted molecular near infrared fluorescence imaging and photothermal destruction of ovarian cancer cells. **Lasers in Surgery and Medicine**, [*s. l.*], v. 46, n. 7, p. 582–592, 2014.

BALDE, A.; KIM, S. K.; BENJAKUL, S.; NAZEER, R. A. Pulmonary drug delivery applications of natural polysaccharide polymer derived nano/micro-carrier systems: A review. **International Journal of Biological Macromolecules**, [*s. l.*], v. 220, p. 1464–1479, 2022. Disponível em: Acesso em: 23 abr. 2023.

BAO, Z.; LIU, X.; LIU, Y.; LIU, H.; ZHAO, K. Near-infrared light-responsive inorganic nanomaterials for photothermal therapy. **Asian Journal of Pharmaceutical Sciences**, [*s. l.*], v. 11, n. 3, p. 349–364, 2016.

BARAKAT, N. S.; TALEB D.A.B; AL SALEHI A.S. Target Nanoparticles: An Appealing Drug Delivery Platform. **Journal of Nanomedicine & Nanotechnology**, [*s. l.*], v. s4, n. 01, 2011.

BARANWAL, J.; BARSE, B.; FAIS, A.; DELOGU, G. L.; KUMAR, A. Biopolymer: A Sustainable Material for Food and Medical Applications. **Polymers**, [*s. l.*], v. 14, n. 5, p. 983, 2022.

BARTH, B. M.; I. ALTINOĞLU, E.; SHANMUGAVELANDY, S. S.; KAISER, J. M.; CRESPO-GONZALEZ, D.; DIVITTORE, N. A.; MCGOVERN, C.; GOFF, T. M.; KEASEY, N. R.; ADAIR, J. H.; LOUGHRAN, T. P.; CLAXTON, D. F.; KESTER, M. Targeted Indocyanine-Green-Loaded Calcium Phosphosilicate Nanoparticles for In Vivo Photodynamic Therapy of Leukemia. **ACS Nano**, [*s. l.*], v. 5, n. 7, p. 5325–5337, 2011.

BASKARAN, R.; LEE, J.; YANG, S.-G. Clinical development of photodynamic agents and therapeutic applications. **Biomaterials Research**, [*s. l.*], v. 22, n. 1, p. 25, 2018.

BECKER PERES, Luana; BECKER PERES, Laize; DE ARAÚJO, P. H. H.; SAYER, C. Solid lipid nanoparticles for encapsulation of hydrophilic drugs by an organic solvent free double emulsion technique. **Colloids and Surfaces B: Biointerfaces**, [*s. l.*], v. 140, p. 317–323, 2016.

BEGINES, B.; ORTIZ, T.; PÉREZ-ARANDA, M.; MARTÍNEZ, G.; MERINERO, M.; ARGÜELLES-ARIAS, F.; ALCUDIA, A. Polymeric Nanoparticles for Drug Delivery: Recent Developments and Future Prospects. **Nanomaterials**, [*s. l.*], v. 10, n. 7, p. 1403, 2020.

BELLTRAME, J. **MODIFICATION OF POLYESTERS AND NANOMATERIAL PRODUCTION FOR BIOMEDICAL APPLICATIONS**. 2022. - Universidade Federal de Santa Catarina, Florianópolis 2022. Disponível em: https://repositorio.ufsc.br/handle/123456789/242622. Acesso em: 5 set. 2023.

BERNARDY, N.; ROMIO, A. P.; BARCELOS, E. I.; PIZZOL, C. D.; DORA, C. L.; LEMOS-SENNA, E.; ARAUJO, P. H. H.; SAYER, C. Nanoencapsulation of Quercetin via Miniemulsion Polymerization. **Journal of Biomedical Nanotechnology**, [*s. l.*], v. 6, n. 2, p. 181–186, 2010.

BERTRAND, N.; WU, J.; XU, X.; KAMALY, N.; FAROKHZAD, O. C. Cancer nanotechnology: The impact of passive and active targeting in the era of modern cancer biology. **Advanced Drug Delivery Reviews**, [*s. l.*], v. 66, p. 2–25, 2014.

BHARATHIRAJA, S.; MANIVASAGAN, P.; SANTHA MOORTHY, M.; BUI, N. Q.; JANG, B.; PHAN, T. T. V.; JUNG, W.-K.; KIM, Y.-M.; LEE, K. D.; OH, J. Photo-based PDT/PTT dual model killing and imaging of cancer cells using phycocyanin-polypyrrole nanoparticles. **European Journal of Pharmaceutics and Biopharmaceutics**, [*s. l.*], v. 123, p. 20–30, 2018.

BILICI, K.; CETIN, S.; CELIKBAS, E.; YAGCI ACAR, H.; KOLEMEN, S. Recent Advances in Cyanine-Based Phototherapy Agents. **Frontiers in Chemistry**, [*s. l.*], v. 9, 2021.

BILICI, K.; MUTI, A.; SENNAROĞLU, A.; YAGCI ACAR, H. Indocyanine green loaded APTMS coated SPIONs for dual phototherapy of cancer. **Journal of Photochemistry and Photobiology B: Biology**, [*s. l.*], v. 201, p. 111648, 2019.

BOONMAN, A. J.; CUYPERS, M.; LEUSINK, G. L.; NAALDENBERG, J.; BLOEMENDAL, H. J. Cancer treatment and decision making in individuals with intellectual disabilities: a scoping literature review. **The Lancet Oncology**, [*s. l.*], v. 23, n. 4, p. e174–e183, 2022.

CALIN, M. A.; DIACONEASA, A.; SAVASTRU, D.; TAUTAN, M. Photosensitizers and light sources for photodynamic therapy of the Bowen's disease. **Archives of Dermatological Research**, [*s. l.*], v. 303, n. 3, p. 145–151, 2011.

CALIXTO, G.; BERNEGOSSI, J.; DE FREITAS, L.; FONTANA, C.; CHORILLI, M. Nanotechnology-Based Drug Delivery Systems for Photodynamic Therapy of Cancer: A Review. **Molecules**, [*s. l.*], v. 21, n. 3, p. 342, 2016.

CALLAGHAN, S.; SENGE, M. O. The good, the bad, and the ugly–controlling singlet oxygen through design of photosensitizers and delivery systems for photodynamic therapy. **Photochemical & Photobiological Sciences**, [*s. l.*], v. 17, n. 11, p. 1490–1514, 2018.

CHANDRA, N. S.; GORANTLA, S.; PRIYA, S.; SINGHVI, G. Insight on updates in polysaccharides for ocular drug delivery. **Carbohydrate Polymers**, [*s. l.*], v. 297, p. 120014, 2022. Disponível em: Acesso em: 23 abr. 2023.

CHANG, M. C.; KUO, Y. J.; HUNG, K. H.; PENG, C. L.; CHEN, K. Y.; YEH, L. K. Liposomal dexamethasone-moxifloxacin nanoparticle combinations with collagen/gelatin/alginate hydrogel for corneal infection treatment and wound healing. **Biomedical Materials (Bristol)**, [*s. l.*], v. 15, n. 5, 2020.

CHANG, D.; MA, Y.; XU, X.; XIE, J.; JU, S. Stimuli-Responsive Polymeric Nanoplatforms for Cancer Therapy. **Frontiers in Bioengineering and Biotechnology**, [*s. l.*], v. 9, 2021.

CHATTERJEE, K.; ZHANG, J.; HONBO, N.; KARLINER, J. S. Doxorubicin Cardiomyopathy. **Cardiology**, [*s. l.*], v. 115, n. 2, p. 155–162, 2010.

CHEN, L.; HUANG, J.; LI, X.; HUANG, M.; ZENG, S.; ZHENG, J.; PENG, S.; LI, S. Progress of Nanomaterials in Photodynamic Therapy Against Tumor. **Frontiers in Bioengineering and Biotechnology**, [*s. l.*], v. 10, 2022.

CHEN, H.-H.; LU, I.-L.; LIU, T.-I.; TSAI, Y.-C.; CHIANG, W.-H.; LIN, S.-C.; CHIU, H.-C. Indocyanine green/doxorubicin-encapsulated functionalized nanoparticles for effective

combination therapy against human MDR breast cancer. **Colloids and Surfaces B: Biointerfaces**, [*s. l.*], v. 177, p. 294–305, 2019.

CHEN, J.; NING, C.; ZHOU, Z.; YU, P.; ZHU, Y.; TAN, G.; MAO, C. Nanomaterials as photothermal therapeutic agents. **Progress in Materials Science**, [*s. l.*], v. 99, p. 1–26, 2019.

CHEN, G.; ROY, I.; YANG, C.; PRASAD, P. N. Nanochemistry and Nanomedicine for Nanoparticle-based Diagnostics and Therapy. **Chemical Reviews**, [*s. l.*], v. 116, n. 5, p. 2826–2885, 2016.

CHEN, H.; WANG, G. D.; CHUANG, Y.-J.; ZHEN, Z.; CHEN, X.; BIDDINGER, P.; HAO, Z.; LIU, F.; SHEN, B.; PAN, Z.; XIE, J. Nanoscintillator-Mediated X-ray Inducible Photodynamic Therapy for In Vivo Cancer Treatment. **Nano Letters**, [*s. l.*], v. 15, n. 4, p. 2249–2256, 2015.

CHEN, Z.; WANG, W.; LI, Y.; WEI, C.; ZHONG, P.; HE, D.; LIU, H.; WANG, P.; HUANG, Z.; ZHU, W.; ZHOU, Y.; QIN, L. Folic Acid-Modified Erythrocyte Membrane Loading Dual Drug for Targeted and Chemo-Photothermal Synergistic Cancer Therapy. **Molecular Pharmaceutics**, [*s. l.*], v. 18, n. 1, p. 386–402, 2021.

CHEN, R.; WANG, X.; YAO, X.; ZHENG, X.; WANG, J.; JIANG, X. Near-IR-triggered photothermal/photodynamic dual-modality therapy system via chitosan hybrid nanospheres. **Biomaterials**, [*s. l.*], v. 34, n. 33, p. 8314–8322, 2013.

CHENTHAMARA, D.; SUBRAMANIAM, S.; RAMAKRISHNAN, S. G.; KRISHNASWAMY, S.; ESSA, M. M.; LIN, F.-H.; QORONFLEH, M. W. Therapeutic efficacy of nanoparticles and routes of administration. **Biomaterials Research**, [*s. l.*], v. 23, n. 1, p. 20, 2019.

CHIARADIA, V. **Unsaturated macrolactone polymerization followed by its modification and crosslinking via click chemistry-based reactions**. 2019. - Universidade Federal de Santa Catarina, Florianópolis 2019.

CHIARADIA, V.; HANAY, S. B.; KIMMINS, S. D.; OLIVEIRA, D. de; ARAÚJO, P. H. H.; SAYER, C.; HEISE, A. Crosslinking of Electrospun Fibres from Unsaturated Polyesters by Bis-Triazolinediones (TAD). **Polymers**, [*s. l.*], v. 11, n. 11, p. 1808, 2019.

CHIARADIA, V.; POLLONI, A. E.; DE OLIVEIRA, D.; DE OLIVEIRA, J. V.; ARAÚJO, P. H. H.; SAYER, C. Polyester nanoparticles from macrolactones via miniemulsion enzymatic ring-opening polymerization. **Colloid and Polymer Science**, [*s. l.*], v. 296, n. 5, p. 861–869, 2018.

CHITGUPI, U.; QIN, Y.; LOVELL, J. F. Targeted Nanomaterials for Phototherapy. **Nanotheranostics**, [*s. l.*], v. 1, n. 1, p. 38–58, 2017.

CHITTASUPHO, C.; XIE, S.-X.; BAOUM, A.; YAKOVLEVA, T.; SIAHAAN, T. J.; BERKLAND, C. J. ICAM-1 targeting of doxorubicin-loaded PLGA nanoparticles to lung epithelial cells. **European Journal of Pharmaceutical Sciences**, [*s. l.*], v. 37, n. 2, p. 141–150, 2009.

CLEMENT, S.; CHEN, W.; DENG, W.; GOLDYS, E. M. X-ray radiation-induced and targeted photodynamic therapy with folic acid-conjugated biodegradable nanoconstructs. **International Journal of Nanomedicine**, [*s. l.*], v. Volume 13, p. 3553–3570, 2018.

COLMÁN, M. M. E.; MOREIRA, R. P. M.; AMARAL, M. do; ARAÚJO, P. H. H.; SAYER, C. Incorporation of PMMA and PS in Styrene and Methyl methacrylate Miniemulsion Homopolymerization. **Macromolecular Symposia**, [*s. l.*], v. 299–300, n. 1, p. 41–47, 2011.

CORBO, C.; MOLINARO, R.; PARODI, A.; TOLEDANO FURMAN, N. E.; SALVATORE, F.; TASCIOTTI, E. The impact of nanoparticle protein corona on cytotoxicity, immunotoxicity and target drug delivery. **Nanomedicine**, [*s. l.*], v. 11, n. 1, p. 81–100, 2016.

CORREIA, J. H.; RODRIGUES, J. A.; PIMENTA, S.; DONG, T.; YANG, Z. Photodynamic Therapy Review: Principles, Photosensitizers, Applications, and Future Directions. **Pharmaceutics**, [*s. l.*], v. 13, n. 9, p. 1332, 2021.

COSTA, R. A.; FARAH, M. E.; FREYMÜLLER, E.; MORALES, P. H.; SMITH, R.; CARDILLO, J. A. Choriocapillaris photodynamic therapy using indocyanine green. **American Journal of Ophthalmology**, [*s. l.*], v. 132, n. 4, p. 557–565, 2001.

CRUCHO, C. I. C.; BARROS, M. T. Polymeric nanoparticles: A study on the preparation variables and characterization methods. **Materials Science and Engineering: C**, [*s. l.*], v. 80, p. 771–784, 2017.

DANHIER, F.; FERON, O.; PRÉAT, V. To exploit the tumor microenvironment: Passive and active tumor targeting of nanocarriers for anti-cancer drug delivery. **Journal of Controlled Release**, [*s. l.*], v. 148, n. 2, p. 135–146, 2010.

DE, R.; MAHATA, M. K.; KIM, K. Structure-Based Varieties of Polymeric Nanocarriers and Influences of Their Physicochemical Properties on Drug Delivery Profiles. **Advanced Science**, [*s. l.*], v. 9, n. 10, p. 2105373, 2022.

DE OLIVEIRA, F. C. S.; OLVERA, D.; SAWKINS, M. J.; CRYAN, S.-A.; KIMMINS, S. D.; DA SILVA, T. E.; KELLY, D. J.; DUFFY, G. P.; KEARNEY, C.; HEISE, A. Direct UV-Triggered Thiol–ene Cross-Linking of Electrospun Polyester Fibers from Unsaturated

Poly(macrolactone)s and Their Drug Loading by Solvent Swelling. **Biomacromolecules**, [*s. l.*], v. 18, n. 12, p. 4292–4298, 2017.

DEBELE, T.; PENG, S.; TSAI, H.-C. Drug Carrier for Photodynamic Cancer Therapy. **International Journal of Molecular Sciences**, [*s. l.*], v. 16, n. 9, p. 22094–22136, 2015.

DENG, K.; HOU, Z.; DENG, X.; YANG, P.; LI, C.; LIN, J. Enhanced Antitumor Efficacy by 808 nm Laser-Induced Synergistic Photothermal and Photodynamic Therapy Based on a Indocyanine-Green-Attached W18O49 Nanostructure. **Advanced Functional Materials**, [*s. l.*], v. 25, n. 47, p. 7280–7290, 2015.

DENG, Y.; WANG, L.; YANG, W.; FU, S.; ELAÏSSARI, A. Preparation of magnetic polymeric particles via inverse microemulsion polymerization process. **Journal of Magnetism and Magnetic Materials**, [*s. l.*], v. 257, n. 1, p. 69–78, 2003.

DESMETTRE, T.; DEVOISSELLE, J. M.; MORDON, S. Fluorescence Properties and Metabolic Features of Indocyanine Green (ICG) as Related to Angiography. **Survey of Ophthalmology**, [*s. l.*], v. 45, n. 1, p. 15–27, 2000.

DEVRIM GÖKBERK, B.; ERDINÇ, N. Design, Optimization, and Characterization of Lysozyme-Loaded Poly(ε-Caprolactone) Microparticles for Pulmonary Delivery. **Journal of Pharmaceutical Innovation**, [*s. l.*], v. 18, n. 1, p. 325–338, 2023.

DOS SANTOS, A. F.; DE ALMEIDA, D. R. Q.; TERRA, L. F.; BAPTISTA, M. S.; LABRIOLA, L. Photodynamic therapy in cancer treatment - an update review. **Journal of Cancer Metastasis and Treatment**, [*s. l.*], v. 2019, 2019.

DOUKA, A.; VOUYIOUKA, S.; PAPASPYRIDI, L. M.; PAPASPYRIDES, C. D. **A review on enzymatic polymerization to produce polycondensation polymers: The case of aliphatic polyesters, polyamides and polyesteramides**. [*S. l.*]: Elsevier Ltd, 2018.

DUDA, A.; KOWALSKI, A.; PENCZEK, S.; UYAMA, H.; KOBAYASHI, S. Kinetics of the Ring-Opening Polymerization of 6-, 7-, 9-, 12-, 13-, 16-, and 17-Membered Lactones. Comparison of Chemical and Enzymatic Polymerizations. **Macromolecules**, [*s. l.*], v. 35, n. 11, p. 4266–4270, 2002.

DURO-CASTANO, A.; SOUSA-HERVES, A.; ARMIÑÁN, A.; CHARBONNIER, D.; ARROYO-CRESPO, J. J.; WEDEPOHL, S.; CALDERÓN, M.; VICENT, M. J. Polyglutamic acid-based crosslinked doxorubicin nanogels as an anti-metastatic treatment for triple negative breast cancer. **Journal of Controlled Release**, [*s. l.*], v. 332, p. 10–20, 2021. Disponível em: Acesso em: 23 abr. 2023.

EBRAHIMIAN, M.; HASHEMI, M.; MALEKI, M.; HASHEMITABAR, G.; ABNOUS, K.; RAMEZANI, M.; HAGHPARAST, A. Co-delivery of Dual Toll-Like Receptor Agonists and Antigen in Poly(Lactic-Co-Glycolic) Acid/Polyethylenimine Cationic Hybrid Nanoparticles Promote Efficient In Vivo Immune Responses. **Frontiers in Immunology**, [*s. l.*], v. 8, 2017.

EBRAHIMIAN, M.; MAHVELATI, F.; MALAEKEH-NIKOUEI, B.; HASHEMI, E.; OROOJALIAN, F.; HASHEMI, M. Bromelain Loaded Lipid-Polymer Hybrid Nanoparticles for Oral Delivery: Formulation and Characterization. **Applied Biochemistry and Biotechnology**, [*s. l.*], v. 194, n. 8, p. 3733–3748, 2022.

EBRAHIMNEJAD, P.; SODAGAR TALEGHANI, A.; ASARE-ADDO, K.; NOKHODCHI, A. An updated review of folate-functionalized nanocarriers: A promising ligand in cancer. **Drug Discovery Today**, [*s. l.*], v. 27, n. 2, p. 471–489, 2022.

EDIRIWICKREMA, A.; SALTZMAN, W. M. Nanotherapy for Cancer: Targeting and Multifunctionality in the Future of Cancer Therapies. **ACS Biomaterials Science & Engineering**, [*s. l.*], v. 1, n. 2, p. 64–78, 2015.

ETCHEVERRY, M. E.; PASQUALE, M. A.; GARAVAGLIA, M. Photodynamic therapy of HeLa cell cultures by using LED or laser sources. **Journal of Photochemistry and Photobiology B: Biology**, [*s. l.*], v. 160, p. 271–277, 2016.

FERREIRA, L. P.; GASPAR, V. M.; MONTEIRO, M. V.; FREITAS, B.; SILVA, N. J. O.; MANO, J. F. Screening of dual chemo-photothermal cellular nanotherapies in organotypic breast cancer 3D spheroids. **Journal of Controlled Release**, [*s. l.*], v. 331, p. 85–102, 2021.

FEUSER, P. E.; GASPAR, P. C.; JACQUES, A. V.; TEDESCO, A. C.; SANTOS SILVA, M. C. dos; RICCI-JÚNIOR, E.; SAYER, C.; DE ARAÚJO, P. H. H. Synthesis of ZnPc loaded poly(methyl methacrylate) nanoparticles via miniemulsion polymerization for photodynamic therapy in leukemic cells. **Materials Science and Engineering: C**, [*s. l.*], v. 60, p. 458–466, 2016.

FICKWEILER, S.; SZEIMIES, R.-M.; BÄUMLER, W.; STEINBACH, P.; KARRER, S.; GOETZ, A. E.; ABELS, C.; HOFSTÄDTER, F. Indocyanine green: Intracellular uptake and phototherapeutic effects in vitro. **Journal of Photochemistry and Photobiology B: Biology**, [*s. l.*], v. 38, n. 2–3, p. 178–183, 1997.

FLORY, P. J. Fundamental Principles of Condensation Polymerization. **Chemical Reviews**, [*s. l.*], v. 39, n. 1, p. 137–197, 1946.

FREIRE, N. F.; FEUSER, P. E.; AMBEL, E. M. T.; CORDANI, M.; PIERI, E. De; MACHADO-DE-ÁVILA, R. A.; ZIELINSKI, A. A. F.; SAYER, C.; DE ARAÚJO, P. H. H.; DÍEZ, G. V.; ALBUQUERQUE, E. C.; FIALHO, R. L. L. Preparation and characterization of full-spectrum cannabis extract loaded poly(thioether-ester) nanoparticles: In vitro evaluation of their antitumoral efficacy. **Colloids and Surfaces A: Physicochemical and Engineering Aspects**, [*s. l.*], v. 658, p. 130676, 2023.

FREIRE, N. F.; FEUSER, P. E.; DA SILVA ABEL, J.; MACHADO-DE-ÁVILA, R. A.; LOPES FIALHO, R.; CABRAL ALBUQUERQUE, E.; SAYER, C.; HERMES DE ARAÚJO, P. H. Zinc phthalocyanine encapsulation via thiol-ene miniemulsion polymerization and *in vitro* photoxicity studies. **International Journal of Polymeric Materials and Polymeric Biomaterials**, [*s. l.*], v. 71, n. 5, p. 349–358, 2022.

FRIZZO, M. S.; FEUSER, P. E.; BERRES, P. H.; RICCI-JÚNIOR, E.; CAMPOS, C. E. M.; COSTA, C.; DE ARAÚJO, P. H. H.; SAYER, C. Simultaneous encapsulation of zinc oxide and octocrylene in poly (methyl methacrylate-co-styrene) nanoparticles obtained by miniemulsion polymerization for use in sunscreen formulations. **Colloids and Surfaces A: Physicochemical and Engineering Aspects**, [*s. l.*], v. 561, p. 39–46, 2019.

FU, Y.; LI, X.; SUN, C.; REN, Z.; WENG, W.; MAO, C.; HAN, G. pH-Triggered $SrTiO_3$:Er Nanofibers with Optically Monitored and Controlled Drug Delivery Functionality. **ACS Applied Materials & Interfaces**, [*s. l.*], v. 7, n. 45, p. 25514–25521, 2015.

G. NAVA-ARZALUZ, M.; PINON-SEGUNDO, E.; GANEM-RONDERO, A.; LECHUGA-BALLESTEROS, D. Single Emulsion-Solvent Evaporation Technique and Modifications for the Preparation of Pharmaceutical Polymeric Nanoparticles. **Recent Patents on Drug Delivery & Formulation**, [*s. l.*], v. 6, n. 3, p. 209–223, 2012.

GAMAGE, R. S.; SMITH, B. D. Spontaneous Transfer of Indocyanine Green from Liposomes to Albumin Is Inhibited by the Antioxidant α-Tocopherol. **Langmuir**, [*s. l.*], v. 38, n. 39, p. 11950–11961, 2022.

GANGOPADHYAY, M.; SINGH, T.; BEHARA, K. K.; KARWA, S.; GHOSH, S. K.; SINGH, N. D. P. Coumarin-containing-star-shaped 4-armpolyethylene glycol: targeted fluorescent organic nanoparticles for dual treatment of photodynamic therapy and chemotherapy. **Photochemical & Photobiological Sciences**, [*s. l.*], v. 14, n. 7, p. 1329–1336, 2015.

GAO, S.; WANG, J.; TIAN, R.; WANG, G.; ZHANG, L.; LI, Y.; LI, L.; MA, Q.; ZHU, L. Construction and Evaluation of a Targeted Hyaluronic Acid Nanoparticle/Photosensitizer

Complex for Cancer Photodynamic Therapy. **ACS Applied Materials & Interfaces**, [*s. l.*], v. 9, n. 38, p. 32509–32519, 2017.

GAUMET, M.; VARGAS, A.; GURNY, R.; DELIE, F. Nanoparticles for drug delivery: The need for precision in reporting particle size parameters. **European Journal of Pharmaceutics and Biopharmaceutics**, [*s. l.*], v. 69, n. 1, p. 1–9, 2008.

GERELKHUU, Z.; LEE, Y.-I.; YOON, T. H. Upconversion Nanomaterials in Bioimaging and Biosensor Applications and Their Biological Response. **Nanomaterials**, [*s. l.*], v. 12, n. 19, p. 3470, 2022.

GERMANOVA, V. N.; KARLOVA, E. V.; VOLOVA, L. T.; ZOLOTAREV, A. V.; ROSSINSKAYA, V. V.; ZAKHAROV, I. D.; KORIGODSKIY, A. R.; BOLTOVSKAYA, V. V.; NEFEDOVA, I. F.; RADAYKINA, M. V. PLA-PEG Implant as a Drug Delivery System in Glaucoma Surgery: Experimental Study. **Polymers**, [*s. l.*], v. 14, n. 16, 2022.

GHARIEH, A.; KHOEE, S.; MAHDAVIAN, A. R. Emulsion and miniemulsion techniques in preparation of polymer nanoparticles with versatile characteristics. **Advances in Colloid and Interface Science**, [*s. l.*], v. 269, p. 152–186, 2019.

GOMARI, H.; FOROUZANDEH MOGHADAM, M.; SOLEIMANI, M.; GHAVAMI, M.; KHODASHENAS, S. Targeted delivery of doxorubicin to HER2 positive tumor models. **International Journal of Nanomedicine**, [*s. l.*], v. Volume 14, p. 5679–5690, 2019.

GOMES, A. J.; LUNARDI, L. O.; MARCHETTI, J. M.; LUNARDI, C. N.; TEDESCO, A. C. Indocyanine Green Nanoparticles Useful for Photomedicine. **Photomedicine and Laser Surgery**, [*s. l.*], v. 24, n. 4, p. 514–521, 2006.

GONÇALVES, F. A. M. M.; FONSECA, A. C.; DOMINGOS, M.; GLORIA, A.; SERRA, A. C.; COELHO, J. F. J. The potential of unsaturated polyesters in biomedicine and tissue engineering: Synthesis, structure-properties relationships and additive manufacturing. **Progress in Polymer Science**, [*s. l.*], v. 68, p. 1–34, 2017.

GUDKOV, A. V; ZELNICK, C. R.; KAZAROV, A. R.; THIMMAPAYA, R.; SUTTLE, D. P.; BECK, W. T.; RONINSON, I. B. Isolation of genetic suppressor elements, inducing resistance to topoisomerase II-interactive cytotoxic drugs, from human topoisomerase II cDNA. **Proceedings of the National Academy of Sciences**, [*s. l.*], v. 90, n. 8, p. 3231–3235, 1993.

GUINDANI, C.; DOZORETZ, P.; VENERAL, J. G.; DA SILVA, D. M.; ARAÚJO, P. H. H.; FERREIRA, S. R. S.; DE OLIVEIRA, D. Enzymatic ring opening copolymerization of globalide and ε-caprolactone under supercritical conditions. **The Journal of Supercritical Fluids**, [*s. l.*], v. 128, p. 404–411, 2017.

GUINDANI, C.; FEUSER, P. E.; CORDEIRO, A. P.; DE MENESES, A. C.; POSSATO, J. C.; DA SILVA ABEL, J.; MACHADO-DE-ÁVILA, R. A.; SAYER, C.; DE ARAÚJO, P. H. H. Bovine serum albumin conjugation on poly(methyl methacrylate) nanoparticles for targeted drug delivery applications. **Journal of Drug Delivery Science and Technology**, [*s. l.*], v. 56, p. 101490, 2020.

GUINDANI, C.; FREY, M.-L.; SIMON, J.; KOYNOV, K.; SCHULTZE, J.; FERREIRA, S. R. S.; ARAÚJO, P. H. H.; DE OLIVEIRA, D.; WURM, F. R.; MAILÄNDER, V.; LANDFESTER, K. Covalently Binding of Bovine Serum Albumin to Unsaturated Poly(Globalide-Co-ε-Caprolactone) Nanoparticles by Thiol-Ene Reactions. **Macromolecular bioscience**, [*s. l.*], v. 19, n. 10, p. e1900145, 2019.

GÜNEY AKKURT, M.; GÜLSOY, M. Polylactide nanoparticles encapsulating indocyanine green for photothermal therapy of prostate cancer cells. **Photodiagnosis and Photodynamic Therapy**, [*s. l.*], v. 37, p. 102693, 2022.

GUO, R.; TIAN, Y.; WANG, Y.; YANG, W. Near-Infrared Laser-Triggered Nitric Oxide Nanogenerators for the Reversal of Multidrug Resistance in Cancer. **Advanced Functional Materials**, [*s. l.*], v. 27, n. 13, p. 1606398, 2017.

HAK, A.; RAVASAHEB SHINDE, V.; RENGAN, A. K. A review of advanced nanoformulations in phototherapy for cancer therapeutics. **Photodiagnosis and Photodynamic Therapy**, [*s. l.*], v. 33, p. 102205, 2021.

HAN, H. S.; CHOI, K. Y. Advances in Nanomaterial-Mediated Photothermal Cancer Therapies: Toward Clinical Applications. **Biomedicines**, [*s. l.*], v. 9, n. 3, p. 305, 2021.

HAQUE, S.; BOYD, B. J.; MCINTOSH, M. P.; POUTON, C. W.; KAMINSKAS, L. M.; WHITTAKER, M. Suggested Procedures for the Reproducible Synthesis of Poly(d,l-lactide-co-glycolide) Nanoparticles Using the Emulsification Solvent Diffusion Platform. **Current Nanoscience**, [*s. l.*], v. 14, n. 5, p. 448–453, 2018.

HENDERSON, I. C.; CANELLOS, G. P. Cancer of the Breast. **New England Journal of Medicine**, [*s. l.*], v. 302, n. 2, p. 78–90, 1980.

HENDERSON, L. A.; SVIRKIN, Y. Y.; GROSS, R. A.; KAPLAN, D. L.; SWIFT, G. Enzyme-Catalyzed Polymerizations of ε-Caprolactone: Effects of Initiator on Product Structure, Propagation Kinetics, and Mechanism. **Macromolecules**, [*s. l.*], v. 29, n. 24, p. 7759–7766, 1996.

HERNÁNDEZ-GIOTTONINI, K. Y.; RODRÍGUEZ-CÓRDOVA, R. J.; GUTIÉRREZ-VALENZUELA, C. A.; PEÑUÑURI-MIRANDA, O.; ZAVALA-RIVERA, P.; GUERRERO-

GERMÁN, P.; LUCERO-ACUÑA, A. PLGA nanoparticle preparations by emulsification and nanoprecipitation techniques: effects of formulation parameters. **RSC Advances**, [*s. l.*], v. 10, n. 8, p. 4218–4231, 2020.

HESHMATI AGHDA, N.; ABDULSAHIB, S. M.; SEVERSON, C.; LARA, E. J.; TORRES HURTADO, S.; YILDIZ, T.; CASTILLO, J. A.; TUNNELL, J. W.; BETANCOURT, T. Induction of immunogenic cell death of cancer cells through nanoparticle-mediated dual chemotherapy and photothermal therapy. **International Journal of Pharmaceutics**, [*s. l.*], v. 589, p. 119787, 2020.

HONG, E. J.; CHOI, D. G.; SHIM, M. S. Targeted and effective photodynamic therapy for cancer using functionalized nanomaterials. **Acta Pharmaceutica Sinica B**, [*s. l.*], v. 6, n. 4, p. 297–307, 2016.

HSU, C.-C.; LIN, S.-L.; CHANG, C. A. Lanthanide-Doped Core–Shell–Shell Nanocomposite for Dual Photodynamic Therapy and Luminescence Imaging by a Single X-ray Excitation Source. **ACS Applied Materials & Interfaces**, [*s. l.*], v. 10, n. 9, p. 7859–7870, 2018.

HU, Z. Photodynamic Therapy as an Emerging Treatment Modality for Cancer and Non-Cancer Diseases. **Journal of Analytical & Bioanalytical Techniques**, [*s. l.*], v. S1, n. e001, 2014.

HU, J.-J.; CHENG, Y.-J.; ZHANG, X.-Z. Recent advances in nanomaterials for enhanced photothermal therapy of tumors. **Nanoscale**, [*s. l.*], v. 10, n. 48, p. 22657–22672, 2018.

HU, H.; LIU, X.; HONG, J.; YE, N.; XIAO, C.; WANG, J.; LI, Z.; XU, D. Mesoporous polydopamine-based multifunctional nanoparticles for enhanced cancer phototherapy. **Journal of Colloid and Interface Science**, [*s. l.*], v. 612, p. 246–260, 2022.

HUANG, R. B.; MOCHERLA, S.; HESLINGA, M. J.; CHAROENPHOL, P.; ENIOLA-ADEFESO, O. Dynamic and cellular interactions of nanoparticles in vascular-targeted drug delivery (review). **Molecular Membrane Biology**, [*s. l.*], v. 27, n. 7, p. 312–327, 2010.

HUANG, Y.-Y.; SHARMA, S. K.; DAI, T.; CHUNG, H.; YAROSLAVSKY, A.; GARCIA-DIAZ, M.; CHANG, J.; CHIANG, L. Y.; HAMBLIN, M. R. Can nanotechnology potentiate photodynamic therapy?. **Nanotechnology Reviews**, [*s. l.*], v. 1, n. 2, p. 111–146, 2012.

HUANG, X.; WU, J.; HE, M.; HOU, X.; WANG, Y.; CAI, X.; XIN, H.; GAO, F.; CHEN, Y. Combined Cancer Chemo-Photodynamic and Photothermal Therapy Based on

ICG/PDA/TPZ-Loaded Nanoparticles. **Molecular Pharmaceutics**, [*s. l.*], v. 16, n. 5, p. 2172–2183, 2019.

HUNG, C.-C.; HUANG, W.-C.; LIN, Y.-W.; YU, T.-W.; CHEN, H.-H.; LIN, S.-C.; CHIANG, W.-H.; CHIU, H.-C. Active Tumor Permeation and Uptake of Surface Charge-Switchable Theranostic Nanoparticles for Imaging-Guided Photothermal/Chemo Combinatorial Therapy. **Theranostics**, [*s. l.*], v. 6, n. 3, p. 302–317, 2016.

IANNAZZO, D.; PISTONE, A.; SALAMÒ, M.; GALVAGNO, S.; ROMEO, R.; GIOFRÉ, S. V.; BRANCA, C.; VISALLI, G.; DI PIETRO, A. Graphene quantum dots for cancer targeted drug delivery. **International Journal of Pharmaceutics**, [*s. l.*], v. 518, n. 1–2, p. 185–192, 2017.

IBRAHEEM, D.; IQBAL, M.; AGUSTI, G.; FESSI, H.; ELAISSARI, A. Effects of process parameters on the colloidal properties of polycaprolactone microparticles prepared by double emulsion like process. **Colloids and Surfaces A: Physicochemical and Engineering Aspects**, [*s. l.*], v. 445, p. 79–91, 2014.

IQBAL, M.; ROBIN, S.; HUMBERT, P.; VIENNET, C.; AGUSTI, G.; FESSI, H.; ELAISSARI, A. Submicron polycaprolactone particles as a carrier for imaging contrast agent for in vitro applications. **Colloids and Surfaces B: Biointerfaces**, [*s. l.*], v. 136, p. 488–495, 2015a.

IQBAL, M.; VALOUR, J.-P.; FESSI, H.; ELAISSARI, A. Preparation of biodegradable PCL particles via double emulsion evaporation method using ultrasound technique. **Colloid and Polymer Science**, [*s. l.*], v. 293, n. 3, p. 861–873, 2015b.

JADIA, R.; KYDD, J.; RAI, P. Remotely Phototriggered, Transferrin-Targeted Polymeric Nanoparticles for the Treatment of Breast Cancer. **Photochemistry and Photobiology**, [*s. l.*], v. 94, n. 4, p. 765–774, 2018.

JAISWAL, M.; DUDHE, R.; SHARMA, P. K. Nanoemulsion: an advanced mode of drug delivery system. **3 Biotech**, [*s. l.*], v. 5, n. 2, p. 123–127, 2015.

JAMALI, Z.; KHOOBI, M.; HEJAZI, S. M.; EIVAZI, N.; ABDOLAHPOUR, S.; IMANPARAST, F.; MORADI-SARDAREH, H.; PAKNEJAD, M. Evaluation of targeted curcumin (CUR) loaded PLGA nanoparticles for in vitro photodynamic therapy on human glioblastoma cell line. **Photodiagnosis and Photodynamic Therapy**, [*s. l.*], v. 23, p. 190–201, 2018.

JAQUE, D.; MARTÍNEZ MAESTRO, L.; DEL ROSAL, B.; HARO-GONZALEZ, P.; BENAYAS, A.; PLAZA, J. L.; MARTÍN RODRÍGUEZ, E.; GARCÍA SOLÉ, J. Nanoparticles for photothermal therapies. **Nanoscale**, [*s. l.*], v. 6, n. 16, p. 9494–9530, 2014.

JAWAHAR, N.; MEYYANATHAN, S. Polymeric nanoparticles for drug delivery and targeting: A comprehensive review. **International Journal of Health & Allied Sciences**, [*s. l.*], v. 1, n. 4, p. 217, 2012.

JELVEHGARI, M.; MONTAZAM, S. Comparison of Microencapsulation by Emulsion-Solvent Extraction/ Evaporation Technique Using Derivatives Cellulose and Acrylate-Methacrylate Copolymer as Carriers. **Jundishapur Journal of Natural Pharmaceutical Products**, [*s. l.*], v. 7, n. 4, p. 144–152, 2012.

JENJOB, R.; PHAKKEEREE, T.; SEIDI, F.; THEERASILP, M.; CRESPY, D. Emulsion Techniques for the Production of Pharmacological Nanoparticles. **Macromolecular Bioscience**, [*s. l.*], v. 19, n. 6, p. 1900063, 2019.

JEON, Y.-M.; LEE, H.-S.; JEONG, D.; OH, H.-K.; RA, K.-H.; LEE, M.-Y. Antimicrobial photodynamic therapy using chlorin e6 with halogen light for acne bacteria-induced inflammation. **Life Sciences**, [*s. l.*], v. 124, p. 56–63, 2015.

JIN, S. G. Production and Application of Biomaterials Based on Polyvinyl alcohol (PVA) as Wound Dressing. **Chemistry an Asian Journal**, [*s. l.*], v. 17, n. 21, 2022.

JOSEPH, X.; AKHIL, V.; ARATHI, A.; MOHANAN, P. Nanobiomaterials in support of drug delivery related issues. **Materials Science and Engineering: B**, [*s. l.*], v. 279, p. 115680, 2022.

JUNG, H. S.; VERWILST, P.; SHARMA, A.; SHIN, J.; SESSLER, J. L.; KIM, J. S. Organic molecule-based photothermal agents: an expanding photothermal therapy universe. **Chemical Society Reviews**, [*s. l.*], v. 47, n. 7, p. 2280–2297, 2018.

KALARIA, D. R.; SHARMA, G.; BENIWAL, V.; RAVI KUMAR, M. N. V. Design of Biodegradable Nanoparticles for Oral Delivery of Doxorubicin: In vivo Pharmacokinetics and Toxicity Studies in Rats. **Pharmaceutical Research**, [*s. l.*], v. 26, n. 3, p. 492–501, 2009.

KAMRA VERMA, A.; LEEKHA, A.; KUMAR, V.; MOIN, I.; KUMAR, S. Biodistribution and In-vivo Efficacy of Doxorubicin Loaded Chitosan Nanoparticles in Ehrlich Ascites Carcinoma (EAC) Bearing Balb/c Mice. **Journal of Nanomedicine & Nanotechnology**, [*s. l.*], v. 09, n. 04, 2018.

KARIMI, M.; BAHRAMI, S.; RAVARI, S. B.; ZANGABAD, P. S.; MIRSHEKARI, H.; BOZORGOMID, M.; SHAHREZA, S.; SORI, M.; HAMBLIN, M. R. Albumin nanostructures

as advanced drug delivery systems. **Expert Opinion on Drug Delivery**, [*s. l.*], v. 13, n. 11, p. 1609–1623, 2016a.

KARIMI, M.; GHASEMI, A.; SAHANDI ZANGABAD, P.; RAHIGHI, R.; MOOSAVI BASRI, S. M.; MIRSHEKARI, H.; AMIRI, M.; SHAFAEI PISHABAD, Z.; ASLANI, A.; BOZORGOMID, M.; GHOSH, D.; BEYZAVI, A.; VASEGHI, A.; AREF, A. R.; HAGHANI, L.; BAHRAMI, S.; HAMBLIN, M. R. Smart micro/nanoparticles in stimulus-responsive drug/gene delivery systems. **Chemical Society Reviews**, [*s. l.*], v. 45, n. 5, p. 1457–1501, 2016b.

KATAOKA, H.; NISHIE, H.; HAYASHI, N.; TANAKA, M.; NOMOTO, A.; YANO, S.; JOH, T. New photodynamic therapy with next-generation photosensitizers. **Annals of Translational Medicine**, [*s. l.*], v. 5, n. 8, p. 183–183, 2017.

KCIUK, M.; GIELECIŃSKA, A.; MUJWAR, S.; KOŁAT, D.; KAŁUZIŃSKA-KOŁAT, Ż.; CELIK, I.; KONTEK, R. Doxorubicin—An Agent with Multiple Mechanisms of Anticancer Activity. **Cells**, [*s. l.*], v. 12, n. 4, p. 659, 2023.

KESHARWANI, P.; CHADAR, R.; SHEIKH, A.; RIZG, W. Y.; SAFHI, A. Y. CD44-Targeted Nanocarrier for Cancer Therapy. **Frontiers in Pharmacology**, [*s. l.*], v. 12, 2022.

KESHARWANI, S. S.; KAUR, S.; TUMMALA, H.; SANGAMWAR, A. T. Multifunctional approaches utilizing polymeric micelles to circumvent multidrug resistant tumors. **Colloids and Surfaces B: Biointerfaces**, [*s. l.*], v. 173, p. 581–590, 2019.

KHULUGUROV, V. M.; IVANOV, N. A.; KIM, B. C.; MAYOROV, A. P.; BORDZILOVSKY, D. S.; MASYCHEVA, V. I.; DANILENKO, E. D. All solid state lasers for photodynamic therapy of the malignant neoplasms. *Em*: PROCEEDINGS, 6TH INTERNATIONAL CONFERENCE ON ACTUAL PROBLEMS OF ELECTRONIC INSTRUMENT ENGINEERING, [*s. d.*], [*s. l.*], . **Anais** [...]. [*S. l.*]: IEEE, [*s. d.*]. p. 208–215.

KIM, T. H.; CHEN, Y.; MOUNT, C. W.; GOMBOTZ, W. R.; LI, X.; PUN, S. H. Evaluation of Temperature-Sensitive, Indocyanine Green-Encapsulating Micelles for Noninvasive Near-Infrared Tumor Imaging. **Pharmaceutical Research**, [*s. l.*], v. 27, n. 9, p. 1900–1913, 2010.

KIM, M. M.; DARAFSHEH, A. Light Sources and Dosimetry Techniques for Photodynamic Therapy. **Photochemistry and Photobiology**, [*s. l.*], v. 96, n. 2, p. 280–294, 2020.

KOBAYASHI, S. Lipase-catalyzed polyester synthesis - A green polymer chemistry. **Proceedings of the Japan Academy, Series B**, [*s. l.*], v. 86, n. 4, p. 338–365, 2010.

KONG, C.; CHEN, X. Combined Photodynamic and Photothermal Therapy and Immunotherapy for Cancer Treatment: A Review. **International Journal of Nanomedicine**, [*s. l.*], v. Volume 17, p. 6427–6446, 2022.

KRISHNAN, V.; MITRAGOTRI, S. Nanoparticles for topical drug delivery: Potential for skin cancer treatment. **Advanced Drug Delivery Reviews**, [*s. l.*], v. 153, p. 87–108, 2020.

KRUGER, C.; ABRAHAMSE, H. Utilisation of Targeted Nanoparticle Photosensitiser Drug Delivery Systems for the Enhancement of Photodynamic Therapy. **Molecules**, [*s. l.*], v. 23, n. 10, p. 2628, 2018.

KYDD, J.; JADIA, R.; VELPURISIVA, P.; GAD, A.; PALIWAL, S.; RAI, P. Targeting Strategies for the Combination Treatment of Cancer Using Drug Delivery Systems. **Pharmaceutics**, [*s. l.*], v. 9, n. 4, p. 46, 2017.

KYRYCHENKO, A.; PASKO, D. A.; KALUGIN, O. N. Poly(vinyl alcohol) as a water protecting agent for silver nanoparticles: the role of polymer size and structure. **Physical Chemistry Chemical Physics**, [*s. l.*], v. 19, n. 13, p. 8742–8756, 2017.

LAKHANI, P.; PATIL, A.; MAJUMDAR, S. Recent advances in topical nano drug-delivery systems for the anterior ocular segment. **Therapeutic Delivery**, [*s. l.*], v. 9, n. 2, p. 137–153, 2018.

LAN, M.; ZHAO, S.; LIU, W.; LEE, C.; ZHANG, W.; WANG, P. Photosensitizers for Photodynamic Therapy. **Advanced Healthcare Materials**, [*s. l.*], v. 8, n. 13, p. 1900132, 2019.

LARUE, L.; BEN MIHOUB, A.; YOUSSEF, Z.; COLOMBEAU, L.; ACHERAR, S.; ANDRÉ, J. C.; ARNOUX, P.; BAROS, F.; VERMANDEL, M.; FROCHOT, C. Using X-rays in photodynamic therapy: an overview. **Photochemical & Photobiological Sciences**, [*s. l.*], v. 17, n. 11, p. 1612–1650, 2018.

LECOMTE, P.; JÉRÔME, C. Recent Developments in Ring-Opening Polymerization of Lactones. *Em*: [*S. l.: s. n.*], 2011. p. 173–217.

LEE, Y.-E. K.; KOPELMAN, R. Polymeric Nanoparticles for Photodynamic Therapy. *Em*: [*S. l.: s. n.*], 2011. p. 151–178.

LEE, D.; KWON, S.; JANG, S.; PARK, E.; LEE, Y.; KOO, H. Overcoming the obstacles of current photodynamic therapy in tumors using nanoparticles. **Bioactive Materials**, [*s. l.*], v. 8, p. 20–34, 2022.

LEE, A.; TSAI, H.-Y.; YATES, M. Z. Steric Stabilization of Thermally Responsive -Isopropylacrylamide Particles by Poly(vinyl alcohol). **Langmuir**, [*s. l.*], v. 26, n. 23, p. 18055–18060, 2010.

LERCHE, C.; HEERFORDT, I.; HEYDENREICH, J.; WULF, H. Alternatives to Outdoor Daylight Illumination for Photodynamic Therapy—Use of Greenhouses and Artificial Light Sources. **International Journal of Molecular Sciences**, [*s. l.*], v. 17, n. 3, p. 309, 2016.

LI, X.; FERREL, G. L.; GUERRA, M. C.; HODE, T.; LUNN, J. A.; ADALSTEINSSON, O.; NORDQUIST, R. E.; LIU, H.; CHEN, W. R. Preliminary safety and efficacy results of laser immunotherapy for the treatment of metastatic breast cancer patients. **Photochemical & Photobiological Sciences**, [*s. l.*], v. 10, n. 5, p. 817–821, 2011.

LI, X.; HE, M.; ZHOU, Q.; DUTTA, D.; LU, N.; LI, S.; GE, Z. Multifunctional Mesoporous Hollow Cobalt Sulfide Nanoreactors for Synergistic Chemodynamic/Photodynamic/Photothermal Therapy with Enhanced Efficacy. **ACS Applied Materials & Interfaces**, [*s. l.*], v. 14, n. 45, p. 50601–50615, 2022.

LI, X.; KOLEMEN, S.; YOON, J.; AKKAYA, E. U. Activatable Photosensitizers: Agents for Selective Photodynamic Therapy. **Advanced Functional Materials**, [*s. l.*], v. 27, n. 5, p. 1604053, 2017.

LI, X.; KWON, N.; GUO, T.; LIU, Z.; YOON, J. Innovative Strategies for Hypoxic-Tumor Photodynamic Therapy. **Angewandte Chemie International Edition**, [*s. l.*], v. 57, n. 36, p. 11522–11531, 2018.

LI, Zhiheng; LI, Zheng; WANG, J. Visualization of Phototherapy Evolution by Optical Imaging. **Molecules**, [*s. l.*], v. 28, n. 10, p. 3992, 2023.

LI, Shuihong; WEI, X.; LI, Sisi; ZHU, C.; WU, C. Up-Conversion Luminescent Nanoparticles for Molecular Imaging, Cancer Diagnosis and Treatment</p>. **International Journal of Nanomedicine**, [*s. l.*], v. Volume 15, p. 9431–9445, 2020.

LI, X.; ZHANG, Q.; AHMAD, Z.; HUANG, J.; REN, Z.; WENG, W.; HAN, G.; MAO, C. Near-infrared luminescent $CaTiO_3:Nd^{3+}$ nanofibers with tunable and trackable drug release kinetics. **Journal of Materials Chemistry B**, [*s. l.*], v. 3, n. 37, p. 7449–7456, 2015.

LI, W.; ZHENG, C.; PAN, Z.; CHEN, C.; HU, D.; GAO, G.; KANG, S.; CUI, H.; GONG, P.; CAI, L. Smart hyaluronidase-actived theranostic micelles for dual-modal imaging guided photodynamic therapy. **Biomaterials**, [*s. l.*], v. 101, p. 10–19, 2016.

LIANG, G.; WANG, Haojie; SHI, H.; WANG, Haitao; ZHU, M.; JING, A.; LI, J.; LI, G. Recent progress in the development of upconversion nanomaterials in bioimaging and disease treatment. **Journal of Nanobiotechnology**, [*s. l.*], v. 18, n. 1, p. 154, 2020.

LIECHTY, W. B.; KRYSCIO, D. R.; SLAUGHTER, B. V.; PEPPAS, N. A. Polymers for Drug Delivery Systems. **Annual Review of Chemical and Biomolecular Engineering**, [*s. l.*], v. 1, n. 1, p. 149–173, 2010.

LIN, L.; SONG, X.; DONG, X.; LI, B. Nano-photosensitizers for enhanced photodynamic therapy. **Photodiagnosis and Photodynamic Therapy**, [*s. l.*], v. 36, p. 102597, 2021.

LIU, F.; CHEN, Y.; LI, Y.; GUO, Y.; CAO, Y.; LI, P.; WANG, Z.; GONG, Y.; RAN, H. Folate-receptor-targeted laser-activable poly(lactide-glycolic acid) nanoparticles loaded with paclitaxel/indocyanine green for photoacoustic/ultrasound imaging and chemo/photothermal therapy. **International Journal of Nanomedicine**, [*s. l.*], v. Volume 13, p. 5139–5158, 2018.

LIU, C.-G.; HAN, Y.-H.; KANKALA, R. K.; WANG, S.-B.; CHEN, A.-Z. Subcellular Performance of Nanoparticles in Cancer Therapy. **International Journal of Nanomedicine**, [*s. l.*], v. Volume 15, p. 675–704, 2020.

LIU, B.; JIN, Z.; CHEN, H.; LIANG, L.; LI, Y.; WANG, G.; ZHANG, J.; XU, T. Electrospun poly (L-lactic acid)/gelatine membranes loaded with doxorubicin for effective suppression of glioblastoma cell growth in vitro and in vivo. **Regenerative Biomaterials**, [*s. l.*], v. 8, n. 5, 2021a.

LIU, B.; JIN, Z.; CHEN, H.; LIANG, L.; LI, Y.; WANG, G.; ZHANG, J.; XU, T. Electrospun poly (L-lactic acid)/gelatine membranes loaded with doxorubicin for effective suppression of glioblastoma cell growth in vitro and in vivo. **Regenerative Biomaterials**, [*s. l.*], v. 8, n. 5, p. rbab043, 2021b. Disponível em: https://doi.org/10.1093/rb/rbab043.

LIU, R.; MA, G.-H.; WAN, Y.-H.; SU, Z.-G. Influence of process parameters on the size distribution of PLA microcapsules prepared by combining membrane emulsification technique and double emulsion-solvent evaporation method. **Colloids and Surfaces B: Biointerfaces**, [*s. l.*], v. 45, n. 3–4, p. 144–153, 2005.

LIU, W.; MADRY, H.; CUCCHIARINI, M. **Application of Alginate Hydrogels for Next-Generation Articular Cartilage Regeneration**. [*S. l.*]: MDPI, 2022.

LIU, S.; MAHESHWARI, R.; KIICK, K. L. Polymer-Based Therapeutics. **Macromolecules**, [*s. l.*], v. 42, n. 1, p. 3–13, 2009.

LIU, J.; YIN, Y.; YANG, L.; LU, B.; YANG, Z.; WANG, W.; LI, R. Nucleus-Targeted Photosensitizer Nanoparticles for Photothermal and Photodynamic Therapy of Breast Carcinoma. **International Journal of Nanomedicine**, [*s. l.*], v. Volume 16, p. 1473–1485, 2021.

LONG, Y.; WU, X.; LI, Z.; FAN, J.; HU, X.; LIU, B. PEGylated WS2 nanodrug system with erythrocyte membrane coating for chemo/photothermal therapy of cervical cancer. **Biomaterials Science**, [*s. l.*], v. 8, n. 18, p. 5088–5105, 2020.

LOVELL, P. A.; SCHORK, F. J. Fundamentals of Emulsion Polymerization. **Biomacromolecules**, [*s. l.*], v. 21, n. 11, p. 4396–4441, 2020.

LOWRY, O. H.; ROSEBROUGH, N. J.; FARR, A. L.; RANDALL, R. J. Protein measurement with the Folin phenol reagent. **The Journal of biological chemistry**, [*s. l.*], v. 193, n. 1, p. 265–75, 1951.

LUO, Z.; LI, M.; ZHOU, M.; LI, H.; CHEN, Y.; REN, X.; DAI, Y. O2-evolving and ROS-activable nanoparticles for treatment of multi-drug resistant Cancer by combination of photodynamic therapy and chemotherapy. **Nanomedicine: Nanotechnology, Biology and Medicine**, [*s. l.*], v. 19, p. 49–57, 2019.

LV, S.; MIAO, Y.; LIU, D.; SONG, F. Recent Development of Photothermal Agents (PTAs) Based on Small Organic Molecular Dyes. **ChemBioChem**, [*s. l.*], v. 21, n. 15, p. 2098–2110, 2020.

MA, Y.; SADOQI, M.; SHAO, J. Biodistribution of indocyanine green-loaded nanoparticles with surface modifications of PEG and folic acid. **International Journal of Pharmaceutics**, [*s. l.*], v. 436, n. 1–2, p. 25–31, 2012.

MACHADO, F. C.; ADUM DE MATOS, R. P.; PRIMO, F. L.; TEDESCO, A. C.; RAHAL, P.; CALMON, M. F. Effect of curcumin-nanoemulsion associated with photodynamic therapy in breast adenocarcinoma cell line. **Bioorganic & Medicinal Chemistry**, [*s. l.*], v. 27, n. 9, p. 1882–1890, 2019.

MANAVITEHRANI, I.; FATHI, A.; BADR, H.; DALY, S.; NEGAHI SHIRAZI, A.; DEHGHANI, F. Biomedical Applications of Biodegradable Polyesters. **Polymers**, [*s. l.*], v. 8, n. 1, p. 20, 2016.

MANCHANDA, R.; FERNANDEZ-FERNANDEZ, A.; NAGESETTI, A.; MCGORON, A. J. Preparation and characterization of a polymeric (PLGA) nanoparticulate drug delivery system with simultaneous incorporation of chemotherapeutic and thermo-optical agents. **Colloids and Surfaces B: Biointerfaces**, [*s. l.*], v. 75, n. 1, p. 260–267, 2010.

MANSOURI, S.; CUIE, Y.; WINNIK, F.; SHI, Q.; LAVIGNE, P.; BENDERDOUR, M.; BEAUMONT, E.; FERNANDES, J. C. Characterization of folate-chitosan-DNA nanoparticles for gene therapy. **Biomaterials**, [*s. l.*], v. 27, n. 9, p. 2060–2065, 2006.

MARASINI, R.; ARYAL, S. Indocyanine-type Infrared-820 Encapsulated Polymeric Nanoparticle-Assisted Photothermal Therapy of Cancer. **ACS Omega**, [*s. l.*], v. 7, n. 14, p. 12056–12065, 2022.

MASARUDIN, M. J.; CUTTS, S. M.; EVISON, B. J.; PHILLIPS, Don. R.; PIGRAM, P. J. Factors determining the stability, size distribution, and cellular accumulation of small, monodisperse chitosan nanoparticles as candidate vectors for anticancer drug delivery: application to the passive encapsulation of [14C]-doxorubicin. **Nanotechnology, Science and Applications**, [*s. l.*], p. 67, 2015.

MASOOD, F. Polymeric nanoparticles for targeted drug delivery system for cancer therapy. **Materials Science and Engineering: C**, [*s. l.*], v. 60, p. 569–578, 2016.

MASTER, A.; LIVINGSTON, M.; SEN GUPTA, A. Photodynamic nanomedicine in the treatment of solid tumors: Perspectives and challenges. **Journal of Controlled Release**, [*s. l.*], v. 168, n. 1, p. 88–102, 2013.

MATICA; AACHMANN; TØNDERVIK; SLETTA; OSTAFE. Chitosan as a Wound Dressing Starting Material: Antimicrobial Properties and Mode of Action. **International Journal of Molecular Sciences**, [*s. l.*], v. 20, n. 23, p. 5889, 2019.

MCBRIDE, R. A.; GILLIES, E. R. Kinetics of Self-Immolative Degradation in a Linear Polymeric System: Demonstrating the Effect of Chain Length. **Macromolecules**, [*s. l.*], v. 46, n. 13, p. 5157–5166, 2013.

MEHRABAN, N.; MUSICH, P.; FREEMAN, H. Synthesis and Encapsulation of a New Zinc Phthalocyanine Photosensitizer into Polymeric Nanoparticles to Enhance Cell Uptake and Phototoxicity. **Applied Sciences**, [*s. l.*], v. 9, n. 3, p. 401, 2019.

MELGAR AGUILAR, A. E.; FAGUNDES, A. P.; MACUVELE, D. L. P.; CESCA, K.; PORTO, L.; PADOIN, N.; SOARES, C.; GRACHER RIELLA, H. Green Synthesis of Nano Hydroxyapatite: morphology variation and its effect on cytotoxicity against fibroblast. **Materials Letters**, [*s. l.*], v. 284, p. 129013, 2021.

MENDOZA-MUÑOZ, N.; ALCALÁ-ALCALÁ, S.; QUINTANAR-GUERRERO, D. Preparation of Polymer Nanoparticles by the Emulsification-Solvent Evaporation Method: From Vanderhoff's Pioneer Approach to Recent Adaptations. *Em*: POLYMER NANOPARTICLES FOR NANOMEDICINES. Cham: Springer International Publishing, 2016. p. 87–121.

MI, P. Stimuli-responsive nanocarriers for drug delivery, tumor imaging, therapy and theranostics. **Theranostics**, [*s. l.*], v. 10, n. 10, p. 4557–4588, 2020.

MINISTÉRIO DA SAÚDE INSTITUTO NACIONAL DE CÂNCER. **ESTIMATIVA 2023 - Incidência de Câncer no Brasil**. [*S. l.: s. n.*], 2023.

MIRZAEI-KALAR, Z.; YAVARI, A.; JOUYBAN, A. Increasing DNA binding affinity of doxorubicin by loading on Fe3O4 nanoparticles: A multi-spectroscopic study. **Spectrochimica Acta Part A: Molecular and Biomolecular Spectroscopy**, [*s. l.*], v. 229, p. 117985, 2020.

MISHRA, R. K.; TIWARI, S. K.; MOHAPATRA, S.; THOMAS, S. Efficient Nanocarriers for Drug-Delivery Systems. *Em*: NANOCARRIERS FOR DRUG DELIVERY. [*S. l.*]: Elsevier, 2019. p. 1–41.

MITCHELL, M. J.; BILLINGSLEY, M. M.; HALEY, R. M.; WECHSLER, M. E.; PEPPAS, N. A.; LANGER, R. Engineering precision nanoparticles for drug delivery. **Nature Reviews Drug Discovery**, [*s. l.*], v. 20, n. 2, p. 101–124, 2021.

MITRA, S.; GAUR, U.; GHOSH, P. C.; MAITRA, A. N. Tumour targeted delivery of encapsulated dextran–doxorubicin conjugate using chitosan nanoparticles as carrier. **Journal of Controlled Release**, [*s. l.*], v. 74, n. 1–3, p. 317–323, 2001.

MOAZZAMI GOUDARZI, Z.; SOLEIMANI, M.; GHASEMI-MOBARAKEH, L.; SAJKIEWICZ, P.; SHARIFIANJAZI, F.; ESMAEILKHANIAN, A.; KHAKSAR, S. Control of drug release from cotton fabric by nanofibrous mat. **International Journal of Biological Macromolecules**, [*s. l.*], v. 217, p. 270–281, 2022.

MOHAMMADI ABANDANSARI, R.; PARSIAN, H.; KAZEROUNI, F.; PORBAGHER, R.; ZABIHI, E.; RAHIMIPOUR, A. Effect of Simultaneous Treatment with Royal Jelly and Doxorubicin on the Survival of the Prostate Cancer Cell Line (PC3): An In Vitro Study. **International Journal of Cancer Management**, [*s. l.*], v. 11, n. 4, 2018.

MOHAN, P.; RAPOPORT, N. Doxorubicin as a Molecular Nanotheranostic Agent: Effect of Doxorubicin Encapsulation in Micelles or Nanoemulsions on the Ultrasound-Mediated Intracellular Delivery and Nuclear Trafficking. **Molecular Pharmaceutics**, [*s. l.*], v. 7, n. 6, p. 1959–1973, 2010.

MOKWENA, M. G.; KRUGER, C. A.; IVAN, M.-T.; HEIDI, A. A review of nanoparticle photosensitizer drug delivery uptake systems for photodynamic treatment of lung cancer. **Photodiagnosis and Photodynamic Therapy**, [*s. l.*], v. 22, p. 147–154, 2018.

MORDON, S.; DEVOISSELLE, J. M.; SOULIE-BEGU, S.; DESMETTRE, T. Indocyanine Green: Physicochemical Factors Affecting Its Fluorescencein Vivo. **Microvascular Research**, [*s. l.*], v. 55, n. 2, p. 146–152, 1998.

MUNCK, C.; MORDON, S.; BETROUNI, N. Illumination profile characterization of a light device for the dosimetry of intra-pleural photodynamic therapy for mesothelioma. **Photodiagnosis and Photodynamic Therapy**, [*s. l.*], v. 16, p. 23–26, 2016.

MUNDEKKAD, D.; CHO, W. C. Nanoparticles in Clinical Translation for Cancer Therapy. **International Journal of Molecular Sciences**, [*s. l.*], v. 23, n. 3, p. 1685, 2022.

MURA-GALELLI, M. J.; VOEGEL, J. C.; BEHR, S.; BRES, E. F.; SCHAAF, P. Adsorption/desorption of human serum albumin on hydroxyapatite: a critical analysis of the Langmuir model. **Proceedings of the National Academy of Sciences**, [*s. l.*], v. 88, n. 13, p. 5557–5561, 1991.

NAKAMURA, Y.; MOCHIDA, A.; CHOYKE, P. L.; KOBAYASHI, H. Nanodrug Delivery: Is the Enhanced Permeability and Retention Effect Sufficient for Curing Cancer?. **Bioconjugate Chemistry**, [*s. l.*], v. 27, n. 10, p. 2225–2238, 2016.

NAZARI, S.; ABDELRASOUL, A. Impact of Membrane Modification and Surface Immobilization Techniques on the Hemocompatibility of Hemodialysis Membranes: A Critical Review. **Membranes**, [*s. l.*], v. 12, n. 11, p. 1063, 2022.

NOMURA, S.; MORIMOTO, Y.; TSUJIMOTO, H.; ARAKE, M.; HARADA, M.; SAITOH, D.; HARA, I.; OZEKI, E.; SATOH, A.; TAKAYAMA, E.; HASE, K.; KISHI, Y.; UENO, H. Highly reliable, targeted photothermal cancer therapy combined with thermal dosimetry using a near-infrared absorbent. **Scientific Reports**, [*s. l.*], v. 10, n. 1, p. 9765, 2020.

OLIVO, M.; BHUVANESWARI, R.; LUCKY, S. S.; DENDUKURI, N.; SOO-PING THONG, P. Targeted Therapy of Cancer Using Photodynamic Therapy in Combination with Multi-faceted Anti-Tumor Modalities. **Pharmaceuticals**, [*s. l.*], v. 3, n. 5, p. 1507–1529, 2010.

ÖZDAL, Z. D.; GÜLTEKIN, Y.; VURAL, İ.; TAKKA, S. Development and characterization of polymeric nanoparticles containing ondansetron hydrochloride as a hydrophilic drug. **Journal of Drug Delivery Science and Technology**, [*s. l.*], v. 74, p. 103599, 2022.

PAGEL, M.; JEFFERY, J.; ABRIL, E.; NAGLE, R.; GUZMAN, R.; MEUILLET, E.; LUCERO-ACUNA, A. Nanoparticle delivery of an AKT/PDK1 inhibitor improves the therapeutic effect in pancreatic cancer. **International Journal of Nanomedicine**, [*s. l.*], p. 5653, 2014.

PALAMOOR, M.; JABLONSKI, M. M. Comparative study on diffusion and evaporation emulsion methods used to load hydrophilic drugs in poly(ortho ester) nanoparticle emulsions. **Powder Technology**, [*s. l.*], v. 253, p. 53–62, 2014.

PALAO-SUAY, R.; MARTÍN-SAAVEDRA, F. M.; ROSA AGUILAR, M.; ESCUDERO-DUCH, C.; MARTÍN-SALDAÑA, S.; PARRA-RUIZ, F. J.; ROHNER, N. A.; THOMAS, S. N.; VILABOA, N.; SAN ROMÁN, J. Photothermal and photodynamic activity of polymeric nanoparticles based on α-tocopheryl succinate-RAFT block copolymers conjugated to IR-780. **Acta Biomaterialia**, [*s. l.*], v. 57, p. 70–84, 2017.

PARK, J.; PEI, Y.; HYUN, H.; CASTANARES, M. A.; COLLINS, D. S.; YEO, Y. Small molecule delivery to solid tumors with chitosan-coated PLGA particles: A lesson learned from comparative imaging. **Journal of Controlled Release**, [*s. l.*], v. 268, p. 407–415, 2017.

PATEL, M.; PRABHU, A. Smart nanocomposite assemblies for multimodal cancer theranostics. **International Journal of Pharmaceutics**, [*s. l.*], v. 618, p. 121697, 2022.

PATEL, R. H.; WADAJKAR, A. S.; PATEL, N. L.; KAVURI, V. C.; NGUYEN, K. T.; LIU, H. Multifunctionality of indocyanine green-loaded biodegradable nanoparticles for enhanced optical imaging and hyperthermia intervention of cancer. **Journal of Biomedical Optics**, [*s. l.*], v. 17, n. 4, p. 046003, 2012.

PATRA, J. K.; DAS, G.; FRACETO, L. F.; CAMPOS, E. V. R.; RODRIGUEZ-TORRES, M. del P.; ACOSTA-TORRES, L. S.; DIAZ-TORRES, L. A.; GRILLO, R.; SWAMY, M. K.; SHARMA, S.; HABTEMARIAM, S.; SHIN, H.-S. Nano based drug delivery systems: recent developments and future prospects. **Journal of Nanobiotechnology**, [*s. l.*], v. 16, n. 1, p. 71, 2018.

PEBAM, M.; P.S., R.; GANGOPADHYAY, M.; THATIKONDA, S.; RENGAN, A. K. Terminalia chebula Polyphenol and Near-Infrared Dye-Loaded Poly(lactic acid) Nanoparticles for Imaging and Photothermal Therapy of Cancer Cells. **ACS Applied Bio Materials**, [*s. l.*], v. 5, n. 11, p. 5333–5346, 2022.

PINTO, A.; POCARD, M. Photodynamic therapy and photothermal therapy for the treatment of peritoneal metastasis: a systematic review. **Pleura and Peritoneum**, [*s. l.*], v. 3, n. 4, 2018.

PIVETTA, T. P.; BOTTEON, C. E. A.; RIBEIRO, P. A.; MARCATO, P. D.; RAPOSO, M. Nanoparticle Systems for Cancer Phototherapy: An Overview. **Nanomaterials**, [*s. l.*], v. 11, n. 11, p. 3132, 2021.

POLLONI, A. E.; CHIARADIA, V.; DO AMARAL, R. J. F. C.; KEARNEY, C.; GOREY, B.; DE OLIVEIRA, D.; DE OLIVEIRA, J. V.; DE ARAÚJO, P. H. H.; SAYER, C.; HEISE, A. Polyesters with main and side chain phosphoesters as structural motives for biocompatible electrospun fibres. **Polymer Chemistry**, [*s. l.*], v. 11, n. 12, p. 2157–2165, 2020.

POLLONI, A. E.; CHIARADIA, V.; FIGURA, E. M.; DE PAOLI, J. P.; DE OLIVEIRA, D.; DE OLIVEIRA, J. V.; DE ARAUJO, P. H. H.; SAYER, C. Polyesters from Macrolactones Using Commercial Lipase NS 88011 and Novozym 435 as Biocatalysts. **Applied Biochemistry and Biotechnology**, [*s. l.*], v. 184, n. 2, p. 659–672, 2018.

POLLONI, A. E.; VENERAL, J. G.; REBELATTO, E. A.; DE OLIVEIRA, D.; OLIVEIRA, J. V.; ARAÚJO, P. H. H.; SAYER, C. Enzymatic ring opening polymerization of ω-pentadecalactone using supercritical carbon dioxide. **The Journal of Supercritical Fluids**, [*s. l.*], v. 119, p. 221–228, 2017.

PRADOS, J.; MELGUIZO, C.; CABEZA, L.; ORTIZ, R.; CABA, O.; RAMA, A. R.; DELGADO, A. V.; ARIAS, J. L. Enhanced antitumoral activity of doxorubicin against lung cancer cells using biodegradable poly(butylcyanoacrylate) nanoparticles. **Drug Design, Development and Therapy**, [*s. l.*], p. 6433, 2015.

PRADOS, J.; MELGUIZO, C.; ORTIZ, R.; VELEZ, C.; J. ALVAREZ, P.; L. ARIAS, J.; A. RUIZ, M.; GALLARDO, V.; ARANEGA, A. Doxorubicin-Loaded Nanoparticles: New Advances in Breast Cancer Therapy. **Anti-Cancer Agents in Medicinal Chemistry**, [*s. l.*], v. 12, n. 9, p. 1058–1070, 2012.

PUJARI-PALMER, S.; CHEN, S.; RUBINO, S.; WENG, H.; XIA, W.; ENGQVIST, H.; TANG, L.; OTT, M. K. In vivo and in vitro evaluation of hydroxyapatite nanoparticle morphology on the acute inflammatory response. **Biomaterials**, [*s. l.*], v. 90, p. 1–11, 2016.

QIAN, B.; YANG, Q.; WANG, M.; HUANG, S.; JIANG, C.; SHI, H.; LONG, Q.; ZHOU, M.; ZHAO, Q.; YE, X. Encapsulation of lyophilized platelet-rich fibrin in alginate-hyaluronic acid hydrogel as a novel vascularized substitution for myocardial infarction. **Bioactive Materials**, [*s. l.*], v. 7, p. 401–411, 2022. Disponível em: Acesso em: 1 maio 2023.

RAO, J. P.; GECKELER, K. E. Polymer nanoparticles: Preparation techniques and size-control parameters. **Progress in Polymer Science**, [*s. l.*], v. 36, n. 7, p. 887–913, 2011.

RAVI KIRAN, A. V. V. V.; KUSUMA KUMARI, G.; KRISHNAMURTHY, P. T.; KHAYDAROV, R. R. Tumor microenvironment and nanotherapeutics: intruding the tumor fort. **Biomaterials Science**, [*s. l.*], v. 9, n. 23, p. 7667–7704, 2021.

REDDY, M. S. B.; PONNAMMA, D.; CHOUDHARY, R.; SADASIVUNI, K. K. A Comparative Review of Natural and Synthetic Biopolymer Composite Scaffolds. **Polymers**, [*s. l.*], v. 13, n. 7, p. 1105, 2021.

REN, X.-D.; HAO, X.-Y.; LI, H.-C.; KE, M.-R.; ZHENG, B.-Y.; HUANG, J.-D. Progress in the development of nanosensitizers for X-ray-induced photodynamic therapy. **Drug Discovery Today**, [*s. l.*], v. 23, n. 10, p. 1791–1800, 2018.

RIZKALLA, N.; RANGE, C.; LACASSE, F.-X.; HILDGEN, P. Effect of various formulation parameters on the properties of polymeric nanoparticles prepared by multiple emulsion method. **Journal of Microencapsulation**, [*s. l.*], v. 23, n. 1, p. 39–57, 2006.

RIZVI, S. A. A.; SALEH, A. M. Applications of nanoparticle systems in drug delivery technology. **Saudi Pharmaceutical Journal**, [*s. l.*], v. 26, n. 1, p. 64–70, 2018.

ROCHA, B. A.; GONÇALVES, O. H.; LEIMANN, F.; REBECCA, E.; SILVA-BUZANELLO, R.; FILHO, L.; ARAÚJO, P.; CUMAN, R. K. N.; BERSANI-AMADO, C. Curcumin encapsulated in poly-L-lactic acid improves its anti-inflammatory efficacy in vivo . **Advancement in Medicinal Plant Research**, [*s. l.*], v. 2, n. 4, p. 62–73, 2014.

RODRIGUEZ, V. B.; HENRY, S. M.; HOFFMAN, A. S.; STAYTON, P. S.; LI, X.; PUN, S. H. Encapsulation and stabilization of indocyanine green within poly(styrene-alt-maleic anhydride) block-poly(styrene) micelles for near-infrared imaging. **Journal of Biomedical Optics**, [*s. l.*], v. 13, n. 1, p. 014025, 2008.

ROUSSAKI, M.; GAITANAROU, A.; DIAMANTI, P. Ch.; VOUYIOUKA, S.; PAPASPYRIDES, C.; KEFALAS, P.; DETSI, A. Encapsulation of the natural antioxidant aureusidin in biodegradable PLA nanoparticles. **Polymer Degradation and Stability**, [*s. l.*], v. 108, p. 182–187, 2014.

ROWLEY, J. V.; WALL, P.; YU, H.; TRONCI, G.; DEVINE, D. A.; VERNON, J. J.; THORNTON, P. D. Antimicrobial Dye-Conjugated Polyglobalide-Based Organogels. **ACS Applied Polymer Materials**, [*s. l.*], v. 2, n. 7, p. 2927–2933, 2020.

RYVOLOVA, M.; CHOMOUCKA, J.; DRBOHLAVOVA, J.; KOPEL, P.; BABULA, P.; HYNEK, D.; ADAM, V.; ECKSCHLAGER, T.; HUBALEK, J.; STIBOROVA, M.; KAISER, J.; KIZEK, R. Modern Micro and Nanoparticle-Based Imaging Techniques. **Sensors**, [*s. l.*], v. 12, n. 11, p. 14792–14820, 2012.

SALABAT, A.; MIRHOSEINI, F. Polymer-based nanocomposites fabricated by microemulsion method. **Polymer Composites**, [*s. l.*], v. 43, n. 3, p. 1282–1294, 2022.

SALATIN, S.; BARAR, J.; BARZEGAR-JALALI, M.; ADIBKIA, K.; KIAFAR, F.; JELVEHGARI, M. Development of a nanoprecipitation method for the entrapment of a very water soluble drug into Eudragit RL nanoparticles. **Research in Pharmaceutical Sciences**, [*s. l.*], v. 12, n. 1, p. 1, 2017.

SARBADHIKARY, P.; GEORGE, B. P.; ABRAHAMSE, H. Recent Advances in Photosensitizers as Multifunctional Theranostic Agents for Imaging-Guided Photodynamic Therapy of Cancer. **Theranostics**, [*s. l.*], v. 11, n. 18, p. 9054–9088, 2021.

SAVIN, C. L.; PEPTU, C.; KRONEKOVÁ, Z.; SEDLAČÍK, M.; MRLIK, M.; SASINKOVÁ, V.; PEPTU, C. A.; POPA, M.; MOSNÁČEK, J. Polyglobalide-Based Porous Networks Containing Poly(ethylene glycol) Structures Prepared by Photoinitiated Thiol–Ene Coupling. **Biomacromolecules**, [*s. l.*], v. 19, n. 8, p. 3331–3342, 2018.

SAXENA, V.; SADOQI, M.; SHAO, J. Enhanced photo-stability, thermal-stability and aqueous-stability of indocyanine green in polymeric nanoparticulate systems. **Journal of Photochemistry and Photobiology B: Biology**, [*s. l.*], v. 74, n. 1, p. 29–38, 2004a.

SAXENA, V.; SADOQI, M.; SHAO, J. Indocyanine green-loaded biodegradable nanoparticles: preparation, physicochemical characterization and in vitro release. **International Journal of Pharmaceutics**, [*s. l.*], v. 278, n. 2, p. 293–301, 2004b.

SCHOPPA, T.; JUNG, D.; RUST, T.; MULAC, D.; KUCKLING, D.; LANGER, K. Light-responsive polymeric nanoparticles based on a novel nitropiperonal based polyester as drug delivery systems for photosensitizers in PDT. **International Journal of Pharmaceutics**, [*s. l.*], v. 597, p. 120326, 2021.

SEYEDNEJAD, H.; GHASSEMI, A. H.; VAN NOSTRUM, C. F.; VERMONDEN, T.; HENNINK, W. E. Functional aliphatic polyesters for biomedical and pharmaceutical applications. **Journal of Controlled Release**, [*s. l.*], v. 152, n. 1, p. 168–176, 2011.

SHANG, L.; ZHOU, X.; ZHANG, J.; SHI, Y.; ZHONG, L. Metal Nanoparticles for Photodynamic Therapy: A Potential Treatment for Breast Cancer. **Molecules**, [*s. l.*], v. 26, n. 21, p. 6532, 2021.

SHANWAR, S.; LIANG, L.; NECHAEV, A. V.; BAUSHEVA, D. K.; BALALAEVA, I. V.; VODENEEV, V. A.; ROY, I.; ZVYAGIN, A. V.; GURYEV, E. L. Controlled Formation of a Protein Corona Composed of Denatured BSA on Upconversion Nanoparticles Improves Their Colloidal Stability. **Materials**, [*s. l.*], v. 14, n. 7, p. 1657, 2021.

SHARIFI, F.; JAHANGIRI, M.; EBRAHIMNEJAD, P. Synthesis of novel polymeric nanoparticles (methoxy-polyethylene glycol-chitosan/hyaluronic acid) containing 7-ethyl-10-hydroxycamptothecin for colon cancer therapy: in vitro, ex vivo and in vivo investigation. **Artificial Cells, Nanomedicine, and Biotechnology**, [*s. l.*], v. 49, n. 1, p. 367–380, 2021.

SHEN, X.; LI, T.; CHEN, Z.; XIE, X.; ZHANG, H.; FENG, Y.; LI, S.; QIN, X.; YANG, H.; WU, C.; ZHENG, C.; ZHU, J.; YOU, F.; LIU, Y. NIR-Light-Triggered Anticancer Strategy

for Dual-Modality Imaging-Guided Combination Therapy via a Bioinspired Hybrid PLGA Nanoplatform. **Molecular Pharmaceutics**, [*s. l.*], v. 16, n. 3, p. 1367–1384, 2019.

SHI, L.; WANG, X.; ZHAO, F.; LUAN, H.; TU, Q.; HUANG, Z.; WANG, Hao; WANG, Hongwei. In vitro evaluation of 5-aminolevulinic acid (ALA) loaded PLGA nanoparticles. **International Journal of Nanomedicine**, [*s. l.*], p. 2669, 2013.

SHIRATA, C.; KANEKO, J.; INAGAKI, Y.; KOKUDO, T.; SATO, M.; KIRITANI, S.; AKAMATSU, N.; ARITA, J.; SAKAMOTO, Y.; HASEGAWA, K.; KOKUDO, N. Near-infrared photothermal/photodynamic therapy with indocyanine green induces apoptosis of hepatocellular carcinoma cells through oxidative stress. **Scientific Reports**, [*s. l.*], v. 7, n. 1, p. 13958, 2017.

SHIRAZIAN, S.; KEYKHA, E.; POURSHAHIDI, S.; EBRAHIMI, H. Effects of 660 nm and 810 nm Low-Power Diode Laser on Proliferation and Invasion of Oral Cancer Cells in Cell Culture Media. **Photochemistry and Photobiology**, [*s. l.*], v. 97, n. 3, p. 618–626, 2021.

SHU, Y.; SONG, R.; ZHENG, A.; HUANG, J.; CHEN, M.; WANG, J. Thermo/pH dual-stimuli-responsive drug delivery for chemo-/photothermal therapy monitored by cell imaging. **Talanta**, [*s. l.*], v. 181, p. 278–285, 2018.

SIMON, J.; MÜLLER, L. K.; KOKKINOPOULOU, M.; LIEBERWIRTH, I.; MORSBACH, S.; LANDFESTER, K.; MAILÄNDER, V. Exploiting the biomolecular corona: pre-coating of nanoparticles enables controlled cellular interactions. **Nanoscale**, [*s. l.*], v. 10, n. 22, p. 10731–10739, 2018.

SINGH, A. P.; BISWAS, A.; SHUKLA, A.; MAITI, P. Targeted therapy in chronic diseases using nanomaterial-based drug delivery vehicles. **Signal Transduction and Targeted Therapy**, [*s. l.*], v. 4, n. 1, p. 33, 2019.

SMITH, M.; ROBERTS, M.; AL-KASSAS, R. Implantable drug delivery systems for the treatment of osteomyelitis. **Drug Development and Industrial Pharmacy**, [*s. l.*], v. 48, n. 10, p. 511–527, 2022.

SODAGAR TALEGHANI, A.; EBRAHIMNEJAD, P.; HEIDARINASAB, A.; AKBARZADEH, A. Sugar-conjugated dendritic mesoporous silica nanoparticles as pH-responsive nanocarriers for tumor targeting and controlled release of deferasirox. **Materials Science and Engineering: C**, [*s. l.*], v. 98, p. 358–368, 2019.

SOKOLOV, K.; CHUMANOV, G.; COTTON, T. M. Enhancement of Molecular Fluorescence near the Surface of Colloidal Metal Films. **Analytical Chemistry**, [*s. l.*], v. 70, n. 18, p. 3898–3905, 1998.

SONG, L.; LI, P.-P.; YANG, W.; LIN, X.-H.; LIANG, H.; CHEN, X.-F.; LIU, G.; LI, J.; YANG, H.-H. Low-Dose X-ray Activation of W(VI)-Doped Persistent Luminescence Nanoparticles for Deep-Tissue Photodynamic Therapy. **Advanced Functional Materials**, [*s. l.*], v. 28, n. 18, p. 1707496, 2018.

SONG, R.; MURPHY, M.; LI, C.; TING, K.; SOO, C.; ZHENG, Z. Current development of biodegradable polymeric materials for biomedical applications. **Drug Design, Development and Therapy**, [*s. l.*], v. Volume 12, p. 3117–3145, 2018.

SONGCA, S. P. Combinations of Photodynamic Therapy with Other Minimally Invasive Therapeutic Technologies against Cancer and Microbial Infections. **International Journal of Molecular Sciences**, [*s. l.*], v. 24, n. 13, p. 10875, 2023.

SPADA, A.; EMAMI, J.; TUSZYNSKI, J. A.; LAVASANIFAR, A. The Uniqueness of Albumin as a Carrier in Nanodrug Delivery. **Molecular Pharmaceutics**, [*s. l.*], v. 18, n. 5, p. 1862–1894, 2021.

SPOIALĂ, A.; ILIE, C. I.; FICAI, D.; FICAI, A.; ANDRONESCU, E. **From Biomedical Applications of Alginate towards CVD Implications Linked to COVID-19**. [*S. l.*]: MDPI, 2022.

SRINIVASAN, S.; MANCHANDA, R.; LEI, T.; NAGESETTI, A.; FERNANDEZ-FERNANDEZ, A.; MCGORON, A. J. Targeted nanoparticles for simultaneous delivery of chemotherapeutic and hyperthermia agents – An in vitro study. **Journal of Photochemistry and Photobiology B: Biology**, [*s. l.*], v. 136, p. 81–90, 2014.

STAGNOLI, S.; GARRO, C.; ERTEKIN, O.; HEID, S.; SEYFERTH, S.; SORIA, G.; MARIANO CORREA, N.; LEAL-EGAÑA, A.; BOCCACCINI, A. R. Topical systems for the controlled release of antineoplastic Drugs: Oxidized Alginate-Gelatin Hydrogel/Unilamellar vesicles. **Journal of Colloid and Interface Science**, [*s. l.*], v. 629, p. 1066–1080, 2023. Disponível em: Acesso em: 1 maio 2023.

SUBHAN, M. A.; PARVEEN, F.; FILIPCZAK, N.; YALAMARTY, S. S. K.; TORCHILIN, V. P. Approaches to Improve EPR-Based Drug Delivery for Cancer Therapy and Diagnosis. **Journal of Personalized Medicine**, [*s. l.*], v. 13, n. 3, p. 389, 2023.

SULMAN, E. M.; MATVEEVA, V. G.; BRONSTEIN, L. M. Design of biocatalysts for efficient catalytic processes. **Current Opinion in Chemical Engineering**, [*s. l.*], v. 26, p. 1–8, 2019.

SUN, L.; LI, Q.; ZHANG, L.; XU, Z.; KANG, Y.; XUE, P. PEGylated Polydopamine Nanoparticles Incorporated with Indocyanine Green and Doxorubicin for Magnetically Guided

Multimodal Cancer Therapy Triggered by Near-Infrared Light. **ACS Applied Nano Materials**, [*s. l.*], v. 1, n. 1, p. 325–336, 2018.

SUN, Z.; WANG, X.; LIU, J.; WANG, Z.; WANG, W.; KONG, D.; LENG, X. ICG/l-Arginine Encapsulated PLGA Nanoparticle-Thermosensitive Hydrogel Hybrid Delivery System for Cascade Cancer Photodynamic-NO Therapy with Promoted Collagen Depletion in Tumor Tissues. **Molecular Pharmaceutics**, [*s. l.*], v. 18, n. 3, p. 928–939, 2021.

TADA, D. B.; BAPTISTA, M. S. Photosensitizing nanoparticles and the modulation of ROS generation. **Frontiers in Chemistry**, [*s. l.*], v. 3, 2015.

TAHA, A.; AHMED, E.; ISMAIEL, A.; ASHOKKUMAR, M.; XU, X.; PAN, S.; HU, H. Ultrasonic emulsification: An overview on the preparation of different emulsifiers-stabilized emulsions. **Trends in Food Science & Technology**, [*s. l.*], v. 105, p. 363–377, 2020.

TAKAHASHI, H.; NAKAJIMA, S.; OGASAWARA, K.; ASANO, R.; NAKAE, Y.; SAKATA, I.; IIZUKA, H. Photodynamic therapy using a novel irradiation source, LED lamp, is similarly effective to photodynamic therapy using diode laser or metal-halide lamp on DMBA- and TPA-induced mouse skin papillomas. **The Journal of Dermatology**, [*s. l.*], v. 41, n. 8, p. 729–731, 2014.

TANG, Z.; HE, C.; TIAN, H.; DING, J.; HSIAO, B. S.; CHU, B.; CHEN, X. Polymeric nanostructured materials for biomedical applications. **Progress in Polymer Science**, [*s. l.*], v. 60, p. 86–128, 2016.

TANG, J.-Q.; HOU, X.-Y.; YANG, C.-S.; LI, Y.-X.; XIN, Y.; GUO, W.-W.; WEI, Z.-P.; LIU, Y.-Q.; JIANG, G. Recent developments in nanomedicine for melanoma treatment. **International Journal of Cancer**, [*s. l.*], v. 141, n. 4, p. 646–653, 2017.

TANG, Y.; LEI, T.; MANCHANDA, R.; NAGESETTI, A.; FERNANDEZ-FERNANDEZ, A.; SRINIVASAN, S.; MCGORON, A. J. Simultaneous Delivery of Chemotherapeutic and Thermal-Optical Agents to Cancer Cells by a Polymeric (PLGA) Nanocarrier: An In Vitro Study. **Pharmaceutical Research**, [*s. l.*], v. 27, n. 10, p. 2242–2253, 2010.

TANG, Y.; MCGORON, A. J. Combined effects of laser-ICG photothermotherapy and doxorubicin chemotherapy on ovarian cancer cells. **Journal of Photochemistry and Photobiology B: Biology**, [*s. l.*], v. 97, n. 3, p. 138–144, 2009.

TAWFIK, M.; TONNELLIER, X.; SANSOM, C. Light source selection for a solar simulator for thermal applications: A review. **Renewable and Sustainable Energy Reviews**, [*s. l.*], v. 90, p. 802–813, 2018.

TEWES, F.; MUNNIER, E.; ANTOON, B.; NGABONI OKASSA, L.; COHEN-JONATHAN, S.; MARCHAIS, H.; DOUZIECH-EYROLLES, L.; SOUCÉ, M.; DUBOIS, P.; CHOURPA, I. Comparative study of doxorubicin-loaded poly(lactide-co-glycolide) nanoparticles prepared by single and double emulsion methods. **European Journal of Pharmaceutics and Biopharmaceutics**, [*s. l.*], v. 66, n. 3, p. 488–492, 2007.

TEYMOURI, F.; FARHAD, S. Z.; GOLESTANEH, H. The Effect of Photodynamic Therapy and Diode Laser as Adjunctive Periodontal Therapy on the Inflammatory Mediators Levels in Gingival Crevicular Fluid and Clinical Periodontal Status. **Journal of dentistry (Shiraz, Iran)**, [*s. l.*], v. 17, n. 3, p. 226–32, 2016.

TIAN, H.; TANG, Z.; ZHUANG, X.; CHEN, X.; JING, X. Biodegradable synthetic polymers: Preparation, functionalization and biomedical application. **Progress in Polymer Science**, [*s. l.*], v. 37, n. 2, p. 237–280, 2012.

TING, C.-W.; CHOU, Y.-H.; HUANG, S.-Y.; CHIANG, W.-H. Indocyanine green-carrying polymeric nanoparticles with acid-triggered detachable PEG coating and drug release for boosting cancer photothermal therapy. **Colloids and Surfaces B: Biointerfaces**, [*s. l.*], v. 208, p. 112048, 2021.

TOGSVERD-BO, K.; LERCHE, C. M.; PHILIPSEN, P. A.; HÆDERSDAL, M.; WULF, H. C. Artificial daylight photodynamic therapy with "non-inflammatory" doses of hexyl aminolevulinate only marginally delays SCC development in UV-exposed hairless mice. **Photochemical & Photobiological Sciences**, [*s. l.*], v. 12, n. 12, p. 2130–2136, 2013.

TSCHAN, M. J.-L.; BRULÉ, E.; HAQUETTE, P.; THOMAS, C. M. Synthesis of biodegradable polymers from renewable resources. **Polym. Chem.**, [*s. l.*], v. 3, n. 4, p. 836–851, 2012.

TURAN, I. S.; YILDIZ, D.; TURKSOY, A.; GUNAYDIN, G.; AKKAYA, E. U. A Bifunctional Photosensitizer for Enhanced Fractional Photodynamic Therapy: Singlet Oxygen Generation in the Presence and Absence of Light. **Angewandte Chemie International Edition**, [*s. l.*], v. 55, n. 8, p. 2875–2878, 2016.

URBÁNEK, T.; JÄGER, E.; JÄGER, A.; HRUBÝ, M. Selectively Biodegradable Polyesters: Nature-Inspired Construction Materials for Future Biomedical Applications. **Polymers**, [*s. l.*], v. 11, n. 6, p. 1061, 2019.

VAN DER MEULEN, I.; DE GEUS, M.; ANTHEUNIS, H.; DEUMENS, R.; JOOSTEN, E. A. J.; KONING, C. E.; HEISE, A. Polymers from Functional Macrolactones as Potential

Biomaterials: Enzymatic Ring Opening Polymerization, Biodegradation, and Biocompatibility. **Biomacromolecules**, [*s. l.*], v. 9, n. 12, p. 3404–3410, 2008.

VAN DER MEULEN, I.; GUBBELS, E.; HUIJSER, S.; SABLONG, R.; KONING, C. E.; HEISE, A.; DUCHATEAU, R. Catalytic Ring-Opening Polymerization of Renewable Macrolactones to High Molecular Weight Polyethylene-like Polymers. **Macromolecules**, [*s. l.*], v. 44, n. 11, p. 4301–4305, 2011.

VAN ECK, N. J.; WALTMAN, L. Visualizing Bibliometric Networks. *Em*: MEASURING SCHOLARLY IMPACT. Cham: Springer International Publishing, 2014. p. 285–320.

VARDY, J. L.; LIEW, A.; WARBY, A.; ELDER, A.; KESHET, I.; DEVINE, R.; OULIARIS, C.; RENTON, C.; TATTERSALL, M. H. N.; DHILLON, H. M. On the receiving end: have patient perceptions of the side-effects of cancer chemotherapy changed since the twentieth century?. **Supportive Care in Cancer**, [*s. l.*], v. 30, n. 4, p. 3503–3512, 2022.

VIVEK, R.; VARUKATTU, N.; CHANDRABABU, R.; ALOK, S.; THONDHI, P.; ALAGARSAMY, V.; KANNAN, S. Multifunctional nanoparticles for trimodal photodynamic therapy-mediated photothermal and chemotherapeutic effects. **Photodiagnosis and Photodynamic Therapy**, [*s. l.*], v. 23, p. 244–253, 2018.

WAKHARDE AA, A. A. B. A. and K. S. Synergistic Activation of Doxorubicin against Cancer: A Review. **American Journal of Clinical Microbiology and Antimicrobials**, [*s. l.*], v. 1, n. 2, 2018.

WANG, X.; GU, Y.; LI, Q.; XU, Y.; SHI, Y.; WANG, Z.; XIA, M.; LI, J.; WANG, D. Synergistic chemo-photothermal cancer therapy of pH-responsive polymeric nanoparticles loaded IR825 and DTX with charge-reversal property. **Colloids and Surfaces B: Biointerfaces**, [*s. l.*], v. 209, p. 112164, 2022.

WANG, R.; HAN, Y.; SUN, B.; ZHAO, Z.; OPOKU-DAMOAH, Y.; CHENG, H.; ZHANG, H.; ZHOU, J.; DING, Y. Cancer Therapy: Deep Tumor Penetrating Bioparticulates Inspired Burst Intracellular Drug Release for Precision Chemo-Phototherapy (Small 12/2018). **Small**, [*s. l.*], v. 14, n. 12, p. 1870049, 2018.

WANG, J.; LI, S.; HAN, Y.; GUAN, J.; CHUNG, S.; WANG, C.; LI, D. Poly(Ethylene Glycol)–Polylactide Micelles for Cancer Therapy. **Frontiers in Pharmacology**, [*s. l.*], v. 9, 2018.

WANG, Y.; LI, P.; TRUONG-DINH TRAN, T.; ZHANG, J.; KONG, L. Manufacturing Techniques and Surface Engineering of Polymer Based Nanoparticles for Targeted Drug Delivery to Cancer. **Nanomaterials**, [*s. l.*], v. 6, n. 2, p. 26, 2016.

WANG, S.; LI, Jingtao; YE, Z.; LI, Jieling; WANG, A.; HU, J.; BAI, S.; YIN, J. Self-assembly of photosensitive and chemotherapeutic drugs for combined photodynamic-chemo cancer therapy with real-time tracing property. **Colloids and Surfaces A: Physicochemical and Engineering Aspects**, [*s. l.*], v. 574, p. 44–51, 2019.

WANG, X.-H.; PENG, H.-S.; YANG, W.; REN, Z.-D.; LIU, X.-M.; LIU, Y.-A. Indocyanine green-platinum porphyrins integrated conjugated polymer hybrid nanoparticles for near-infrared-triggered photothermal and two-photon photodynamic therapy. **Journal of Materials Chemistry B**, [*s. l.*], v. 5, n. 9, p. 1856–1862, 2017.

WANG, X.; RONSIN, O.; GRAVEZ, B.; FARMAN, N.; BAUMBERGER, T.; JAISSER, F.; CORADIN, T.; HÉLARY, C. Nanostructured Dense Collagen-Polyester Composite Hydrogels as Amphiphilic Platforms for Drug Delivery. **Advanced Science**, [*s. l.*], v. 8, n. 7, 2021.

WANG, Y.; WEI, X.; ZHANG, C.; ZHANG, F.; LIANG, W. Nanoparticle delivery strategies to target doxorubicin to tumor cells and reduce side effects. **Therapeutic Delivery**, [*s. l.*], v. 1, n. 2, p. 273–287, 2010.

WANG, Q.; XIA, B.; XU, J.; NIU, X.; CAI, J.; SHEN, Q.; WANG, W.; HUANG, W.; FAN, Q. Biocompatible small organic molecule phototheranostics for NIR-II fluorescence/photoacoustic imaging and simultaneous photodynamic/photothermal combination therapy. **Materials Chemistry Frontiers**, [*s. l.*], v. 3, n. 4, p. 650–655, 2019.

WATANABE, T.; SAKAMOTO, Y.; INOOKA, T.; KIMURA, Y.; ONO, T. Indocyanine green-laden poly(ethylene glycol)-block-polylactide (PEG-b-PLA) nanocapsules incorporating reverse micelles: Effects of PEG-b-PLA composition on the nanocapsule diameter and encapsulation efficiency. **Colloids and Surfaces A: Physicochemical and Engineering Aspects**, [*s. l.*], v. 520, p. 764–770, 2017.

WEI, G.; YANG, G.; WEI, B.; WANG, Y.; ZHOU, S. Near-infrared light switching nitric oxide nanoemitter for triple-combination therapy of multidrug resistant cancer. **Acta Biomaterialia**, [*s. l.*], v. 100, p. 365–377, 2019.

WEIJER, R.; BROEKGAARDEN, M.; KOS, M.; VAN VUGHT, R.; RAUWS, E. A. J.; BREUKINK, E.; VAN GULIK, T. M.; STORM, G.; HEGER, M. Enhancing photodynamic therapy of refractory solid cancers: Combining second-generation photosensitizers with multi-

targeted liposomal delivery. **Journal of Photochemistry and Photobiology C: Photochemistry Reviews**, [*s. l.*], v. 23, p. 103–131, 2015.

WIEGELL, S. R.; FABRICIUS, S.; GNIADECKA, M.; STENDER, I. M.; BERNE, B.; KROON, S.; ANDERSEN, B. L.; MØRK, C.; SANDBERG, C.; IBLER, K. S.; JEMEC, G. B. E.; BROCKS, K. M.; PHILIPSEN, P. A.; HEYDENREICH, J.; HAEDERSDAL, M.; WULF, H. C. Daylight-mediated photodynamic therapy of moderate to thick actinic keratoses of the face and scalp: a randomized multicentre study. **British Journal of Dermatology**, [*s. l.*], v. 166, n. 6, p. 1327–1332, 2012.

WIEGELL, S. R.; HÆDERSDAL, M.; PHILIPSEN, P. A.; ERIKSEN, P.; ENK, C. D.; WULF, H. C. Continuous activation of PpIX by daylight is as effective as and less painful than conventional photodynamic therapy for actinic keratoses; a randomized, controlled, single-blinded study. **British Journal of Dermatology**, [*s. l.*], v. 158, n. 4, p. 740–746, 2008.

WILSON, J. A.; ATES, Z.; PFLUGHAUPT, R. L.; DOVE, A. P.; HEISE, A. Polymers from macrolactones: From pheromones to functional materials. **Progress in Polymer Science**, [*s. l.*], v. 91, p. 29–50, 2019.

WU, C.-P.; HSIEH, C.-H.; WU, Y.-S. The Emergence of Drug Transporter-Mediated Multidrug Resistance to Cancer Chemotherapy. **Molecular Pharmaceutics**, [*s. l.*], v. 8, n. 6, p. 1996–2011, 2011.

WU, M.; MEI, T.; LIN, C.; WANG, Y.; CHEN, J.; LE, W.; SUN, M.; XU, J.; DAI, H.; ZHANG, Y.; XUE, C.; LIU, Z.; CHEN, B. Melanoma Cell Membrane Biomimetic Versatile CuS Nanoprobes for Homologous Targeting Photoacoustic Imaging and Photothermal Chemotherapy. **ACS Applied Materials & Interfaces**, [*s. l.*], v. 12, n. 14, p. 16031–16039, 2020.

WU, H.; WEI, M.; XU, Y.; LI, Y.; ZHAI, X.; SU, P.; MA, Q.; ZHANG, H. PDA-Based Drug Delivery Nanosystems: A Potential Approach for Glioma Treatment. **International Journal of Nanomedicine**, [*s. l.*], v. Volume 17, p. 3751–3775, 2022.

XIA, F.; NIU, J.; HONG, Y.; LI, C.; CAO, W.; WANG, L.; HOU, W.; LIU, Y.; CUI, D. Matrix metallopeptidase 2 targeted delivery of gold nanostars decorated with IR-780 iodide for dual-modal imaging and enhanced photothermal/photodynamic therapy. **Acta Biomaterialia**, [*s. l.*], v. 89, p. 289–299, 2019.

XIA, W.; TAO, Z.; ZHU, B.; ZHANG, W.; LIU, C.; CHEN, S.; SONG, M. Targeted Delivery of Drugs and Genes Using Polymer Nanocarriers for Cancer Therapy. **International Journal of Molecular Sciences**, [*s. l.*], v. 22, n. 17, p. 9118, 2021.

XIA, C.; XIAO, C. Preparation and characterization of dual responsive sodium alginate-g-poly(vinyl alcohol) hydrogel. **Journal of Applied Polymer Science**, [*s. l.*], v. 123, n. 4, p. 2244–2249, 2012.

XIAO, X.; TENG, F.; SHI, C.; CHEN, J.; WU, S.; WANG, B.; MENG, X.; ESSIET IMEH, A.; LI, W. Polymeric nanoparticles—Promising carriers for cancer therapy. **Frontiers in Bioengineering and Biotechnology**, [*s. l.*], v. 10, 2022.

XU, M.; HAN, X.; XIONG, H.; GAO, Y.; XU, B.; ZHU, G.; LI, J. Cancer Nanomedicine: Emerging Strategies and Therapeutic Potentials. **Molecules**, [*s. l.*], v. 28, n. 13, p. 5145, 2023.

XU, R. X.; HUANG, J.; XU, J. S.; SUN, D.; HINKLE, G. H.; MARTIN, E. W.; POVOSKI, S. P. Fabrication of indocyanine green encapsulated biodegradable microbubbles for structural and functional imaging of cancer. **Journal of Biomedical Optics**, [*s. l.*], v. 14, n. 3, p. 034020, 2009.

XU, X.; LIU, Y.; FU, W.; YAO, M.; DING, Z.; XUAN, J.; LI, D.; WANG, S.; XIA, Y.; CAO, M. Poly(N-isopropylacrylamide)-Based Thermoresponsive Composite Hydrogels for Biomedical Applications. **Polymers**, [*s. l.*], v. 12, n. 3, p. 580, 2020.

YANG, S.; GAO, H. Nanoparticles for modulating tumor microenvironment to improve drug delivery and tumor therapy. **Pharmacological Research**, [*s. l.*], v. 126, p. 97–108, 2017.

YANG, J.; HAN, S.; ZHENG, H.; DONG, H.; LIU, J. Preparation and application of micro/nanoparticles based on natural polysaccharides. **Carbohydrate Polymers**, [*s. l.*], v. 123, p. 53–66, 2015.

YANG, J.; LEE, C.-H.; PARK, J.; SEO, S.; LIM, E.-K.; SONG, Y. J.; SUH, J.-S.; YOON, H.-G.; HUH, Y.-M.; HAAM, S. Antibody conjugated magnetic PLGA nanoparticles for diagnosis and treatment of breast cancer. **Journal of Materials Chemistry**, [*s. l.*], v. 17, n. 26, p. 2695, 2007.

YANG, C.; SU, M.; LUO, P.; LIU, Y.; YANG, F.; LI, C. A Photosensitive Polymeric Carrier with a Renewable Singlet Oxygen Reservoir Regulated by Two NIR Beams for Enhanced Antitumor Phototherapy. **Small**, [*s. l.*], v. 17, n. 29, p. 2101180, 2021.

YANG, M.; YANG, T.; MAO, C. Enhancement of Photodynamic Cancer Therapy by Physical and Chemical Factors. **Angewandte Chemie International Edition**, [*s. l.*], v. 58, n. 40, p. 14066–14080, 2019.

YAO, S.; JIN, X.; WANG, C.; CAO, A.; HU, J.; CHEN, B.; WANG, B. ICG/5-Fu coencapsulated temperature stimulus response nanogel drug delivery platform for chemo-

photothermal/photodynamic synergetic therapy. **Journal of Biomaterials Applications**, [*s. l.*], v. 36, n. 4, p. 565–578, 2021.

YE, Y.; WANG, J.; SUN, W.; BOMBA, H. N.; GU, Z. Topical and Transdermal Nanomedicines for Cancer Therapy. *Em*: [*S. l.: s. n.*], 2019. p. 231–251.

YOON, H. Y.; KOO, H.; CHOI, K. Y.; LEE, S. J.; KIM, K.; KWON, I. C.; LEARY, J. F.; PARK, K.; YUK, S. H.; PARK, J. H.; CHOI, K. Tumor-targeting hyaluronic acid nanoparticles for photodynamic imaging and therapy. **Biomaterials**, [*s. l.*], v. 33, n. 15, p. 3980–3989, 2012.

YOUSEFI RIZI, H. A.; SHIN, D. H.; YOUSEFI RIZI, S. Polymeric Nanoparticles in Cancer Chemotherapy: A Narrative Review. **Iranian Journal of Public Health**, [*s. l.*], 2022.

YU, J. J.; LEE, H. A.; KIM, J. H.; KONG, W. H.; KIM, Y.; CUI, Z. Y.; PARK, K. G.; KIM, W. S.; LEE, H. G.; SEO, S. W. Bio-distribution and anti-tumor efficacy of PEG/PLA nano particles loaded doxorubicin. **Journal of Drug Targeting**, [*s. l.*], v. 15, n. 4, p. 279–284, 2007.

YU, J.; WANG, L.; XIE, X.; YU, H.; XU, J.; REN, J.; ZHU, W.; LEI, Z.; LV, L. Multifunctional Nanoparticles Codelivering Doxorubicin and Amorphous Calcium Carbonate Preloaded with Indocyanine Green for Enhanced Chemo-Photothermal Cancer Therapy. **International Journal of Nanomedicine**, [*s. l.*], v. 18, p. 323–337, 2023.

YUSUF, A.; ALMOTAIRY, A. R. Z.; HENIDI, H.; ALSHEHRI, O. Y.; ALDUGHAIM, M. S. Nanoparticles as Drug Delivery Systems: A Review of the Implication of Nanoparticles' Physicochemical Properties on Responses in Biological Systems. **Polymers**, [*s. l.*], v. 15, n. 7, p. 1596, 2023.

ZENG, W.-N.; YU, Q.-P.; WANG, D.; LIU, J.-L.; YANG, Q.-J.; ZHOU, Z.-K.; ZENG, Y.-P. Mitochondria-targeting graphene oxide nanocomposites for fluorescence imaging-guided synergistic phototherapy of drug-resistant osteosarcoma. **Journal of Nanobiotechnology**, [*s. l.*], v. 19, n. 1, p. 79, 2021.

ZHANG, J.; LIN, Y.; LIN, Z.; WEI, Q.; QIAN, J.; RUAN, R.; JIANG, X.; HOU, L.; SONG, J.; DING, J.; YANG, H. Stimuli-Responsive Nanoparticles for Controlled Drug Delivery in Synergistic Cancer Immunotherapy. **Advanced Science**, [*s. l.*], v. 9, n. 5, p. 2103444, 2022.

ZHANG, L.; QIN, Y.; ZHANG, Z.; FAN, F.; HUANG, C.; LU, L.; WANG, H.; JIN, X.; ZHAO, H.; KONG, D.; WANG, C.; SUN, H.; LENG, X.; ZHU, D. Dual pH/reduction-

responsive hybrid polymeric micelles for targeted chemo-photothermal combination therapy. **Acta Biomaterialia**, [*s. l.*], v. 75, p. 371–385, 2018.

ZHANG, J.; SHI, H.; WU, D.; XING, Z.; ZHANG, A.; YANG, Y.; LI, Q. Recent developments in lipase-catalyzed synthesis of polymeric materials. **Process Biochemistry**, [*s. l.*], v. 49, n. 5, p. 797–806, 2014.

ZHANG, S.; WANG, J.; KONG, Z.; SUN, X.; HE, Z.; SUN, B.; LUO, C.; SUN, J. Emerging photodynamic nanotherapeutics for inducing immunogenic cell death and potentiating cancer immunotherapy. **Biomaterials**, [*s. l.*], v. 282, p. 121433, 2022.

ZHAO, X.; LIU, J.; FAN, J.; CHAO, H.; PENG, X. Recent progress in photosensitizers for overcoming the challenges of photodynamic therapy: from molecular design to application. **Chemical Society Reviews**, [*s. l.*], v. 50, n. 6, p. 4185–4219, 2021.

ZHAO, X.; YANG, C.-X.; CHEN, L.-G.; YAN, X.-P. Dual-stimuli responsive and reversibly activatable theranostic nanoprobe for precision tumor-targeting and fluorescence-guided photothermal therapy. **Nature Communications**, [*s. l.*], v. 8, n. 1, p. 14998, 2017.

ZHAO, H.; YIN, R.; CHEN, D.; REN, J.; WANG, Yucheng; ZHANGA, J.; DENG, H.; WANG, Ying; QIU, H.; HUANG, N.; ZOU, Q.; ZHAO, J.; GU, Y. In vitro and in vivo antitumor activity of a novel hypocrellin B derivative for photodynamic therapy. **Photodiagnosis and Photodynamic Therapy**, [*s. l.*], v. 11, n. 2, p. 204–212, 2014.

ZHENG, X.; XING, D.; ZHOU, F.; WU, B.; CHEN, W. R. Indocyanine Green-Containing Nanostructure as Near Infrared Dual-Functional Targeting Probes for Optical Imaging and Photothermal Therapy. **Molecular Pharmaceutics**, [*s. l.*], v. 8, n. 2, p. 447–456, 2011.

ZHENG, M.; YUE, C.; MA, Y.; GONG, P.; ZHAO, P.; ZHENG, C.; SHENG, Z.; ZHANG, P.; WANG, Z.; CAI, L. Single-Step Assembly of DOX/ICG Loaded Lipid–Polymer Nanoparticles for Highly Effective Chemo-photothermal Combination Therapy. **ACS Nano**, [*s. l.*], v. 7, n. 3, p. 2056–2067, 2013.

ZHOU, M.; HUANG, H.; WANG, D.; LU, H.; CHEN, J.; CHAI, Z.; YAO, S. Q.; HU, Y. Light-Triggered PEGylation/dePEGylation of the Nanocarriers for Enhanced Tumor Penetration. **Nano Letters**, [*s. l.*], v. 19, n. 6, p. 3671–3675, 2019.

ZHOU, Z.; SONG, J.; NIE, L.; CHEN, X. Reactive oxygen species generating systems meeting challenges of photodynamic cancer therapy. **Chemical Society Reviews**, [*s. l.*], v. 45, n. 23, p. 6597–6626, 2016.

ZHU, J.; ZHOU, H.; GERHARD, E. M.; ZHANG, S.; PARRA RODRÍGUEZ, F. I.; PAN, T.; YANG, H.; LIN, Y.; YANG, J.; CHENG, H. Smart bioadhesives for wound healing and closure. **Bioactive Materials**, [*s. l.*], v. 19, p. 360–375, 2023. Disponível em: Acesso em: 1 maio 2023.

ZIAUDDIN; HUSSAIN, T.; NAZIR, A.; MAHMOOD, U.; HAMEED, M.; RAMAKRISHNA, S.; ABID, S. Nanoengineered Therapeutic Scaffolds for Burn Wound Management. **Current Pharmaceutical Biotechnology**, [*s. l.*], v. 23, n. 12, p. 1417–1435, 2022.

ZOLNIK, B. S.; GONZÁLEZ-FERNÁNDEZ, A.; SADRIEH, N.; DOBROVOLSKAIA, M. A. Minireview: Nanoparticles and the Immune System. **Endocrinology**, [*s. l.*], v. 151, n. 2, p. 458–465, 2010.

ZUO, H.; GU, Z.; COOPER, H.; XU, Z. P. Crosslinking to enhance colloidal stability and redispersity of layered double hydroxide nanoparticles. **Journal of Colloid and Interface Science**, [*s. l.*], v. 459, p. 10–16, 2015.